# APPENDIX K
# BC MINISTRY OF ENVIRONMENT EIS

## Part C: Appendix A
## Multiport Diffuser Design and Dilution Modelling Report
## Attachments E to J

### Annacis Island WWTP New Outfall System

**Vancouver Fraser Port Authority**
**Project and Environmental Review Application**

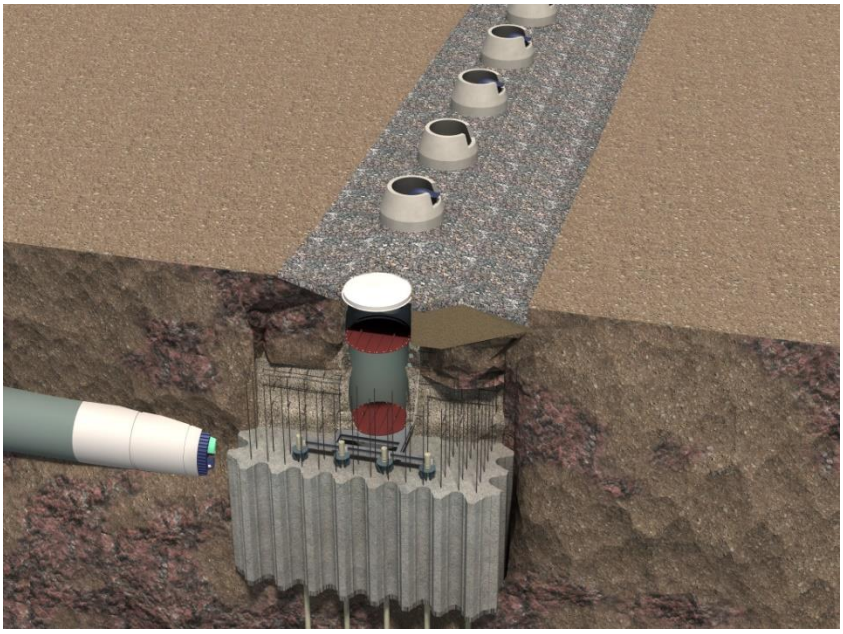

metrovancouver
SERVICES AND SOLUTIONS FOR A LIVABLE REGION

CDM Smith

Golder Associates

This page intentionally left blank

# Attachment E

# Annacis Island WWTP Salinity Monitoring Program

This page intentionally left blank.

20 April 2017

## SEPTEMBER 2016 TO MARCH 2017

# Annacis Island WWTP Salinity Monitoring Program

**Submitted to:**
CDM Smith Canada ULC
4720 Kingsway, Suite 1001
Burnaby, BC
V5H 4N2

**Report Number: 1525010-083-R-Rev1-703**

**Distribution:**

1 copy - CDM Smith
1 copy - Golder Associates Ltd

REPORT

Golder Associates

# Executive Summary

Golder Associates Ltd. (Golder) was retained by CDM Smith Canada ULC (CDM Smith) to provide a baseline water density sampling program to support the characterization of existing conditions during the pre-freshet period in the Fraser River near Annacis Island, Delta, BC. Water density measurements are needed to support modelling of the wastewater effluent plume and design of the outfall as part of the Environmental Impact Study (EIS) that is being prepared for the proposed Annacis Island Wastewater Treatment Plant (AIWWTP) transient migration and outfall system.

The project objectives are to measure water column density structure (defined by salinity and temperature) and temporal variations at the site during non-freshet (low flow) conditions. The data measurement program consisted of the following:

- Continuous monitoring of salinity and temperature at a single point moored instrument from September 2016 to March 2017 located on the Brewery Pier on the north bank approximately 200 m downstream of the proposed outfall.
- Continuous monitoring of near bed salinity, temperature, turbidity, and current speed and direction through the water column near the proposed outfall location from a seabed frame (QuadPod) for a 30 day period.
- Water column profiling of Conductivity and Temperature with Depth (CTD) during select tidal conditions over five days at six specified sampling locations.

The salinity monitoring program at the proposed Annacis Island WWTP outfall captured salinity present at the project site during low flows. Nearly six months of continuous data collection at Brewery Pier provides insight on the trends in salinity in relation to river discharge levels and tidal phases. The QuadPod measurements and CTD profiles provide detailed data during low flow conditions at the project site from 7 February to 9 March 2017. This data analysis provides key information on salinity conditions at the project site and will support the development and design of the proposed outfall and work undertaken as part of the permit application process. This analysis has illustrated the following:

- Salinity of values ranging from a baseline of 0.06 to a maximum of 19.9 were measured during the course of the data collection program.
- Salinity values of 0.5 or higher occurred 55 days out of the 176 day deployment at the Brewery Pier station and on 22 days of the 31 day deployment at the QuadPod station.
- Salinity events at the Brewery Pier and QuadPod stations most often occurred when river flows were below 1,000 $m^3/s$ at the Hope station, however, some salinity events occurred when flows were higher. The largest recorded river flow at Hope was 1,800 $m^3/s$ when a salinity event was recorded at the Brewery Pier station.
- Tidal asymmetry, in the form of diurnal inequality caused by a smaller differences between the higher high water of the tidal cycle and higher low water, tended to coincide with the occurrence of the salt wedge presence at the site (along with lower river discharge levels).

- Current conditions measured by the QuadPod at the project site were predominantly to the southwest (downriver). Current measurements collected during lower discharge levels showed that at least once per tidal cycle, the flow direction reversed through the water column to flow northeast (upriver) during the larger flood tide of the day. When tidal asymmetry was not as strong (diurnal inequality was minimal), the flow reversal occurred twice each cycle, during both flood tides.
- Mean current speeds were between 0.48 to 0.71 m/s and reached maximum values of 1.4 to 2.12 m/s through the water column from the bottom to surface respectively. Flow speed and direction were relatively uniform through the water column, with speeds slightly higher near the surface and decreasing with depth. Current direction through the water column became stratified for a few select salt wedge intrusion events, and current speed was slower near the bottom where the salt wedge was present.
- Based on current speed at the Quad Pod and downstream CTD profiles, the salt wedge was observed approaching the site from downstream, moving upstream during the flood tide, and elevated salinity would remain present at the site until the early or middle of the ebb tide.
- Salinity events recorded at the Brewery Pier and QuadPod typically increased in salinity during the flood tide and continued to increase past slack high. Peak salinity values for each event corresponded with the early to middle of the ebb tide. Near bed current flow measurements showed that the peak salinity values corresponded with southwesterly current flow and often the downriver flow had been sustained for a few hours before peak salinity was reached.
- The salt wedge was likely present further upstream of the project site during events when the peak salinity corresponded to downriver flows.
- Other characteristics of the salt wedge besides increased salinity, included increased water temperature, and decreased turbidity and pH.
- The pycnocline was typically present at -5 to -10 m CGVD in the CTD profiles measured at the site.

# Important Information and Limitations of This Report

Golder Associates Ltd. (Golder) has prepared this document in a manner consistent with that level of care and skill ordinarily exercised by members of the engineering and science professions currently practising under similar conditions in the jurisdiction in which the services are provided, subject to the time limits and physical constraints applicable to this document. No warranty, express or implied, is made.

This document, including all text, data, tables, plans, figures, drawings and other documents contained herein, has been prepared by Golder for the sole benefit of CDM Smith. It represents Golder's professional judgement based on the knowledge and information available at the time of completion. Golder is not responsible for any unauthorized use or modification of this document. All third parties relying on this document do so at their own risk.

The factual data, interpretations, suggestions, recommendations and opinions expressed in this document pertain to the specific project, site conditions, design objective, development and purpose described to Golder by CDM Smith, and are not applicable to any other project or site location. In order to properly understand the factual data, interpretations, suggestions, recommendations and opinions expressed in this document, reference must be made to the entire document.

This document, including all text, data, tables, plans, figures, drawings and other documents contained herein, as well as all electronic media prepared by Golder are considered its professional work product and shall remain the copyright property of Golder. CDM Smith may make copies of the document in such quantities as are reasonably necessary for those parties conducting business specifically related to the subject of this document or in support of or in response to regulatory inquiries and proceedings. Electronic media is susceptible to unauthorized modification, deterioration and incompatibility and therefore no party can rely solely on the electronic media versions of this document.

# Table of Contents

**TABLES**



**FIGURES**

**APPENDICES**

# 1.0 INTRODUCTION

Golder Associates Ltd. (Golder) was retained by CDM Smith Canada ULC (CDM Smith) to provide a baseline water density sampling program to support the characterization of existing conditions during the pre-freshet period in the Fraser River near Annacis Island, Delta, BC. Water density measurements are needed to support modelling of the wastewater effluent plume and design of the outfall as part of the Environmental Impact Study (EIS) that is being prepared for the proposed Annacis Island Wastewater Treatment Plant (AIWWTP) transient migration and outfall system.

The project objectives are to measure water column density structure (defined by salinity and temperature) and temporal variations at the site during non-freshet (low flow) conditions. The data measurement program consisted of the following:

- Continuous monitoring of salinity and temperature at a single point moored instrument from September 2016 to March 2017 located on the Brewery Pier on the north bank approximately 200 m downstream of the proposed outfall.
- Continuous monitoring of near bed salinity, temperature, turbidity, and current speed and direction through the water column near the proposed outfall location from a seabed frame (QuadPod) for a 30 day period.
- Water column profiling of Conductivity and Temperature with Depth (CTD) during select tidal conditions over five days at six specified sampling locations.

Figure 1 shows the project area, current outfall, single point moored instrument at Brewery Pier, the six sampling locations for CTD profiles, and the two deployment positions of the QuadPod during the baseline data collection effort.

This technical memorandum should be read in conjunction with **"Important Information and Limitations of This Report"** which is appended following the executive summary of the report. The reader's attention is specifically drawn to this information, as it is essential that it is followed for the proper use and interpretation of this report.


## LEGEND

PROJECT DATA
- PROJECT AREA
- CONDUCTIVITY AND TEMPERATURE WITH DEPTH (CTD) PROFILE LOCATION
- MOORING - BREWERY PIER
- QUADPOD
- EXISTING WWPT OUTFALL

BASE DATA
- HIGHWAY
- MAJOR ROAD

FRASER RIVER SHIPPING CHANNEL
- CENTRE OF CHANNEL
- OUTER CHANNEL BOUNDARY
- WATERCOURSE
- WATER

0 200 400
1:10,000 METRES

**REFERENCES**
1. SHIPPING CHANNEL SUPPLIED BY BLACK & VEATCH
2. ROADS, WATERCOURSE AND WATERBODY DATA OBTAINED FROM GEOGRATIS, © DEPARTMENT OF NATURAL RESOURCES CANADA. ALL RIGHTS RESERVED
3. IMAGERY © DIGITALGLOBE, INC. ALL RIGHTS RESERVED, IMAGE DATE 09/25/2009. COORDINATE SYSTEM: NAD 1983 UTM ZONE 10N

CLIENT
CDM SMITH INC.

CONSULTANT
Golder Associates

| | |
|---|---|
| YYYY-MM-DD | 2017-03-29 |
| DESIGNED | DO |
| PREPARED | MH |
| REVIEWED | |
| APPROVED | |

PROJECT
ANNACIS ISLAND WWTP TRANSIENT MITIGATION & OUTFALL UPGRADE
DELTA, B.C.

TITLE
ANNACIS ISLAND WWPT OUTFALL SALINITY MONITORING PROGRAM

| PROJECT NO. | CONTROL | REV. | FIGURE |
|---|---|---|---|
| 1525010 | 703.2 | A | 01 |

PATH: \\golder.gds\gal\burnaby\CAD-GIS\Client\CDM_Smith\Annacis_Island\99_PROJECTS\1525010_WWTP\02_PRODUCTION\703\MXD\Report\Figure_01_Outfall_Salinity_Monitoring_Program.mxd

IF THIS MEASUREMENT DOES NOT MATCH WHAT IS SHOWN, THE SHEET SIZE HAS BEEN MODIFIED FROM: ANSI B

0 25mm

# 2.0 METHODS

The Annacis Island WWTP salinity and water density monitoring program included two continuously logging stations and five days of CTD profile measurements in the project area during low flow river conditions. Data collection began 16 September 2016 at the Brewery Pier moored sensor and continued until 10 March 2017. Continuous measurements at the proposed outfall were obtained from 7 February to 9 March 2017, and CTD profiles were collected on five select days with low river flow and tidal conditions conducive to salt wedge presence at the site between 25 January and 9 March 2017.

## 2.1 Mooring and Frame Design

The Brewery Pier moored instrument consisted of a Seabird Electronics SBE37 SM microCAT CT recorder (SBE37) with pressure sensor and YSI EXO2 water quality sonde mounted in a steel frame attached to a 10 m line (Figure 2). The mooring line was suspended from a railing on the Brewery Pier with the base of the steel frame resting on the river bed to keep the line taut. The mooring and instrumentation was installed on 16 September 2016 at 17:30 UTC. The SBE37 CT was set to sample every 60 seconds, and the YSI EXO2 was programmed to sample every 120 seconds. The different sampling intervals were set based on the different power consumption requirements of the respective instruments. The YSI EXO2 was recovered 25 October 2016 at 21:40 UTC. The CT sensor remained deployed until 10 March 2017 at 19:15 UTC.

The YSI EXO2 recorded conductivity (salinity), temperature, depth, turbidity, and pH. The pH sensor was replaced or verified once every 2 weeks. During each data download, an independent pH meter was used to collect data for comparison with the pH sensor. The SBE37 recorded conductivity (salinity), temperature, and depth. Following a data download on 2 February 2017, there were errors in the data file, caused from the download. No data was lost, but the SBE37 was replaced on 3 February 2017 with an RBRduo sensor that only measures conductivity (salinity) and temperature.

The moored instruments were installed at 49.1589° N, -122.9509° W. The position was surveyed and the pier elevation was recorded as 3.84 m Canadian Geodetic Vertical Datum 1928 (CGVD28). The sensors of the instruments were 8.12 m below the survey point, meaning the station was installed at -4.28 m CGVD28.

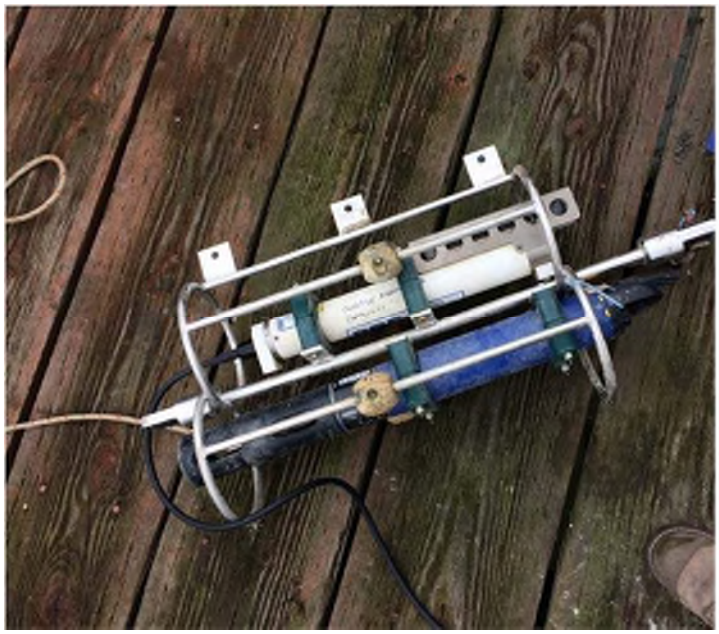

*Figure 2: (Left) Brewery Pier steel frame with SBE37 and YSI EXO2.*

The QuadPod is a lead ballasted and powder coated aluminum seabed frame supporting a Teledyne RD Instruments (TRDI) 600 kHz Acoustic Doppler Current Profiler (ADCP), two Seabird SBE37 conductivity-temperature (CT) sensors, an RBRduo pressure sensor, a JFE Advantech Infinity optical turbidity sensor, and an acoustic release pop-up recovery mechanism and back up pop-up recovery system (Figure 3). The sampling protocols and parameters measured by the instruments on the QuadPod are summarized in Table 1.

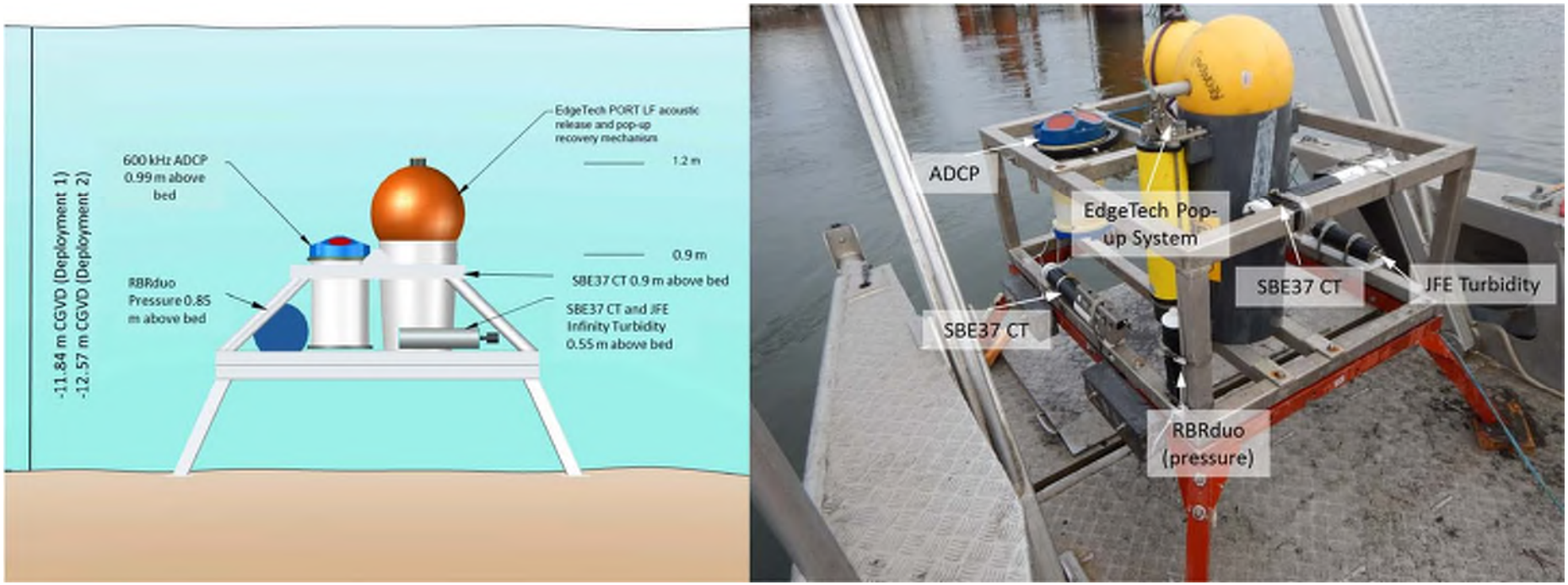


*Figure 3: (Left) Conceptual Diagram of QuadPod with deployment elevations and elevations above the river bed, (Right) Photo of QuadPod prepared for deployment.*

**Table 1: QuadPod Instrumentation and Sampling Strategy**

| Instrumentation | Sampling Strategy | Sensor Elevation Deploy1 and Deploy2 | Instrument Uncertainty |
|---|---|---|---|
| 1 TRDI 600 kHz WorkHorse Sentinel ADCP SN# 21100 upward-looking measuring water column currents (u, v, w) and relative water levels | Ensemble interval: 360 seconds<br>Pings per ensemble: 60 pings<br>Ping interval: 6 s<br>Bin size: 0.5 metres (m)<br>Blanking distance: 1.6 m<br>Number of bins: 35 | -10.85 m and -11.58 m CGVD28 | Horizontal standard deviation: 1.76 centimetres per second (cm/s)<br>Compass direction accuracy: ±2° |
| SeaBird Electronics (SBE37) SM MicroCat CT, SN# 12344 and SN# 12345, measuring conductivity and temperature | Sampling Interval: 1 minute<br>Sampling duration: 1 second | SBE12344: -10.89 m and -11.62 m CGVD28<br>SBE12345: -11.29 m and -12.02 m CGVD28 | Temperature accuracy: ±0.002°C<br>Conductivity accuracy: ±0.003 mS/cm |
| RBR Duo SN# 50517 measuring pressure (depth) and temperature | Sampling Interval: 1 minute<br>Sampling duration: 1 second | -10.99 m and -11.72 m CGVD28 | Temperature accuracy: ±0.002°C<br>Pressure accuracy: ±0.05% full scale (20 m decibar range) |
| JFE Advantech Infinity turbidity logger SN# 142 | Measurement Interval: 1 second<br>Samples per burst: 10<br>Burst Interval: 5 minutes | -11.29 m and -12.02 m CGVD28 | Temperature accuracy: ±0.02 ˚C<br>Turbidity accuracy: ±0.3 FTU |

The ADCP compass was calibrated onshore prior to deployment to account for hard and soft iron effects and then fixed in the QuadPod. The ADCP compass was calibrated successfully with a reported error of 0.3° which is within the manufacturers' recommended maximum error of 2.0 °.

## 2.2 Instrument Deployment and Recovery

The Brewery Pier mooring was deployed and recovered from land by accessing the pier through the Turning Point Brewery property. The mooring was accessed by pulling up the line and system and lowering into the water again. The QuadPod was recovered and deployed onboard the M/V Plan B using the vessel A-frame and winch to lower and lift the frame. The frame and instruments were recovered in good condition. There was substantial sand accumulation around the instrumentation and most notably inside the rope canister of the pop-up recovery system (Figure 4). The QuadPod was deployed 7 February 2017 at 17:30 and recovered on 14 February 2017 for an interim data download. The QuadPod was recovered on 9 March 2017 at 18:54 to complete the 30 day data collection program. Table 2 summarizes the deployment locations and elevation of the frame.

**Table 2: QuadPod deployment position and elevation**

| Deployment Location | Latitude, Longitude (DD.ddddd) | UTM NAD83 Zone 10 | UTM with GVRD Ground Units. Combined Scale Factor = 0.9996026 | Elevation (m, CGVD28) |
|---|---|---|---|---|
| Deploy1 (7 February to 14 February 2017) | 49.1586°N, -122.9485°W | 503754.87E, 5445088.11N | 503955.14E, 5447252.84N | -11.84 |
| Deploy2 (14 February to 9 March 2017) | 49.15816°N, -122.948197°W | 503777.33E, 5445039.12N | 503977.61E, 5447203.8N | -12.57 |

Notes: UTM=Universal Transverse Mercator; NAD= North American Datum; GVRD= Greater Vancouver Regional District

*Figure 4: Frame redeployment on 14 February 2017 (Left) and Sand accumulation inside the EdgeTech rope canister (Right).*

## 2.3 CTD Profiles

A SeaBird 19plus V2 profiler with auxiliary sensors was used to measure CTD profiles at the project site at six sampling locations (Figure 1). CTD profiles were collected on five sampling days and opportunistically on days while deploying and servicing the QuadPod. The samples were collected in successive order to complete one iteration. The sampling order was CTD1, CTD2, CTD3, CTD4, CTD5, and CTD6. Station CTD2 and CTD4 are the same location. Additional samples were collected at a station called CTD7 at the western end of Annacis Island when the salt wedge was possibly downstream of the site. CTD profiles were collected on 25 January, 26 January, 31 January, 1 February, 7 February, 9 February, and 9 March 2017.

The SBE 19plus V2 SeaCAT profiler (SN: 19P72752-7329) is equipped with instruments to measure conductivity, temperature, turbidity, pH, and pressure. The SBE 19plus V2 uses an internally mounted strain-gauge pressure sensor, a T-C Duct, which ensures the temperature and conductivity measurements are made on the same parcel of water. The auxiliary sensors include a pH probe SBE18 (SN: 181093) and a WETLabs optical turbidity sensor (SN: NTURT-548). The SBE 19plus V2 samples continuously at a rate of 4 Hertz (Hz).

## 2.4 Data Processing and Quality Assurance/Quality Control (QA/QC)

Quality checks include reviewing time series measured by the instruments including various diagnostic parameters; checking the instrument clock for drift during the deployment; checking internal recorder and file status; and plotting and viewing the time series in various formats specific to each instrument. Instrument clocks were compared upon recovery to a GPS receiver clock in order to determine if the instrument clock drifted ahead (fast) or behind (slow) GPS time. Data were not corrected for clock drift for the purposes of this report as all measured clock drift was less than 10 seconds. The following sections describe the processing methods for the moored instruments and CTD profiles. Quality-controlled data are provided electronically as Appendix A with this report.

### 2.4.1 Currents

The current profiler data were exported from raw binary format to ASCII format using the manufacturer's software. Further processing was completed using the MATLAB® (Mathworks 2015) scientific computing software. This report presents the concatenated full deployment data-set. Processing and quality-checking of the time series data consisted of the following steps:

- Plotting quality control parameters: instrument heading, tilt (vector sum of pitch and roll angles), battery voltage, depth, and temperature. The tilt was inspected to identify periods when the transducer might have deviated from vertical which could affect the integrity of current measurements.
- Measured water temperature and estimated salinity were converted to water density using the International Equation of State of Seawater 1980 (IES80) (Fofonoff and Millard 1983). Depths were output directly from the TRDI software and converted to CGVD28 elevations based on the deployment location and mounting height.

Current velocity measurements recorded by the current profilers were processed in nine steps:

1) Speed of sound is calculated by the instrument during the deployment based on the user-entered water salinity and using the measured temperature and pressure. The calculated speed of sound is applied in real time to internally calculate current velocity, which is stored on the instrument recorder. Horizontal velocities were corrected in post processing, as necessary, for the variation in sound speed. Local variations in speed of sound due to salinity changes were generally expected to be less than 5%. Changes in speed of sound through the profile do not influence horizontal velocity but may have a minor influence on vertical velocity and range calculations (TRDI 2006).

2) East and North horizontal components of velocities were corrected from magnetic north to true north direction using the magnetic declination for the location and time of deployment. A magnetic declination of 16° E was applied based on the Natural Resources Canada numerical model for the International Geomagnetic Reference Field (Natural Resources Canada 2017).

3) Acoustic amplitude (echo intensity) was plotted to check the quality of the instrument signal return and filtered for amplitudes below the noise floor for the respective instrument (TRDI 2010).

4) Data were filtered for sidelobe interference using the 20° beam slant angle of the TRDI instrument. The filter correction was calculated as the product of the instrument depth and the cosine of the slant angle plus one range bin. Filtered data entries were replaced with -999.99 in the data records; the filtered range approximately corresponds to the top 10% of the range to surface or bottom depending on whether the instrument was up-looking or down-looking, respectively.

5) Measurements made by the instrument while it was out of the water, as determined from pressure readings, were removed and replaced with -999.99.

6) Instrument elevations were referenced to CGVD28, using the deployment coordinates and recently collected bathymetric data to determine elevation of the QuadPod position for deployment 1 and deployment 2.

7) Additional manual editing to remove or flag suspicious data was performed as necessary.

8) Time series data from ancillary sensors on the current profilers were inspected for quality assurance/quality control (QA/QC) purposes. Figure 5 shows time series of instrument depth, battery voltage, temperature, heading, tilt, and temperature, measured by the ADCP from 7 February to 9 March 2017. TRDI recommends a maximum tilt limit of 15° (TRDI 2010). The tilt is within the recommended limit for the full deployment period.

9) The currents in the Fraser River were strong, up to 2 m/s, and therefore increased turbulence is observed in the data. At times high vertical velocities (up to 0.3 m/s) and error velocities were observed. TRDI (2010) calculates an error velocity as the difference of two different vertical velocities measured by independent beam pairs. The error velocity is a measure of the homogeneity of the water mass that is measured. The data were filtered for vertical velocities greater than 0.3 m/s and error velocities greater than 0.15 m/s. The data removed due to vertical velocity error accounted for less than 3% of the total removed data during the QA/QC process and was greatest near the bottom where vertical velocities were the greatest.

10) Simple descriptive statistics were calculated for each bin depth of each instrument: minimum, median, mean, maximum, standard deviation, and percentile values: 1$^{st}$, 5$^{th}$, 25$^{th}$, 75$^{th}$, 95$^{th}$, and 99$^{th}$ percentiles.

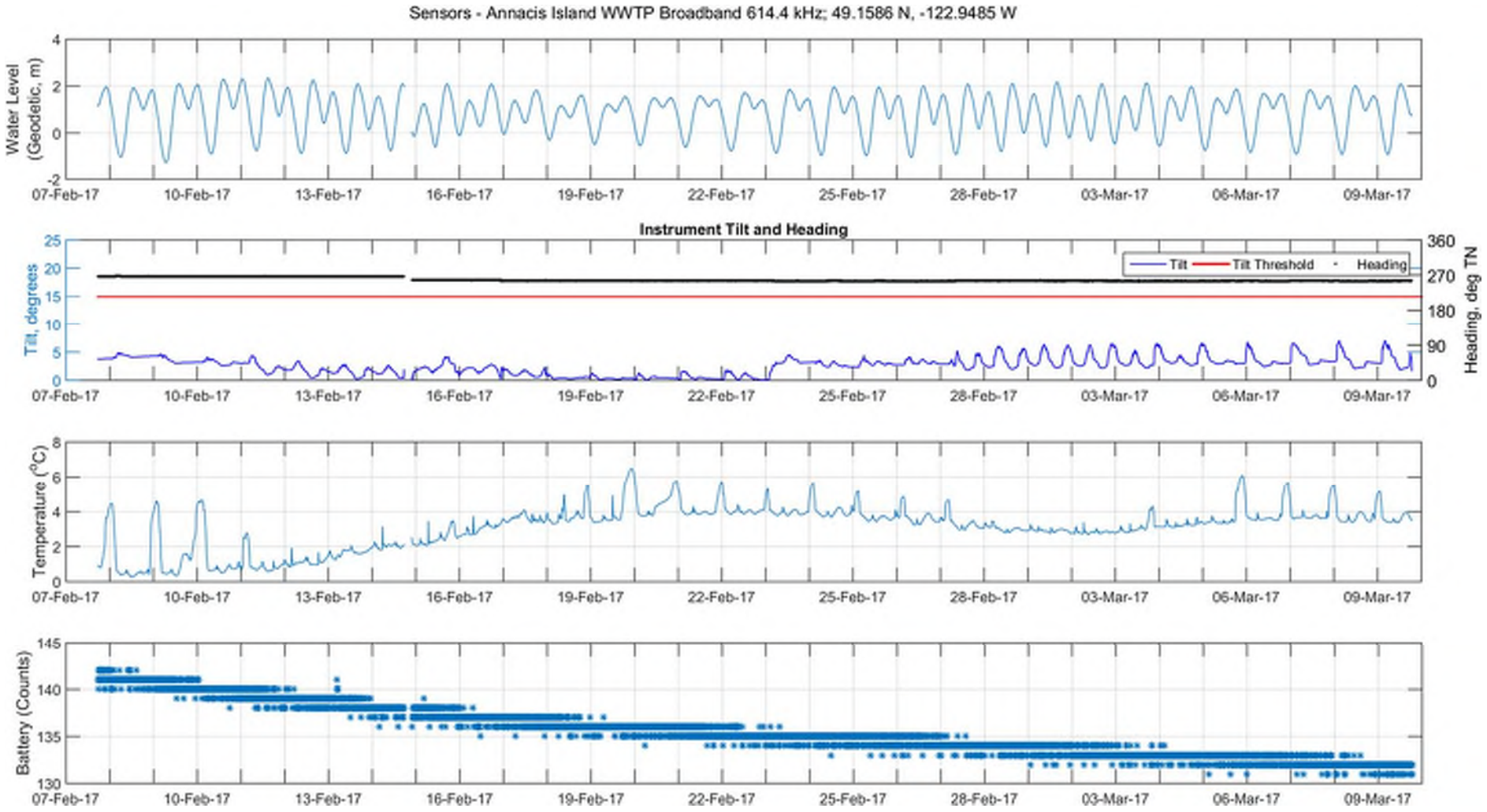


*Figure 5: Time series of quality control parameters for the TRDI 600 kHz ADCP deployed on the QuadPod including water level, instrument tilt and heading, water temperature, and battery voltage for 7 February to 9 March 2017*

### 2.4.2 Water Quality

Four types of water quality sensors were used on the QuadPod and Brewery Pier:

- RBRduo pressure and temperature data loggers.
- Seabird Electronics (SBE) 37 CT integrated conductivity and temperature sensor.
- JFE Advantech Infinity Turbidity sensor.
- YSI EXO2 water quality sonde

All of the water quality sensors returned complete datasets. Data from the sensors were filtered for out of water values and evaluated for data quality. Salinity, temperature, and depth data were plotted and reviewed for visual outliers. Those outliers are flagged and removed from the filtered data. Turbidity values are reviewed visually, and outliers are flagged and removed from the filtered data. In addition, an automated filter is applied to the data. This filter removes values that exceed the 99% turbidity value plus twice the standard deviation. Bulk statistics (minimum, median, mean, maximum, standard deviation, 1%, 5%, 25%, 75%, 95%, 99% values) were then calculated for the filtered dataset.

Additional steps were taken to verify pH data measured by the YSI EXO2. During installation and subsequent site visits, an independent pH meter was calibrated to measure pH while on site. Following recovery of the sonde, pH probe was subjected to a verification process to asses sensor drift. During the 30 day deployment the pH probe was replaced after 2 weeks. Each probe was calibrated prior to the deployment, however drift and inconsistencies with the independent pH meter meant the continuous pH data from the sonde could not be verified, and are therefore not included in the data set. The pH ranges measured by the independent pH meter are provided in the data summary below.

### 2.4.3 CTD Profiles

CTD profile data was downloaded from the instruments and imported to the SBE Data Processing software (v.7.23.2) for quality checking and conversion. Data processing routines included ‘Align CTD’, which corrected for transit delays of pumped sensors and response time mismatches, and ‘Filter’ which matched response times of temperature and conductivity instruments, and filtered digital noise in the pressure signal. The data was then exported to ASCII-formatted text files for further processing using MATLAB® scientific and technical computing software. This included isolating and extracting the downcast data, quality assurance checks, statistical analysis and profile plotting. The CTD profile naming convention for samples combine the station location (i.e., “CTD1”) with the sampling iteration number (i.e., “1”). For example, the first CTD profile collected at the CTD1 location is named CTD1-1.

CTD profiles were collected on five sampling days and opportunistically on three additional days while deploying and servicing the QuadPod. CTD profiles were collected at six sampling stations (Figure 1). The samples were collected in successive order to complete one iteration. The sampling order was CTD1, CTD2, CTD3, CTD4, CTD5, and CTD6. Station CTD2 and CTD4 are at the same location. Additional samples were collected at a station called CTD7 at the western end of Annacis Island when the salt wedge was possibly downstream of the site. CTD profiles were collected on 25 January, 26 January, 31 January, 1 February, 7 February, 9 February, 14 February, and 9 March 2017.

# 3.0 DATA SUMMARY

## 3.1 Brewery Pier

Figure 6 is a time series of salinity, temperature, and instrument depth measured by the SBE37 (and RBRduo) at the Brewery Pier near the project site from 16 September 2016 to 10 March 2017. Figure 6 also shows the discharge measured at the Hope water level gage station for the same time frame (#08MF005, Water Office, 2017) and observed water levels recorded at the New Westminster tide gauge station (9354). The New Westminster tide gauge data were converted to CGVD28 data using a conversion of -1.8 m to convert from Chart Datum (CD) to CGVD28 provided by CDM Smith (personal communication, 20 March, 2017). Summary statistics of data measured by the SBE37 are provided in Table 4. Water pressure was corrected using recorded barometric pressure from the nearest meteorological station at Burns Bog (WMO: 71042).

Water temperature gradually decreases during the data collection period from 16.3 deg C to near 0 deg C between 19 December 2016 and 13 February 2017 followed by a slight increase through 10 March 2017. Temperature averaged 6.8 deg C during the entire data collection period. Salinity was near zero for the majority of the deployment but reached a maximum value of 12.6 on 5 February 2017. Salinity values that exceeded 0.5 occurred during 2.83% of the measurements collected in 60 second intervals for approximately 6 months. There were 55 days with salinity over 0.5 during the 176 day deployment. The measured discharge at Hope reached a maximum of 3560 $m^3/s$ on 17 November 2016 and a minimum of 778 $m^3/s$ on 9 February 2017 during the deployment. Salinity was present frequently at the site beginning on 2 February 2017 when discharge levels reached values of 1050 $m^3/s$ and lower and was present for a portion of almost every day until the instrument recovery on 10 March 2017. There were two multiple-day salinity events during which salinity exceeded 1 that occurred when flows were above 1050 $m^3/s$: 7 October to 14 October 2016 and 8 December to 16 December 2016. During the October event discharge values averaged 1830 $m^3/s$, while peak salinity values ranged from 1 to 6. During the mid-December event discharge flows began at 1760 $m^3/s$ and decreased to 1130 $m^3/s$ by the end of the event while the peak salinity values ranged from 1 to 6.7.

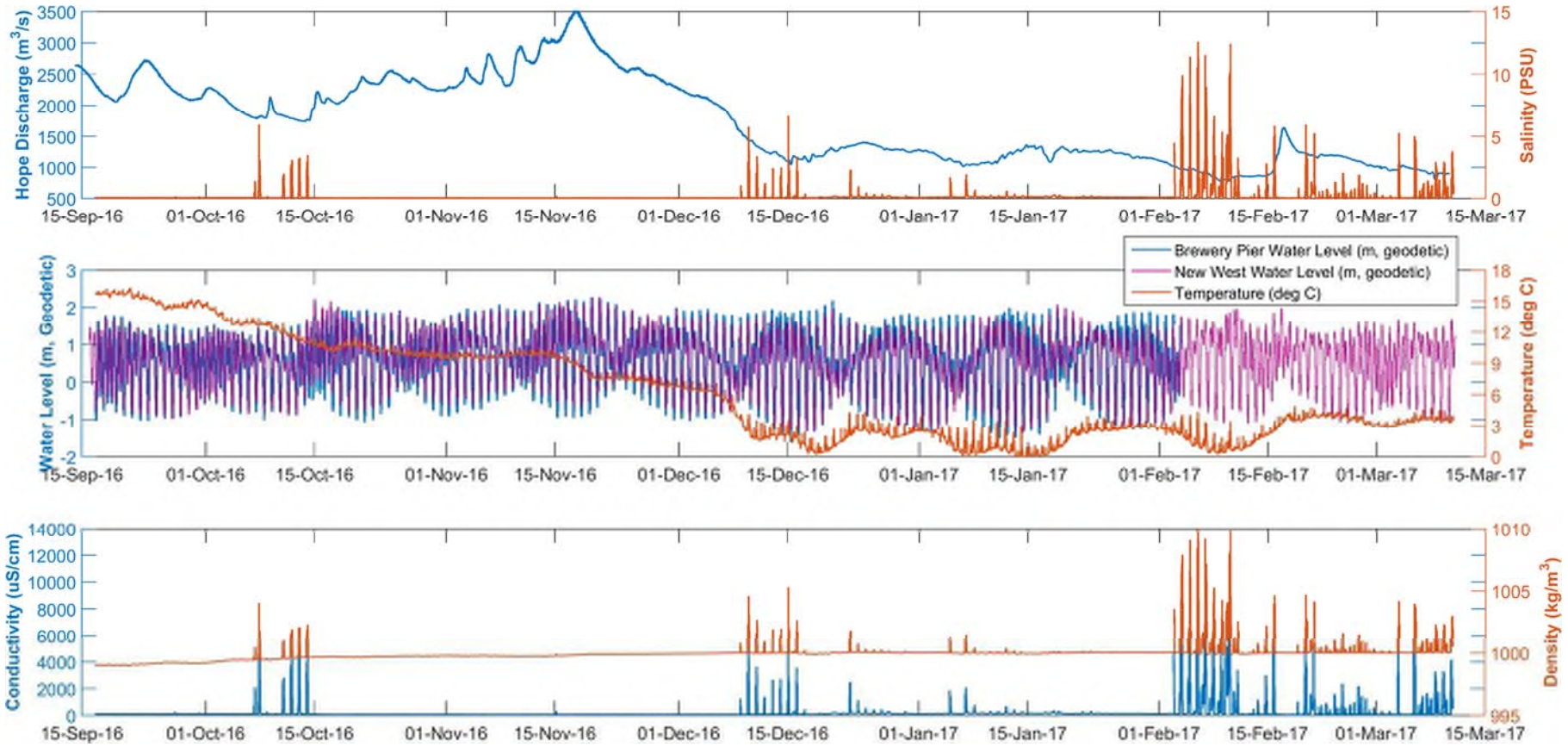


*Figure 6: Timeseries of salinity at the Brewery Pier and discharge measured at the Hope Station (08MF005) (top) water temperature and water level measured at the Brewery Pier and water level measured at the New Westminster Tide Gauge (7654) (middle), conductivity and water density (bottom) measured by the SBE37 at the Brewery Pier from 16 September 2016 to 10 March 2017.*

**Table 3: Summary Statistics of Parameters Measured by the SBE37 and RBRduo from 16 September 2016 to 10 March 2017 on the Brewery Pier**

| | Minimum | 1%-ile | 5%-ile | 25%-ile | 50%-ile | Mean | 75%-ile | 95%-ile | 99%-ile | Maximum | Standard Deviation | % Valid Data |
|---|---|---|---|---|---|---|---|---|---|---|---|---|
| Conductivity [µS/cm] | 31.6 | 48.0 | 54.8 | 62.8 | 88.7 | 154.7 | 123.1 | 237.7 | 2,281.1 | 12,827.8 | 429.1 | 100% |
| Specific Conductivity [µS/cm] | 52.5 | 69.7 | 79.8 | 95.7 | 118.3 | 256.6 | 225.1 | 443.4 | 3,661.1 | 21,334.7 | 721.0 | 100% |
| Salinity | 0.0 | 0.0 | 0.0 | 0.0 | 0.1 | 0.1 | 0.1 | 0.2 | 1.9 | 12.6 | 0.4 | 100% |
| Temperature [deg C] | 0.0 | 0.1 | 0.4 | 2.3 | 6.9 | 6.8 | 10.2 | 15.1 | 15.8 | 16.3 | 4.8 | 100% |
| Water Level [m, CGVD28] | -1.6 | -1.2 | -0.9 | 0.0 | 0.8 | 0.6 | 1.3 | 1.8 | 2.0 | 2.3 | 0.8 | 95.2% |
| Water Pressure [dbar-corrected] | 2.6 | 3.0 | 3.4 | 4.2 | 4.9 | 4.8 | 5.5 | 6.0 | 6.2 | 6.4 | 0.8 | 95.2% |
| Density [kg/m$^3$] | 998.9 | 999.0 | 999.1 | 999.7 | 999.9 | 999.8 | 1000.0 | 1000.1 | 1001.3 | 1010.0 | 0.4 | 100% |

Note: The % valid data for water level and pressure is reduced due to the replacement of the SBE37 sensor by the RBRduo CT sensor which does not measure pressure and depth.

Figure 7 is a timeseries of parameters measured by the YSI EXO2 from 16 September to 25 October 2016. Summary statistics of parameters measured by the YSI EXO2 are provided in Table 4. The pH timeseries is not presented as the pH measurements could not be verified. Average pH values measured by the independent pH meters are presented in Table 5 along with the corresponding pH value measured at the Gravesend Reach Buoy near Tilbury Island (~7 km downstream) maintained by Environment Canada. Environment Canada note that the pH data had not been verified and are subject to sensor drift.

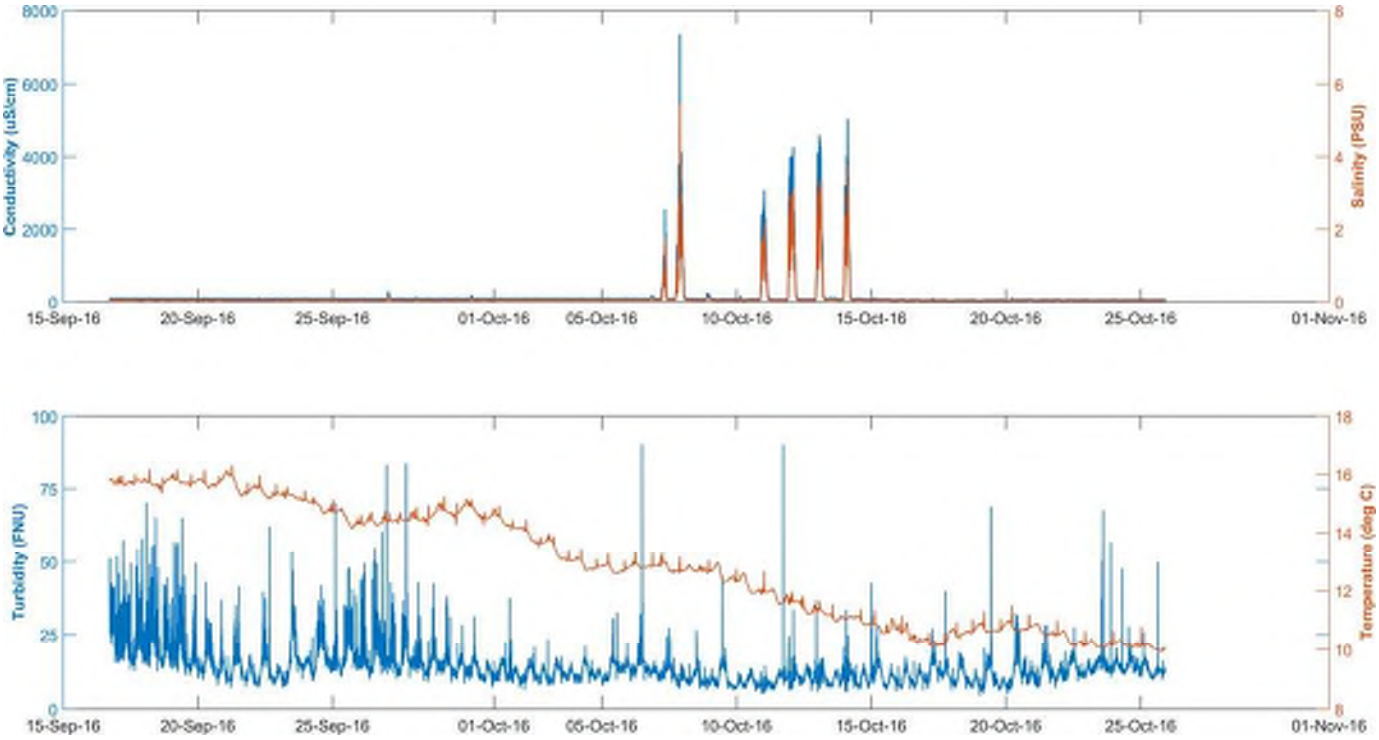


*Figure 7: Timeseries of YSI EXO2 data measured at the Brewery Pier mooring from 16 September to 25 October 2016.*

**Table 4: Summary Statistics of Parameters Measured by the YSI EXO2 from 16 September to 25 October 2016 on the Brewery Pier**

| | Minimum | 1%-ile | 5%-ile | 25%-ile | 50%-ile | Mean | 75%-ile | 95%-ile | 99%-ile | Maximum | Standard Deviation | % Valid Data |
|---|---|---|---|---|---|---|---|---|---|---|---|---|
| Conductivity [µS/cm] | 46.0 | 50.1 | 59.5 | 71.3 | 92.1 | 155.7 | 95.8 | 131.7 | 2,726.1 | 7,357.5 | 414.4 | 99.9% |
| Specific Conductivity [µS/cm] | 63.4 | 68.7 | 82.7 | 97.5 | 115.3 | 204.5 | 120.2 | 171.2 | 3,650.0 | 9,640.4 | 555.4 | 99.9% |
| Salinity | 0.0 | 0.0 | 0.0 | 0.1 | 0.1 | 0.1 | 0.1 | 0.1 | 1.9 | 5.4 | 0.3 | 99.9% |
| Temperature [deg C] | 9.9 | 10.0 | 10.2 | 10.8 | 12.8 | 12.9 | 14.7 | 15.8 | 15.9 | 16.3 | 2.0 | 99.9% |
| Instrument Depth [m] | 3.5 | 3.6 | 3.7 | 4.5 | 5.2 | 5.1 | 5.7 | 6.2 | 6.5 | 6.7 | 0.8 | 99.9% |
| Turbidity [FNU] | 4.4 | 6.8 | 7.8 | 10.1 | 12.6 | 13.8 | 15.9 | 24.8 | 33.2 | 90.6 | 5.5 | 99.8% |
| pH | NA | NA | NA | NA | NA | NA | NA | NA | NA | NA | NA | 0% |

NA=not applicable

**Table 5: Summary of Independent pH meter average compared with continuous hourly Gravesend Reach Buoy data provided by Environment Canada**

| Sampling Date and Time (UTC) | Average pH ±St Dev[1] | Gravesend Reach Buoy pH[2] |
|---|---|---|
| 16 September 2016 17:38-17:42 | 7.47± 0.02 | 7.80 |
| 6 October 2016 20:15-20:23 | 7.84± 0.05 | 7.89 |
| 25 October 2016 22:39-22:47 | 7.62± 0.02 | 7.67 |

Note: 1) St Dev=Standard Deviation. 2) Environment Canada data have not been verified and are subject to sensor drift.

## 3.2 QuadPod

### 3.2.1 Currents

A contour plot of current speed, direction, and acoustic backscatter amplitude (echo intensity) from 7 February to 9 March 2017 measured by the TRDI 600 kHz ADCP at the QuadPod frame is provided in Figure 8. Current speeds and direction are generally uniform through the water column and follow tidal trends. The highest current speeds are near the surface and decrease slightly with depth. Flow is predominantly in the downstream direction to the southwest. However, a full flow reversal occurs at least once per tidal cycle during the flood tide. The flow reversal to the northwest is typically associated with slower flow speeds. The salt wedge intrusion is often visible in the current direction signal showing some stratification of flow directions. The interaction of salinity at the site and near bed flow characteristics are reviewed further in Section 4.0.

Summary statistics calculated for the current measurements are presented in Table 6 for each vertical bin. Bin depths (defined by the mid-point of each 0.5 m vertical bin) are referenced vertically in metres datum (m CGVD28). The valid data return for this instrument was 99.9%.

The mean current speed throughout the deployment was in the range 0.48 to 0.71 m/s (for all valid bins). The highest mean current speeds (greater than 0.65 m/s) and instantaneous maximum speeds (exceeding 2 m/s) were measured at the near surface bins of -3.55 to -1.55 m CGVD28 elevations. The strongest current speeds (greater than 1.5 m/s) were typically measured during the middle and end of the ebbing tide. Peak current speeds typically coincided with large ebb ranges associated with spring tides.

Rose plots of current speed and direction for selected near surface (-2.55 m geo), mid-range (-6.05 m geo), and near river bed (-9.55 m geo) bins for the ADCP are provided in Figure 9. Directions in the rose plots were binned into 10° increments and plotted by frequency of occurrence (percentage). Bimodal current directions were aligned from the southwest to the northeast on the flood, with an ebb (and down river) flow dominance to the southwest. Overall, flow direction was constant through the water column with peak speeds occurring in the upper water column and gradually reducing with depth. On select tidal conditions a full flow reversal occurs where flows are to the northwest. The flow reversal occurred during flood tides and near slack high tides. Instances where flow direction changes through the water column correspond with salinity events measured at the QuadPod. Patterns and possible dynamics of the salt wedge and current flow will be discussed further in 4.0 Analysis and Conclusions.

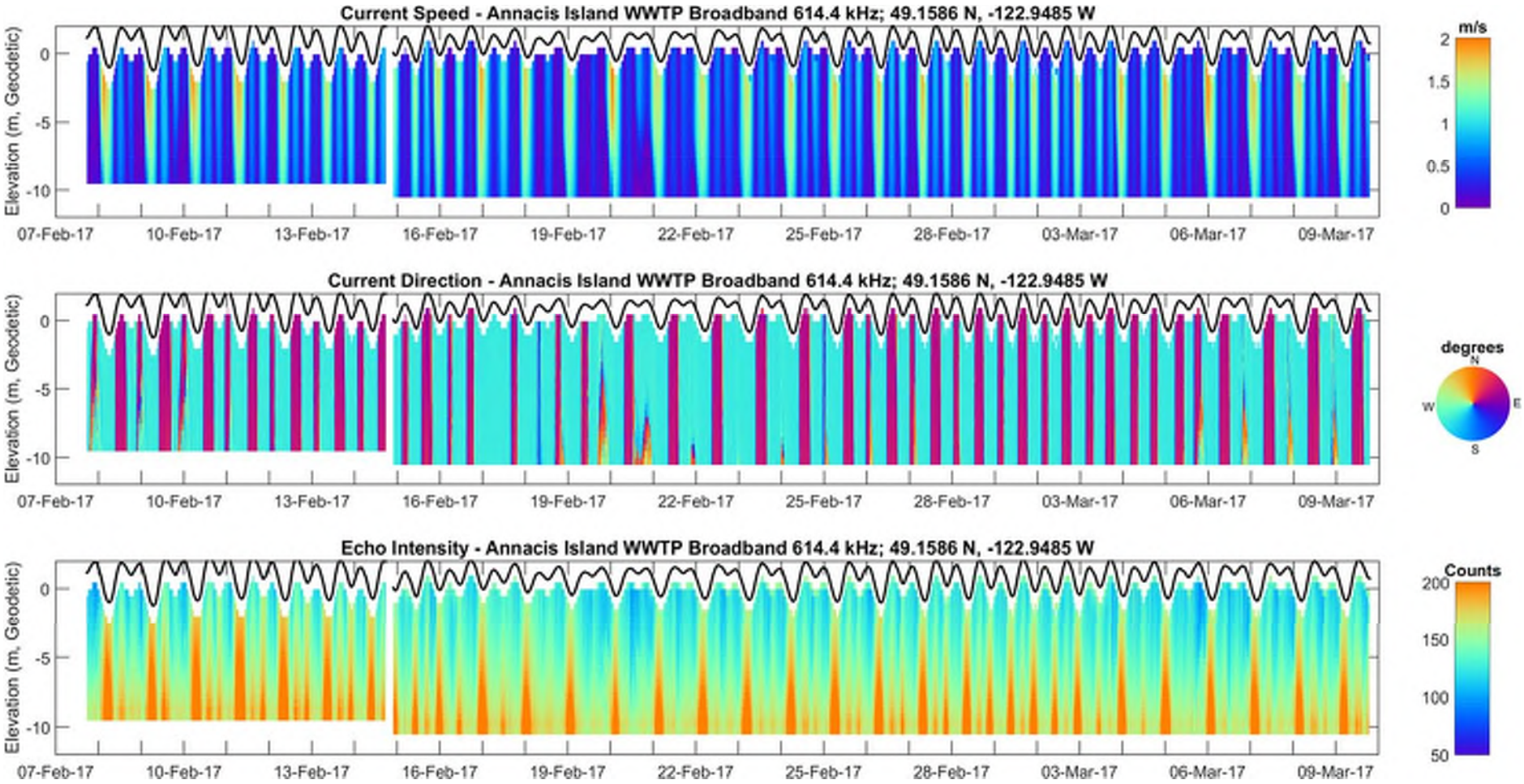


*Figure 8: Profiles of current speed, direction, and echo intensity measured by the 600 kHz ADCP on the QuadPod station from 7 February to 9 March 2017*

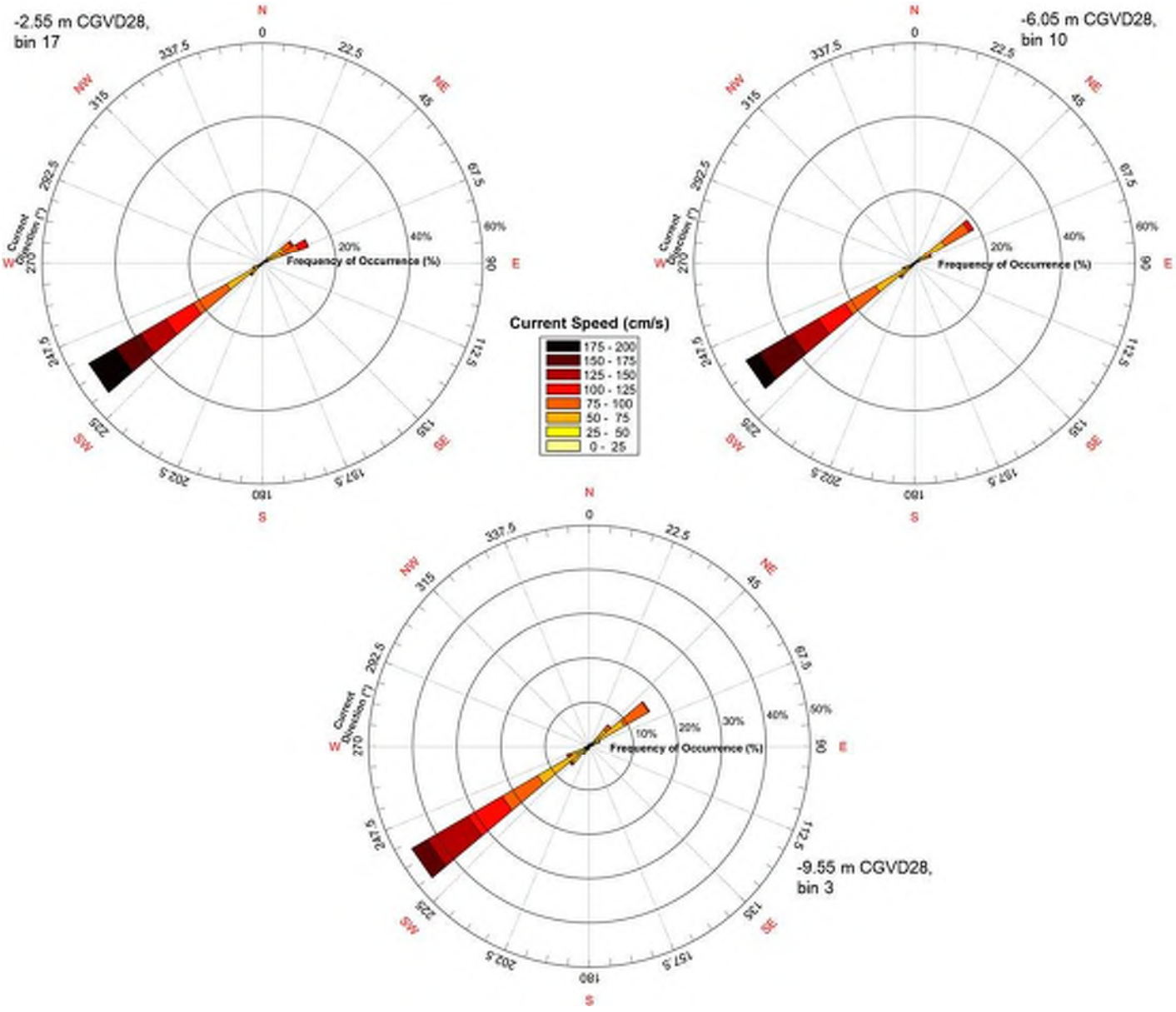


*Figure 9: Current roses for -2.55 m, -6.05 m, and -9.55 m CGVD28 bin elevation measured by the 600 kHz ADCP from 7 February to 9 March 2017 at QuadPod.*

**Table 6: Statistics of current speed and average direction by bin measured by the 600 kHz ADCP at the QuadPod**

| Elev (m geo) | Bin No. | Min Speed (m/s) | 1%ile (m/s) | 5%ile (m/s) | 25%ile (m/s) | Median Speed (m/s) | Mean Speed (m/s) | 75%ile (m/s) | 95%ile (m/s) | 99%ile (m/s) | Max Speed (m/s) | Std Speed (m/s) | Average Direction (Degree, TN)[1] |
|---|---|---|---|---|---|---|---|---|---|---|---|---|---|
| -1.55 | 19 | 0.01 | 0.03 | 0.08 | 0.26 | 0.51 | 0.58 | 0.80 | 1.43 | 1.74 | 2.12 | 0.41 | 225.9 |
| -2.05 | 18 | 0.00 | 0.04 | 0.09 | 0.29 | 0.57 | 0.67 | 0.95 | 1.59 | 1.83 | 2.08 | 0.47 | 228.3 |
| -2.55 | 17 | 0.01 | 0.04 | 0.09 | 0.30 | 0.59 | 0.71 | 1.04 | 1.65 | 1.81 | 2.05 | 0.50 | 229.5 |
| -3.05 | 16 | 0.00 | 0.04 | 0.09 | 0.30 | 0.59 | 0.71 | 1.05 | 1.63 | 1.80 | 2.03 | 0.49 | 229.2 |
| -3.55 | 15 | 0.01 | 0.03 | 0.09 | 0.30 | 0.59 | 0.70 | 1.03 | 1.61 | 1.77 | 2.01 | 0.49 | 229.4 |
| -4.05 | 14 | 0.00 | 0.03 | 0.09 | 0.29 | 0.58 | 0.69 | 1.02 | 1.59 | 1.74 | 1.98 | 0.48 | 229.2 |
| -4.55 | 13 | 0.01 | 0.03 | 0.09 | 0.29 | 0.57 | 0.68 | 1.01 | 1.57 | 1.72 | 1.92 | 0.47 | 229.7 |
| -5.05 | 12 | 0.00 | 0.03 | 0.08 | 0.28 | 0.56 | 0.67 | 0.99 | 1.54 | 1.68 | 1.90 | 0.46 | 230.0 |
| -5.55 | 11 | 0.00 | 0.03 | 0.08 | 0.28 | 0.54 | 0.65 | 0.97 | 1.51 | 1.64 | 1.78 | 0.46 | 230.4 |
| -6.05 | 10 | 0.00 | 0.03 | 0.08 | 0.27 | 0.53 | 0.64 | 0.95 | 1.48 | 1.60 | 1.76 | 0.45 | 230.4 |
| -6.55 | 9 | 0.01 | 0.03 | 0.08 | 0.27 | 0.52 | 0.62 | 0.93 | 1.45 | 1.57 | 1.70 | 0.44 | 231.4 |
| -7.05 | 8 | 0.01 | 0.03 | 0.08 | 0.26 | 0.50 | 0.61 | 0.90 | 1.41 | 1.53 | 1.70 | 0.42 | 232.5 |
| -7.55 | 7 | 0.00 | 0.03 | 0.07 | 0.25 | 0.49 | 0.59 | 0.88 | 1.38 | 1.49 | 1.63 | 0.41 | 233.7 |
| -8.05 | 6 | 0.00 | 0.03 | 0.07 | 0.24 | 0.48 | 0.57 | 0.85 | 1.35 | 1.46 | 1.60 | 0.40 | 235.1 |
| -8.55 | 5 | 0.01 | 0.04 | 0.08 | 0.23 | 0.46 | 0.56 | 0.81 | 1.31 | 1.43 | 1.55 | 0.39 | 236.4 |
| -9.05 | 4 | 0.00 | 0.03 | 0.08 | 0.22 | 0.44 | 0.54 | 0.78 | 1.27 | 1.38 | 1.53 | 0.38 | 237.1 |
| -9.55 | 3 | 0.00 | 0.03 | 0.07 | 0.22 | 0.43 | 0.52 | 0.75 | 1.23 | 1.35 | 1.53 | 0.36 | 238.2 |
| -10.05 | 2 | 0.00 | 0.03 | 0.07 | 0.21 | 0.40 | 0.50 | 0.72 | 1.20 | 1.32 | 1.46 | 0.36 | 239.8 |
| -10.55 | 1 | 0.00 | 0.03 | 0.07 | 0.20 | 0.38 | 0.48 | 0.68 | 1.15 | 1.27 | 1.37 | 0.34 | 242.1 |

1) Direction units (degrees True North (TN), to where current is heading).

Elev= elevation; m geo = metres above CGVD28 datum; %ile = percentile; Min = minimum; Max = maximum; Std = standard deviation

.

### 3.2.2 Salinity and Temperature

Time series of temperature and salinity recorded by the SBE 37SM CT's near the river bed bottom at the QuadPod station from 7 February to 9 March 2017 are provided in Figure 10 and Figure 11. The summary statistics for these variables are presented in Table 7 and Table 8.

Average salinity at the QuadPod was measured as 1.7 by both SBE37 sensors. The ambient river water salinity tends to vary from 0.04 to 0.08. Spikes in salinity from salt wedge intrusion occurred frequently during the approximately 30 day deployment during low river flows. Salinity measurements (recorded every 60 seconds) exceeded salinity values greater than 0.5 for 23% of the measurements and approximately 23 different salinity events with a peak value of 1 or greater occurred during the full deployment. A maximum salinity value of 19.9 was recorded on 19 February 2017 at approximately 22:20. Near bed water temperature ranged from 0.3 deg C to 6.5 deg C and averaged 3.12 deg C during the full deployment. River water temperature was colder than the water associated with the salt wedge intrusions.

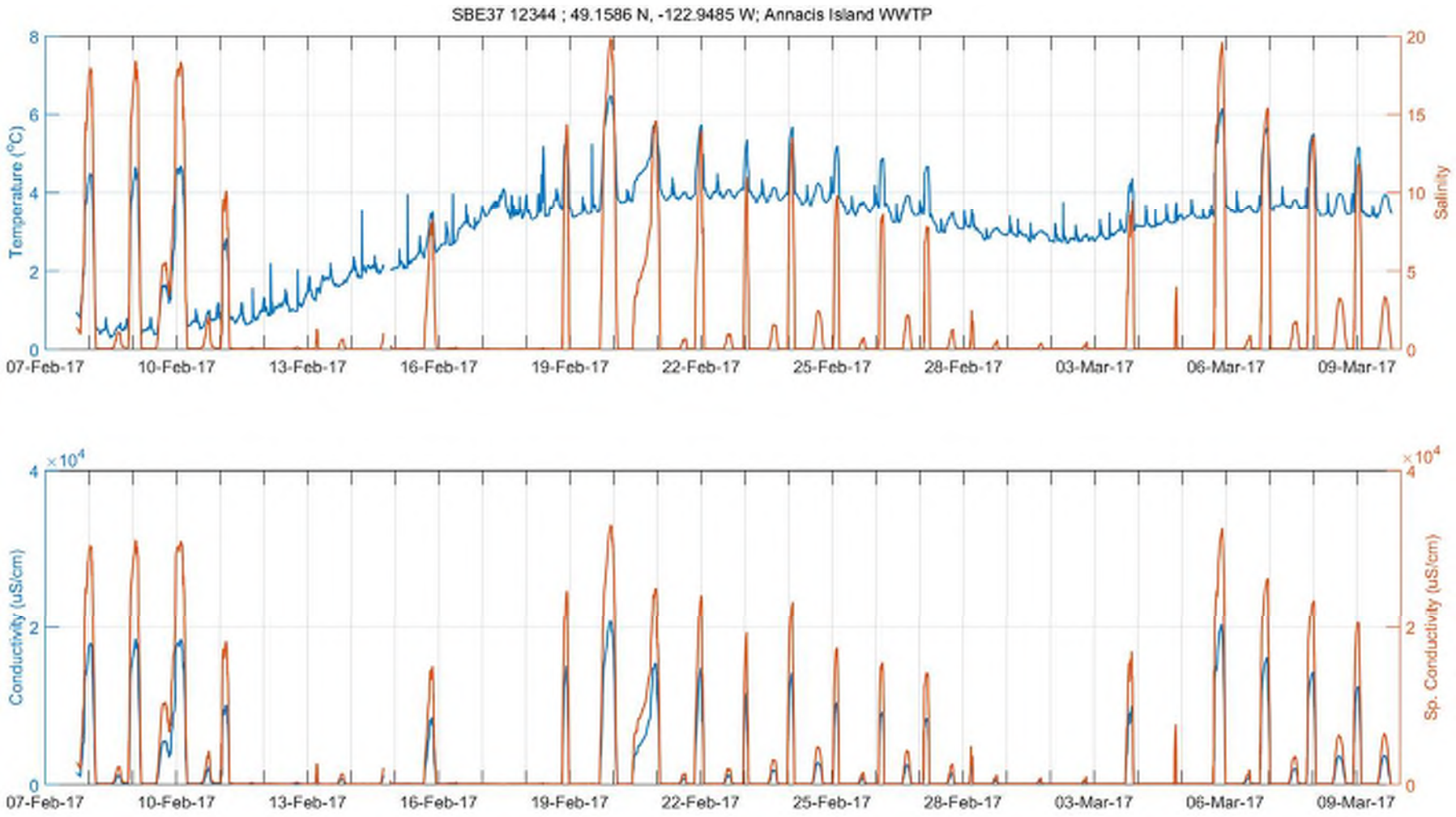


*Figure 10: Timeseries of temperature, salinity, conductivity, and specific conductivity as measured by SBE37 12344 at the QuadPod station mounted 99 cm above the river bed. See Table 1 for deployment elevations.*

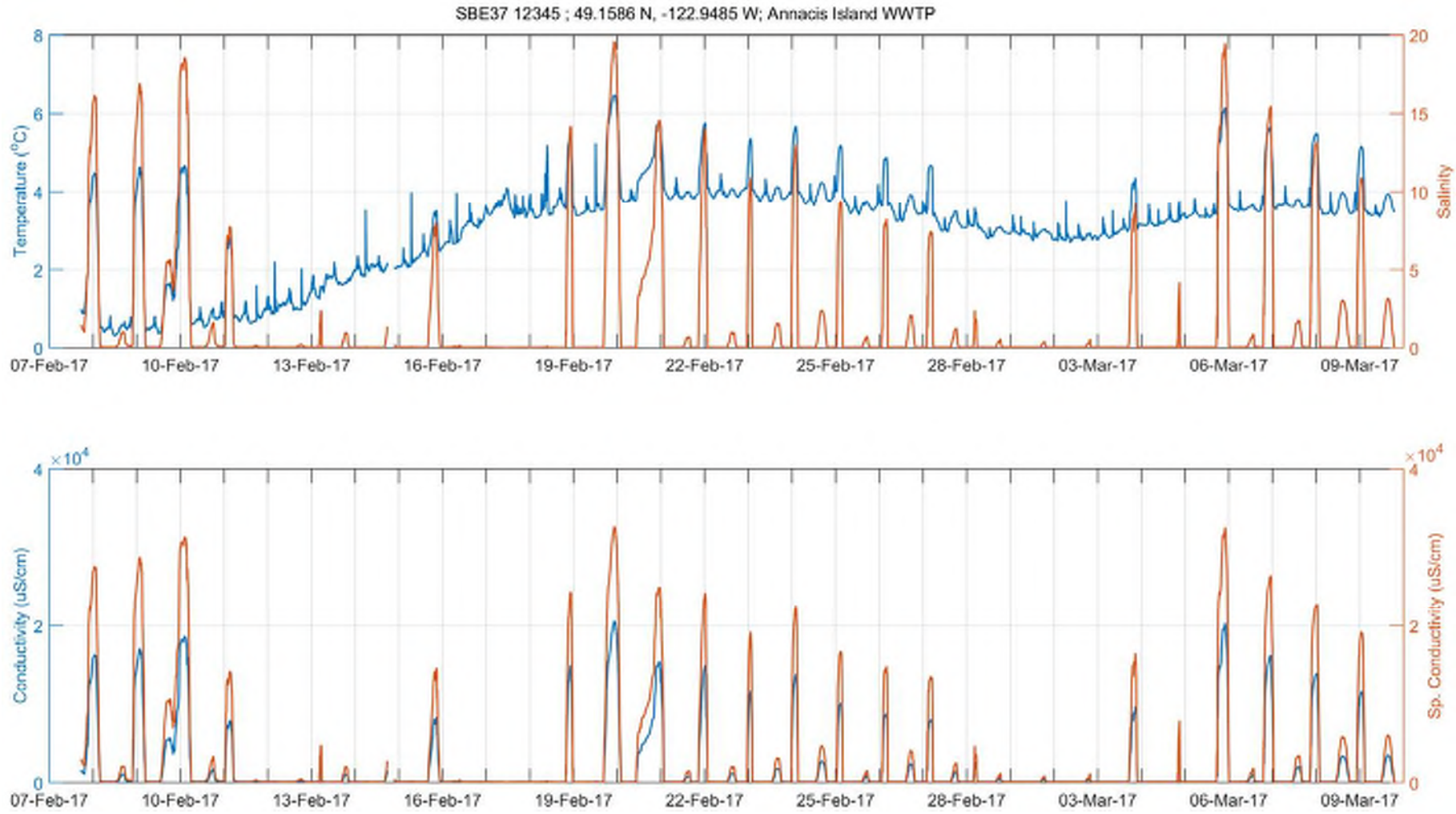


*Figure 11: Timeseries of temperature, salinity, conductivity, and specific conductivity as measured by SBE37 12345 at the QuadPod station mounted 55 cm above the river bed. See Table 1 for deployment elevations.*

**Table 7: Summary statistics for SBE 37SM 12344 at 99 cm above the river bed on the QuadPod from 7 February to 9 March 2017**

| | Min | 1%ile | 5%ile | 25%ile | Median | Mean | 75%ile | 95%ile | 99%ile | Max | Std | % Valid |
|---|---|---|---|---|---|---|---|---|---|---|---|---|
| Conductivity (µS/cm) | 37.3 | 41.4 | 47.4 | 63.5 | 68.4 | 1772.0 | 463.1 | 13169.0 | 18129.0 | 20817.0 | 4136.5 | 100% |
| Salinity | 0.03 | 0.03 | 0.04 | 0.05 | 0.05 | 1.68 | 0.39 | 12.60 | 17.92 | 19.87 | 4.00 | 100% |
| Specific Conductivity (µS/cm) | 64.1 | 76.4 | 85.5 | 112.9 | 122.2 | 3007.8 | 828.2 | 21888.8 | 30353.3 | 33055.5 | 6906.1 | 100% |
| Temperature (°C) | 0.30 | 0.43 | 0.69 | 2.71 | 3.42 | 3.12 | 3.81 | 4.96 | 5.80 | 6.49 | 1.21 | 100% |

Min = minimum; Max = maximum; %ile = percentile; Std = standard deviation; µS/cm = microsiemens per centimetre.

**Table 8: Summary statistics for SBE 37SM 12345 at 55 cm above the river bed on the QuadPod from 7 February to 9 March 2017**

| | Min | 1%ile | 5%ile | 25%ile | Median | Mean | 75%ile | 95%ile | 99%ile | Max | Std | % Valid |
|---|---|---|---|---|---|---|---|---|---|---|---|---|
| Conductivity (µS/cm) | 40.5 | 50.3 | 56.0 | 66.4 | 71.8 | 1759.0 | 489.2 | 13013.0 | 18208.0 | 20577.0 | 4076.5 | 100% |
| Salinity | 0.03 | 0.04 | 0.04 | 0.05 | 0.06 | 1.66 | 0.41 | 12.52 | 18.05 | 19.62 | 3.93 | 100% |
| Specific Conductivity (µS/cm) | 69.5 | 88.1 | 98.3 | 118.1 | 128.7 | 2983.1 | 880.8 | 21827.1 | 30445.1 | 32672.6 | 6792.2 | 100% |
| Temperature (°C) | 0.29 | 0.44 | 0.69 | 2.72 | 3.42 | 3.12 | 3.82 | 5.03 | 5.81 | 6.49 | 1.22 | 100% |

Min = minimum; Max = maximum; %ile = percentile; Std = standard deviation; µS/cm = microsiemens per centimetre.

### 3.2.3 Turbidity and Depth

Figure 12 is a time series of filtered (despiked) turbidity data recorded by the JFE Infinity sensor and water level recorded by the RBRduo pressure sensor deployed at the QuadPod station from 7 February to 9 March 2017. Summary statistics of turbidity and water level are presented in Table 9. Average turbidity was 9.8 FTU, and reached a maximum of 89.2 FTU on 11 February 2017. The Port of Vancouver was conducting dredging in the area from 10 February to 20 February 2017 and had communicated that turbidity may be elevated as a result. The turbidity signal appears to be tidally driven. The pattern begins with increased turbidity near the bed during peak ebb flows. Turbidity gradually decreases over the subsequent tidal cycle. A sharp decrease in turbidity occurs when the salt wedge is present.

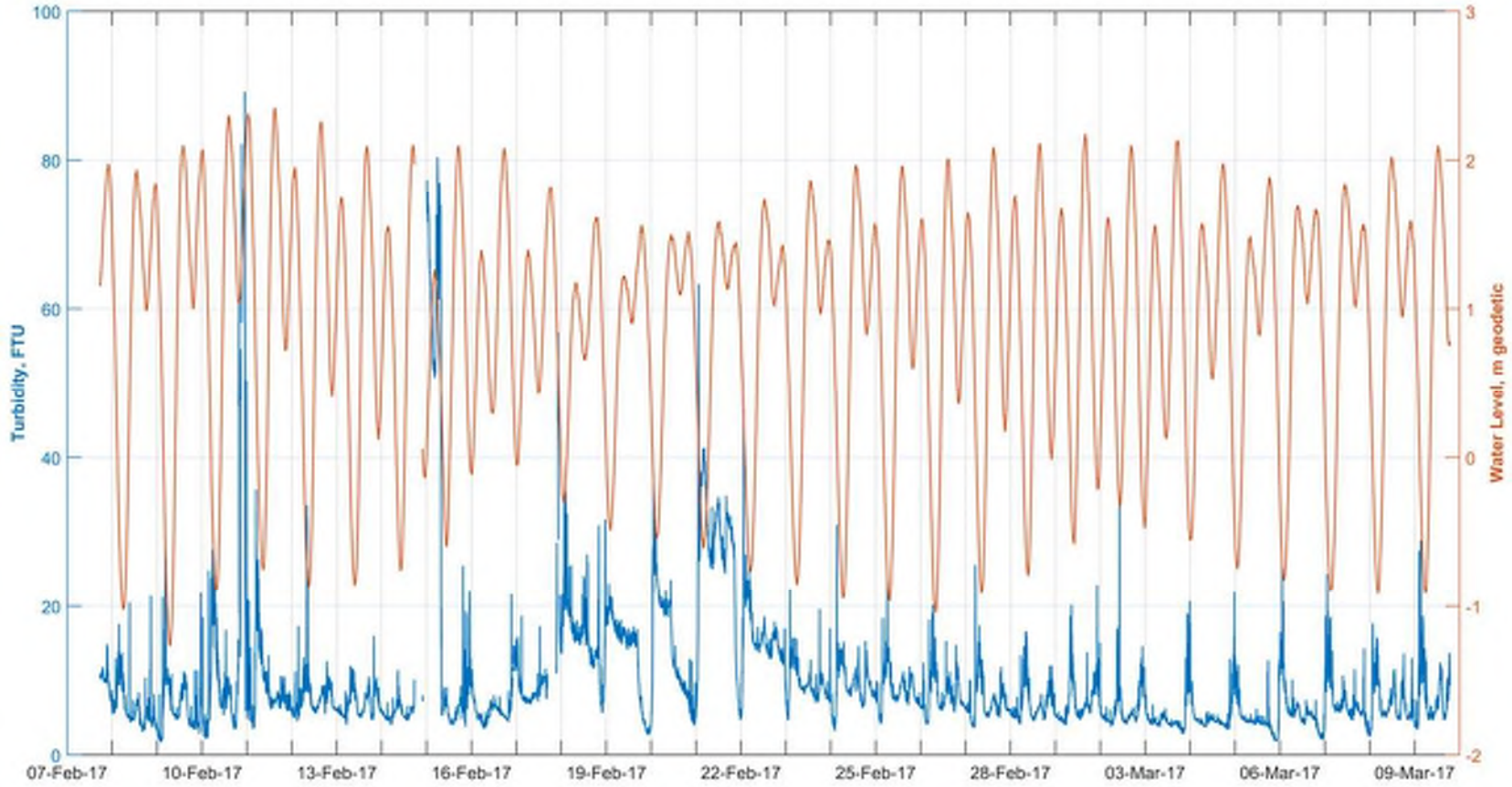


*Figure 12: Timeseries of filtered turbidity and water level measured at the QuadPod station from 7 February to 9 March 2017. See Table 1 for sensor mounting elevation.*

**Table 9: Summary statistics for JFE Infinity and RBRduo on the QuadPod from 7 February to 9 March 2017**

| | Min | 1%ile | 5%ile | 25%ile | Median | Mean | 75%ile | 95%ile | 99%ile | Max | Std | % Valid |
|---|---|---|---|---|---|---|---|---|---|---|---|---|
| Turbidity (FTU) | 1.7 | 2.6 | 3.9 | 5.3 | 7.2 | 9.8 | 10.8 | 24.2 | 54.3 | 89.2 | 8.7 | 97.8% |
| Water Level (m, CGVD28) | -1.32 | -0.89 | -0.60 | 0.34 | 1.12 | 0.91 | 1.54 | 1.97 | 2.14 | 2.23 | 0.80 | 100% |

## 3.3 CTD Profiles

Figure 13 shows the observed tide at New Westminster Station (#7654) along with the stage of the tide CTD profiles were collected converted to CGVD28 datum (conversion of 1.8 m, CDM Smith personal communication, March 2017). Appendix B provides summary tables of each profile collected, the time, stage of the tide, and corresponding text data file for each profile collected. The geographic coordinates of each profile, parameters measured and units are provided in the metadata of each data file provided electronically in Appendix A. The percentage of good data for the downcasts of the profiles is 99.9%. Turbidity and pH occasionally needed to be filtered to remove slow sensor response time and the presence of floating debris in the river interfering with the turbidity values. The tidal range during the CTD profiling campaign was approximately 3 m and includes both spring and neap tides. Table 10 summarizes the daily average discharge measured at Hope during each day CTD profiles were collected.

**Table 10: Daily average discharge at Hope during CTD profile collection**

| CTD Profile Date | Average Hope Discharge ($m^3/s$) |
|---|---|
| 25 January 2017 | 1,268 |
| 26 January 2017 | 1,231 |
| 31 January 2017 | 1,089 |
| 1 February 2017 | 878 |
| 7 February 2017 | 878 |
| 9 February 2017 | 795 |
| 14 February 2017 | 866 |
| 9 March 2017 | 898 |

In total, 45 CTD profiles were collected at each of the six sampling stations, for a total of 270 profiles, and 12 additional profiles at CTD7. A complete set of the profiles measured are provided in Appendix B. The figures presented in the report focus on 7 February and 9 February 2017 which captured large peaks in salinity at the site. Figure 14 provides the 40$^{th}$ iteration of profiles at CTD1, CTD3, CTD4, CTD5, and CTD6 collected on 9 February 2017 during peak salinity. The profiles are overlaid on a 2002 Google Earth image and shown relative to cross channel and along channel position. The pycnocline occurs between -5 to -10 m elevation at all the profile locations. The maximum salinity measured is observed in the deeper water measured at CTD3-40, with values reaching 18.85.

Figure 15 and Figure 16 are timeseries of observed water level at New Westminster station, near bed salinity measured at the QuadPod, and CTD profiles measured at the CTD2/4 station location nearest to the QuadPod on 7 February and 9 February 2017 respectively. Profiles and timeseries of salinity show a small initial peak in salinity corresponding with the first high tide (and early ebb) tide, followed by salinity increasing at the site during the small secondary flood tide of the day. Salinity reaches a peak after the tide has turned and the flow begins to ebb. Salinity declines quickly during peak ebb flows. With the progression of the salt wedge (increased salinity and water temperature) turbidity and pH decrease.

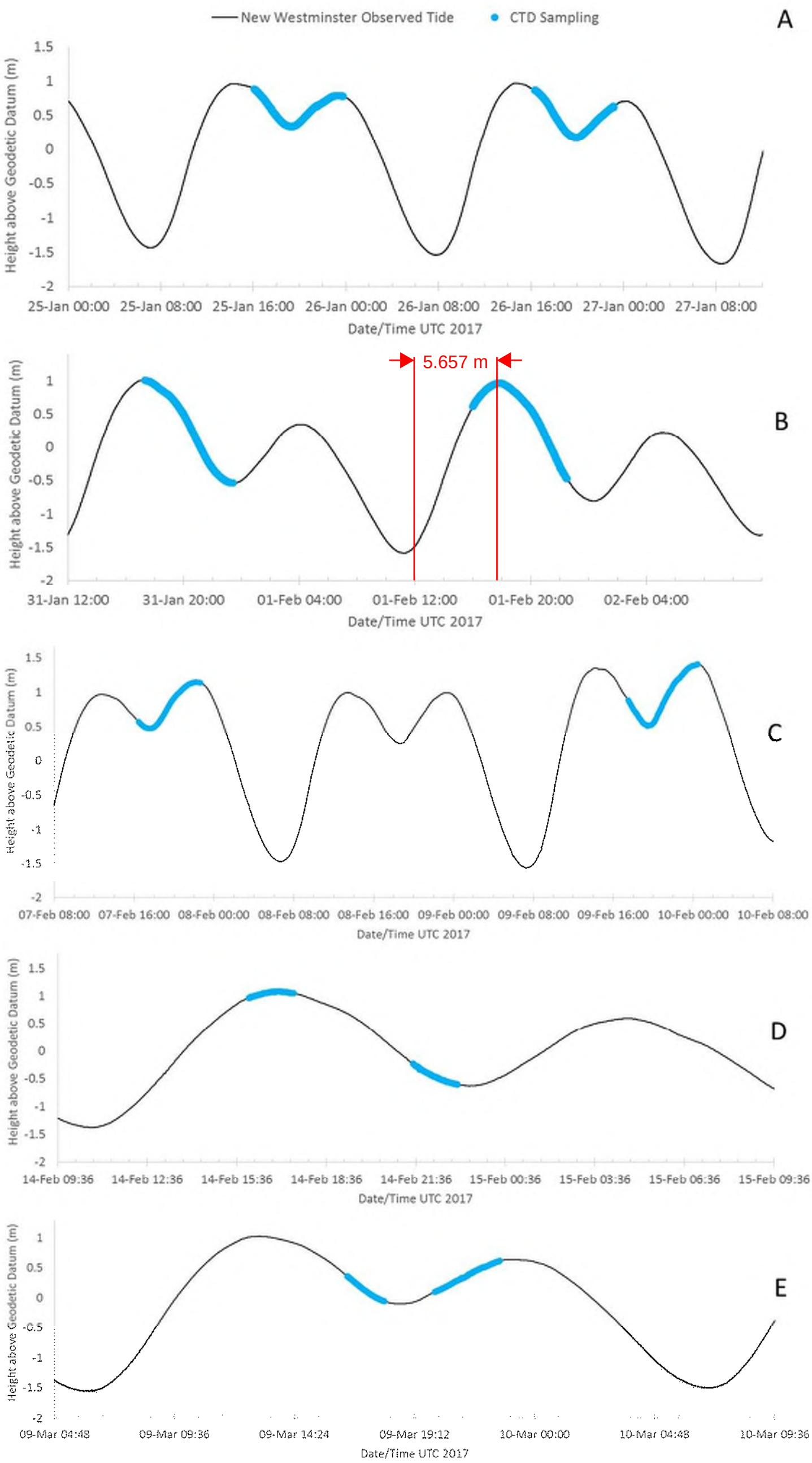


*Figure 13: Timeseries of observed water levels measured at New Westminster station (#7654) converted to CGVD28 elevation for A) 25 and 26 January 2017 B) 31 January and 1 February 2017 C) 7 and 9 February 2017 D) 14 February 2017 and E) 9 March 2017.*

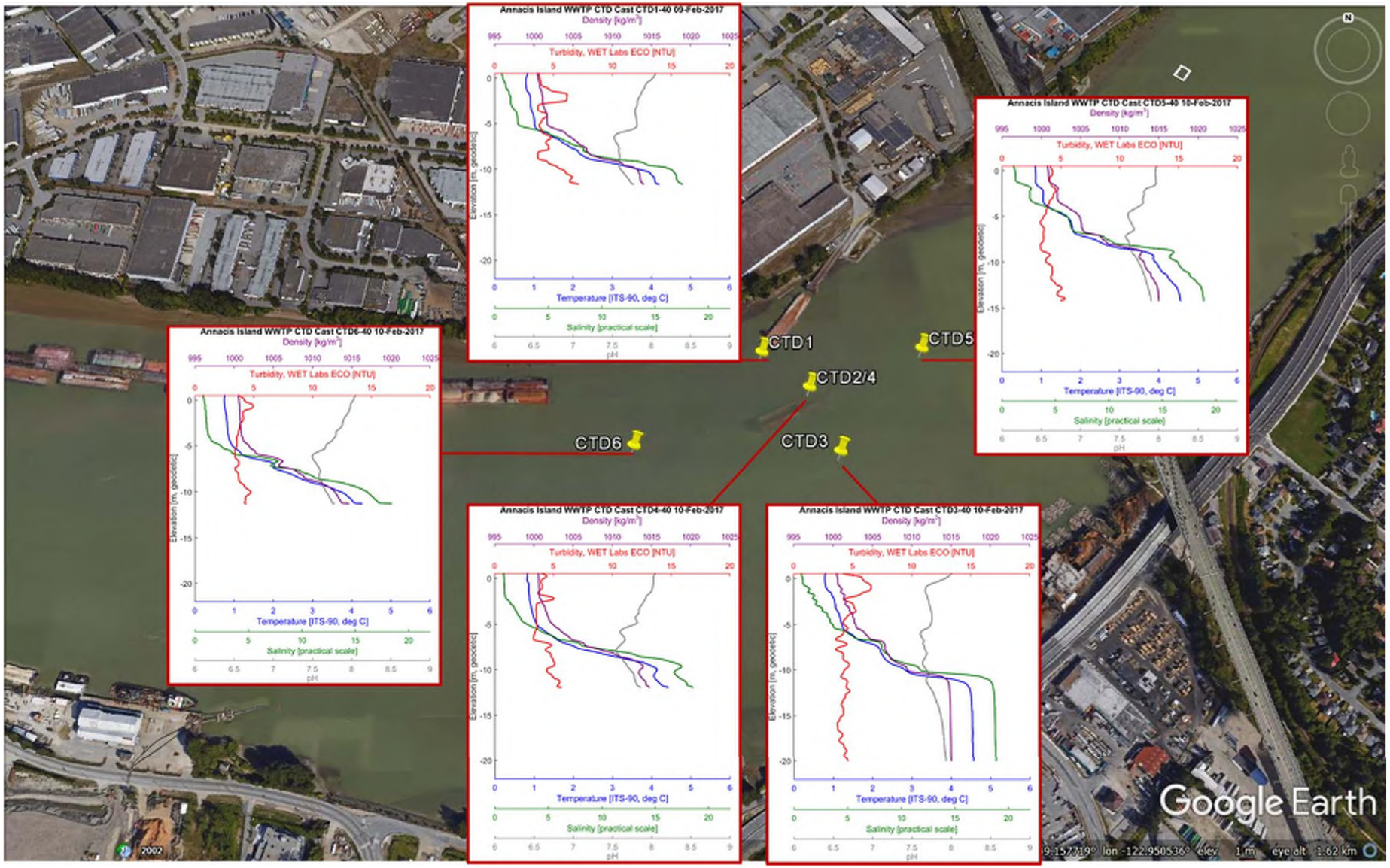


*Figure 14: CTD profiles collected on 9 February 2017 during the 40th iteration overlaid on a Google Earth image.*

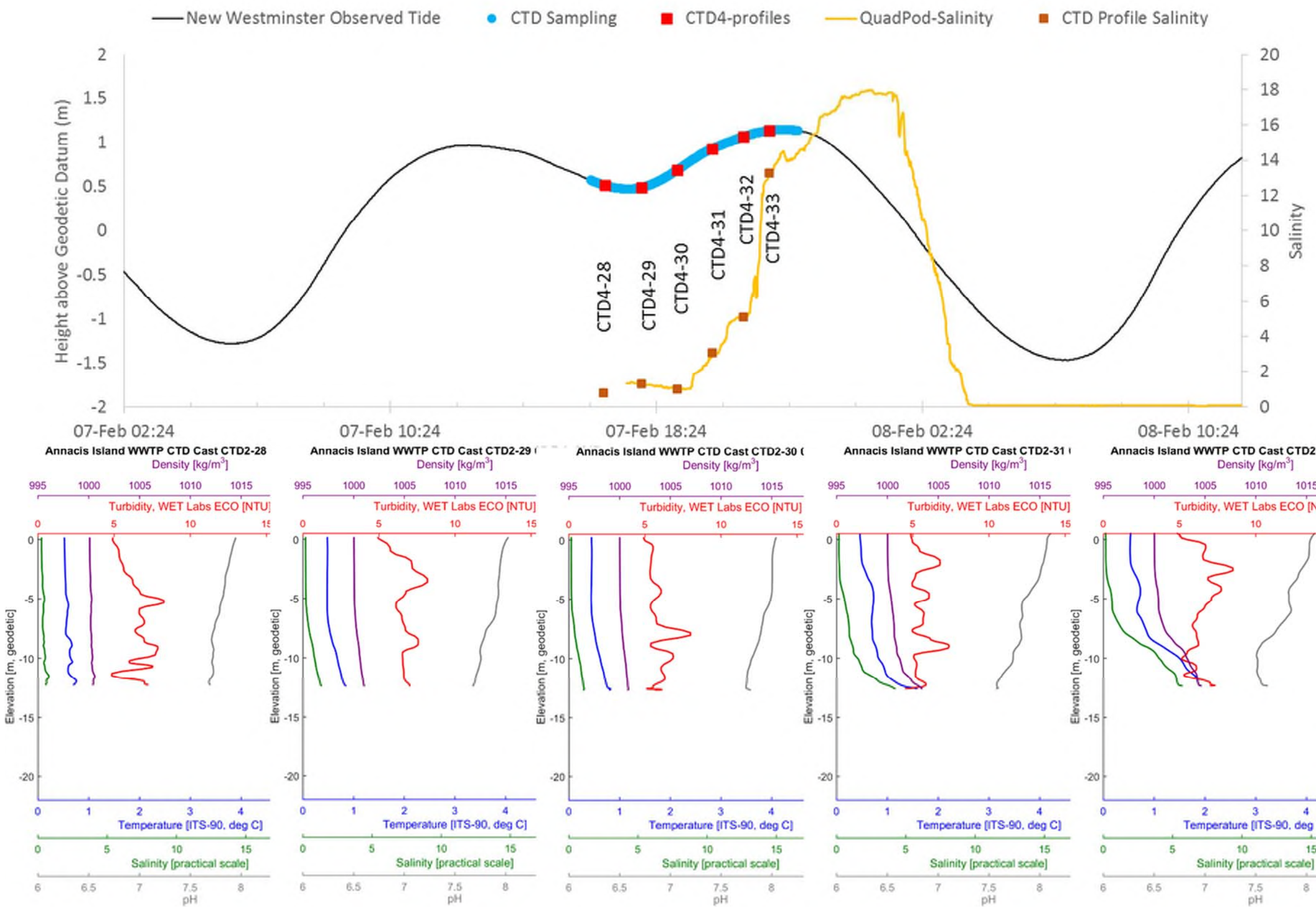


*Figure 15: Timeseries of observed tide at New Westminster, near bed salinity measured at the QuadPod and CTD profiles measured at location CTD2/4 on 7 February 2017.*

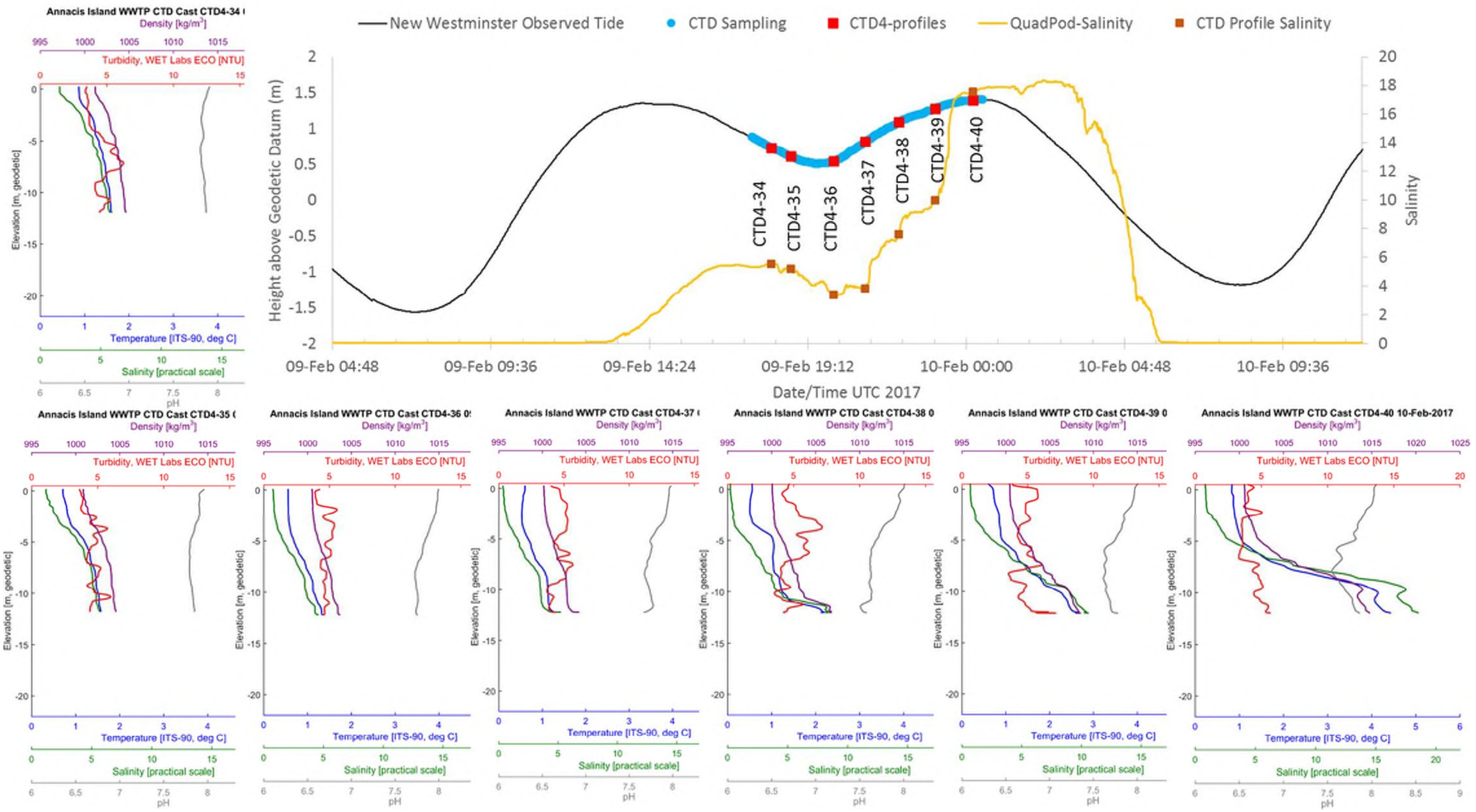


*Figure 16: Timeseries of observed tide at New Westminster, near bed salinity measured at the QuadPod and CTD profiles measured at location CTD2/4 on 9 February 2017.*

# 4.0 ANALYSIS AND DISCUSSION

## 4.1 Tidal Harmonic Analysis

The presence of salinity at the project site is determined by two main factors, the river discharge and the tidal conditions. The interaction between these two factors in relation to salinity is complex (Kostaschuk and Atwood 1990). Salinity was measured at the project site most frequently when the river flows at Hope were below 1,000 $m^3/s$, however, there were also salinity events measured when the river flows at Hope were as high as 1,800 $m^3/s$. The water levels measured at the Brewery Pier were used to assess tidal harmonics and temporal trends that correlate to salinity at the project site.

The water level data measured at the Brewery Pier was used to derive primary tidal constituents at the project site through harmonic analysis using the T-Tide Matlab Toolbox (Pawlowicz et al. 2002). This toolbox performs classical harmonic analysis for periods of 1 year or shorter and computes 95% confidence intervals for each analyzed component (referred to as Phase Error). It accounts for unresolved constituents using nodal corrections and can predict up to 38 tidal constituents, including shallow water constituents. The harmonic analysis conducted on the depth values measured by the SBE37 sensor explained 91.7% of the total variance through 23 significant constituents (Table 11). As expected, the primary constituents with largest amplitude include M2, the principal lunar component and K1, the Luni-solar diurnal component. The tides in the lower mainland are mixed semidiurnal tides that are predominantly semidiurnal.

A timeseries of measured water level and predicted tides by the harmonic analysis is presented in Figure 17. Differences between measured water levels and the predicted tidal elevations (water level residual) suggest there is a temporal offset between predicted components and observed water levels at the project site. Figure 18 provides a timeseries of predicted tides at Point Atkinson and a measure of tidal asymmetry represented by the difference between the daily higher high tide and the higher low tide which is associated with, but not identical to the diurnal inequality. The latter is defined as the difference between the higher high water and lower high water in a diurnal tide or the difference between the higher low water and lower low water in a diurnal tide. Predicted tides at Point Atkinson were used to reference a tidal signal that is not affected by river flows or time lags. Observed tides at New Westminster and salinity measured at the Brewery Pier are presented for comparison. Although this trend was not always consistent during low river flows (below 1,000 $m^3/s$), the salt wedge was present more often during tidal phases when the tides were asymmetric and the difference between the higher high tide and higher low tide was small. Meaning the ebb between the higher high and lower high is short in duration and weak. The cycle of asymmetry in the tidal signal generally follows the spring – neap periodicity of approximately 12 to 14 days due to the interaction of diurnal and semidiurnal constituents (e.g., M2 and K1) causing the diurnal inequality (Nidzieko & Ralston 2012).

Kostaschuk and Atwood (1990) noted a similar trend using multivariate analysis of salt wedge position related to tides and discharge. The analysis revealed a 14 day cycle of low tide elevations that was mirrored by the predicted position of the salt wedge (Kostaschuk and Atwood 1990).

**Table 11: Results from the Harmonic Analysis Conducted on Water Levels Measured at the Brewery Pier**

| Constituent | Frequency (cycles per hour) | Amplitude (m) | Amplitude Error (m) | Phase (degrees GMT) | Phase Error (degrees GMT)[1] | Signal-to-Noise Ratio[2] |
|---|---|---|---|---|---|---|
| M2 | 0.081 | 0.726 | 0.014 | 66.3 | 1.1 | 2500.0 |
| K1 | 0.042 | 0.691 | 0.014 | 305.6 | 1.4 | 2400.0 |
| O1 | 0.039 | 0.372 | 0.020 | 278.1 | 2.4 | 360.0 |
| P1 | 0.042 | 0.229 | 0.013 | 312.7 | 3.2 | 310.0 |
| S2 | 0.083 | 0.162 | 0.012 | 95.1 | 5.1 | 180.0 |
| N2 | 0.079 | 0.162 | 0.012 | 37.5 | 4.5 | 180.0 |
| Q1 | 0.037 | 0.067 | 0.016 | 269.6 | 13.7 | 19.0 |
| NO1 | 0.040 | 0.063 | 0.015 | 326.4 | 17.0 | 19.0 |
| MSF | 0.003 | 0.051 | 0.013 | 18.9 | 15.7 | 15.0 |
| K2 | 0.084 | 0.044 | 0.018 | 117.5 | 26.1 | 5.9 |
| MM | 0.002 | 0.042 | 0.014 | 92.7 | 16.8 | 8.6 |
| L2 | 0.082 | 0.039 | 0.014 | 90.1 | 21.4 | 8.0 |
| OO1 | 0.045 | 0.033 | 0.024 | 332.1 | 46.8 | 1.9 |
| J1 | 0.043 | 0.029 | 0.017 | 352.3 | 33.0 | 3.0 |
| M4 | 0.161 | 0.027 | 0.012 | 13.8 | 27.0 | 5.1 |
| MO3 | 0.119 | 0.025 | 0.016 | 309.8 | 36.9 | 2.4 |
| MK3 | 0.122 | 0.024 | 0.014 | 285.3 | 33.0 | 3.0 |
| MS4 | 0.164 | 0.019 | 0.012 | 61.4 | 36.1 | 2.4 |
| 2Q1 | 0.036 | 0.016 | 0.016 | 310.0 | 55.4 | 1.0 |
| UPS1 | 0.046 | 0.015 | 0.021 | 44.9 | 102.2 | 0.5 |
| EPS2 | 0.076 | 0.015 | 0.012 | 209.8 | 42.2 | 1.5 |
| MU2 | 0.078 | 0.013 | 0.014 | 239.0 | 60.9 | 0.9 |
| ETA2 | 0.085 | 0.013 | 0.017 | 39.1 | 85.4 | 0.6 |

Note:

[1] Phase Error is the 95% confidence interval for each analyzed component.

[2] The signal-to-noise power ratio (SNR) is computed based on the square of the ratio of the amplitude to amplitude error.

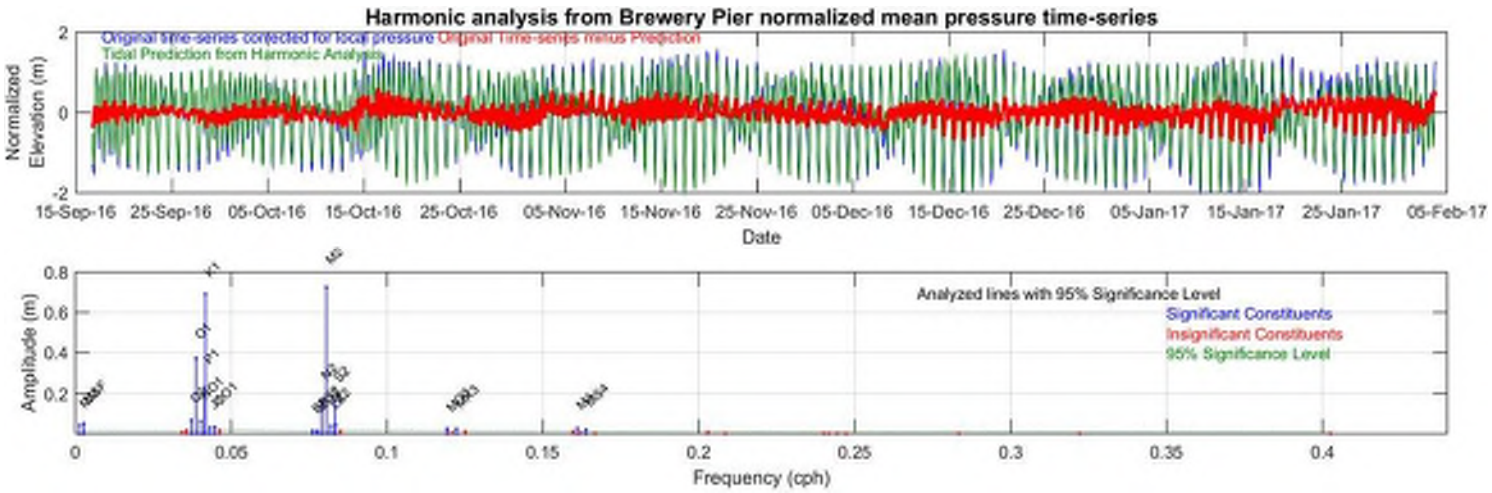


*Figure 17: Time series of measured water level and T-Tide harmonic analysis prediction based on measurements (upper panel), Significant and insignificant constituent (lower panel).*

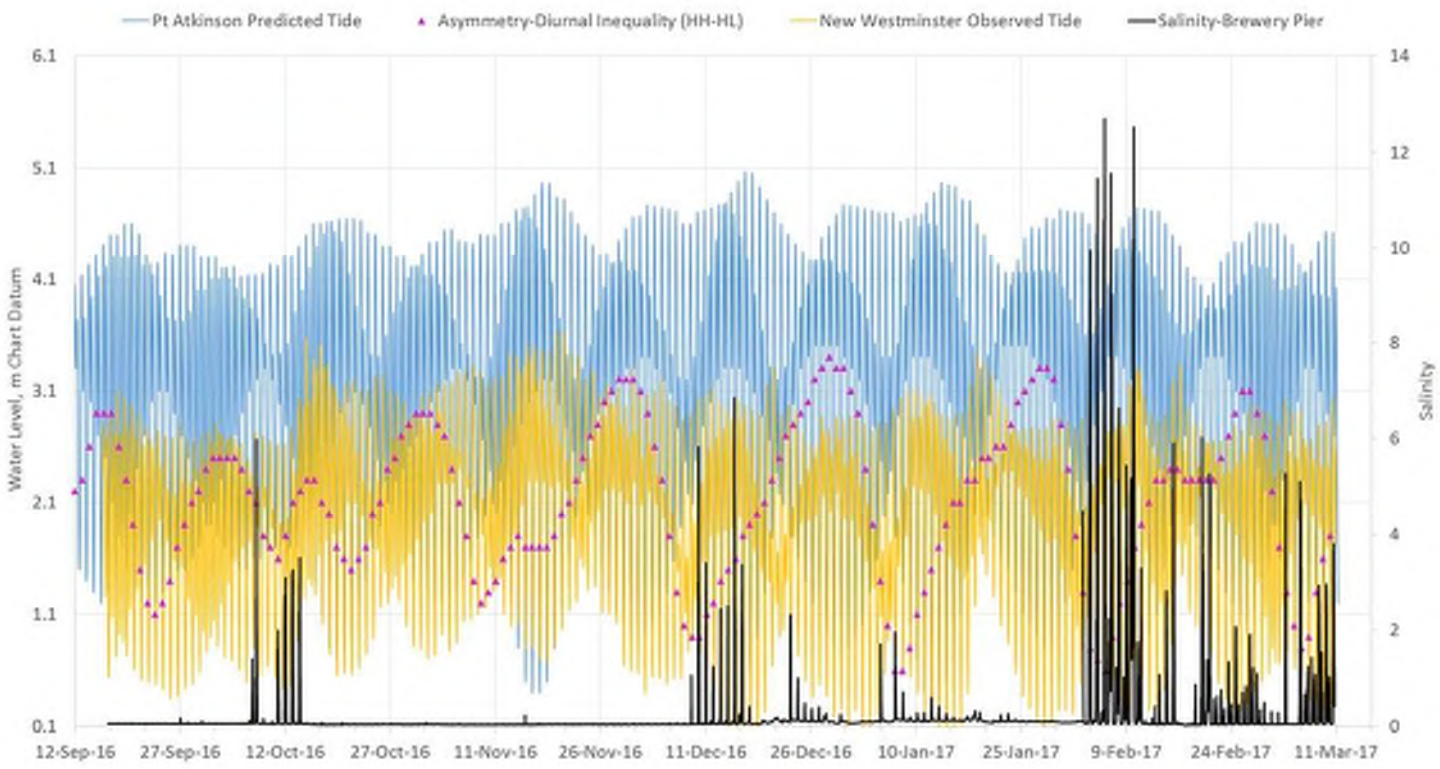


*Figure 18: Timeseries of predicted tide at Point Atkinson, tidal asymmetry represented by a diurnal inequality of the difference between the daily higher high and higher low, observed tide at New Westminster, and measured salinity at the Brewery Pier.*

## 4.2 Salt Wedge and River Flow

Figure 19 and Figure 20 present the timeseries comparing river discharge measured at Hope and the water level measured at the QuadPod with temperature, salinity, turbidity and near bed current direction and echo intensity. Figure 20 focuses on the salinity events recorded from 18 February to 26 February 2017. In most salinity events recorded at the QuadPod and Brewery Pier stations, peak salinity is reached after peak high water, when the water level begins falling. Observations of current direction measured by the ADCP on the QuadPod with salinity show that flow moves north to northwest (upriver) during the onset of salinity measured at the site. However, peak salinity values occur after the flow has shifted to flowing back southwest (downriver). When the southwest current speeds increase, the salinity is quickly flushed from the site. Salinity increasing during the onset of the ebb and southwesterly flows suggests that saline water penetrated further upriver than the project site. The source of the saline water is unknown and only speculative at this point. It is possible that the salt wedge moves up the river along the thalweg (consistent with behavior observed near Tilbury Island in Golder 2016) past the project site and when the tide changes the salt wedge loses its structure and returns downstream over the project site from the northeast. Another possibility is the salt wedge penetrates upriver along the north arm or along the north side of Annacis Island and flows back over the project site. Or a combination of both processes are being measured at the project site.

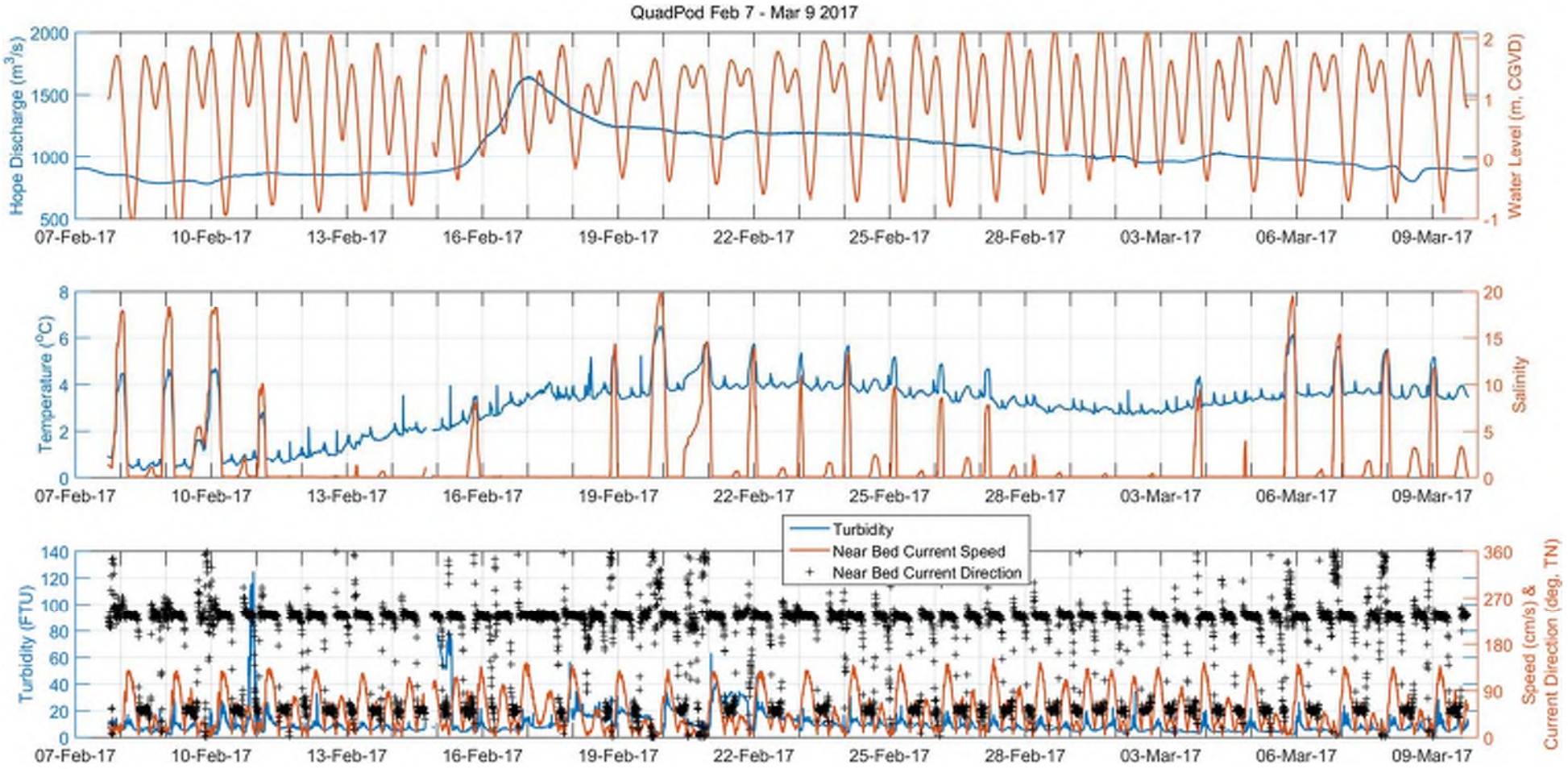


*Figure 19: Timeseries of discharge measured at Hope Station and water level measured at the QuadPod (top panel), compared with water temperature, salinity (middle panel), and near bed turbidity, near bed current direction, and near bed current speed (bottom panel) measured at the QuadPod from 7 February to 9 March, 2017.*

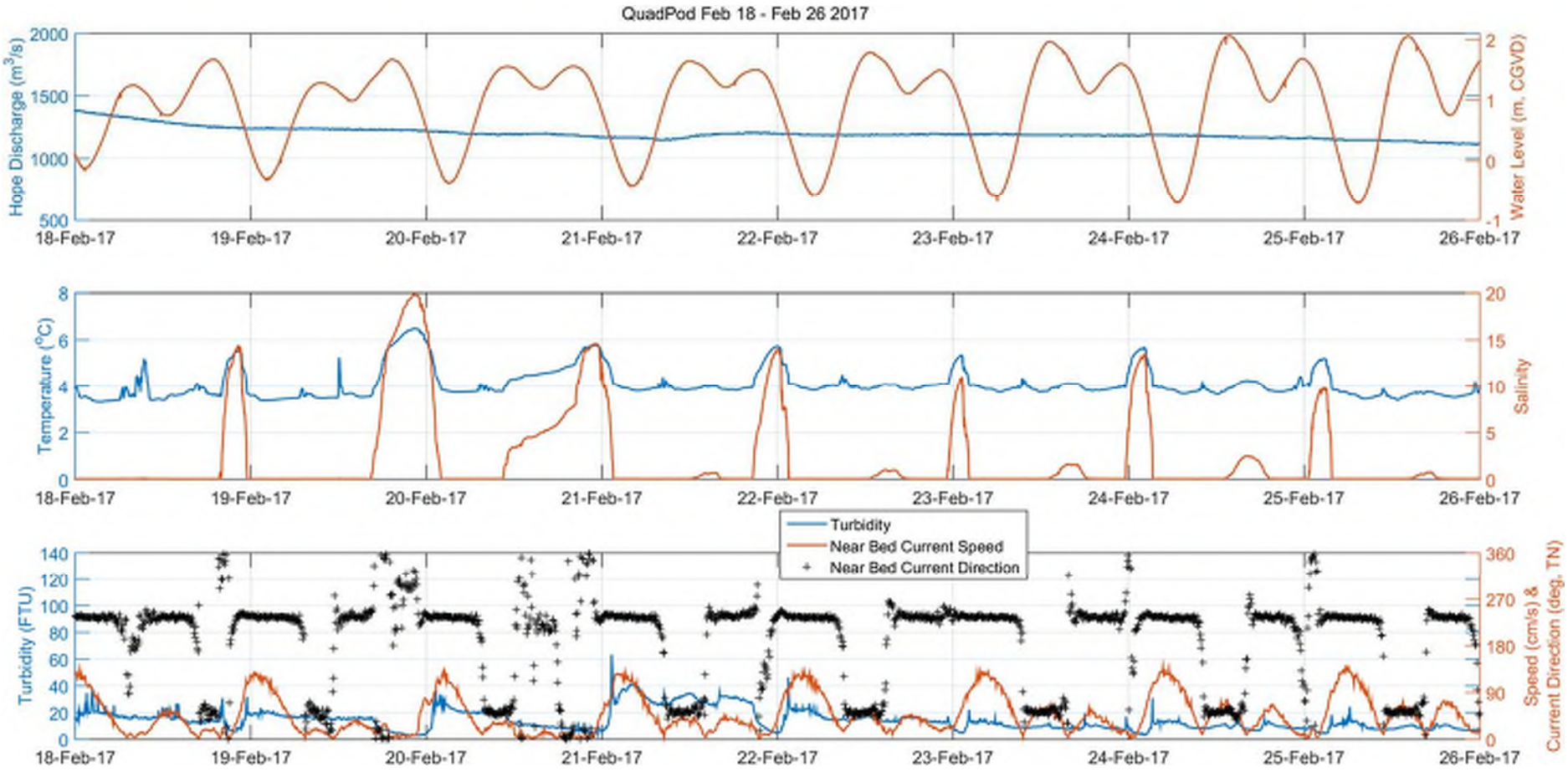


*Figure 20: Timeseries of discharge measured at Hope Station and water level measured at the QuadPod (top panel), compared with water temperature, salinity (middle panel), and near bed turbidity, near bed current direction, and near bed current speed (bottom panel) measured at the QuadPod from 18 February to 26 February, 2017.*

## 4.3 Longitudinal CTD Profile Review

Figure 21 and Figure 22 provide contour plots salinity on a longitudinal transect between CTD7 (if profile was taken at that station), CTD6, CTD2/4, and CTD5 to provide a 2D snapshot image of the salinity and temperature gradient through the water column. Both plots show the progression of the salt wedge front approaching the project site. The salt wedge is typically visible within the bottom 5 m of the profile. The general structure observed in the CTD profiles showed the pycnocline between the 5 to 10 m water depth, and the salt wedge was below 10 m water depth, with typically profiles extending to 15 m water depth. Although the contour plots are not well defined between CTD7 and CTD6, the shape of the salt wedge front is similar to vessel based ADCP transects and CTD profiles measured in March 2016 along the thalweg near Tilbury Island (Golder, 2016). The Salt wedge front was observed to have a relatively constant structure for a long distance along the river bed. That shape is consistent with the contour plot structure, where the elevation of the salt wedge and pycnocline are similar along the longitudinal transect. A similar profile structure was observed in 2006 and 2008 further downstream by Tedford et al. (2009).

The Temperature-Salinity (T-S) plots show the transition of colder fresh river water to warmer more saline water associated with the salt wedge.

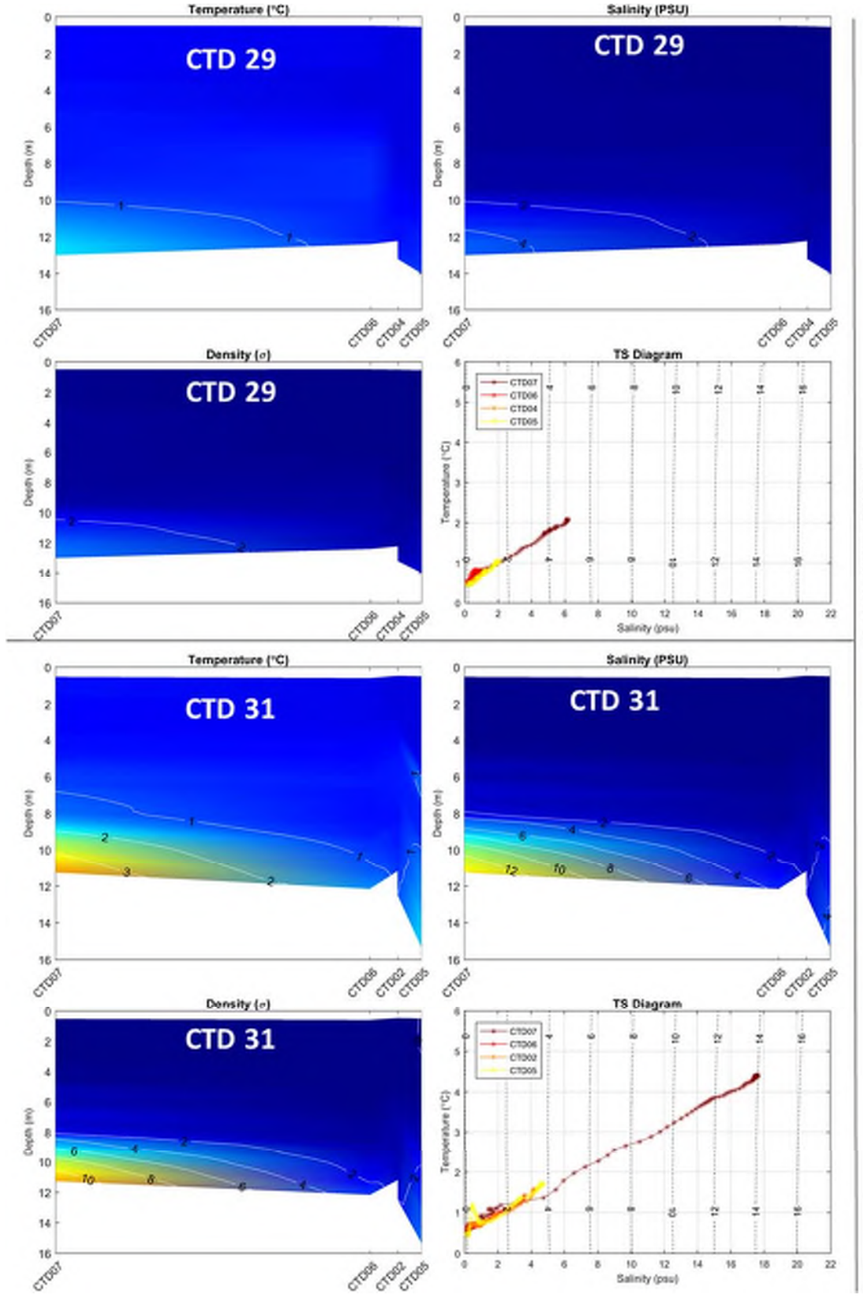


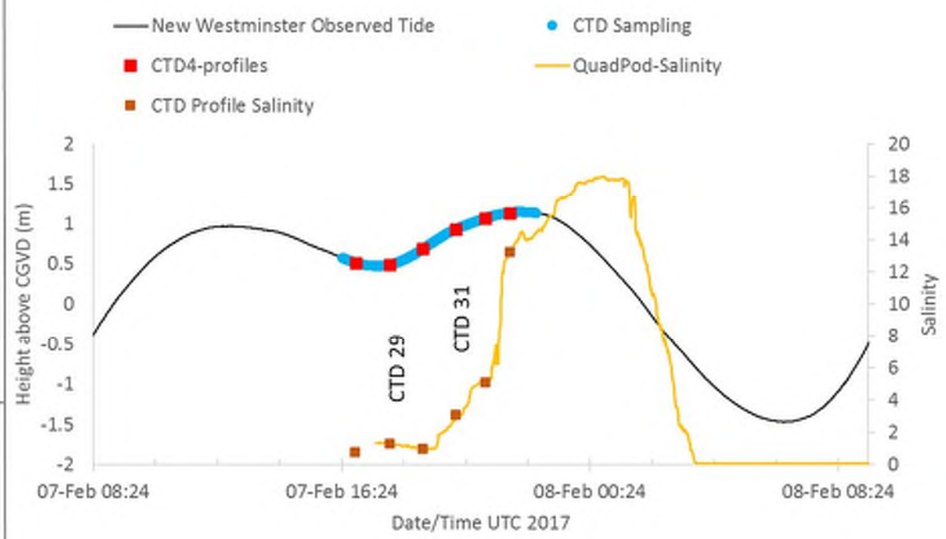


*Figure 21: Longitudinal contour plots of CTD profiles measured on 7 February 2017 during iteration 29 and 31.*

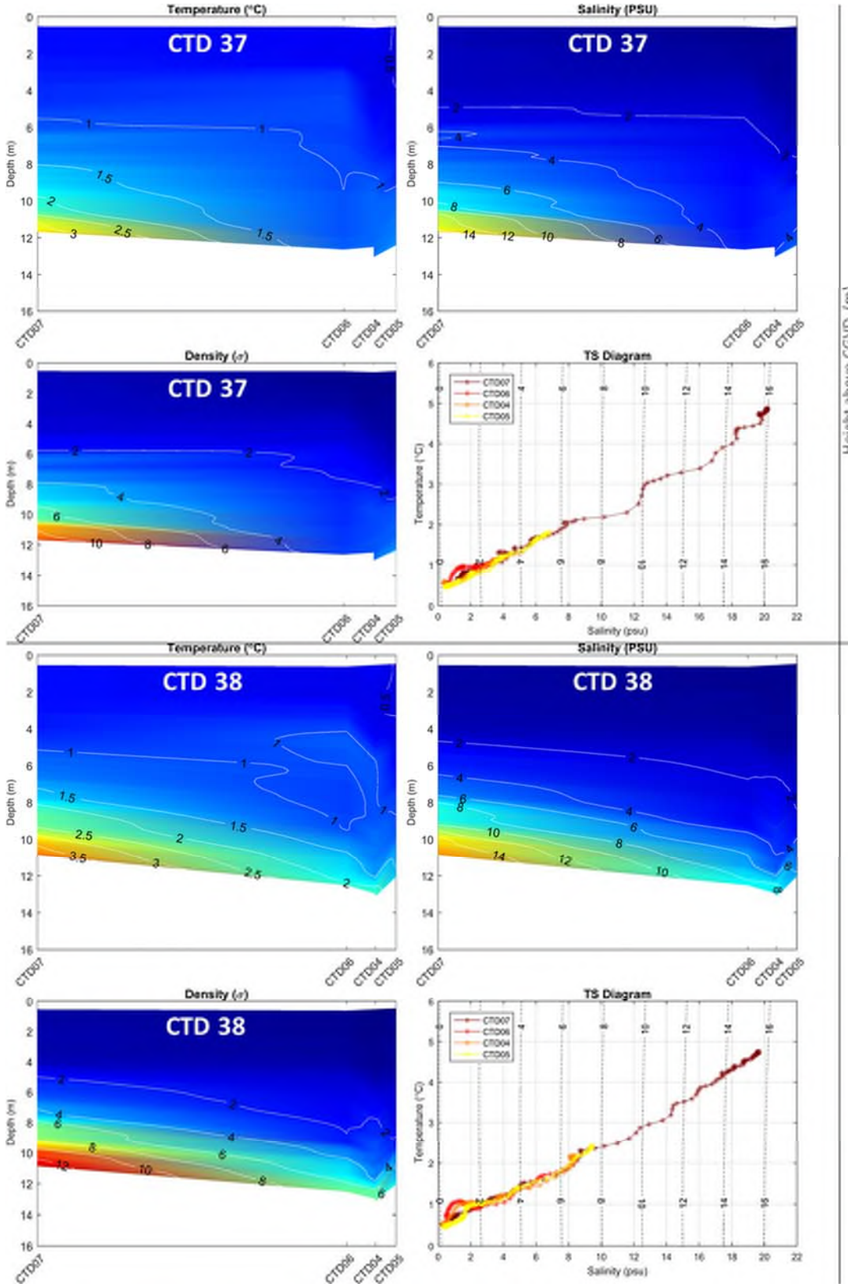


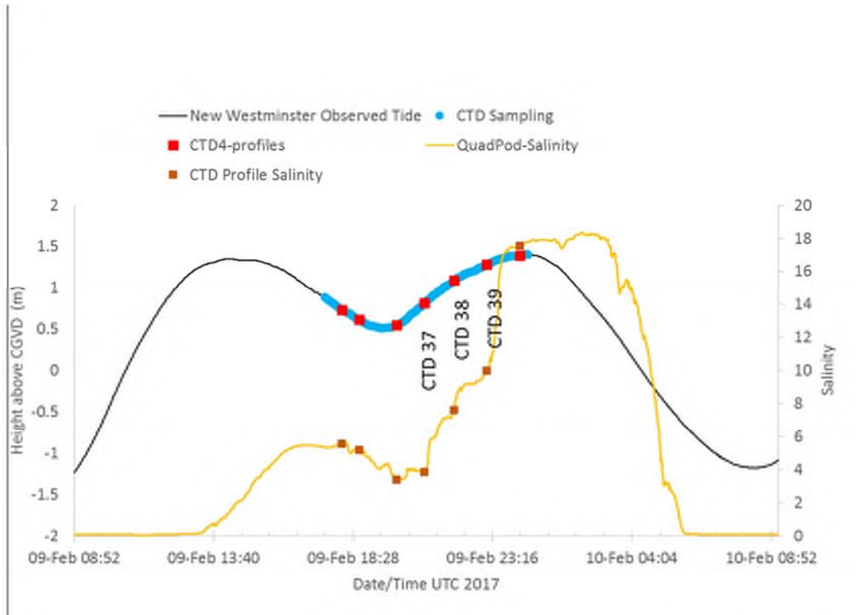


*Figure 22: Longitudinal contour plots of CTD profiles measured on 9 February 2017 during iteration 37, 38 and 39.*

# 5.0 SUMMARY

The salinity monitoring program at the proposed Annacis Island WWTP outfall captured salinity present at the project site during low flows. Nearly six months of continuous data collection at Brewery Pier provides insight on the trends in salinity in relation to river discharge and tidal phase. The QuadPod measurements and CTD profiles provided detailed data during low flow conditions at the project site from 7 February to 9 March 2017. This data analysis provides key information on salinity conditions at the project site and will support the development and design of the proposed outfall as well as work undertaken as part of the permit application process. This analysis has illustrated the following:

- Salinity of values ranging from a baseline of 0.06 to a maximum of 19.9 were measured during the course of the data collection program at the project site.
- Salinity values of 0.5 or higher occurred 55 days out of the 176 day deployment at the Brewery Pier station and on 22 days of the 31 day deployment at the QuadPod station.
- Salinity events at the Brewery Pier and QuadPod stations most often occurred when river flows were below 1,000 $m^3/s$ at the Hope station, however, some salinity events occurred when flows were higher. The largest recorded river flow at Hope was 1,800 $m^3/s$ when a salinity event was recorded at the Brewery Pier station.
- Tidal asymmetry, in the form of diurnal inequality caused by smaller differences between the higher high water of the tidal cycle and higher low water, tended to coincide with the occurrence of the salt wedge presence at the site (along with lower river discharge levels).
- Current conditions measured by the QuadPod at the project site were predominantly to the southwest (downriver). Current measurements collected during lower discharge levels showed that at least once per tidal cycle, the flow direction reversed through the water column to flow northeast (upriver) during the larger flood tide of the day. When tidal asymmetry was not as strong (diurnal inequality was minimal), the flow reversal occurred twice each cycle, during both flood tides.
- Mean current speeds were between 0.48 to 0.71 m/s and reached maximum values of 1.4 to 2.12 m/s through the water column from the bottom to surface respectively. Flow speed and direction were relatively uniform through the water column, with speeds slightly higher near the surface and decreasing with depth. Current direction through the water column became stratified for a few select salt wedge intrusion events, and current speed was slower near the bottom where the salt wedge was present.
- Based on current speed at the Quad Pod and downstream CTD profiles, the salt wedge was observed approaching the site from downstream, moving upstream during the flood tide, and elevated salinity would remain present at the site until the early or middle of the ebb tide.
- Salinity events recorded at the Brewery Pier and QuadPod typically increased in salinity during the flood tide and continued to increase past slack high. Peak salinity values for each event corresponded with the early to middle of the ebb tide. Near bed current flow measurements showed that the peak salinity values corresponded with southwesterly current flow and often the downriver flow had been sustained for a few hours before peak salinity was reached.
- The salt wedge was likely present further upstream of the project site during events when the peak salinity corresponded to downriver flows.
- Other characteristics of the salt wedge besides increased salinity, included increased water temperature, and decreased turbidity and pH.
- The pycnocline was typically present at -5 to -10 m CGVD in the CTD profiles measured at the site.

# 6.0 ELECTRONIC DATA DELIVERABLES

In addition to this report, Golder is issuing the processed data in ASCII format (Appendix A) electronically. The data provided and names of the files are listed below:

- Brewery Pier Data:
  - Brewery Pier SBE37 and RBRCT_Header&Data.txt
  - Brewery Pier YSI EXO2_12F10131_Header&Data.txt
- QuadPod Data:
  - Annacis Island WWTP_SBE37CT_12344_Header.txt
  - Annacis Island WWTP_SBE37CT_12345_Header.txt
  - Annacis Island WWTP_RBRduo_pressure_50517_Header.txt
  - Annacis Island WWTP_JFEInfinity_turbidity_0142_Header.txt
  - ADCP Data Files:
    - Annacis Island WWTP_QuadPod_21100_Header.txt
    - Annacis Island WWTP_QuadPod_21100_adcp_EAA.txt
    - Annacis Island WWTP_QuadPod_21100_adcp_battery.txt
    - Annacis Island WWTP_QuadPod_21100_adcp_bindepth.txt
    - Annacis Island WWTP_QuadPod_21100_adcp_datenum.txt
    - Annacis Island WWTP_QuadPod_21100_adcp_depth.txt
    - Annacis Island WWTP_QuadPod_21100_adcp_heading.txt
    - Annacis Island WWTP_QuadPod_21100_adcp_pitch.txt
    - Annacis Island WWTP_QuadPod_21100_adcp_roll.txt
    - Annacis Island WWTP_QuadPod_21100_adcp_temperature.txt
    - Annacis Island WWTP_QuadPod_21100_adcp_tilt.txt
    - Annacis Island WWTP_QuadPod_21100_adcp_veldir.txt
    - Annacis Island WWTP_QuadPod_21100_adcp_veleast.txt
    - Annacis Island WWTP_QuadPod_21100_adcp_velmag.txt
    - Annacis Island WWTP_QuadPod_21100_adcp_velnorth.txt
    - Annacis Island WWTP_QuadPod_21100_adcp_waterlevel.txt
- CTD Profiles:
  - See Appendix B for tables with complete list of file names

## 7.0 CLOSING

We appreciate the opportunity to conduct this work and trust that this final report and data meet your immediate requirements for final data. If you have any questions concerning this report, please do not hesitate to contact us.

**GOLDER ASSOCIATES LTD.**

Dana Oster, MSc
Coastal Geoscience Specialist

Phil Osborne, PhD, PGeo
Principal, Senior Coastal Geomorphologist

DO/PO/syd



o:\final\2015\3 proj\1525010 cdm_annacis island wwtp\1525010-083-r-rev1-703\1525010-083-r-rev1-703-salinity monitoring 20apr_17.docx

# 8.0 REFERENCES

Fofonoff, N.P. and R.C. Millard Jr. 1983. Algorithms for computation of fundamental properties of seawater (UNESCO Tech. Papers in Marine Science 44). Paris, France: Division of Marine Science, UNESCO.

Kostaschuk, R.A. and Atwood, L.A., 1990. River discharge and tidal controls on salt-wedge position and implications for channel shoaling: Fraser River, British Columbia. *Canadian Journal of Civil Engineering*, *17*(3), pp.452-459.

Golder Associates Ltd., 2016. Baseline Characterization of Water Density to the Proposed Annacis Island Transient Mitigation and Outfall, Delta, BC. 1525010-027-TM-RevA.

Mathworks (The MathWorks, Inc.). 2015. MATLAB and Statistics Toolbox Release 2014b [software], Natick, Massachusetts, United States.

Natural Resources Canada. 2017. Magnetic Declination Calculator. Available at: http://www.geomag.nrcan.gc.ca/calc/mdcal-eng.php. Accessed: February 15, 2017.

Nidzieko, N.J., & Ralston, D.K. 2012. Tidal asymmetry and velocity skew over tidal flats and shallow channels within a macrotidal river delta, J. Geophys. Res., 117, C03001.

Pawlowicz, R., Beardsley, B., & Lentz, S. 2002. Classical tidal harmonic analysis including error estimates in MATLAB using T_TIDE. Computers & Geosciences, 28(8), 929-937.

SBE (Sea-Bird Electronics). 2014. Seasoft V2: SBE Data Processing User's Manual. Software Release 7.23.2 and later. Available at: http://www.seabird.com/sites/default/files/documents/SBEDataProcessing_7.23.2.pdf. Accessed: November 15, 2014.

Tedford, E.W., Carpenter, J.R., Pawlowicz, R., Pieters, R. and Lawrence, G.A., 2009. Observation and analysis of shear instability in the Fraser River estuary. *Journal of Geophysical Research: Oceans*, *114*(C11).

TRDI (Teledyne RDI). 2010. WorkHorse Acoustic Doppler Current Profiler Technical Manual; P/N 957-6150-00 (August 2010).

Unesco 1983. Algorithms for computation of fundamental properties of seawater, 1983. Unesco Tech. Pap. in Mar. Sci., No. 44, 53 pp.

# APPENDIX A

## Data Files (electronic)

# APPENDIX B

## CTD Profiles

# 1.0 CTD PROFILES

Table 1 to Table 8 provide a summary of the CTD station name, iteration, time collected, observed water level at New Westminster (CGVD), and the corresponding data file name. Figure 1 to Figure 52 provide the CTD profile for each station grouped by each of the eight sampling days.

**Table 1: 25 January 2017 CTD Profile Summary**

| CTD Profile Name | Station | Iteration | Time (UTC) | Tide Level at New Westminster (7654) | Data File Name |
|---|---|---|---|---|---|
| CTD1-1 | CTD1 | 1 | 16:21:29 | 0.84 | 'Annacis_Island_CTD1-1_25-Jan-17.txt' |
| CTD1-2 | CTD1 | 2 | 17:17:40 | 0.66 | 'Annacis_Island_CTD1-2_25-Jan-17.txt' |
| CTD1-3 | CTD1 | 3 | 18:12:25 | 0.45 | 'Annacis_Island_CTD1-3_25-Jan-17.txt' |
| CTD1-4 | CTD1 | 4 | 19:28:49 | 0.34 | 'Annacis_Island_CTD1-4_25-Jan-17.txt' |
| CTD1-5 | CTD1 | 5 | 20:29:44 | 0.49 | 'Annacis_Island_CTD1-5_25-Jan-17.txt' |
| CTD1-6 | CTD1 | 6 | 21:29:57 | 0.64 | 'Annacis_Island_CTD1-6_25-Jan-17.txt' |
| CTD1-7 | CTD1 | 7 | 22:15:18 | 0.71 | 'Annacis_Island_CTD1-7_25-Jan-17.txt' |
| CTD1-8 | CTD1 | 8 | 22:55:44 | 0.78 | 'Annacis_Island_CTD1-8_25-Jan-17.txt' |
| CTD2-1 | CTD2 | 1 | 16:28:03 | 0.82 | 'Annacis_Island_CTD2-1_25-Jan-17.txt' |
| CTD2-2 | CTD2 | 2 | 17:29:42 | 0.60 | 'Annacis_Island_CTD2-2_25-Jan-17.txt' |
| CTD2-3 | CTD2 | 3 | 18:17:01 | 0.43 | 'Annacis_Island_CTD2-3_25-Jan-17.txt' |
| CTD2-4 | CTD2 | 4 | 19:33:05 | 0.35 | 'Annacis_Island_CTD2-4_25-Jan-17.txt' |
| CTD2-5 | CTD2 | 5 | 20:34:33 | 0.50 | 'Annacis_Island_CTD2-5_25-Jan-17.txt' |
| CTD2-6 | CTD2 | 6 | 21:36:34 | 0.65 | 'Annacis_Island_CTD2-6_25-Jan-17.txt' |
| CTD2-7 | CTD2 | 7 | 22:19:13 | 0.72 | 'Annacis_Island_CTD2-7_25-Jan-17.txt' |
| CTD2-8 | CTD2 | 8 | 23:04:27 | 0.78 | 'Annacis_Island_CTD2-8_25-Jan-17.txt' |
| CTD3-1 | CTD3 | 1 | 16:35:26 | 0.80 | 'Annacis_Island_CTD3-1_25-Jan-17.txt' |
| CTD3-2 | CTD3 | 2 | 17:35:19 | 0.58 | 'Annacis_Island_CTD3-2_25-Jan-17.txt' |
| CTD3-3* | CTD3 | 3 | 18:31:33 | 0.39 | N/A |
| CTD3-4 | CTD3 | 4 | 19:38:51 | 0.35 | 'Annacis_Island_CTD3-4_25-Jan-17.txt' |
| CTD3-5 | CTD3 | 5 | 20:40:17 | 0.52 | 'Annacis_Island_CTD3-5_25-Jan-17.txt' |
| CTD3-6 | CTD3 | 6 | 21:42:50 | 0.66 | 'Annacis_Island_CTD3-6_25-Jan-17.txt' |
| CTD3-7 | CTD3 | 7 | 22:24:08 | 0.73 | 'Annacis_Island_CTD3-7_25-Jan-17.txt' |
| CTD3-8 | CTD3 | 8 | 23:13:43 | 0.79 | 'Annacis_Island_CTD3-8_25-Jan-17.txt' |
| CTD4-1 | CTD4 | 1 | 16:40:46 | 0.78 | 'Annacis_Island_CTD4-1_25-Jan-17.txt' |
| CTD4-2 | CTD4 | 2 | 17:40:53 | 0.56 | 'Annacis_Island_CTD4-2_25-Jan-17.txt' |
| CTD4-3 | CTD4 | 3 | 18:40:04 | 0.37 | 'Annacis_Island_CTD4-3_25-Jan-17.txt' |
| CTD4-4 | CTD4 | 4 | 19:46:02 | 0.37 | 'Annacis_Island_CTD4-4_25-Jan-17.txt' |
| CTD4-5 | CTD4 | 5 | 20:50:01 | 0.55 | 'Annacis_Island_CTD4-5_25-Jan-17.txt' |
| CTD4-6 | CTD4 | 6 | 21:48:20 | 0.67 | 'Annacis_Island_CTD4-6_25-Jan-17.txt' |
| CTD4-7 | CTD4 | 7 | 22:31:04 | 0.75 | 'Annacis_Island_CTD4-7_25-Jan-17.txt' |
| CTD4-8 | CTD4 | 8 | 23:19:21 | 0.79 | 'Annacis_Island_CTD4-8_25-Jan-17.txt' |
| CTD5-1 | CTD5 | 1 | 16:47:15 | 0.76 | 'Annacis_Island_CTD5-1_25-Jan-17.txt' |
| CTD5-2 | CTD5 | 2 | 17:51:15 | 0.52 | 'Annacis_Island_CTD5-2_25-Jan-17.txt' |
| CTD5-3 | CTD5 | 3 | 18:46:45 | 0.36 | 'Annacis_Island_CTD5-3_25-Jan-17.txt' |
| CTD5-4 | CTD5 | 4 | 19:53:30 | 0.39 | 'Annacis_Island_CTD5-4_25-Jan-17.txt' |
| CTD5-5 | CTD5 | 5 | 20:55:21 | 0.56 | 'Annacis_Island_CTD5-5_25-Jan-17.txt' |
| CTD5-6 | CTD5 | 6 | 21:53:37 | 0.68 | 'Annacis_Island_CTD5-6_25-Jan-17.txt' |

| CTD Profile Name | Station | Iteration | Time (UTC) | Tide Level at New Westminster (7654) | Data File Name |
|---|---|---|---|---|---|
| CTD5-7 | CTD5 | 7 | 22:36:32 | 0.76 | 'Annacis_Island_CTD5-7_25-Jan-17.txt' |
| CTD5-8 | CTD5 | 8 | 23:25:05 | 0.79 | 'Annacis_Island_CTD5-8_25-Jan-17.txt' |
| CTD6-1 | CTD6 | 1 | 16:57:39 | 0.73 | 'Annacis_Island_CTD6-1_25-Jan-17.txt' |
| CTD6-2 | CTD6 | 2 | 17:56:52 | 0.50 | 'Annacis_Island_CTD6-2_25-Jan-17.txt' |
| CTD6-3 | CTD6 | 3 | 18:53:43 | 0.35 | 'Annacis_Island_CTD6-3_25-Jan-17.txt' |
| CTD6-4 | CTD6 | 4 | 20:02:30 | 0.41 | 'Annacis_Island_CTD6-4_25-Jan-17.txt' |
| CTD6-5 | CTD6 | 5 | 21:02:29 | 0.58 | 'Annacis_Island_CTD6-5_25-Jan-17.txt' |
| CTD6-6 | CTD6 | 6 | 22:00:48 | 0.69 | 'Annacis_Island_CTD6-6_25-Jan-17.txt' |
| CTD6-7 | CTD6 | 7 | 22:43:53 | 0.76 | 'Annacis_Island_CTD6-7_25-Jan-17.txt' |
| CTD6-8 | CTD6 | 8 | 23:34:40 | 0.78 | 'Annacis_Island_CTD6-8_25-Jan-17.txt' |

* Profile did not record correctly

**Table 2: 26 January 2017 CTD Profile Summary**

| CTD Profile Name | Station | Iteration | Time (UTC) | Tide Level at New Westminster (7654) | Data File Name |
|---|---|---|---|---|---|
| CTD1-9 | CTD1 | 9 | 16:05:22 | 0.89 | 'Annacis_Island_CTD1-9_26-Jan-17.txt' |
| CTD1-10 | CTD1 | 10 | 16:54:31 | 0.79 | 'Annacis_Island_CTD1-10_26-Jan-17.txt' |
| CTD1-11 | CTD1 | 11 | 17:54:52 | 0.54 | 'Annacis_Island_CTD1-11_26-Jan-17.txt' |
| CTD1-12 | CTD1 | 12 | 18:47:21 | 0.31 | 'Annacis_Island_CTD1-12_26-Jan-17.txt' |
| CTD1-13 | CTD1 | 13 | 19:46:13 | 0.18 | 'Annacis_Island_CTD1-13_26-Jan-17.txt' |
| CTD1-14 | CTD1 | 14 | 20:37:34 | 0.24 | 'Annacis_Island_CTD1-14_26-Jan-17.txt' |
| CTD1-15 | CTD1 | 15 | 21:26:42 | 0.38 | 'Annacis_Island_CTD1-15_26-Jan-17.txt' |
| CTD1-16 | CTD1 | 16 | 22:11:47 | 0.50 | 'Annacis_Island_CTD1-16_26-Jan-17.txt' |
| CTD2-9 | CTD2 | 9 | 16:11:02 | 0.88 | 'Annacis_Island_CTD2-9_26-Jan-17.txt' |
| CTD2-10 | CTD2 | 10 | 17:08:38 | 0.74 | 'Annacis_Island_CTD2-10_26-Jan-17.txt' |
| CTD2-11 | CTD2 | 11 | 17:59:26 | 0.51 | 'Annacis_Island_CTD2-11_26-Jan-17.txt' |
| CTD2-12 | CTD2 | 12 | 18:53:12 | 0.29 | 'Annacis_Island_CTD2-12_26-Jan-17.txt' |
| CTD2-13 | CTD2 | 13 | 19:52:04 | 0.17 | 'Annacis_Island_CTD2-13_26-Jan-17.txt' |
| CTD2-14 | CTD2 | 14 | 20:42:25 | 0.26 | 'Annacis_Island_CTD2-14_26-Jan-17.txt' |
| CTD2-15 | CTD2 | 15 | 21:36:00 | 0.41 | 'Annacis_Island_CTD2-15_26-Jan-17.txt' |
| CTD2-16 | CTD2 | 16 | 22:15:34 | 0.51 | 'Annacis_Island_CTD2-16_26-Jan-17.txt' |
| CTD3-9 | CTD3 | 9 | 16:16:31 | 0.88 | 'Annacis_Island_CTD3-9_26-Jan-17.txt' |
| CTD3-10 | CTD3 | 10 | 17:27:01 | 0.67 | 'Annacis_Island_CTD3-10_26-Jan-17.txt' |
| CTD3-11 | CTD3 | 11 | 18:04:38 | 0.49 | 'Annacis_Island_CTD3-11_26-Jan-17.txt' |
| CTD3-12 | CTD3 | 12 | 19:01:12 | 0.26 | 'Annacis_Island_CTD3-12_26-Jan-17.txt' |
| CTD3-13 | CTD3 | 13 | 19:57:39 | 0.17 | 'Annacis_Island_CTD3-13_26-Jan-17.txt' |
| CTD3-14 | CTD3 | 14 | 20:49:51 | 0.28 | 'Annacis_Island_CTD3-14_26-Jan-17.txt' |
| CTD3-15 | CTD3 | 15 | 21:40:45 | 0.42 | 'Annacis_Island_CTD3-15_26-Jan-17.txt' |
| CTD3-16 | CTD3 | 16 | 22:19:49 | 0.52 | 'Annacis_Island_CTD3-16_26-Jan-17.txt' |
| CTD4-9 | CTD4 | 9 | 16:23:06 | 0.87 | 'Annacis_Island_CTD4-9_26-Jan-17.txt' |
| CTD4-10 | CTD4 | 10 | 17:32:51 | 0.65 | 'Annacis_Island_CTD4-10_26-Jan-17.txt' |
| CTD4-11 | CTD4 | 11 | 18:09:53 | 0.47 | 'Annacis_Island_CTD4-11_26-Jan-17.txt' |

| CTD Profile Name | Station | Iteration | Time (UTC) | Tide Level at New Westminster (7654) | Data File Name |
|---|---|---|---|---|---|
| CTD4-12 | CTD4 | 12 | 19:15:44 | 0.22 | 'Annacis_Island_CTD4-12_26-Jan-17.txt' |
| CTD4-13 | CTD4 | 13 | 20:03:06 | 0.18 | 'Annacis_Island_CTD4-13_26-Jan-17.txt' |
| CTD4-14 | CTD4 | 14 | 20:54:59 | 0.29 | 'Annacis_Island_CTD4-14_26-Jan-17.txt' |
| CTD4-15 | CTD4 | 15 | 21:46:51 | 0.44 | 'Annacis_Island_CTD4-15_26-Jan-17.txt' |
| CTD4-16 | CTD4 | 16 | 22:27:32 | 0.54 | 'Annacis_Island_CTD4-16_26-Jan-17.txt' |
| CTD5-9 | CTD5 | 9 | 16:29:37 | 0.85 | 'Annacis_Island_CTD5-9_26-Jan-17.txt' |
| CTD5-10 | CTD5 | 10 | 17:39:47 | 0.61 | 'Annacis_Island_CTD5-10_26-Jan-17.txt' |
| CTD5-11 | CTD5 | 11 | 18:17:31 | 0.43 | 'Annacis_Island_CTD5-11_26-Jan-17.txt' |
| CTD5-12 | CTD5 | 12 | 19:21:43 | 0.21 | 'Annacis_Island_CTD5-12_26-Jan-17.txt' |
| CTD5-13 | CTD5 | 13 | 20:08:36 | 0.18 | 'Annacis_Island_CTD5-13_26-Jan-17.txt' |
| CTD5-14 | CTD5 | 14 | 21:06:37 | 0.32 | 'Annacis_Island_CTD5-14_26-Jan-17.txt' |
| CTD5-15 | CTD5 | 15 | 21:52:18 | 0.45 | 'Annacis_Island_CTD5-15_26-Jan-17.txt' |
| CTD5-16 | CTD5 | 16 | 22:31:57 | 0.55 | 'Annacis_Island_CTD5-16_26-Jan-17.txt' |
| CTD6-9 | CTD6 | 9 | 16:37:46 | 0.83 | 'Annacis_Island_CTD6-9_26-Jan-17.txt' |
| CTD6-10 | CTD6 | 10 | 17:01:26 | 0.77 | 'Annacis_Island_CTD6-10_26-Jan-17.txt' |
| CTD6-11 | CTD6 | 11 | 18:24:38 | 0.40 | 'Annacis_Island_CTD6-11_26-Jan-17.txt' |
| CTD6-12 | CTD6 | 12 | 19:28:10 | 0.20 | 'Annacis_Island_CTD6-12_26-Jan-17.txt' |
| CTD6-13 | CTD6 | 13 | 20:22:15 | 0.21 | 'Annacis_Island_CTD6-13_26-Jan-17.txt' |
| CTD6-14 | CTD6 | 14 | 21:12:56 | 0.34 | 'Annacis_Island_CTD6-14_26-Jan-17.txt' |
| CTD6-15 | CTD6 | 15 | 21:58:24 | 0.47 | 'Annacis_Island_CTD6-15_26-Jan-17.txt' |
| CTD6-16 | CTD6 | 16 | 22:37:29 | 0.56 | 'Annacis_Island_CTD6-16_26-Jan-17.txt' |

**Table 3: 31 January 2017 CTD Profile Summary**

| CTD Profile Name | Station | Iteration | Time (UTC) | Tide Level at New Westminster (7654) | Data File Name |
|---|---|---|---|---|---|
| CTD1-17 | CTD1 | 17 | 18:24:42 | 0.87 | 'Annacis_Island_CTD1-17_31-Jan-17.txt' |
| CTD1-18 | CTD1 | 18 | 19:21:08 | 0.70 | 'Annacis_Island_CTD1-18_31-Jan-17.txt' |
| CTD1-19 | CTD1 | 19 | 20:16:23 | 0.38 | 'Annacis_Island_CTD1-19_31-Jan-17.txt' |
| CTD1-20 | CTD1 | 20 | 21:14:22 | -0.04 | 'Annacis_Island_CTD1-20_31-Jan-17.txt' |
| CTD1-21 | CTD1 | 21 | 22:18:54 | -0.40 | 'Annacis_Island_CTD1-21_31-Jan-17.txt' |
| CTD2-17 | CTD2 | 17 | 18:29:16 | 0.86 | 'Annacis_Island_CTD2-17_31-Jan-17.txt' |
| CTD2-18 | CTD2 | 18 | 19:24:52 | 0.68 | 'Annacis_Island_CTD2-18_31-Jan-17.txt' |
| CTD2-19 | CTD2 | 19 | 20:22:21 | 0.34 | 'Annacis_Island_CTD2-19_31-Jan-17.txt' |
| CTD2-20* | CTD2 | 20 | 21:18:31 | -0.07 | N/A |
| CTD2-21 | CTD2 | 21 | 22:26:04 | -0.43 | 'Annacis_Island_CTD2-21_31-Jan-17.txt' |
| CTD3-17 | CTD3 | 17 | 18:35:36 | 0.85 | 'Annacis_Island_CTD3-17_31-Jan-17.txt' |
| CTD3-18 | CTD3 | 18 | 19:30:11 | 0.66 | 'Annacis_Island_CTD3-18_31-Jan-17.txt' |
| CTD3-19 | CTD3 | 19 | 20:28:52 | 0.30 | 'Annacis_Island_CTD3-19_31-Jan-17.txt' |
| CTD3-20 | CTD3 | 20 | 21:27:50 | -0.13 | 'Annacis_Island_CTD3-20_31-Jan-17.txt' |
| CTD3-21 | CTD3 | 21 | 22:31:17 | -0.45 | 'Annacis_Island_CTD3-21_31-Jan-17.txt' |
| CTD4-17 | CTD4 | 17 | 18:51:48 | 0.80 | 'Annacis_Island_CTD4-17_31-Jan-17.txt' |
| CTD4-18 | CTD4 | 18 | 19:36:26 | 0.62 | 'Annacis_Island_CTD4-18_31-Jan-17.txt' |

| CTD Profile Name | Station | Iteration | Time (UTC) | Tide Level at New Westminster (7654) | Data File Name |
|---|---|---|---|---|---|
| CTD4-19 | CTD4 | 19 | 20:35:17 | 0.25 | 'Annacis_Island_CTD4-19_31-Jan-17.txt' |
| CTD4-20 | CTD4 | 20 | 21:33:26 | -0.17 | 'Annacis_Island_CTD4-20_31-Jan-17.txt' |
| CTD4-21 | CTD4 | 21 | 22:37:45 | -0.46 | 'Annacis_Island_CTD4-21_31-Jan-17.txt' |
| CTD5-17 | CTD5 | 17 | 18:57:01 | 0.79 | 'Annacis_Island_CTD5-17_31-Jan-17.txt' |
| CTD5-18 | CTD5 | 18 | 19:44:16 | 0.58 | 'Annacis_Island_CTD5-18_31-Jan-17.txt' |
| CTD5-19 | CTD5 | 19 | 20:42:31 | 0.20 | 'Annacis_Island_CTD5-19_31-Jan-17.txt' |
| CTD5-20 | CTD5 | 20 | 21:42:42 | -0.22 | 'Annacis_Island_CTD5-20_31-Jan-17.txt' |
| CTD5-21 | CTD5 | 21 | 22:43:26 | -0.48 | 'Annacis_Island_CTD5-21_31-Jan-17.txt' |
| CTD6-17 | CTD6 | 17 | 19:03:11 | 0.77 | 'Annacis_Island_CTD6-17_31-Jan-17.txt' |
| CTD6-18 | CTD6 | 18 | 19:50:25 | 0.55 | 'Annacis_Island_CTD6-18_31-Jan-17.txt' |
| CTD6-19 | CTD6 | 19 | 20:52:41 | 0.12 | 'Annacis_Island_CTD6-19_31-Jan-17.txt' |
| CTD6-20 | CTD6 | 20 | 21:50:23 | -0.28 | 'Annacis_Island_CTD6-20_31-Jan-17.txt' |
| CTD6-21 | CTD6 | 21 | 22:49:37 | -0.49 | 'Annacis_Island_CTD6-21_31-Jan-17.txt' |

* Profile did not record correctly

**Table 4: 1 February 2017 CTD Profile Summary**

| CTD Profile Name | Station | Iteration | Time (UTC) | Tide Level at New Westminster (7654) | Data File Name |
|---|---|---|---|---|---|
| CTD1-22* | CTD1 | 22 | 16:10:54 | 0.68 | N/A |
| CTD1-23 | CTD1 | 23 | 17:23:06 | 0.94 | 'Annacis_Island_CTD1-23_01-Feb-17.txt' |
| CTD1-24 | CTD1 | 24 | 18:36:52 | 0.89 | 'Annacis_Island_CTD1-24_01-Feb-17.txt' |
| CTD1-25 | CTD1 | 25 | 19:28:38 | 0.71 | 'Annacis_Island_CTD1-25_01-Feb-17.txt' |
| CTD1-26 | CTD1 | 26 | 20:36:29 | 0.36 | 'Annacis_Island_CTD1-26_01-Feb-17.txt' |
| CTD1-27 | CTD1 | 27 | 21:22:22 | 0.01 | 'Annacis_Island_CTD1-27_01-Feb-17.txt' |
| CTD2-22 | CTD2 | 22 | 16:42:12 | 0.83 | 'Annacis_Island_CTD2-22_01-Feb-17.txt' |
| CTD2-23 | CTD2 | 23 | 17:29:43 | 0.95 | 'Annacis_Island_CTD2-23_01-Feb-17.txt' |
| CTD2-24 | CTD2 | 24 | 18:43:17 | 0.86 | 'Annacis_Island_CTD2-24_01-Feb-17.txt' |
| CTD2-25 | CTD2 | 25 | 19:32:27 | 0.69 | 'Annacis_Island_CTD2-25_01-Feb-17.txt' |
| CTD2-26 | CTD2 | 26 | 20:40:35 | 0.33 | 'Annacis_Island_CTD2-26_01-Feb-17.txt' |
| CTD2-27 | CTD2 | 27 | 21:27:28 | -0.03 | 'Annacis_Island_CTD2-27_01-Feb-17.txt' |
| CTD3-22 | CTD3 | 22 | 16:35:58 | 0.80 | 'Annacis_Island_CTD3-22_01-Feb-17.txt' |
| CTD3-23 | CTD3 | 23 | 17:35:12 | 0.96 | 'Annacis_Island_CTD3-23_01-Feb-17.txt' |
| CTD3-24 | CTD3 | 24 | 18:48:34 | 0.85 | 'Annacis_Island_CTD3-24_01-Feb-17.txt' |
| CTD3-25 | CTD3 | 25 | 19:40:15 | 0.66 | 'Annacis_Island_CTD3-25_01-Feb-17.txt' |
| CTD3-26 | CTD3 | 26 | 20:45:38 | 0.29 | 'Annacis_Island_CTD3-26_01-Feb-17.txt' |
| CTD3-27 | CTD3 | 27 | 21:44:14 | -0.16 | 'Annacis_Island_CTD3-27_01-Feb-17.txt' |
| CTD4-22 | CTD4 | 22 | 16:56:17 | 0.88 | 'Annacis_Island_CTD4-22_01-Feb-17.txt' |
| CTD4-23 | CTD4 | 23 | 17:43:46 | 0.96 | 'Annacis_Island_CTD4-23_01-Feb-17.txt' |
| CTD4-24 | CTD4 | 24 | 18:55:19 | 0.83 | 'Annacis_Island_CTD4-24_01-Feb-17.txt' |
| CTD4-25 | CTD4 | 25 | 19:45:32 | 0.64 | 'Annacis_Island_CTD4-25_01-Feb-17.txt' |
| CTD4-26 | CTD4 | 26 | 20:51:45 | 0.25 | 'Annacis_Island_CTD4-26_01-Feb-17.txt' |
| CTD4-27 | CTD4 | 27 | 22:00:09 | -0.27 | 'Annacis_Island_CTD4-27_01-Feb-17.txt' |

| CTD Profile Name | Station | Iteration | Time (UTC) | Tide Level at New Westminster (7654) | Data File Name |
|---|---|---|---|---|---|
| CTD5-22 | CTD5 | 22 | 16:29:41 | 0.77 | 'Annacis_Island_CTD5-22_01-Feb-17.txt' |
| CTD5-23 | CTD5 | 23 | 17:51:25 | 0.97 | 'Annacis_Island_CTD5-23_01-Feb-17.txt' |
| CTD5-24 | CTD5 | 24 | 19:03:00 | 0.80 | 'Annacis_Island_CTD5-24_01-Feb-17.txt' |
| CTD5-25 | CTD5 | 25 | 19:50:34 | 0.62 | 'Annacis_Island_CTD5-25_01-Feb-17.txt' |
| CTD5-26 | CTD5 | 26 | 20:58:40 | 0.19 | 'Annacis_Island_CTD5-26_01-Feb-17.txt' |
| CTD5-27 | CTD5 | 27 | 22:05:44 | -0.31 | 'Annacis_Island_CTD5-27_01-Feb-17.txt' |
| CTD6-22 | CTD6 | 22 | 16:49:36 | 0.85 | 'Annacis_Island_CTD6-22_01-Feb-17.txt' |
| CTD6-23 | CTD6 | 23 | 17:59:21 | 0.96 | 'Annacis_Island_CTD6-23_01-Feb-17.txt' |
| CTD6-24 | CTD6 | 24 | 19:09:06 | 0.78 | 'Annacis_Island_CTD6-24_01-Feb-17.txt' |
| CTD6-25 | CTD6 | 25 | 19:57:42 | 0.59 | 'Annacis_Island_CTD6-25_01-Feb-17.txt' |
| CTD6-26 | CTD6 | 26 | 21:06:45 | 0.13 | 'Annacis_Island_CTD6-26_01-Feb-17.txt' |
| CTD6-27 | CTD6 | 27 | 22:11:17 | -0.37 | 'Annacis_Island_CTD6-27_01-Feb-17.txt' |
| CTD7-22 | CTD7 | 22 | 17:09:53 | 0.91 | 'Annacis_Island_CTD7-22_01-Feb-17.txt' |
| CTD7-23 | CTD7 | 23 | 18:11:21 | 0.95 | 'Annacis_Island_CTD7-23_01-Feb-17.txt' |
| CTD7-24 | CTD7 | 24 | 19:17:56 | 0.75 | 'Annacis_Island_CTD7-24_01-Feb-17.txt' |

* Profile did not record correctly

**Table 5: 7 February 2017 CTD Profile Summary**

| CTD Profile Name | Station | Iteration | Time (UTC) | Tide Level at New Westminster (7654) | Data File Name |
|---|---|---|---|---|---|
| CTD1-28 | CTD1 | 28 | 16:47:05 | 0.52 | 'Annacis_Island_CTD1-28_07-Feb-17.txt' |
| CTD1-29 | CTD1 | 29 | 17:52:39 | 0.48 | 'Annacis_Island_CTD1-29_07-Feb-17.txt' |
| CTD1-30 | CTD1 | 30 | 18:51:12 | 0.65 | 'Annacis_Island_CTD1-30_07-Feb-17.txt' |
| CTD1-31 | CTD1 | 31 | 20:01:18 | 0.92 | 'Annacis_Island_CTD1-31_07-Feb-17.txt' |
| CTD1-32 | CTD1 | 32 | 20:50:36 | 1.04 | 'Annacis_Island_CTD1-32_07-Feb-17.txt' |
| CTD1-33 | CTD1 | 33 | 21:44:30 | 1.13 | 'Annacis_Island_CTD1-33_07-Feb-17.txt' |
| CTD2-28 | CTD2 | 28 | 16:51:10 | 0.51 | 'Annacis_Island_CTD2-28_07-Feb-17.txt' |
| CTD2-29 | CTD2 | 29 | 17:57:11 | 0.49 | 'Annacis_Island_CTD2-29_07-Feb-17.txt' |
| CTD2-30 | CTD2 | 30 | 19:01:59 | 0.69 | 'Annacis_Island_CTD2-30_07-Feb-17.txt' |
| CTD2-31 | CTD2 | 31 | 20:05:52 | 0.93 | 'Annacis_Island_CTD2-31_07-Feb-17.txt' |
| CTD2-32 | CTD2 | 32 | 21:01:25 | 1.07 | 'Annacis_Island_CTD2-32_07-Feb-17.txt' |
| CTD2-33 | CTD2 | 33 | 21:48:43 | 1.14 | 'Annacis_Island_CTD2-33_07-Feb-17.txt' |
| CTD3-28 | CTD3 | 28 | 17:02:59 | 0.49 | 'Annacis_Island_CTD3-28_07-Feb-17.txt' |
| CTD3-29 | CTD3 | 29 | 18:02:32 | 0.50 | 'Annacis_Island_CTD3-29_07-Feb-17.txt' |
| CTD3-30 | CTD3 | 30 | 19:06:19 | 0.71 | 'Annacis_Island_CTD3-30_07-Feb-17.txt' |
| CTD3-31 | CTD3 | 31 | 20:11:04 | 0.95 | 'Annacis_Island_CTD3-31_07-Feb-17.txt' |
| CTD3-32 | CTD3 | 32 | 21:05:49 | 1.08 | 'Annacis_Island_CTD3-32_07-Feb-17.txt' |
| CTD3-33 | CTD3 | 33 | 21:53:11 | 1.14 | 'Annacis_Island_CTD3-33_07-Feb-17.txt' |
| CTD4-28 | CTD4 | 28 | 17:08:28 | 0.49 | 'Annacis_Island_CTD4-28_07-Feb-17.txt' |
| CTD4-29 | CTD4 | 29 | 18:08:41 | 0.51 | 'Annacis_Island_CTD4-29_07-Feb-17.txt' |
| CTD4-30 | CTD4 | 30 | 19:21:22 | 0.77 | 'Annacis_Island_CTD4-30_07-Feb-17.txt' |
| CTD4-31 | CTD4 | 31 | 20:17:01 | 0.97 | 'Annacis_Island_CTD4-31_07-Feb-17.txt' |

| CTD Profile Name | Station | Iteration | Time (UTC) | Tide Level at New Westminster (7654) | Data File Name |
|---|---|---|---|---|---|
| CTD4-32 | CTD4 | 32 | 21:14:53 | 1.09 | 'Annacis_Island_CTD4-32_07-Feb-17.txt' |
| CTD4-33* | CTD4 | 33 | 21:58:10 | 1.14 | N/A |
| CTD5-28 | CTD5 | 28 | 17:14:59 | 0.48 | 'Annacis_Island_CTD5-28_07-Feb-17.txt' |
| CTD5-29 | CTD5 | 29 | 18:14:28 | 0.52 | 'Annacis_Island_CTD5-29_07-Feb-17.txt' |
| CTD5-30 | CTD5 | 30 | 19:25:50 | 0.79 | 'Annacis_Island_CTD5-30_07-Feb-17.txt' |
| CTD5-31 | CTD5 | 31 | 20:21:41 | 0.97 | 'Annacis_Island_CTD5-31_07-Feb-17.txt' |
| CTD5-32 | CTD5 | 32 | 21:21:44 | 1.11 | 'Annacis_Island_CTD5-32_07-Feb-17.txt' |
| CTD5-33 | CTD5 | 33 | 22:04:36 | 1.15 | 'Annacis_Island_CTD5-33_07-Feb-17.txt' |
| CTD6-28 | CTD6 | 28 | 17:25:36 | 0.47 | 'Annacis_Island_CTD6-28_07-Feb-17.txt' |
| CTD6-29 | CTD6 | 29 | 18:22:26 | 0.54 | 'Annacis_Island_CTD6-29_07-Feb-17.txt' |
| CTD6-30 | CTD6 | 30 | 19:37:28 | 0.84 | 'Annacis_Island_CTD6-30_07-Feb-17.txt' |
| CTD6-31 | CTD6 | 31 | 20:30:27 | 1.00 | 'Annacis_Island_CTD6-31_07-Feb-17.txt' |
| CTD6-32 | CTD6 | 32 | 21:28:06 | 1.11 | 'Annacis_Island_CTD6-32_07-Feb-17.txt' |
| CTD6-33 | CTD6 | 33 | 22:12:52 | 1.15 | 'Annacis_Island_CTD6-33_07-Feb-17.txt' |
| CTD7-29 | CTD7 | 29 | 18:34:47 | 0.58 | 'Annacis_Island_CTD7-29_07-Feb-17.txt' |
| CTD7-30 | CTD7 | 30 | 19:47:44 | 0.88 | 'Annacis_Island_CTD7-30_07-Feb-17.txt' |
| CTD7-31 | CTD7 | 31 | 20:38:49 | 1.02 | 'Annacis_Island_CTD7-31_07-Feb-17.txt' |

* Profile did not record correctly

**Table 6: 9 February 2017 CTD Profile Summary**

| CTD Profile Name | Station | Iteration | Time (UTC) | Tide Level at New Westminster (7654) | Data File Name |
|---|---|---|---|---|---|
| CTD1-34 | CTD1 | 34 | 17:51:26 | 0.80 | 'Annacis_Island_CTD1-34_09-Feb-17.txt' |
| CTD1-35 | CTD1 | 35 | 18:26:32 | 0.67 | 'Annacis_Island_CTD1-35_09-Feb-17.txt' |
| CTD1-36 | CTD1 | 36 | 19:43:06 | 0.52 | 'Annacis_Island_CTD1-36_09-Feb-17.txt' |
| CTD1-37 | CTD1 | 37 | 20:42:19 | 0.74 | 'Annacis_Island_CTD1-37_09-Feb-17.txt' |
| CTD1-38 | CTD1 | 38 | 21:41:07 | 1.02 | 'Annacis_Island_CTD1-38_09-Feb-17.txt' |
| CTD1-39 | CTD1 | 39 | 22:50:53 | 1.25 | 'Annacis_Island_CTD1-39_09-Feb-17.txt' |
| CTD1-40 | CTD1 | 40 | 23:52:29 | 1.38 | 'Annacis_Island_CTD1-40_09-Feb-17.txt' |
| CTD2-34 | CTD2 | 34 | 17:55:46 | 0.78 | 'Annacis_Island_CTD2-34_09-Feb-17.txt' |
| CTD2-35 | CTD2 | 35 | 18:30:55 | 0.65 | 'Annacis_Island_CTD2-35_09-Feb-17.txt' |
| CTD2-36 | CTD2 | 36 | 19:49:23 | 0.52 | 'Annacis_Island_CTD2-36_09-Feb-17.txt' |
| CTD2-37 | CTD2 | 37 | 20:47:12 | 0.77 | 'Annacis_Island_CTD2-37_09-Feb-17.txt' |
| CTD2-38 | CTD2 | 38 | 21:45:27 | 1.04 | 'Annacis_Island_CTD2-38_09-Feb-17.txt' |
| CTD2-39 | CTD2 | 39 | 22:55:23 | 1.25 | 'Annacis_Island_CTD2-39_09-Feb-17.txt' |
| CTD2-40 | CTD2 | 40 | 23:56:09 | 1.39 | 'Annacis_Island_CTD2-40_09-Feb-17.txt' |
| CTD3-34 | CTD3 | 34 | 18:00:46 | 0.76 | 'Annacis_Island_CTD3-34_09-Feb-17.txt' |
| CTD3-35 | CTD3 | 35 | 18:35:43 | 0.63 | 'Annacis_Island_CTD3-35_09-Feb-17.txt' |
| CTD3-36 | CTD3 | 36 | 19:54:48 | 0.54 | 'Annacis_Island_CTD3-36_09-Feb-17.txt' |
| CTD3-37 | CTD3 | 37 | 20:51:34 | 0.78 | 'Annacis_Island_CTD3-37_09-Feb-17.txt' |
| CTD3-38 | CTD3 | 38 | 21:52:38 | 1.06 | 'Annacis_Island_CTD3-38_09-Feb-17.txt' |
| CTD3-39 | CTD3 | 39 | 22:59:20 | 1.26 | 'Annacis_Island_CTD3-39_09-Feb-17.txt' |
| CTD3-40** | CTD3 | 40 | 0:09:54 | 1.39 | 'Annacis_Island_CTD3-40_10-Feb-17.txt' |

| CTD Profile Name | Station | Iteration | Time (UTC) | Tide Level at New Westminster (7654) | Data File Name |
|---|---|---|---|---|---|
| CTD4-34 | CTD4 | 34 | 18:06:41 | 0.74 | 'Annacis_Island_CTD4-34_09-Feb-17.txt' |
| CTD4-35 | CTD4 | 35 | 18:41:05 | 0.62 | 'Annacis_Island_CTD4-35_09-Feb-17.txt' |
| CTD4-36 | CTD4 | 36 | 19:59:57 | 0.55 | 'Annacis_Island_CTD4-36_09-Feb-17.txt' |
| CTD4-37 | CTD4 | 37 | 20:56:48 | 0.82 | 'Annacis_Island_CTD4-37_09-Feb-17.txt' |
| CTD4-38 | CTD4 | 38 | 21:57:35 | 1.09 | 'Annacis_Island_CTD4-38_09-Feb-17.txt' |
| CTD4-39 | CTD4 | 39 | 23:04:31 | 1.28 | 'Annacis_Island_CTD4-39_09-Feb-17.txt' |
| CTD4-40** | CTD4 | 40 | 0:13:54 | 1.40 | 'Annacis_Island_CTD4-40_10-Feb-17.txt' |
| CTD5-34 | CTD5 | 34 | 18:12:32 | 0.72 | 'Annacis_Island_CTD5-34_09-Feb-17.txt' |
| CTD5-35 | CTD5 | 35 | 18:48:34 | 0.59 | 'Annacis_Island_CTD5-35_09-Feb-17.txt' |
| CTD5-36 | CTD5 | 36 | 20:07:06 | 0.57 | 'Annacis_Island_CTD5-36_09-Feb-17.txt' |
| CTD5-37 | CTD5 | 37 | 21:04:12 | 0.86 | 'Annacis_Island_CTD5-37_09-Feb-17.txt' |
| CTD5-38 | CTD5 | 38 | 22:02:21 | 1.11 | 'Annacis_Island_CTD5-38_09-Feb-17.txt' |
| CTD5-39 | CTD5 | 39 | 23:09:03 | 1.30 | 'Annacis_Island_CTD5-39_09-Feb-17.txt' |
| CTD5-40** | CTD5 | 40 | 0:17:29 | 1.40 | 'Annacis_Island_CTD5-40_10-Feb-17.txt' |
| CTD6-34 | CTD6 | 34 | 18:19:44 | 0.70 | 'Annacis_Island_CTD6-34_09-Feb-17.txt' |
| CTD6-35 | CTD6 | 35 | 18:56:43 | 0.56 | 'Annacis_Island_CTD6-35_09-Feb-17.txt' |
| CTD6-36 | CTD6 | 36 | 20:16:46 | 0.61 | 'Annacis_Island_CTD6-36_09-Feb-17.txt' |
| CTD6-37 | CTD6 | 37 | 21:11:48 | 0.89 | 'Annacis_Island_CTD6-37_09-Feb-17.txt' |
| CTD6-38 | CTD6 | 38 | 22:08:53 | 1.13 | 'Annacis_Island_CTD6-38_09-Feb-17.txt' |
| CTD6-39 | CTD6 | 39 | 23:15:57 | 1.31 | 'Annacis_Island_CTD6-39_09-Feb-17.txt' |
| CTD6-40** | CTD6 | 40 | 0:22:41 | 1.40 | 'Annacis_Island_CTD6-40_10-Feb-17.txt' |
| CTD7-35 | CTD7 | 35 | 19:05:37 | 0.54 | 'Annacis_Island_CTD7-35_09-Feb-17.txt' |
| CTD7-37 | CTD7 | 37 | 21:24:58 | 0.95 | 'Annacis_Island_CTD7-37_09-Feb-17.txt' |
| CTD7-38 | CTD7 | 38 | 22:25:05 | 1.18 | 'Annacis_Island_CTD7-38_09-Feb-17.txt' |
| CTD7-39 | CTD7 | 39 | 23:23:42 | 1.33 | 'Annacis_Island_CTD7-39_09-Feb-17.txt' |

** UTC Date is 10 February 2017

**Table 7: 14 February 2017 CTD Profile Summary**

| CTD Profile Name | Station | Iteration | Time (UTC) | Tide Level at New Westminster (7654) | Data File Name |
|---|---|---|---|---|---|
| CTD1-41 | CTD1 | 41 | 16:23:13 | 1.03 | 'Annacis_Island_CTD1-41_14-Feb-17.txt' |
| CTD1-42 | CTD1 | 42 | 21:56:14 | -0.38 | 'Annacis_Island_CTD1-42_14-Feb-17.txt' |
| CTD2-41 | CTD2 | 41 | 16:31:12 | 1.05 | 'Annacis_Island_CTD2-41_14-Feb-17.txt' |
| CTD2-42 | CTD2 | 42 | 22:01:08 | -0.41 | 'Annacis_Island_CTD2-42_14-Feb-17.txt' |
| CTD3-41 | CTD3 | 41 | 16:36:09 | 1.06 | 'Annacis_Island_CTD3-41_14-Feb-17.txt' |
| CTD3-42 | CTD3 | 42 | 22:07:21 | -0.43 | 'Annacis_Island_CTD3-42_14-Feb-17.txt' |
| CTD4-41 | CTD4 | 41 | 16:43:11 | 1.07 | 'Annacis_Island_CTD4-41_14-Feb-17.txt' |
| CTD4-42 | CTD4 | 42 | 22:13:45 | -0.46 | 'Annacis_Island_CTD4-42_14-Feb-17.txt' |
| CTD5-41 | CTD5 | 41 | 16:49:03 | 1.08 | 'Annacis_Island_CTD5-41_14-Feb-17.txt' |
| CTD5-42 | CTD5 | 42 | 22:22:36 | -0.50 | 'Annacis_Island_CTD5-42_14-Feb-17.txt' |
| CTD6-41 | CTD6 | 41 | 16:57:16 | 1.08 | 'Annacis_Island_CTD6-41_14-Feb-17.txt' |
| CTD6-42 | CTD6 | 42 | 22:30:05 | -0.53 | 'Annacis_Island_CTD6-42_14-Feb-17.txt' |

**Table 8: 9 March 2017 CTD Profile Summary**

| CTD Profile Name | Station | Iteration | Time (UTC) | Tide Level at New Westminster (7654) | Data File Name |
|---|---|---|---|---|---|
| CTD1-43 | CTD1 | 43 | 16:42:11 | 0.30 | 'Annacis_Island_CTD1-43_09-Mar-17.txt' |
| CTD1-44 | CTD1 | 44 | 20:24:34 | 0.17 | 'Annacis_Island_CTD1-44_09-Mar-17.txt' |
| CTD1-45 | CTD1 | 45 | 22:09:43 | 0.54 | 'Annacis_Island_CTD1-45_09-Mar-17.txt' |
| CTD2-43 | CTD2 | 43 | 16:45:57 | 0.28 | 'Annacis_Island_CTD2-43_09-Mar-17.txt' |
| CTD2-44 | CTD2 | 44 | 20:31:06 | 0.20 | 'Annacis_Island_CTD2-44_09-Mar-17.txt' |
| CTD2-45 | CTD2 | 45 | 22:14:54 | 0.56 | 'Annacis_Island_CTD2-45_09-Mar-17.txt' |
| CTD3-43 | CTD3 | 43 | 16:56:38 | 0.21 | 'Annacis_Island_CTD3-43_09-Mar-17.txt' |
| CTD3-44 | CTD3 | 44 | 20:48:22 | 0.26 | 'Annacis_Island_CTD3-44_09-Mar-17.txt' |
| CTD3-45 | CTD3 | 45 | 22:19:14 | 0.57 | 'Annacis_Island_CTD3-45_09-Mar-17.txt' |
| CTD4-43 | CTD4 | 43 | 17:10:43 | 0.14 | 'Annacis_Island_CTD4-43_09-Mar-17.txt' |
| CTD4-44 | CTD4 | 44 | 21:11:41 | 0.34 | 'Annacis_Island_CTD4-44_09-Mar-17.txt' |
| CTD4-45 | CTD4 | 45 | 22:24:29 | 0.58 | 'Annacis_Island_CTD4-45_09-Mar-17.txt' |
| CTD5-43 | CTD5 | 43 | 17:16:33 | 0.11 | 'Annacis_Island_CTD5-43_09-Mar-17.txt' |
| CTD5-44 | CTD5 | 44 | 21:36:01 | 0.44 | 'Annacis_Island_CTD5-44_09-Mar-17.txt' |
| CTD5-45 | CTD5 | 45 | 22:28:50 | 0.60 | 'Annacis_Island_CTD5-45_09-Mar-17.txt' |
| CTD6-43 | CTD6 | 43 | 17:24:57 | 0.07 | 'Annacis_Island_CTD6-43_09-Mar-17.txt' |
| CTD6-44 | CTD6 | 44 | 21:42:26 | 0.46 | 'Annacis_Island_CTD6-44_09-Mar-17.txt' |
| CTD6-45 | CTD6 | 45 | 22:35:29 | 0.61 | 'Annacis_Island_CTD6-45_09-Mar-17.txt' |
| CTD7-43 | CTD7 | 43 | 17:36:59 | 0.02 | 'Annacis_Island_CTD7-43_09-Mar-17.txt' |
| CTD7-44 | CTD7 | 44 | 21:57:10 | 0.51 | 'Annacis_Island_CTD7-44_09-Mar-17.txt' |

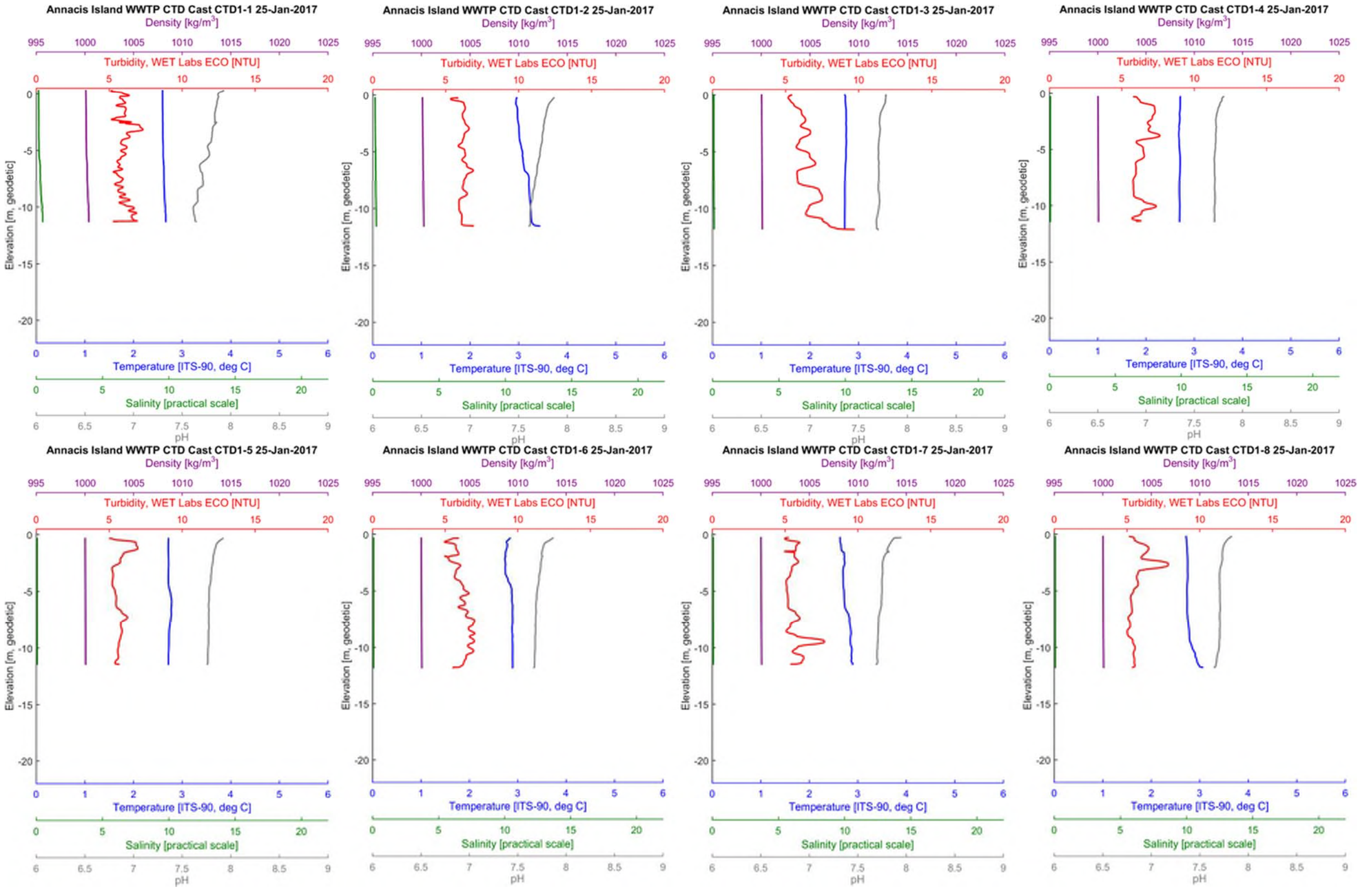


*Figure 1: CTD profiles measured at CTD1 on 25 January 2017*

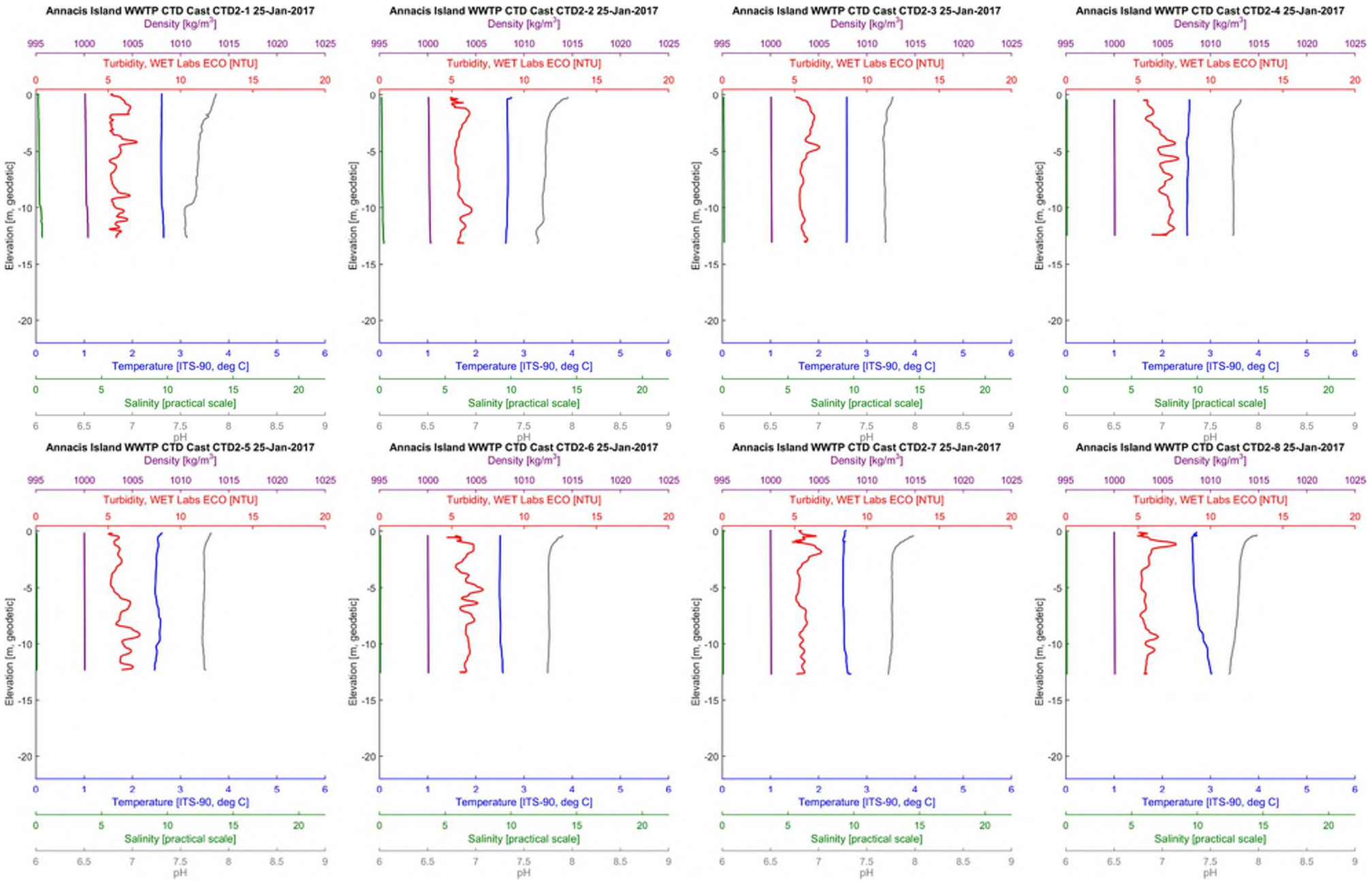


*Figure 2: CTD profiles measured at CTD2 on 25 January 2017*

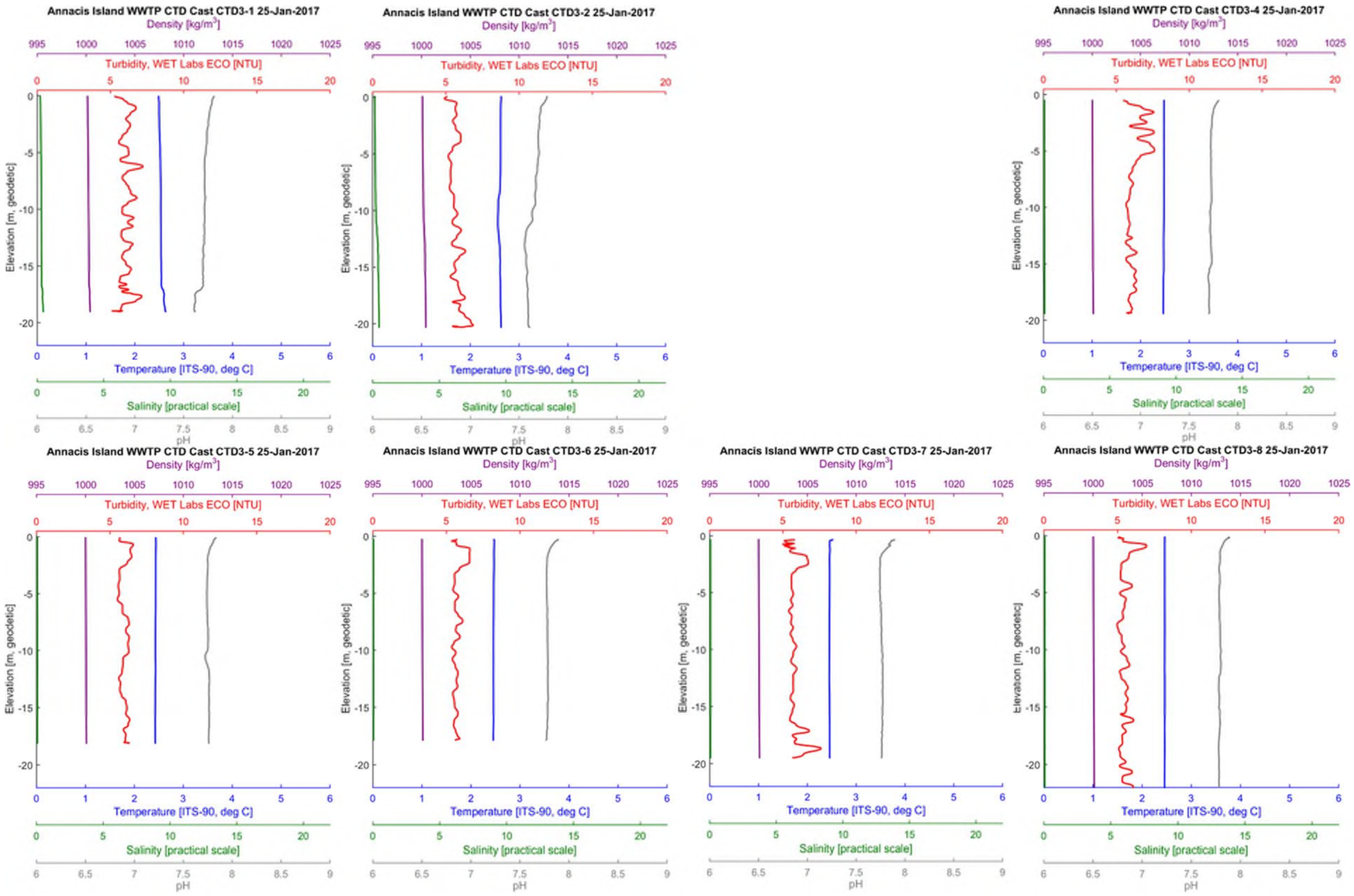


*Figure 3: CTD profiles measured at CTD3 on 25 January 2017*

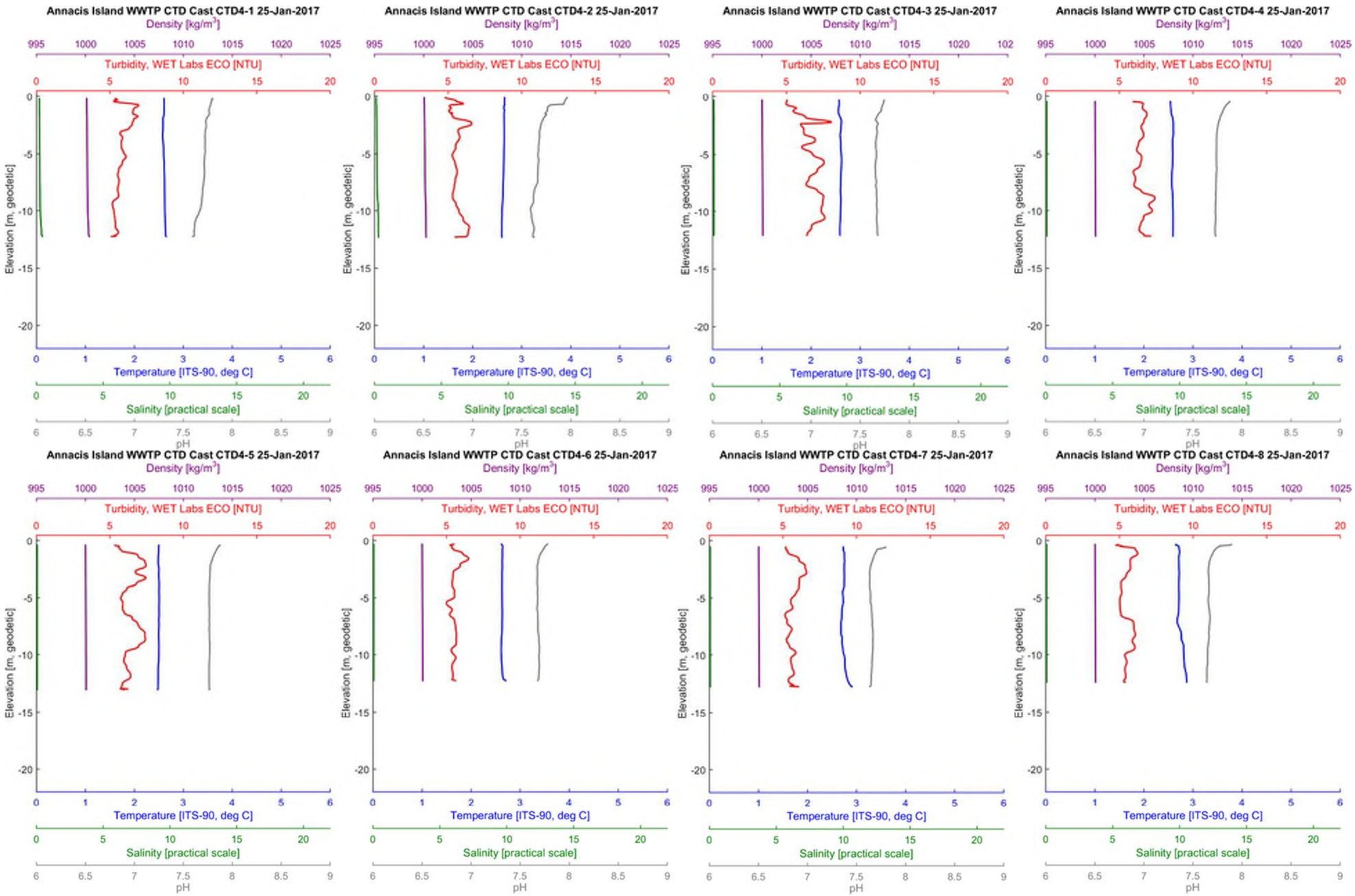


*Figure 4: CTD profiles measured at CTD4 on 25 January 2017*

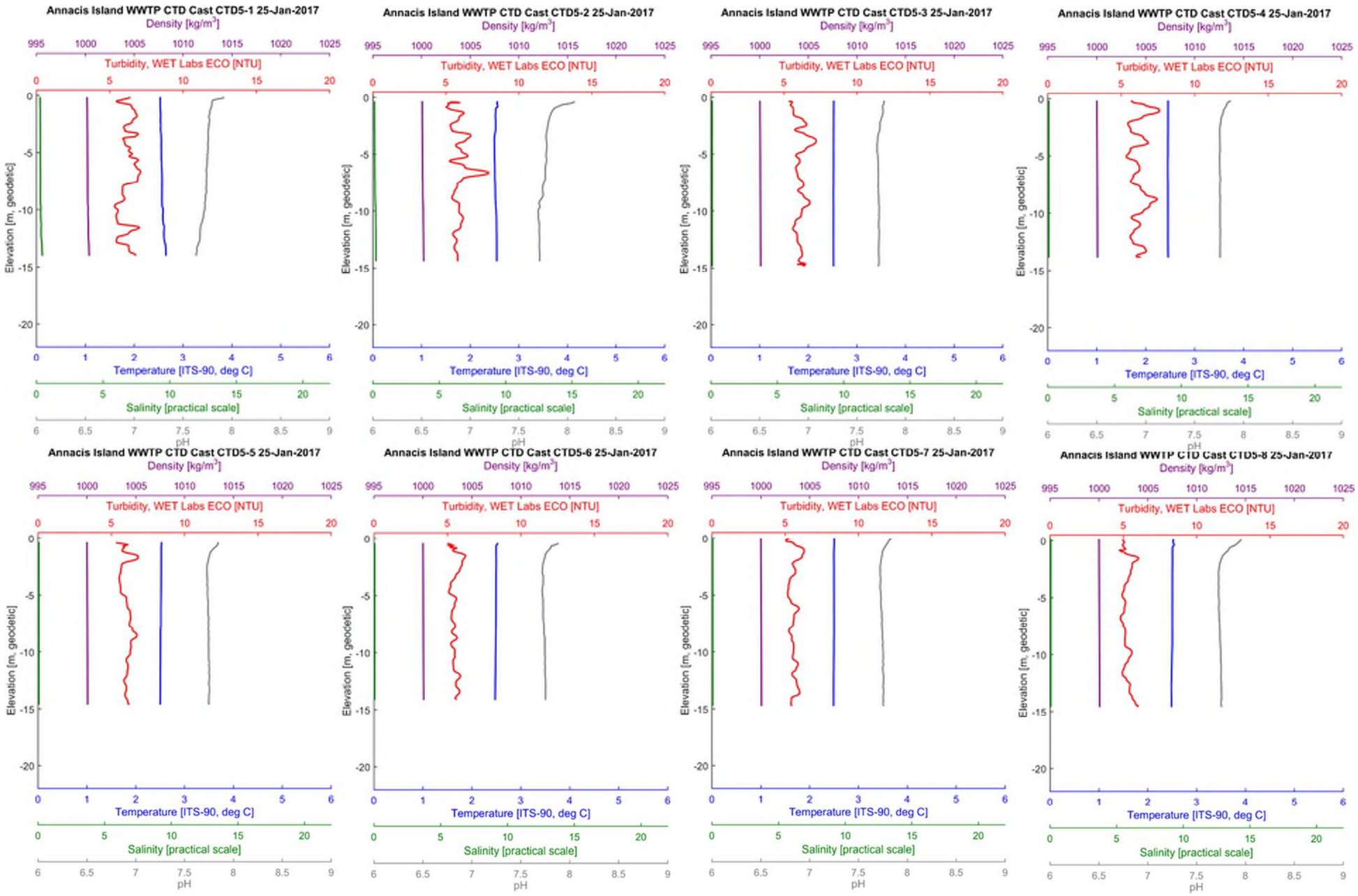


*Figure 5: CTD profiles measured at CTD5 on 25 January 2017*

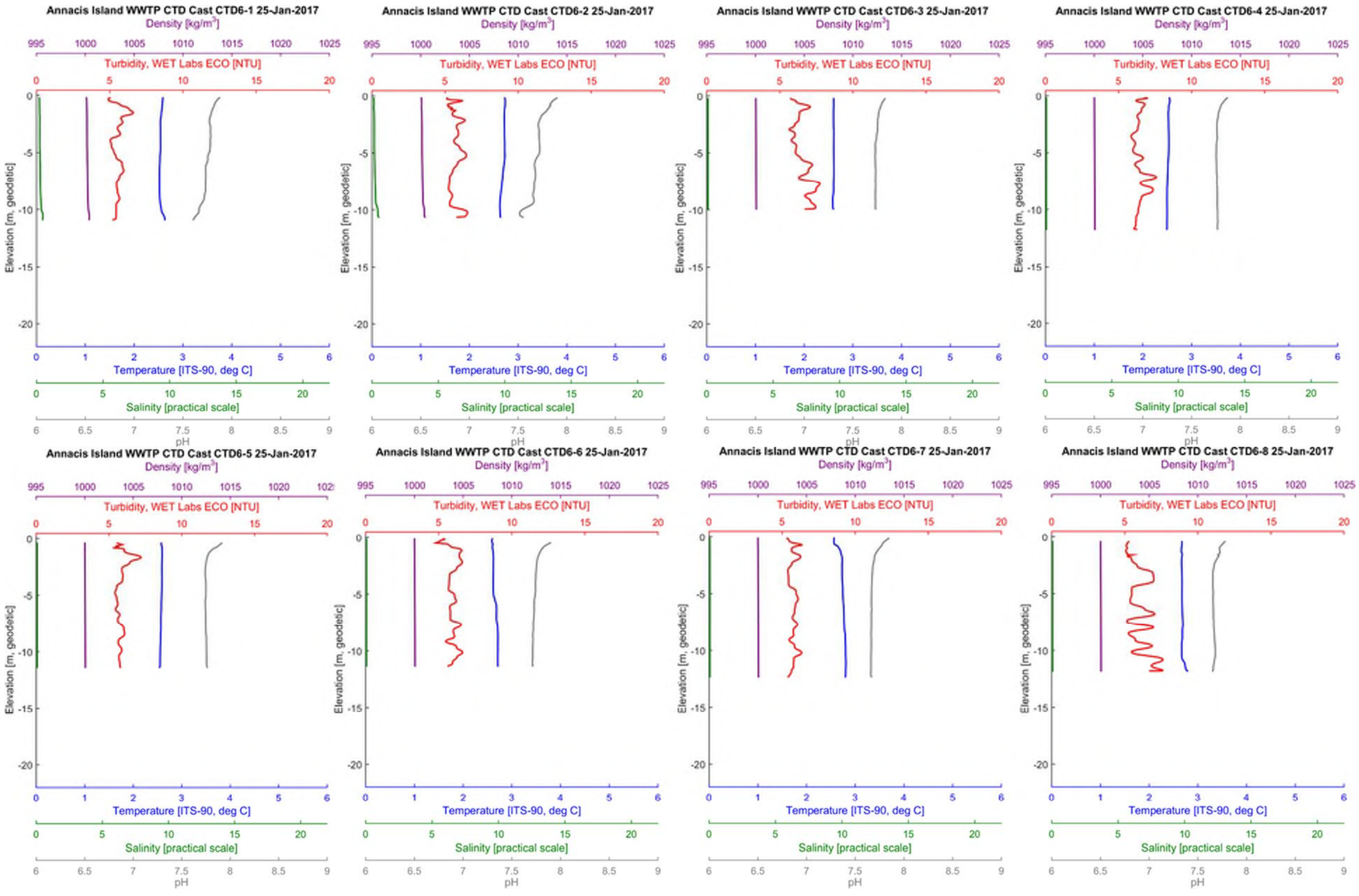


*Figure 6: CTD profiles measured at CTD6 on 25 January 2017*

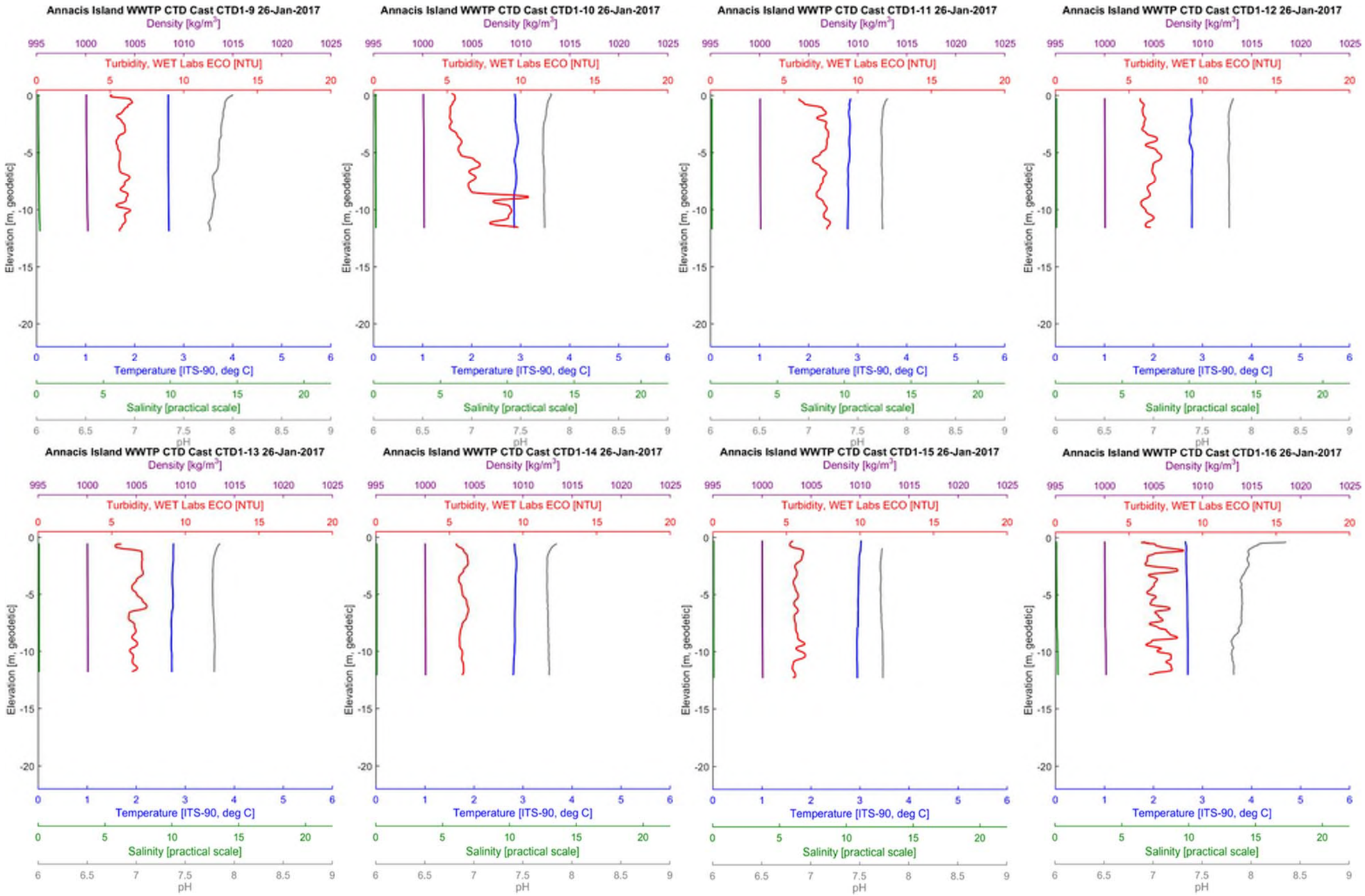


*Figure 7: CTD profiles measured at CTD1 on 26 January 2017*

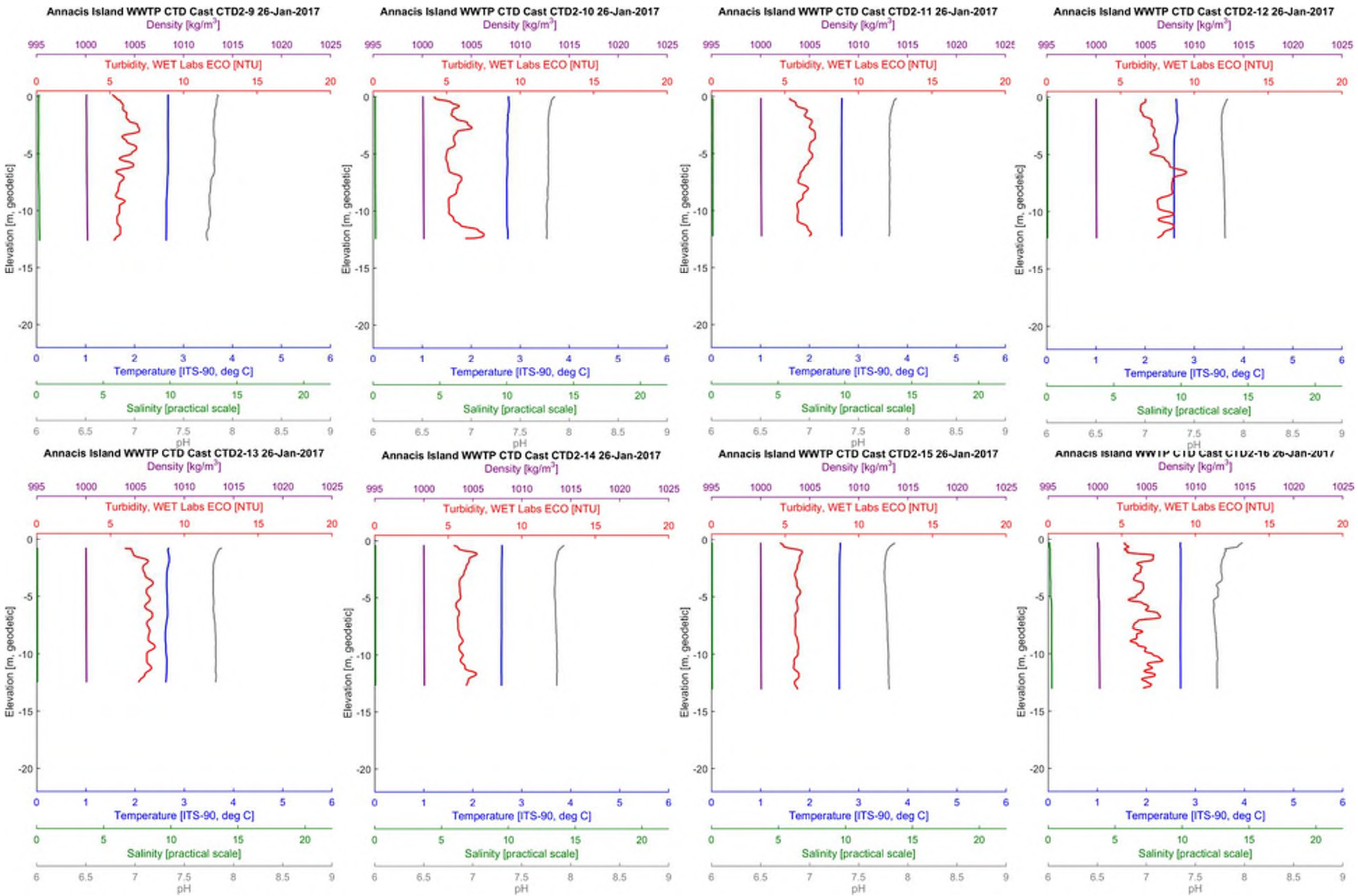


*Figure 8: CTD profiles measured at CTD2 on 26 January 2017*

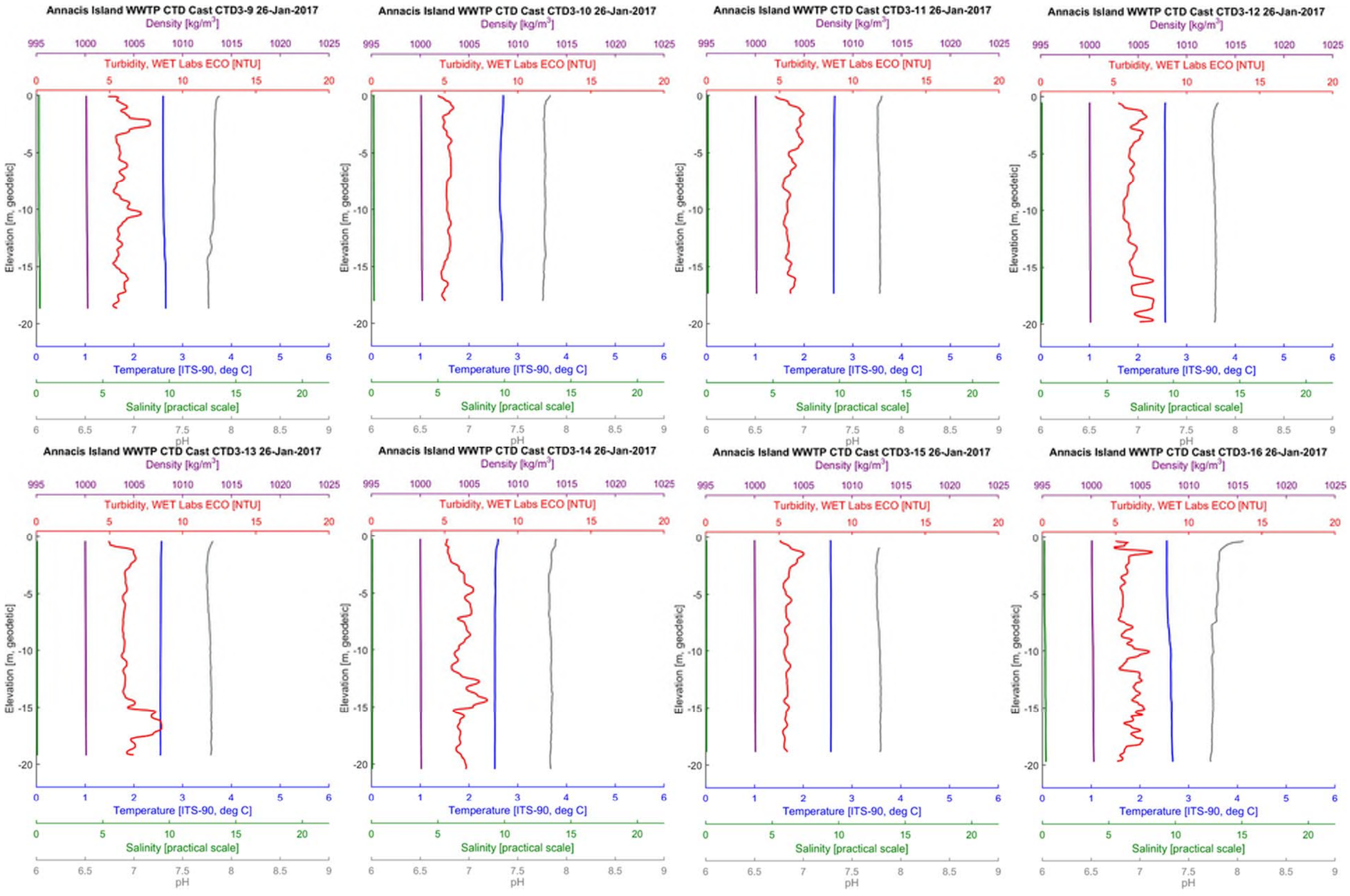


*Figure 9: CTD profiles measured at CTD3 on 26 January 2017*

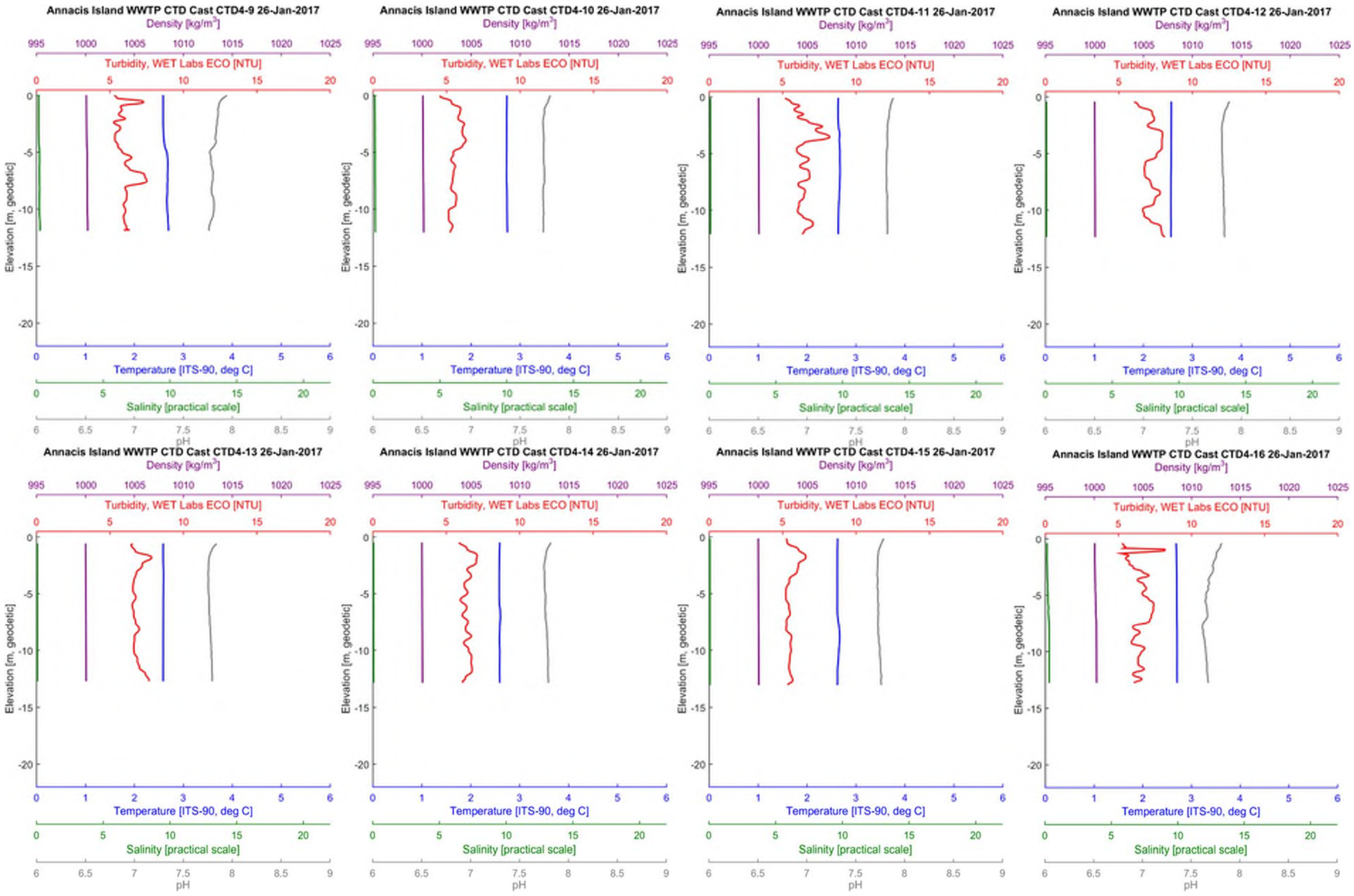


*Figure 10: CTD profiles measured at CTD4 on 26 January 2017*

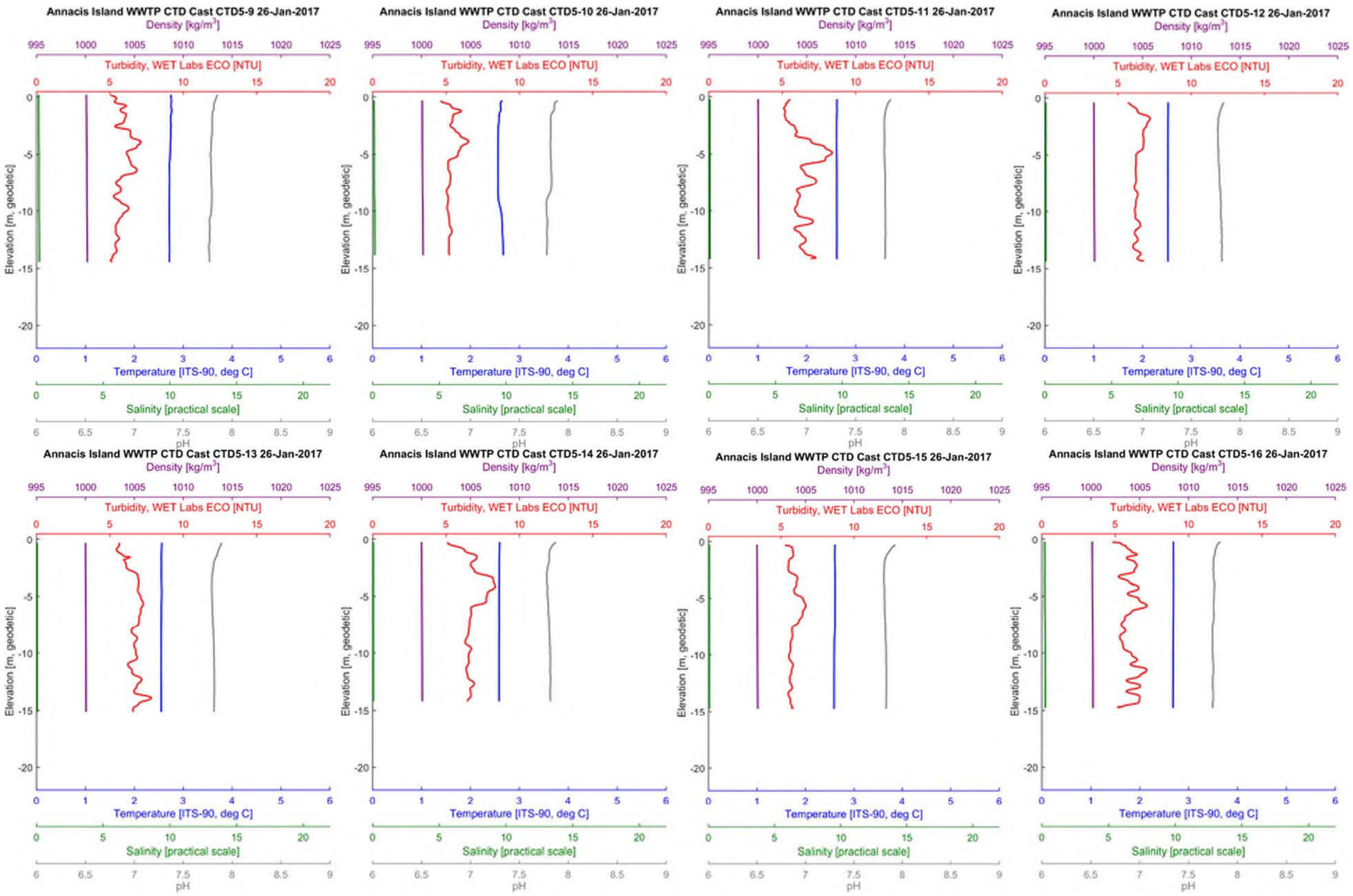


*Figure 11: CTD profiles measured at CTD5 on 26 January 2017*

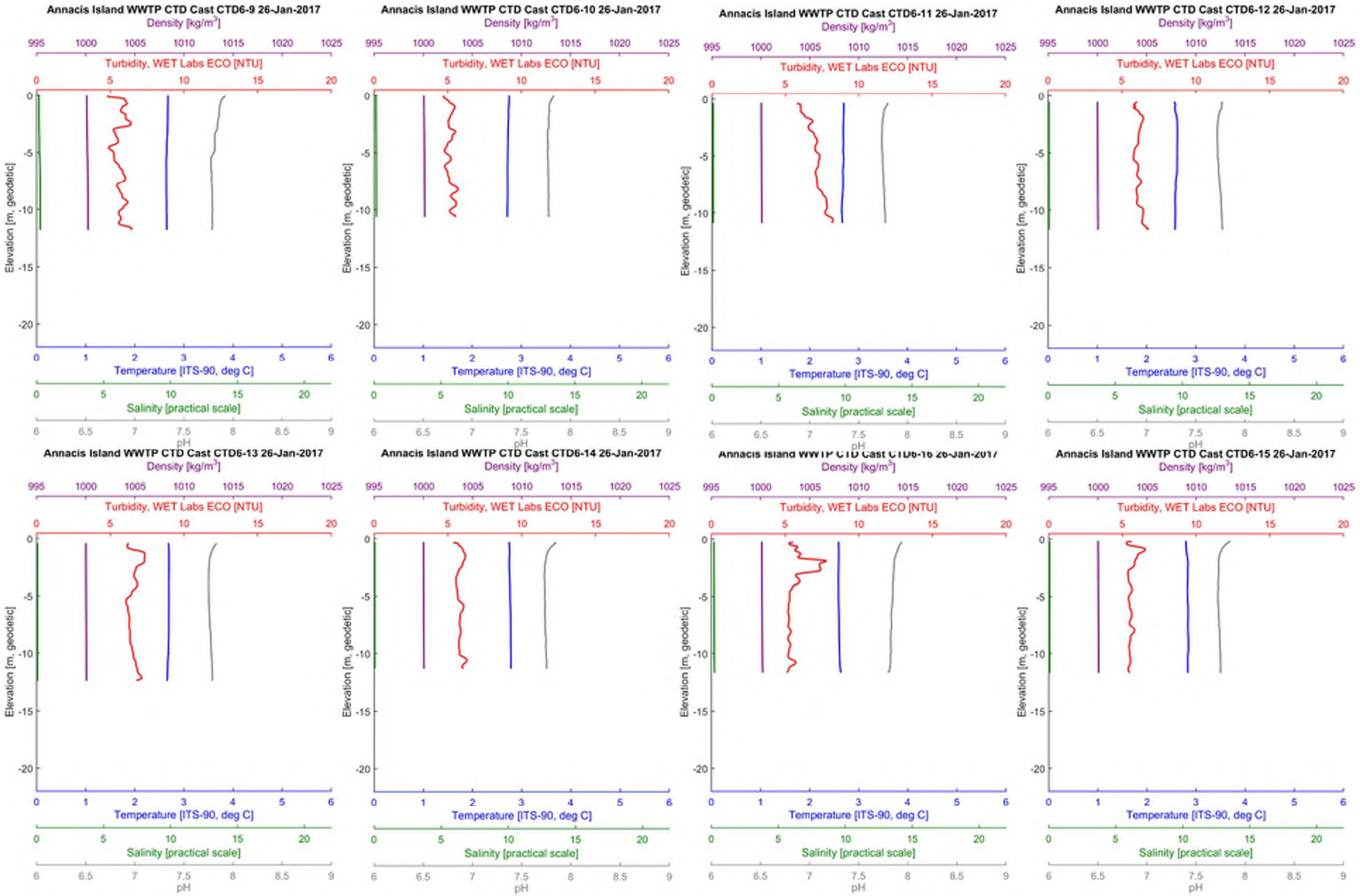


*Figure 12: CTD profiles measured at CTD6 on 26 January 2017*

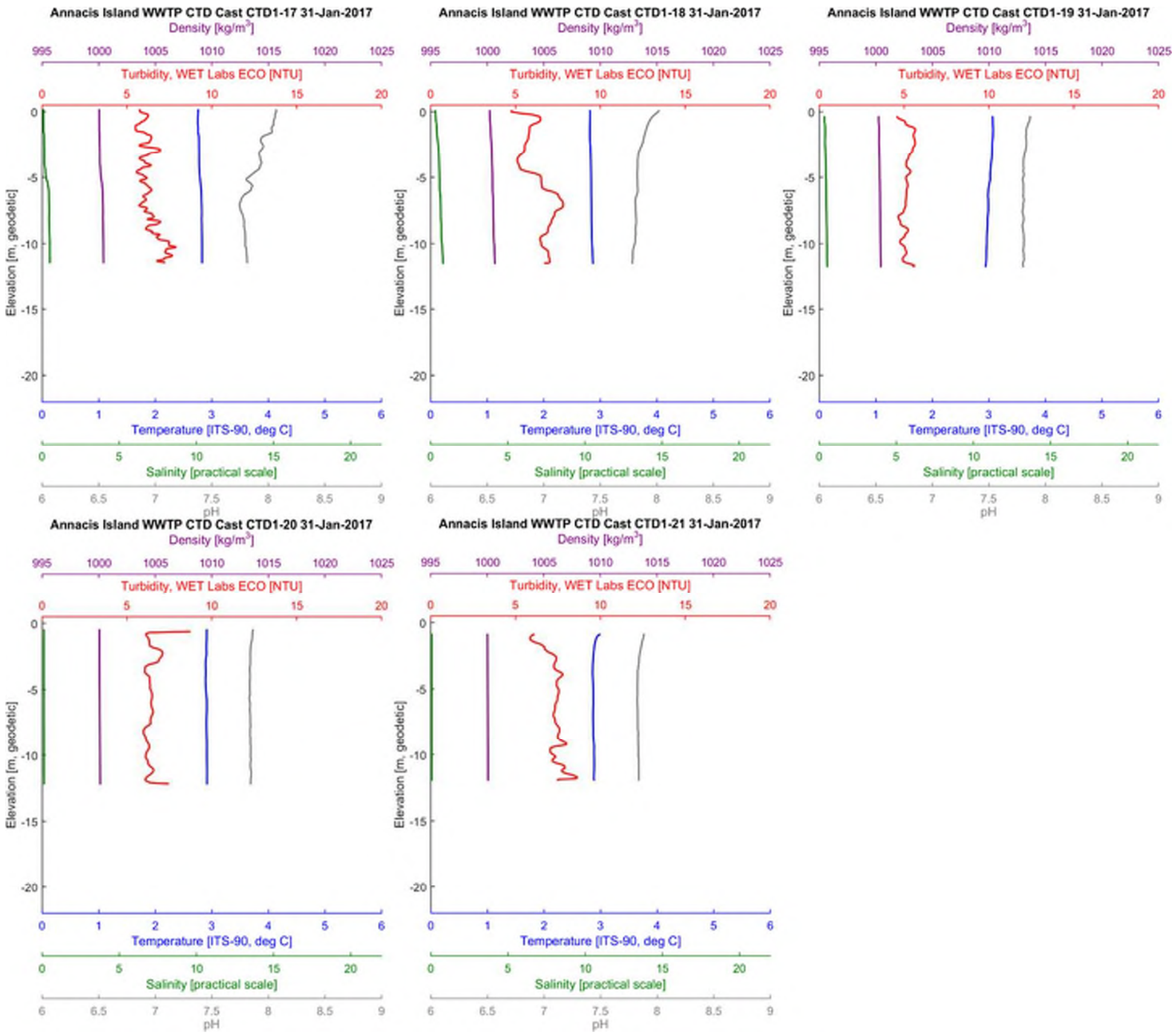


*Figure 13: CTD profiles measured at CTD1 on 31 January 2017*

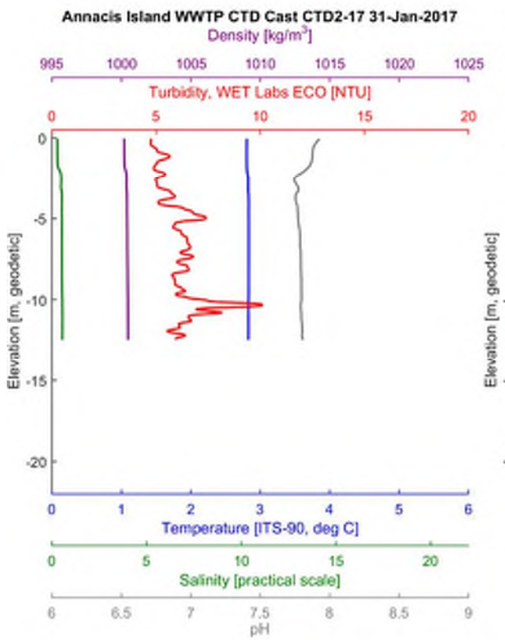


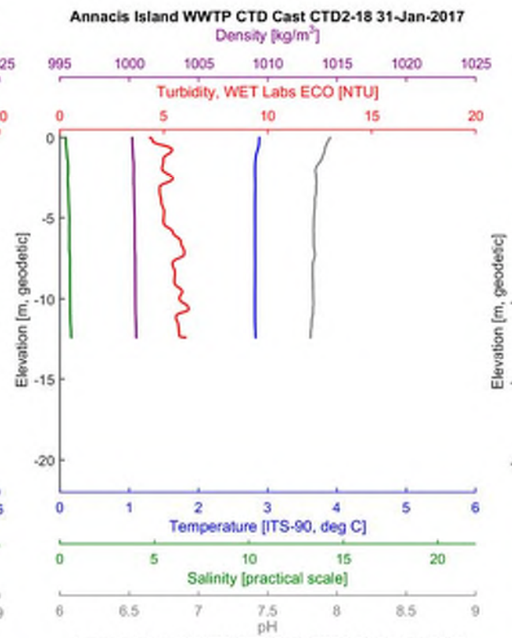


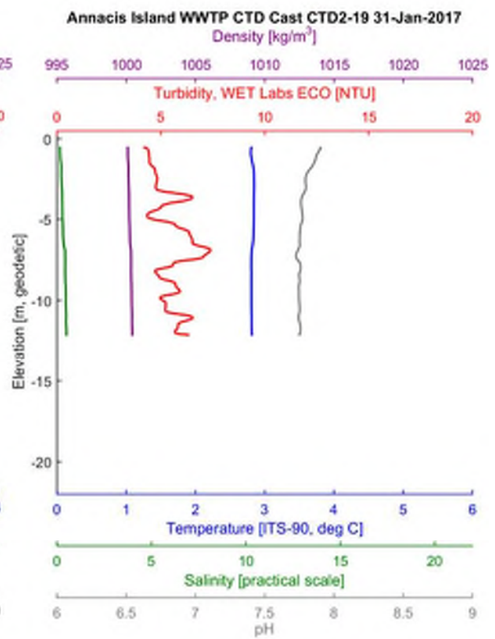


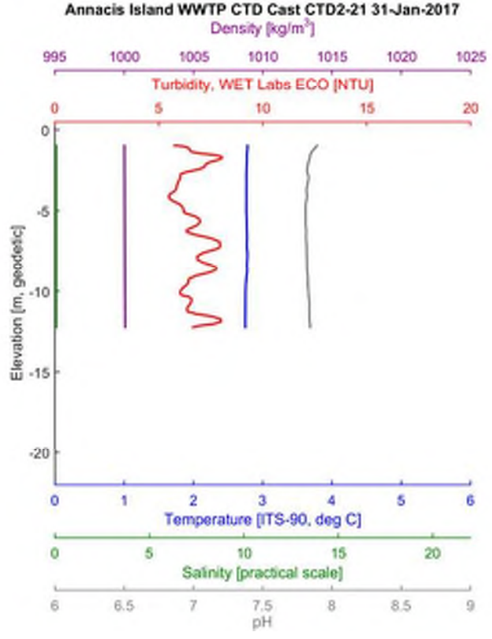


*Figure 14: CTD profiles measured at CTD2 on 31 January 2017*

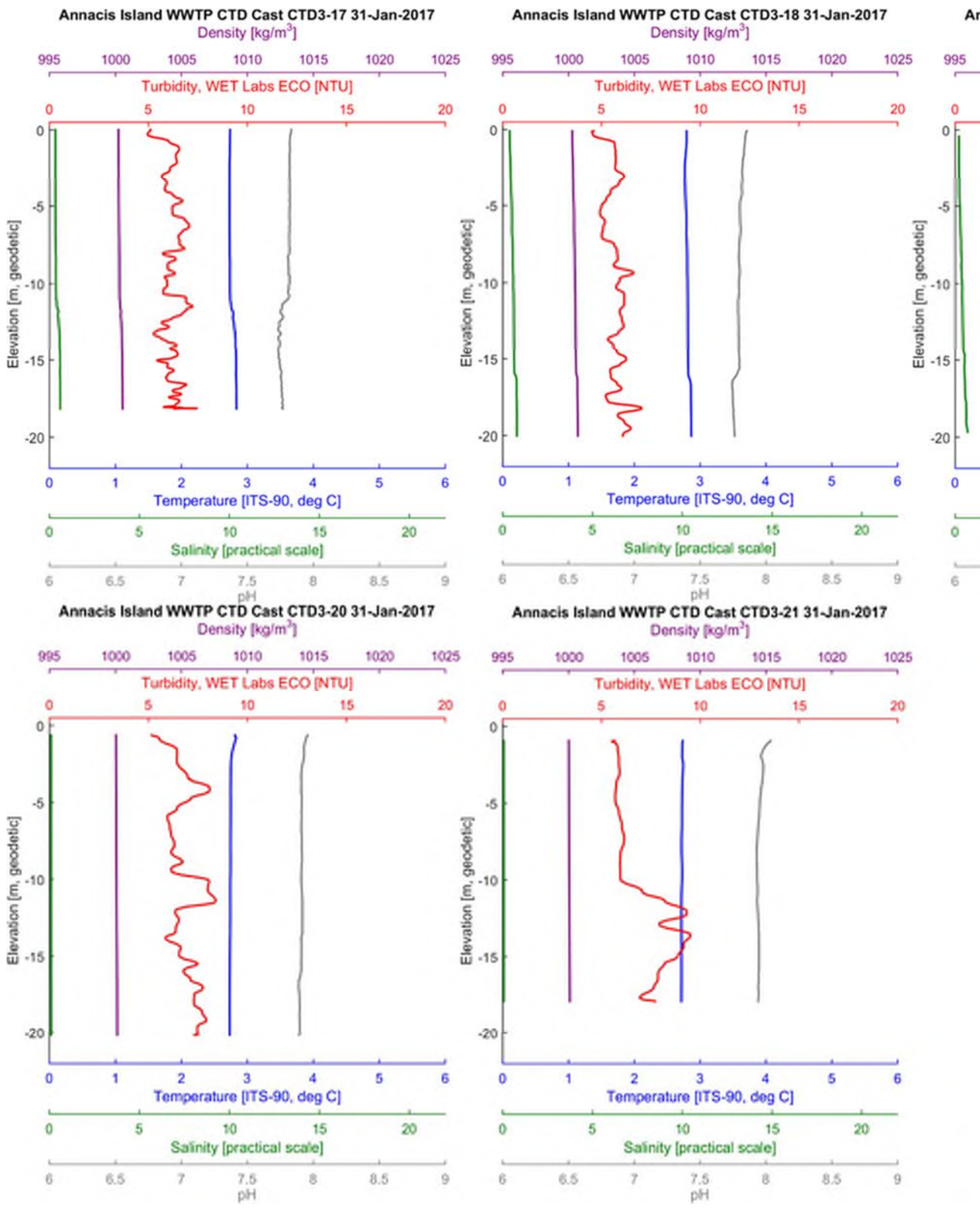


*Figure 15: CTD profiles measured at CTD3 on 31 January 2017*

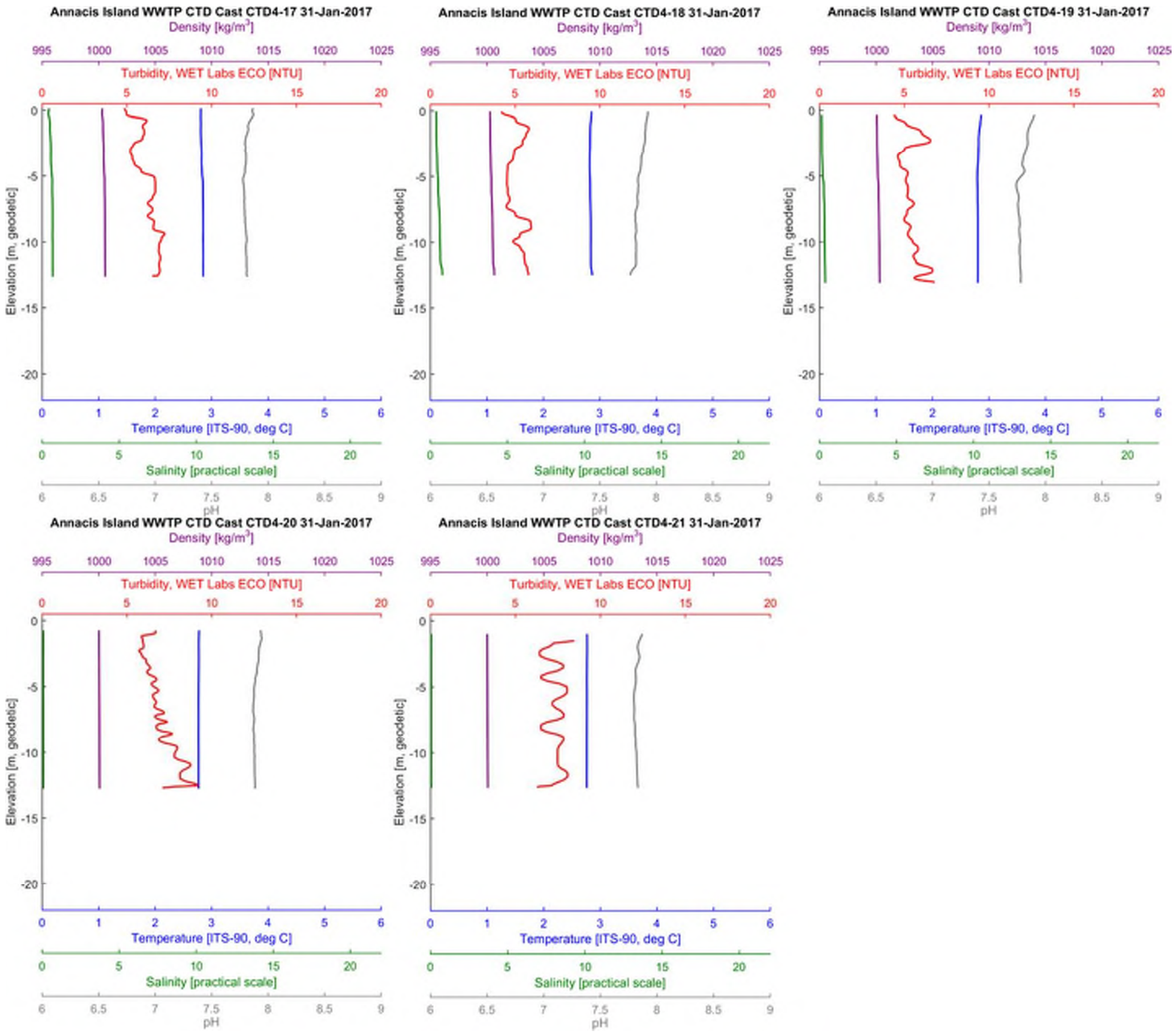


*Figure 16: CTD profiles measured at CTD4 on 31 January 2017*

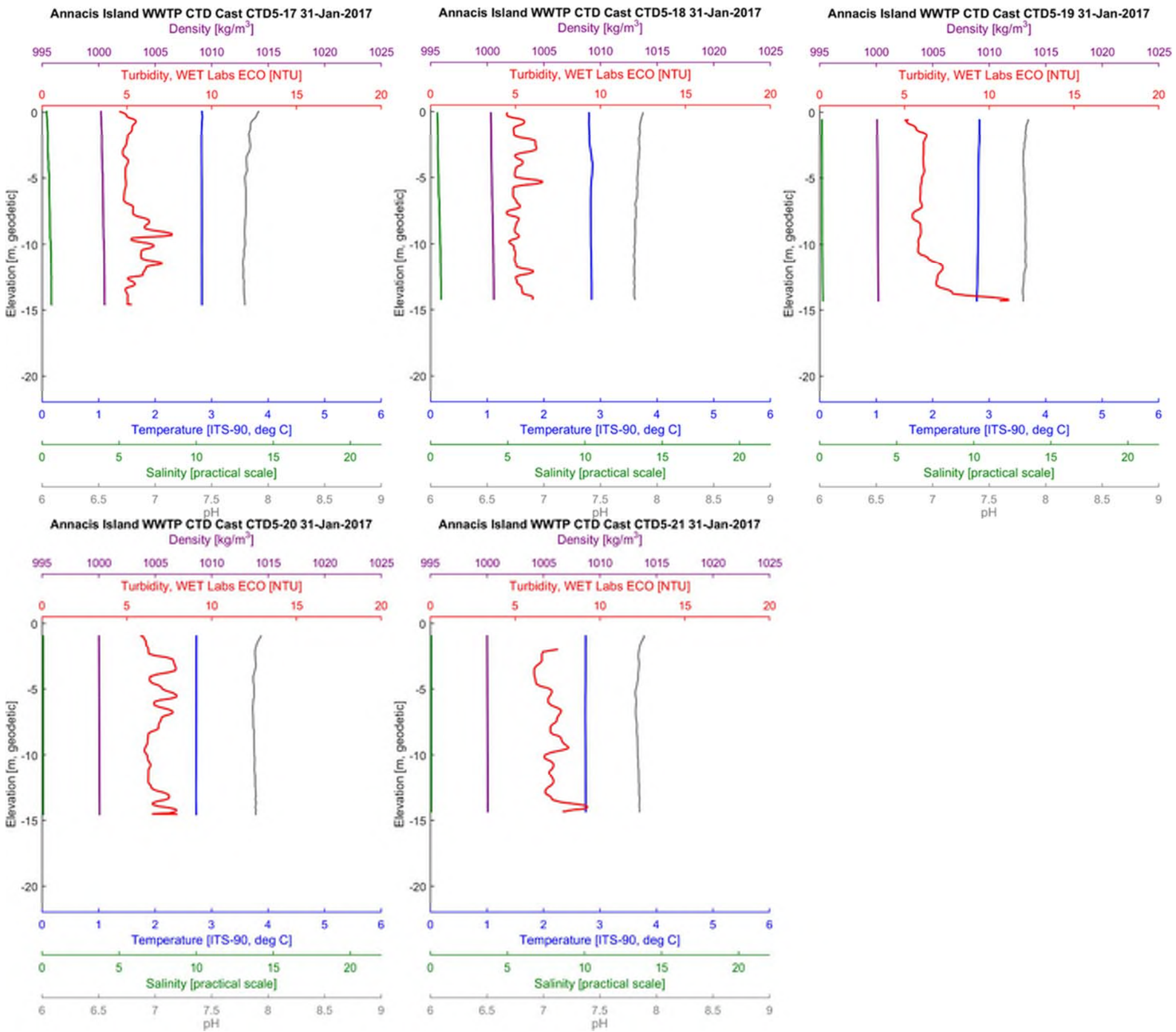


*Figure 17: CTD profiles measured at CTD5 on 31 January 2017*

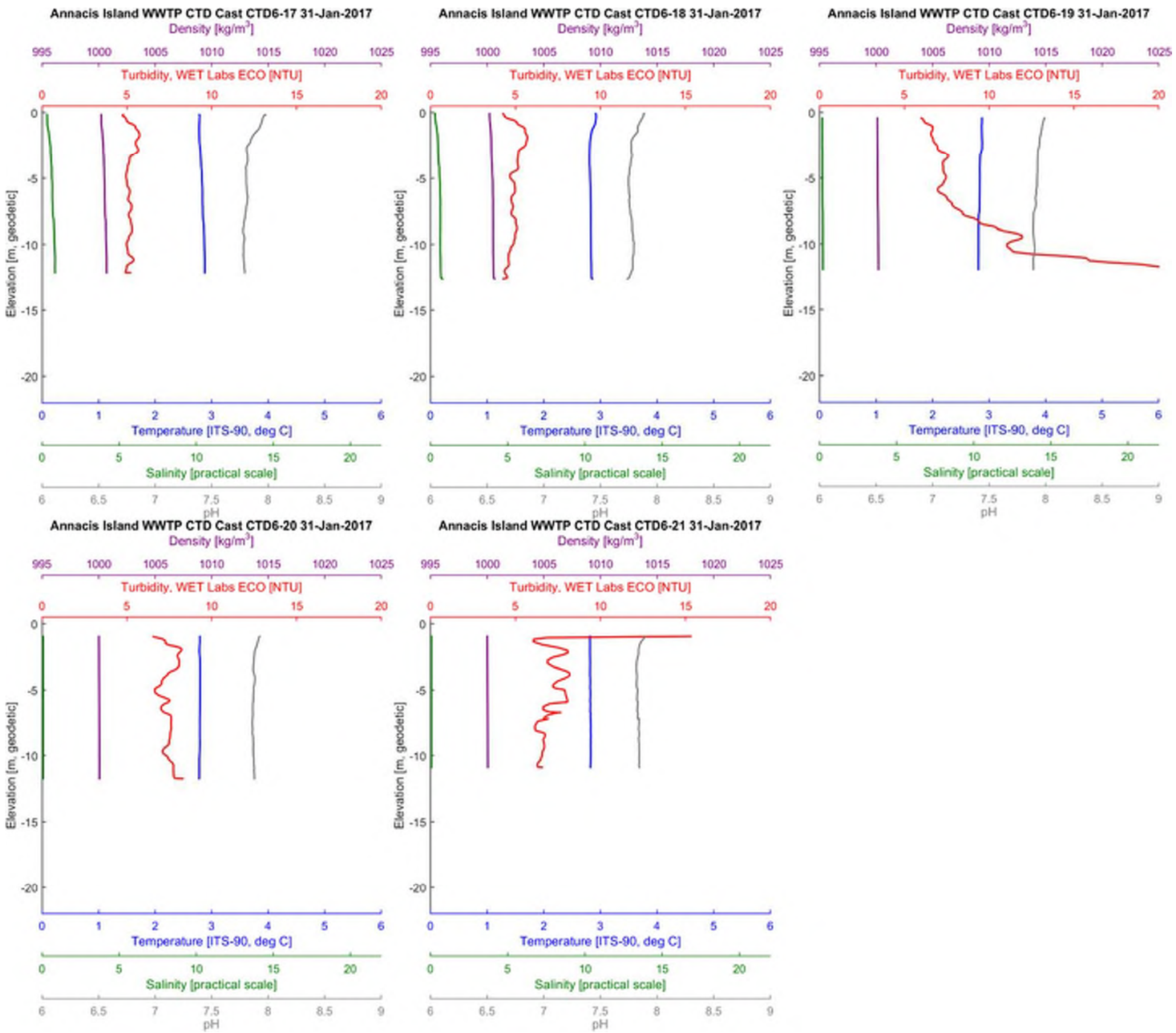


*Figure 18: CTD profiles measured at CTD6 on 31 January 2017*

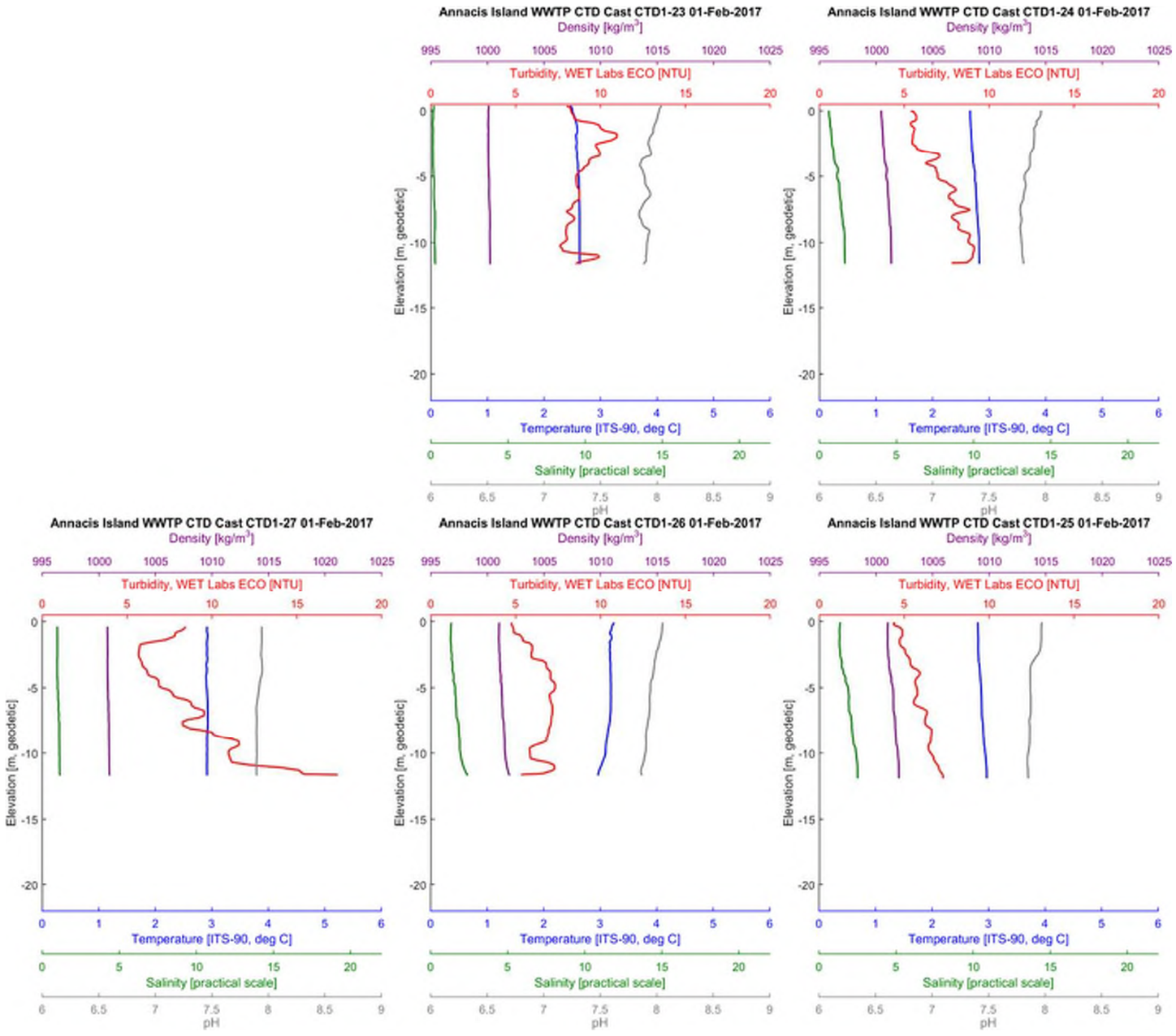


*Figure 19: CTD profiles measured at CTD1 on 1 February 2017*

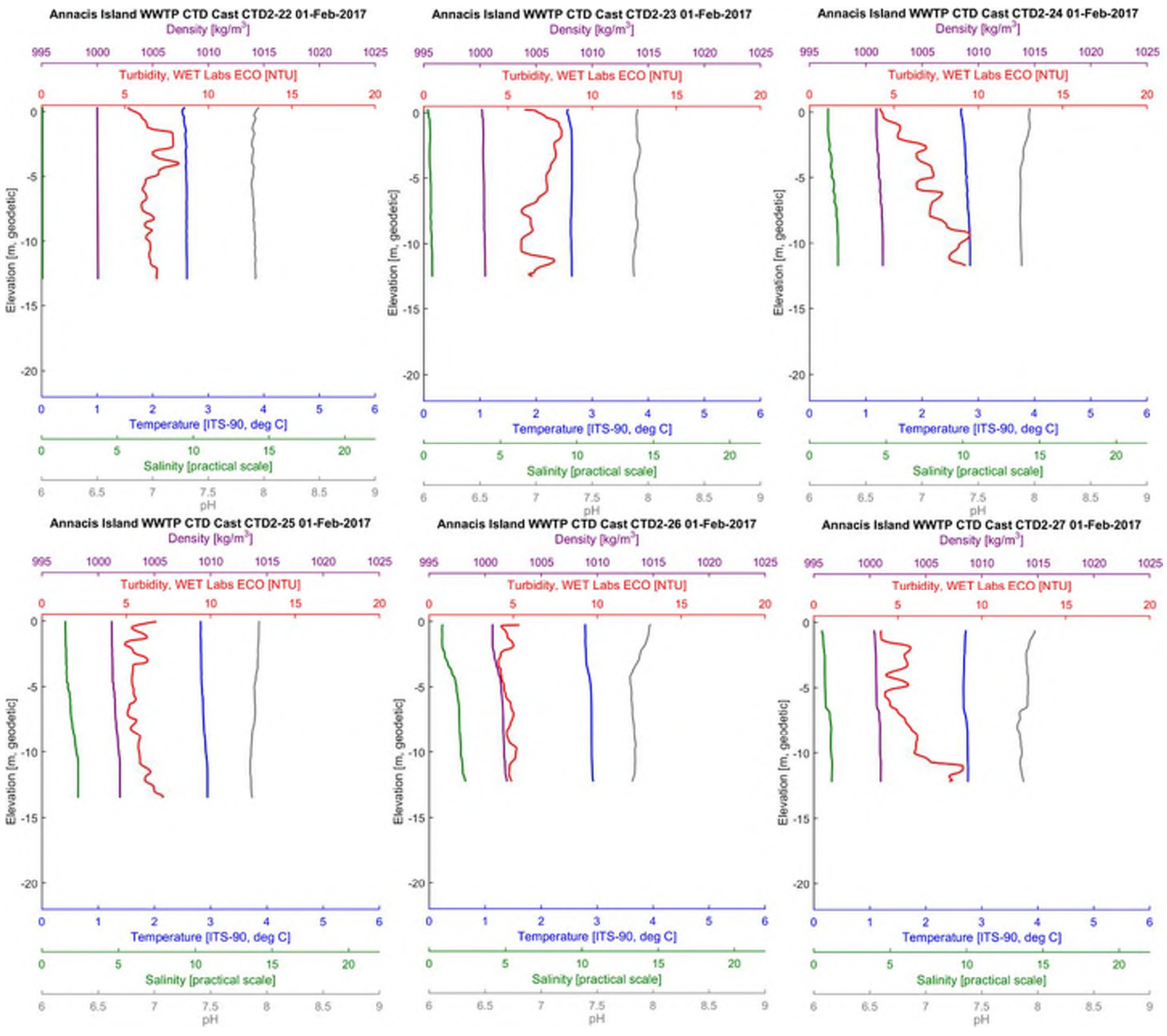


*Figure 20: CTD profiles measured at CTD2 on 1 February 2017*

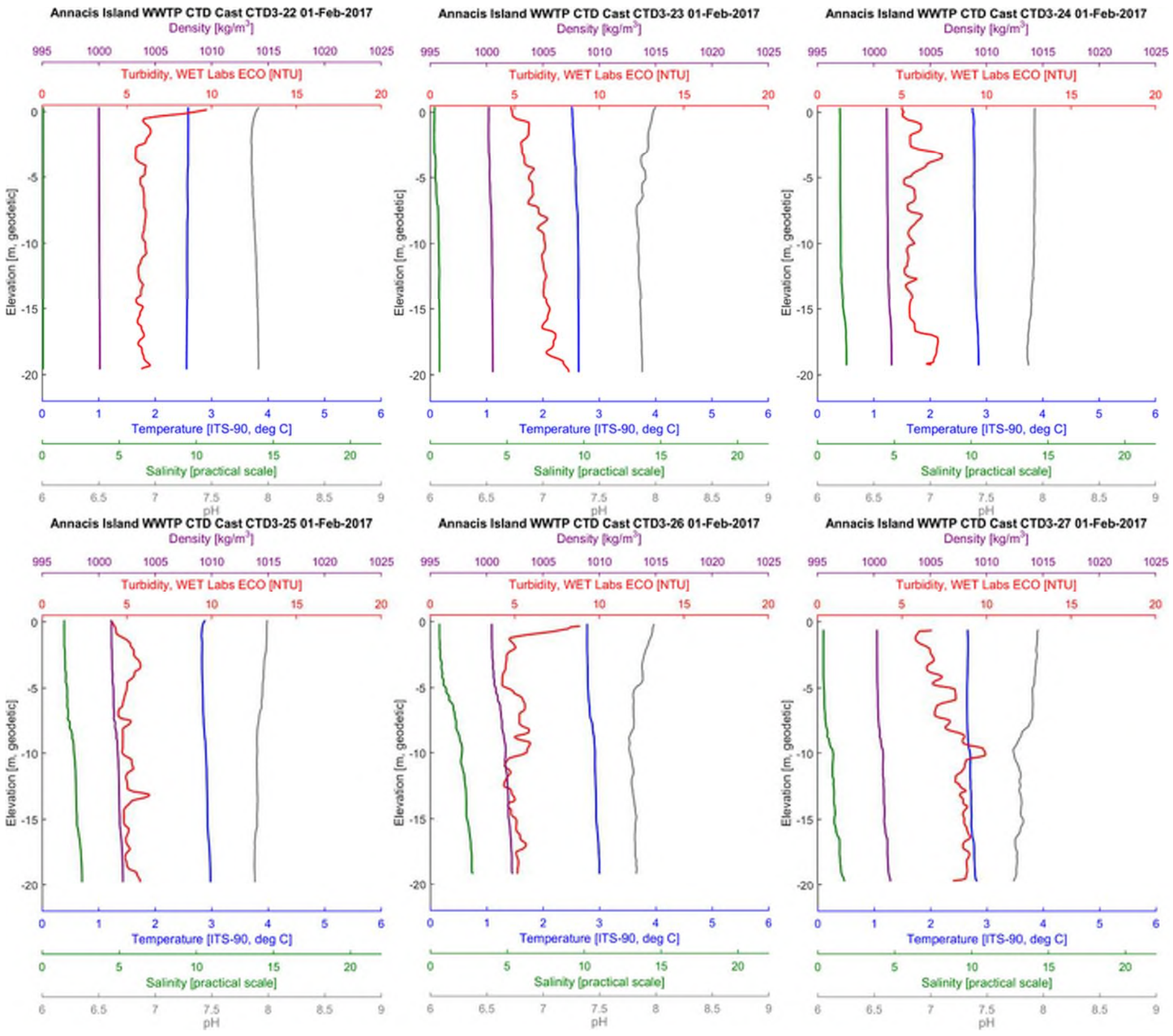


*Figure 21: CTD profiles measured at CTD3 on 1 February 2017*

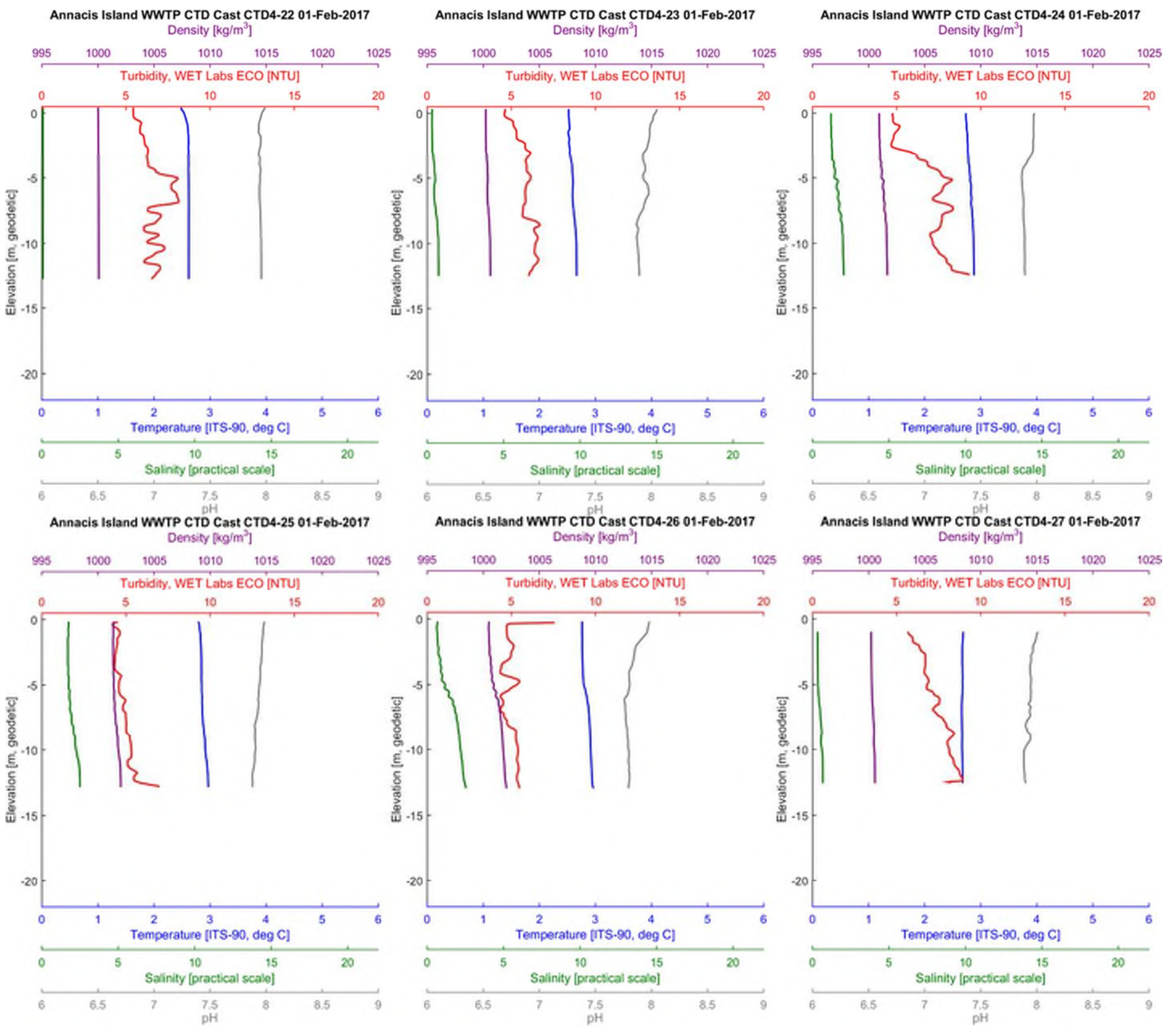


*Figure 22: CTD profiles measured at CTD4 on 1 February 2017*

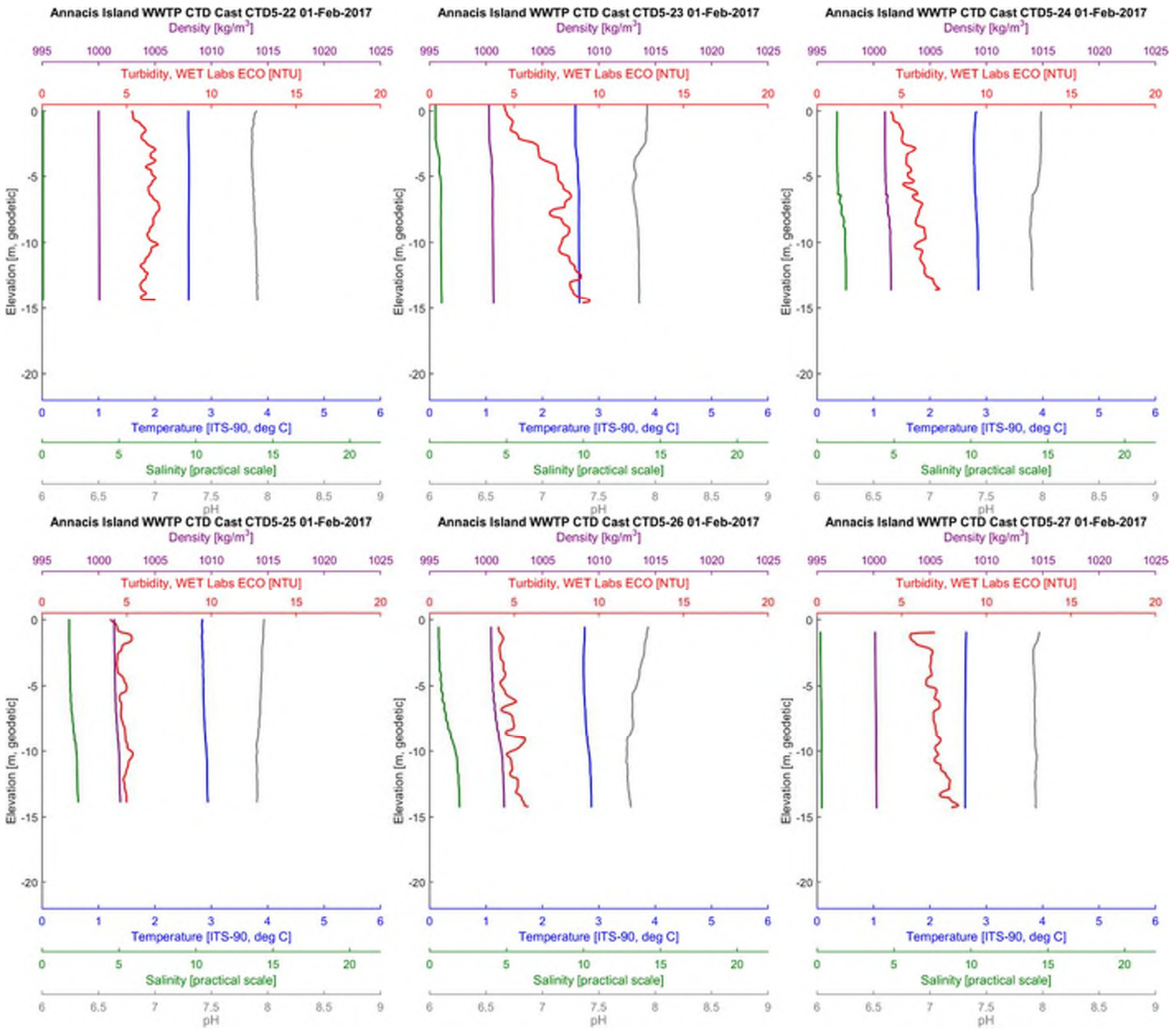


*Figure 23: CTD profiles measured at CTD5 on 1 February 2017*

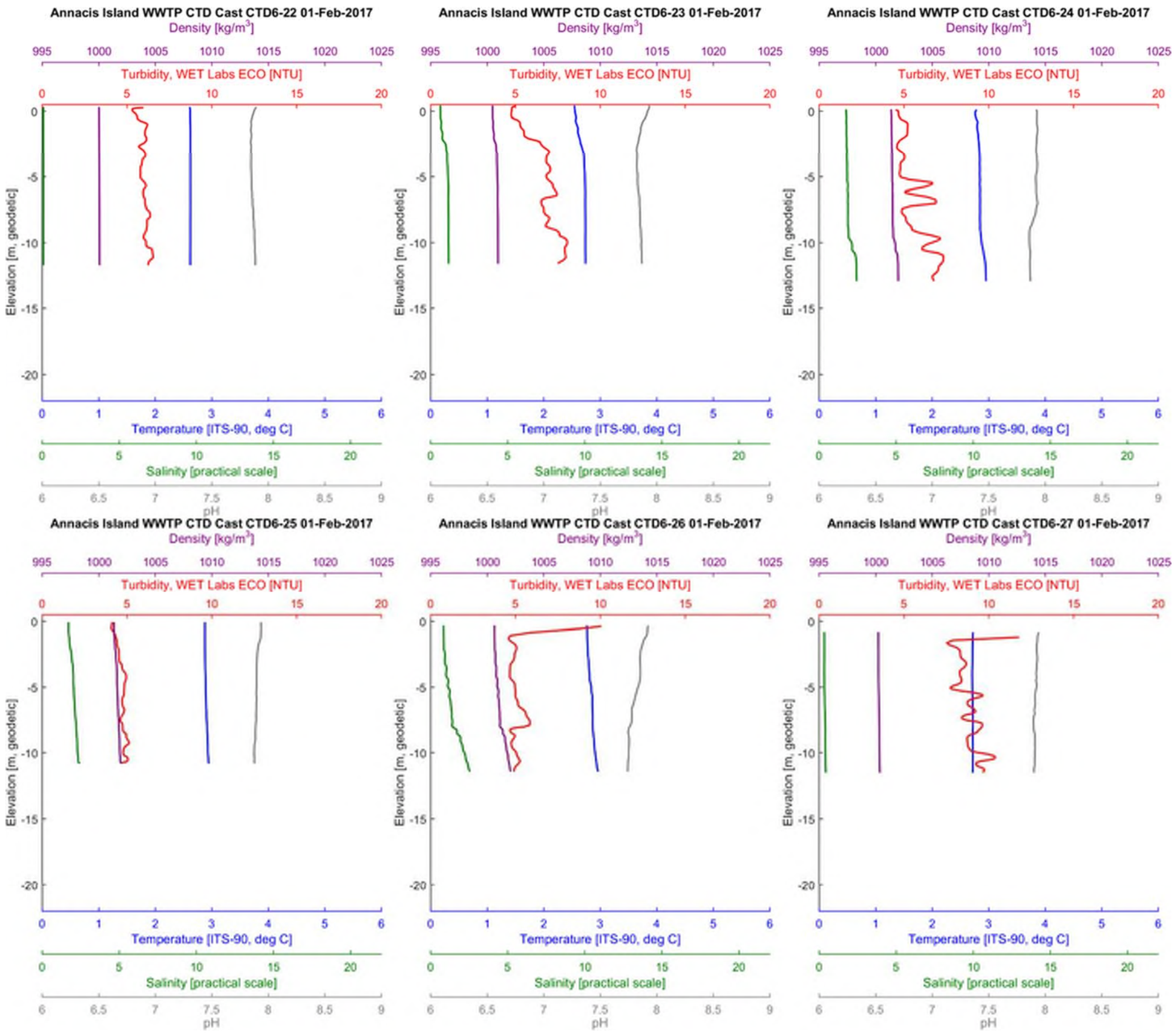


*Figure 24: CTD profiles measured at CTD6 on 1 February 2017*

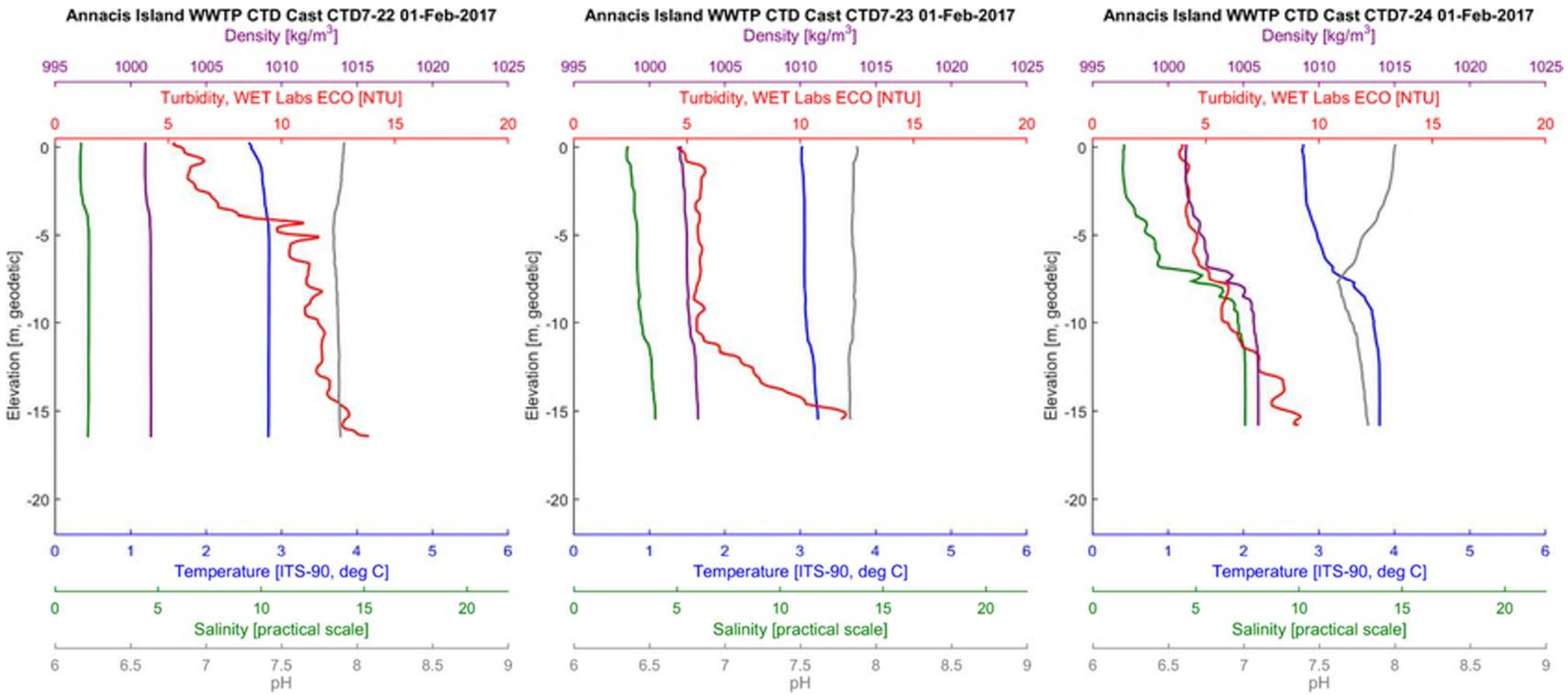


*Figure 25: CTD profiles measured at CTD7 on 1 February 2017*

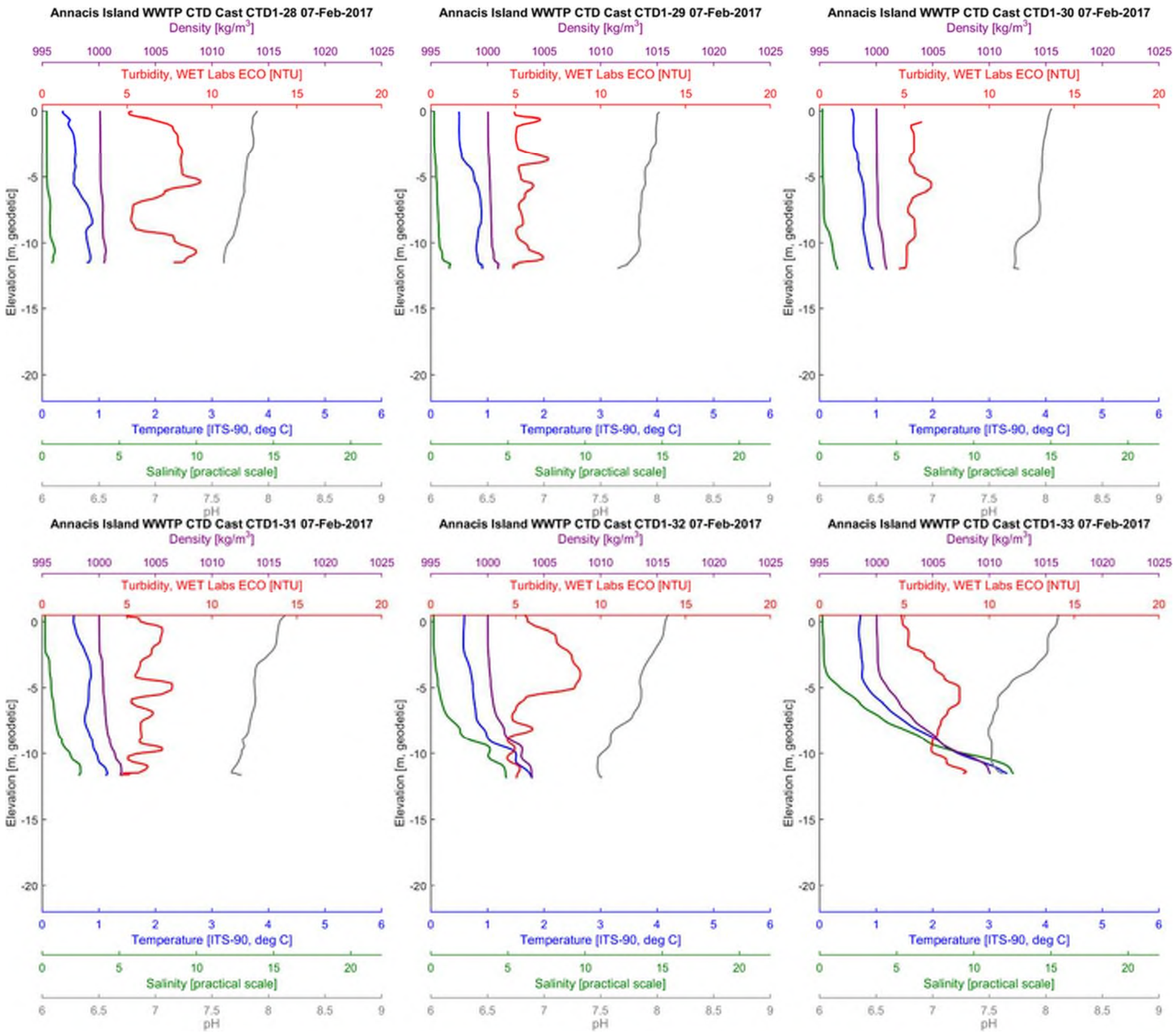


*Figure 26: CTD profiles measured at CTD1 on 7 February 2017*

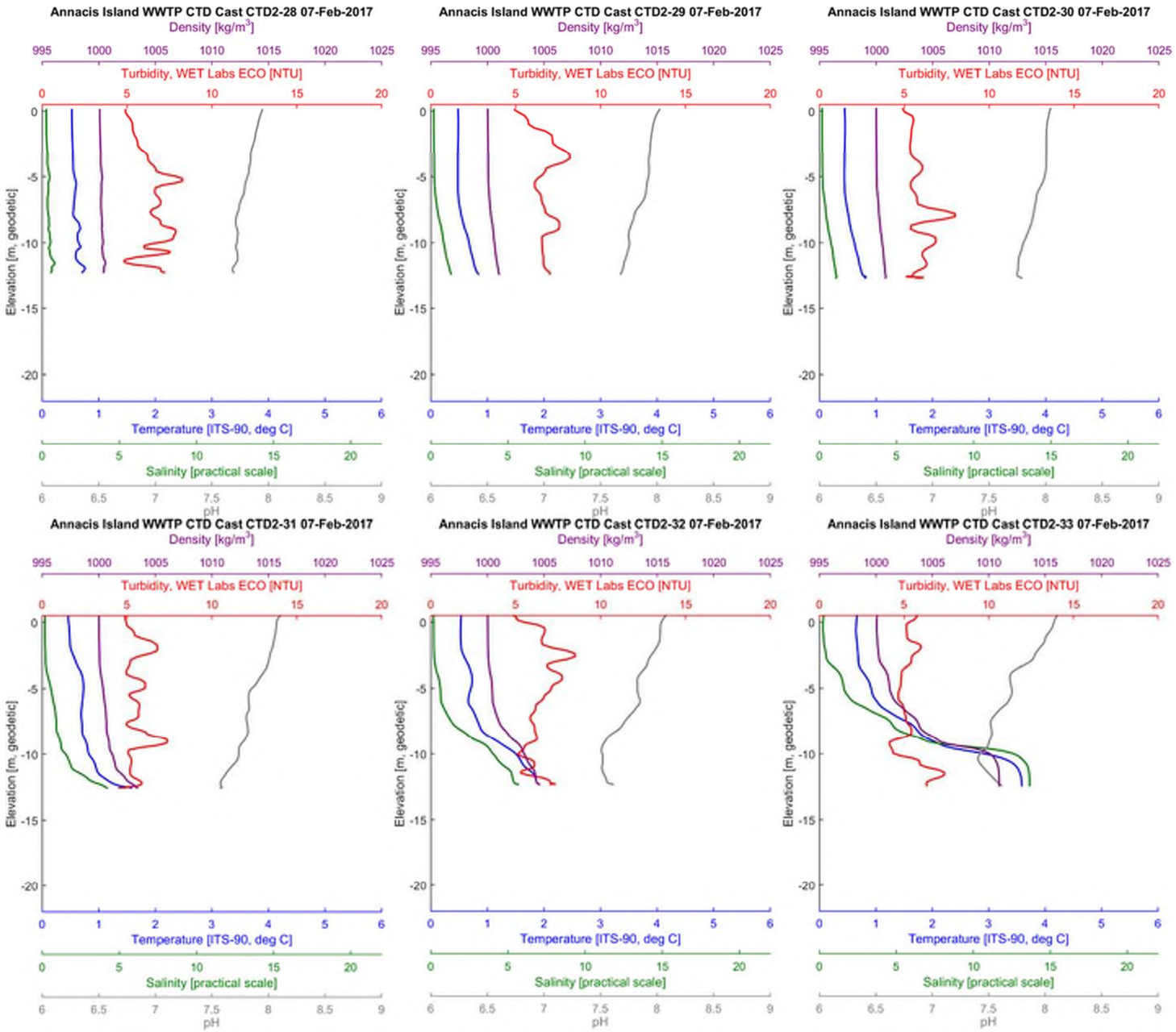


*Figure 27: CTD profiles measured at CTD2 on 7 February 2017*

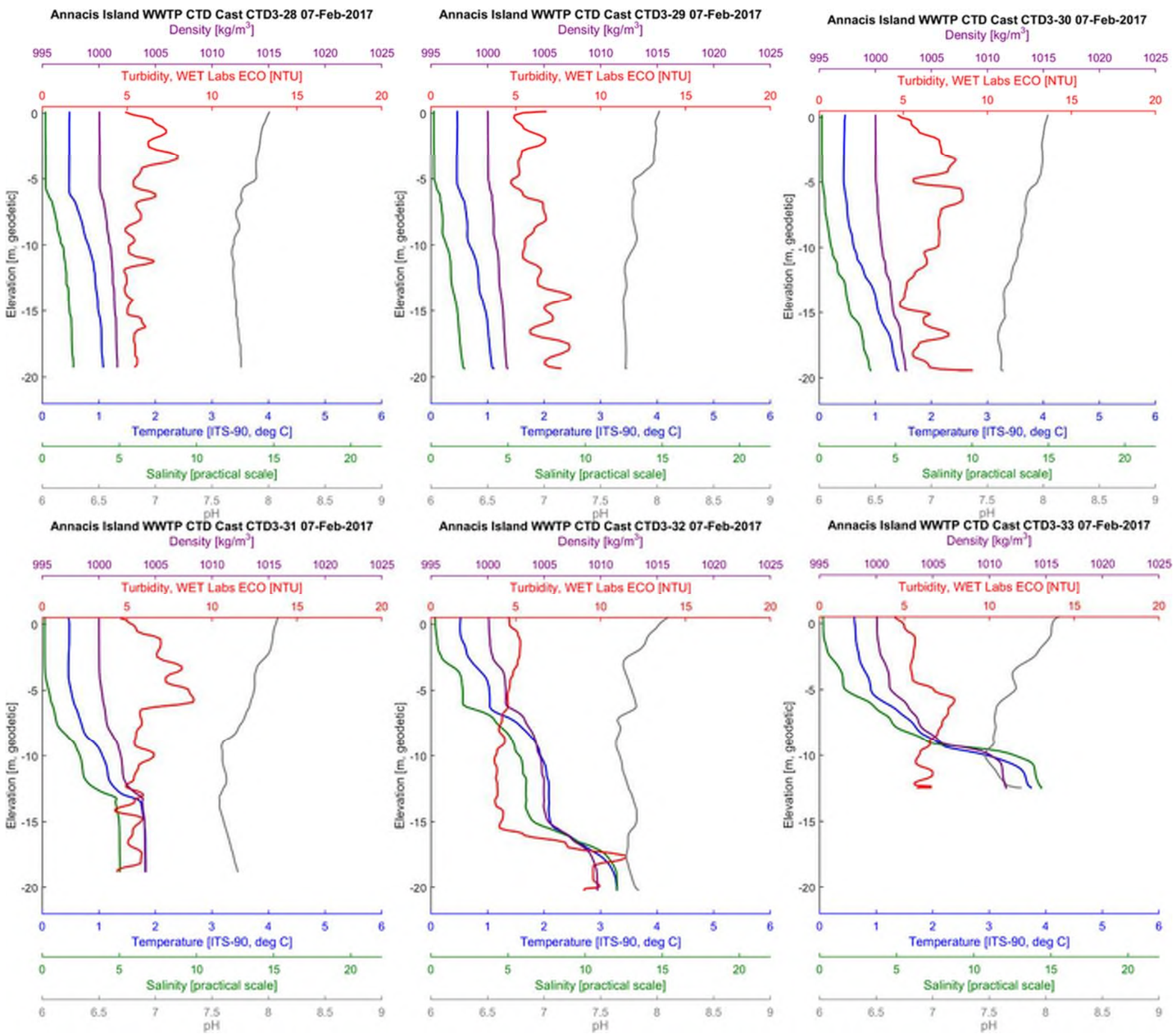


*Figure 28: CTD profiles measured at CTD3 on 7 February 2017*

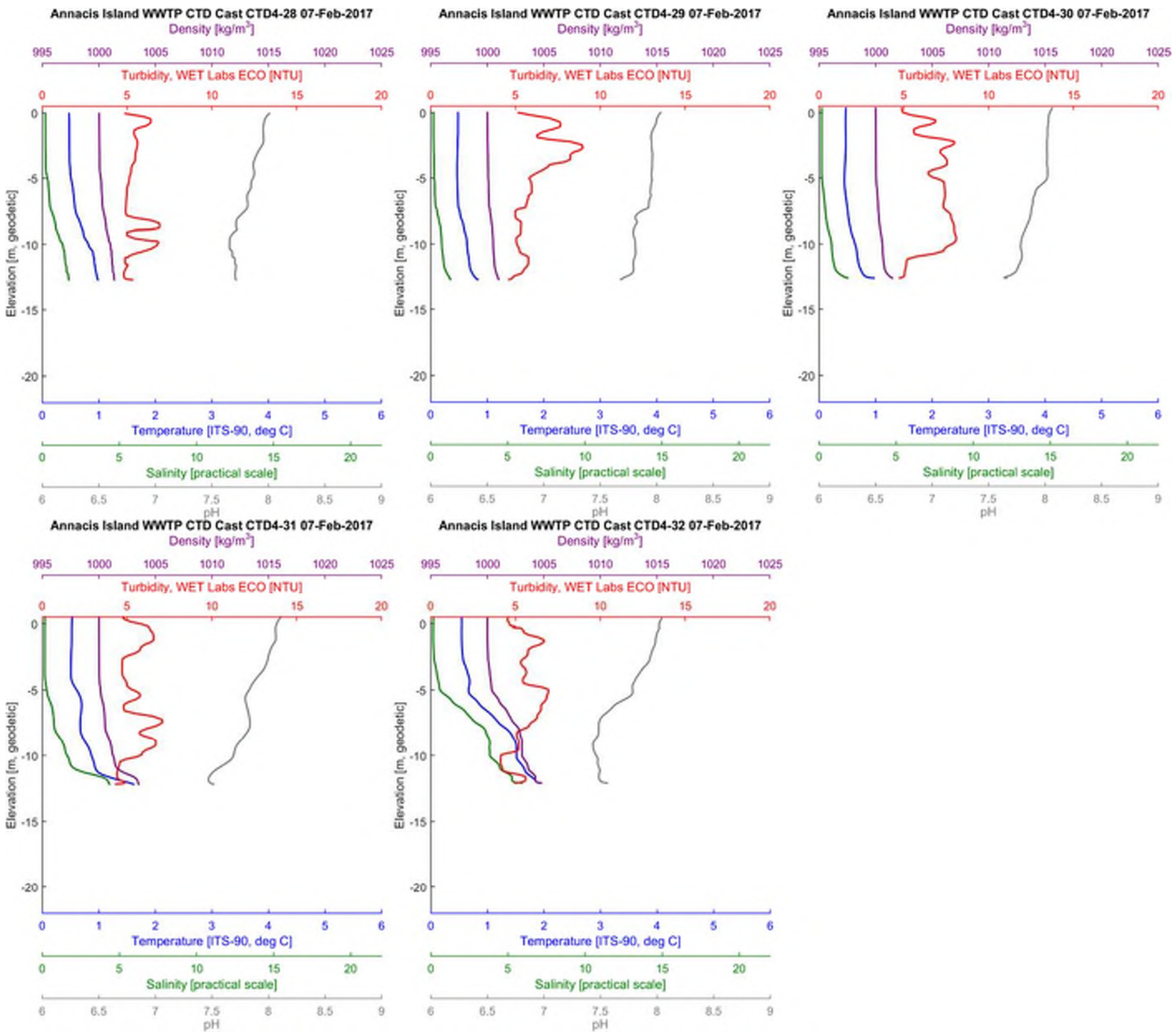


*Figure 29: CTD profiles measured at CTD4 on 7 February 2017*

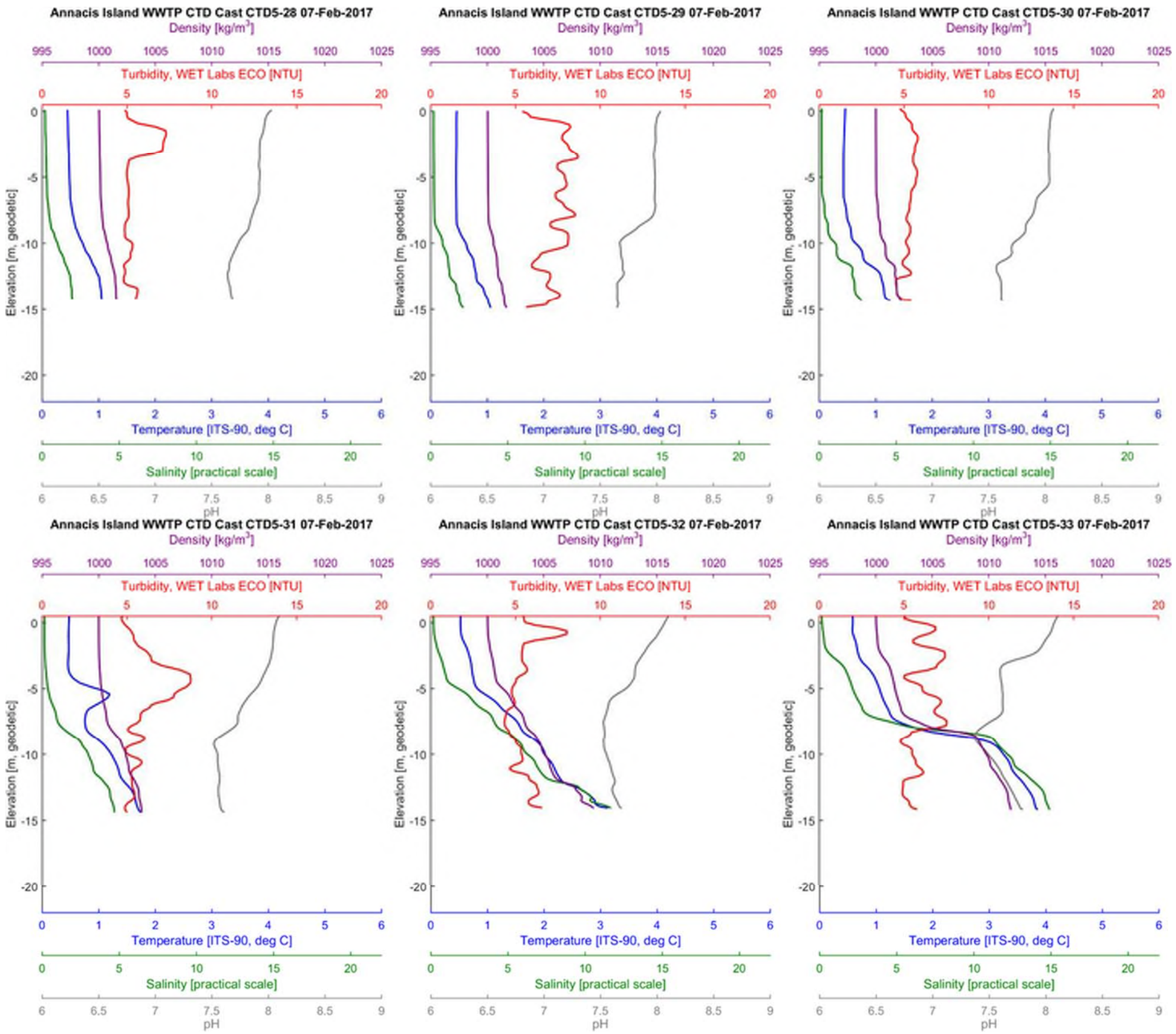


*Figure 30: CTD profiles measured at CTD5 on 7 February 2017*

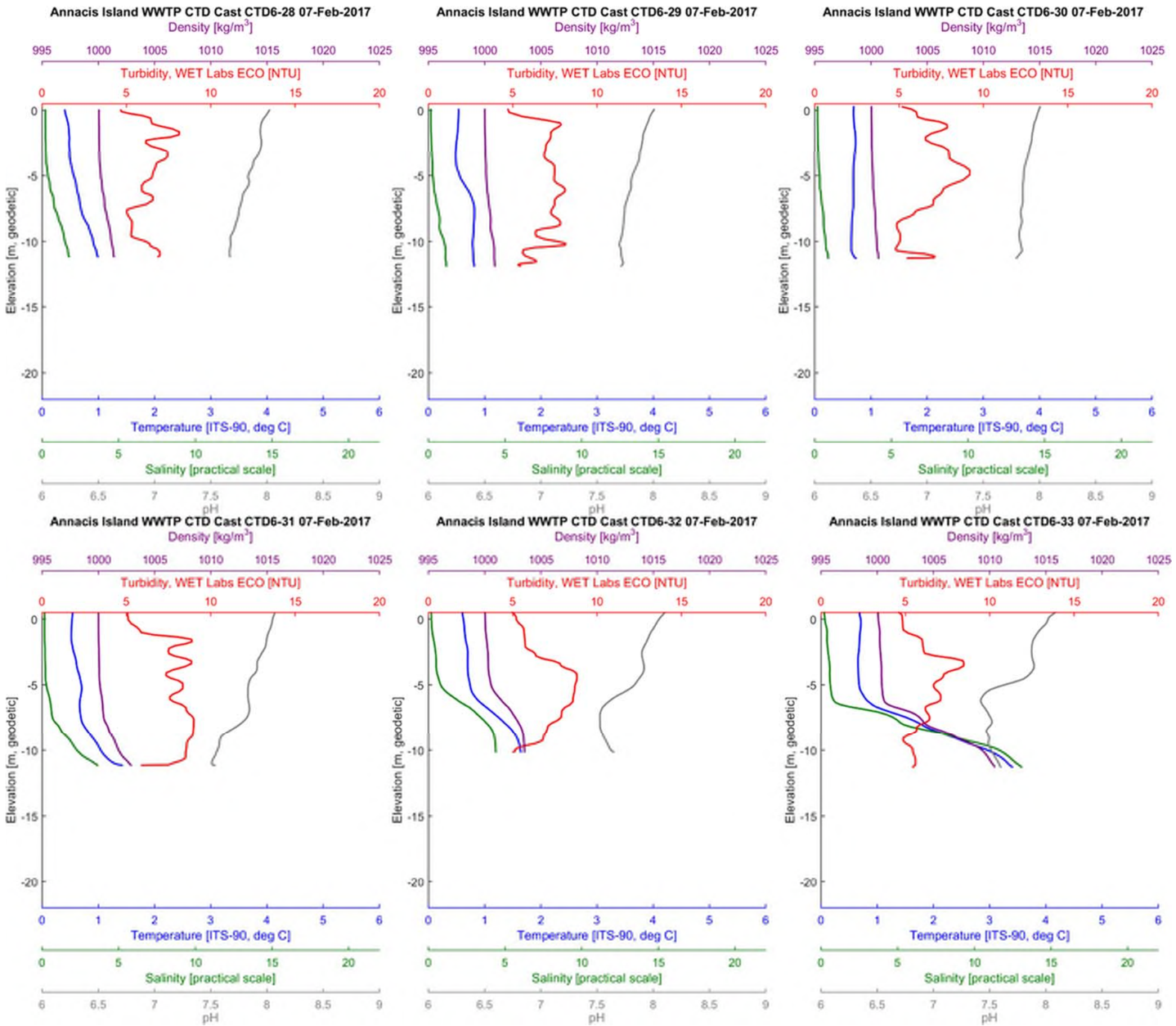


*Figure 31: CTD profiles measured at CTD6 on 7 February 2017*

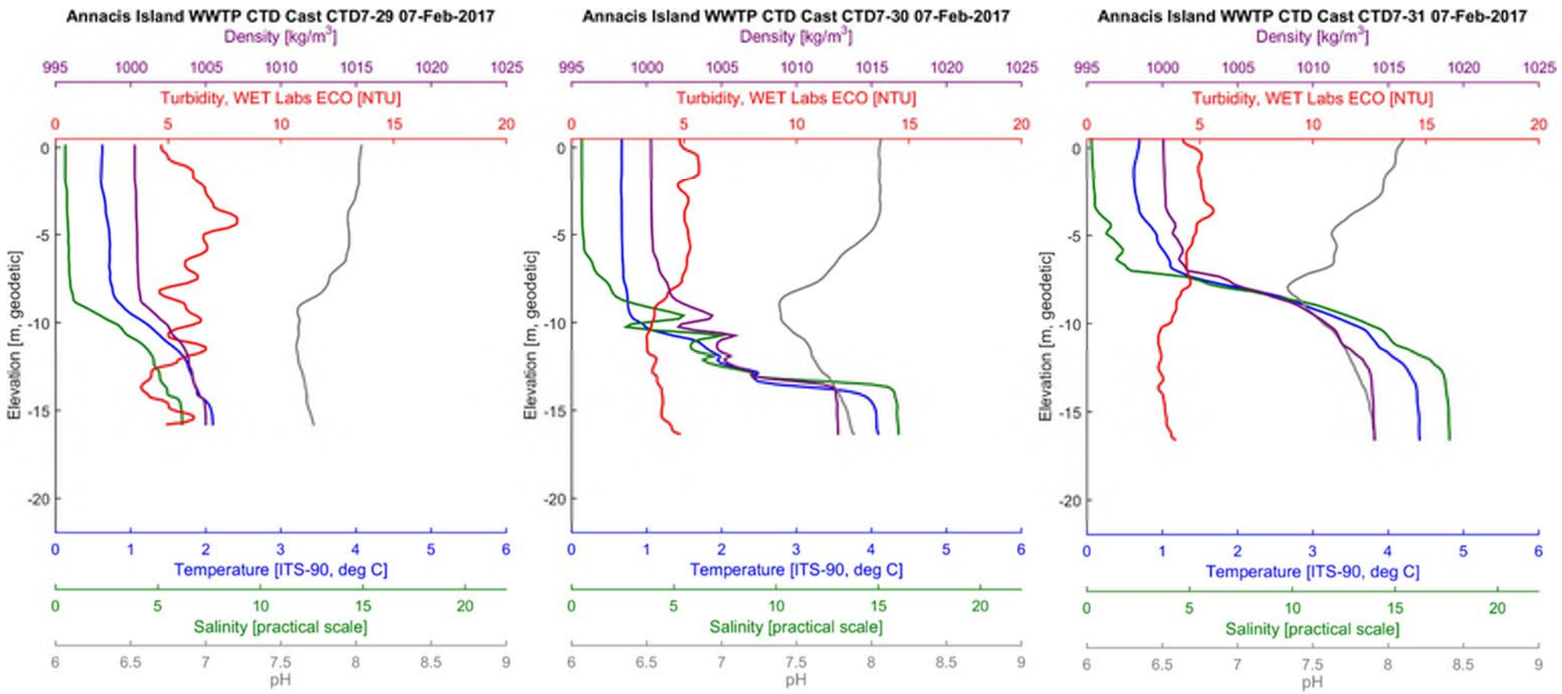


*Figure 32: CTD profiles measured at CTD7 on 7 February 2017*

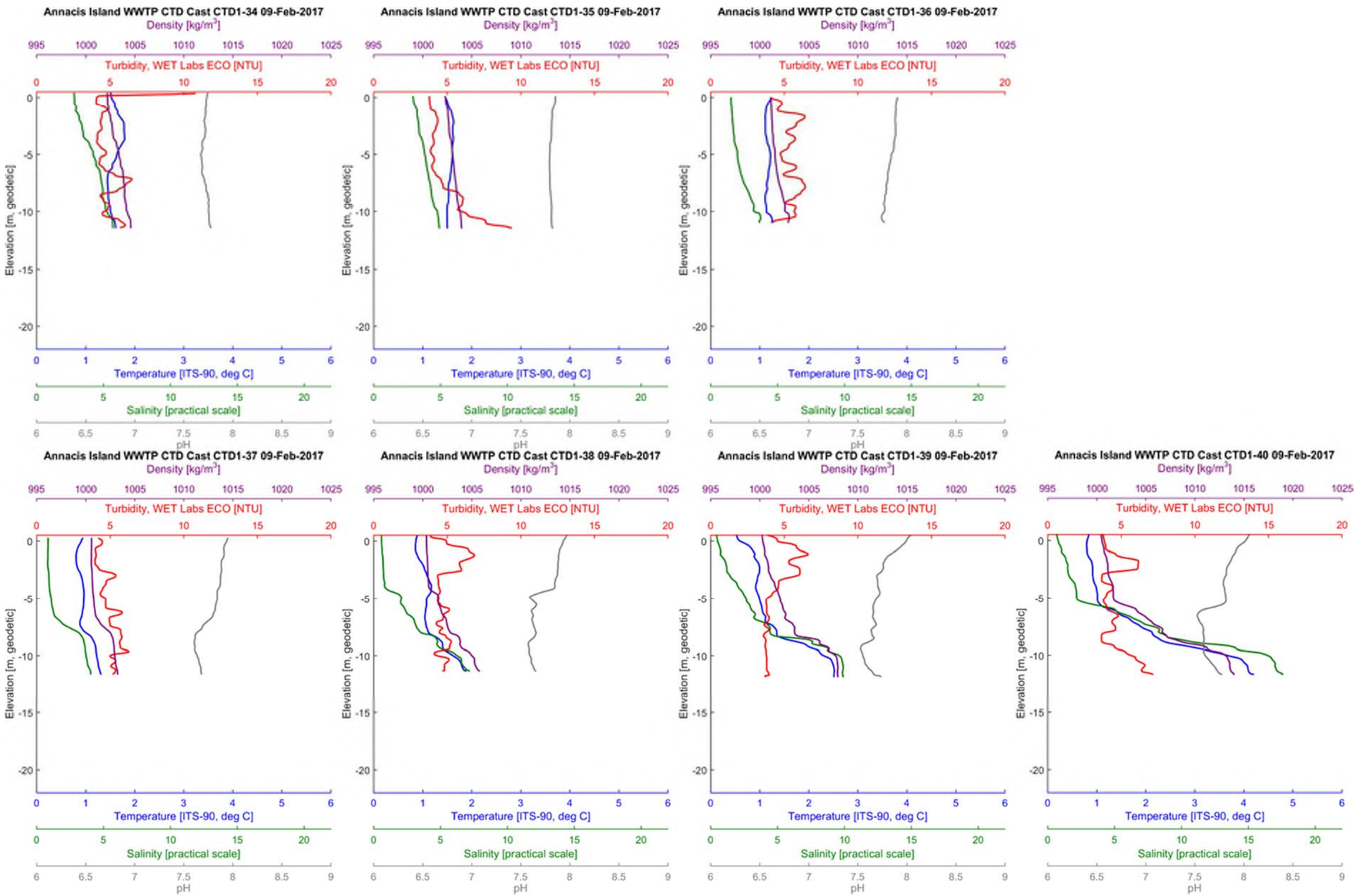


*Figure 33: CTD profiles measured at CTD1 on 9 February 2017*

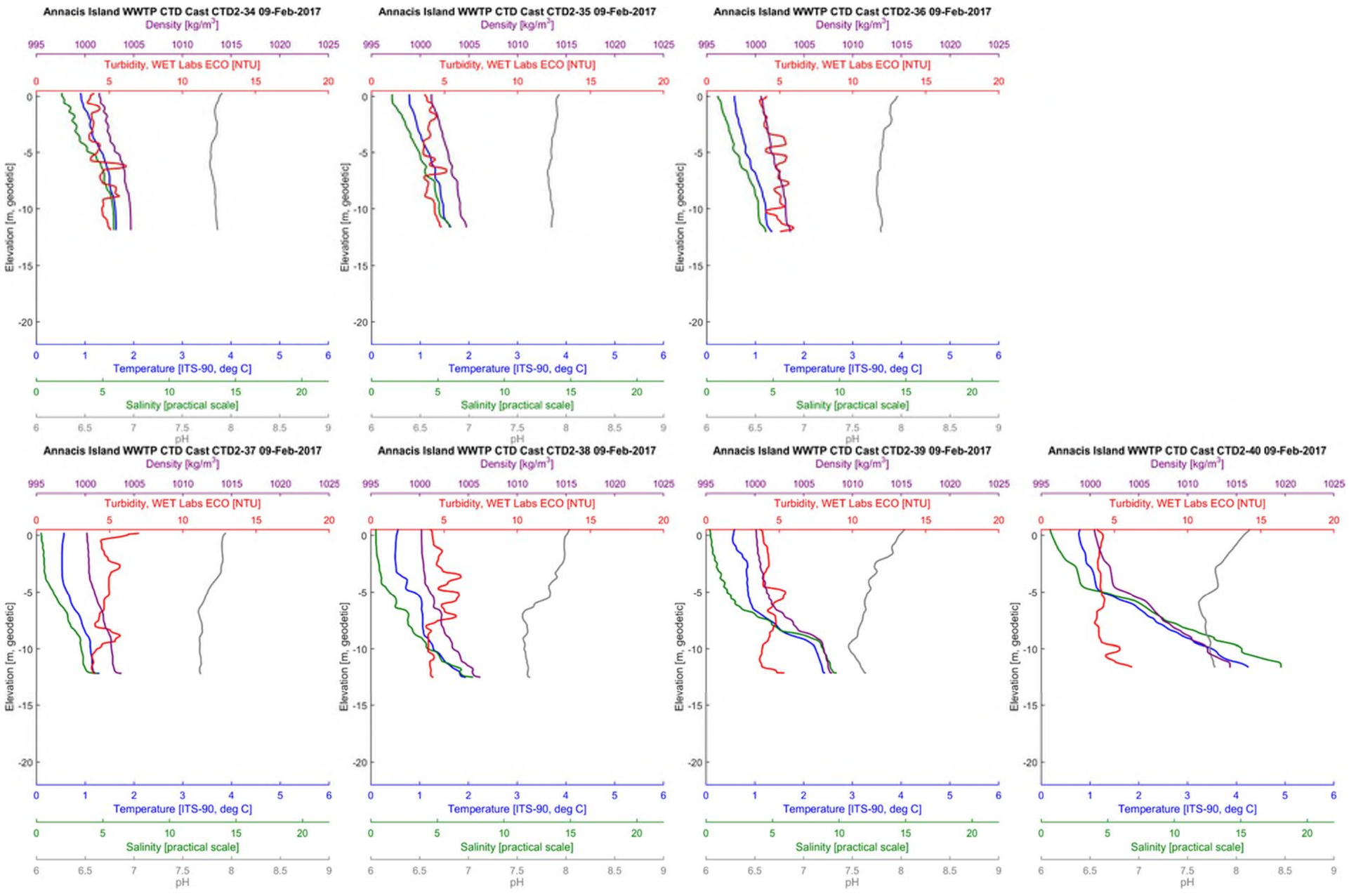


*Figure 34: CTD profiles measured at CTD2 on 9 February 2017*

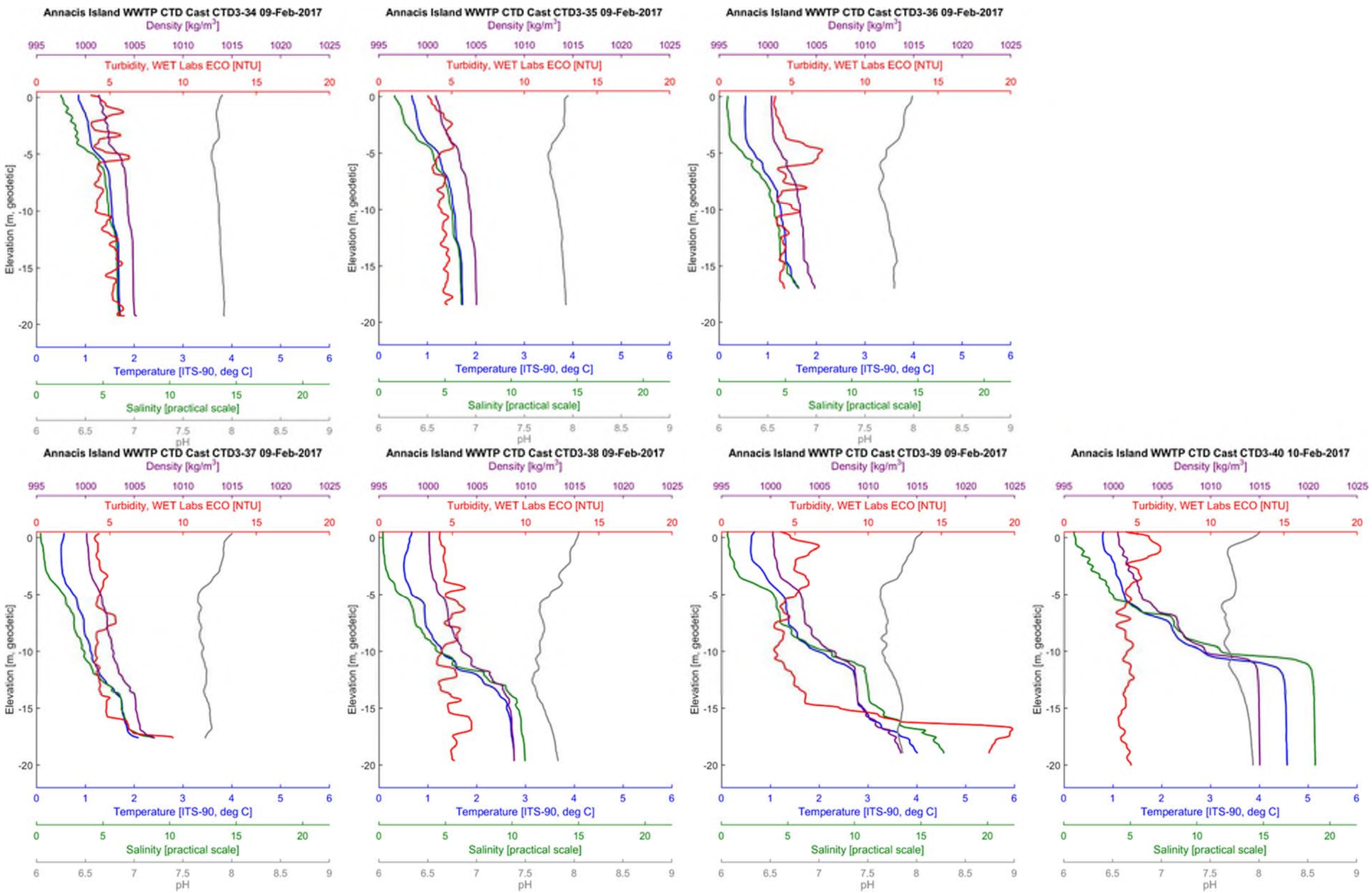


*Figure 35: CTD profiles measured at CTD3 on 9 February 2017*

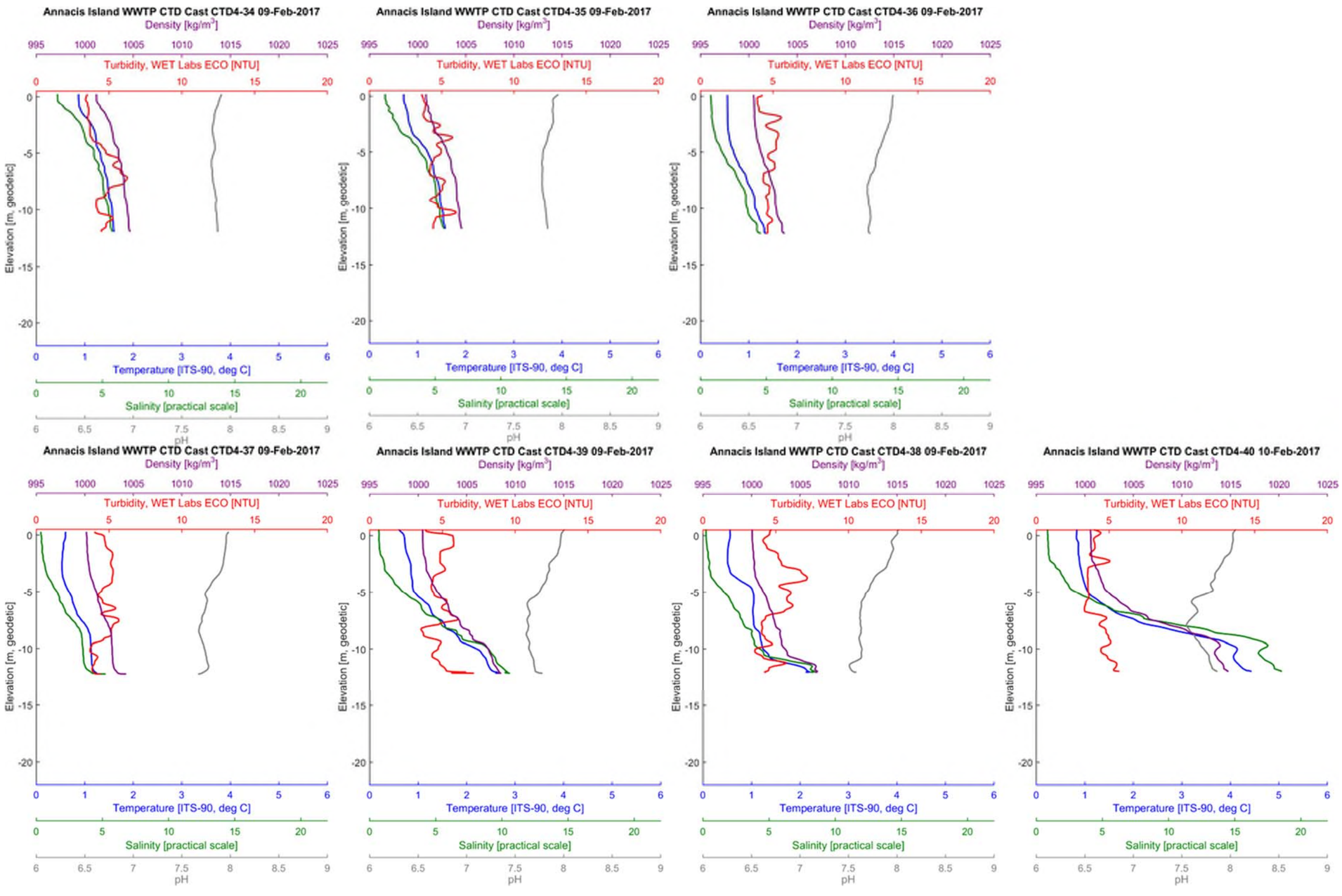


*Figure 36: CTD profiles measured at CTD4 on 9 February 2017*

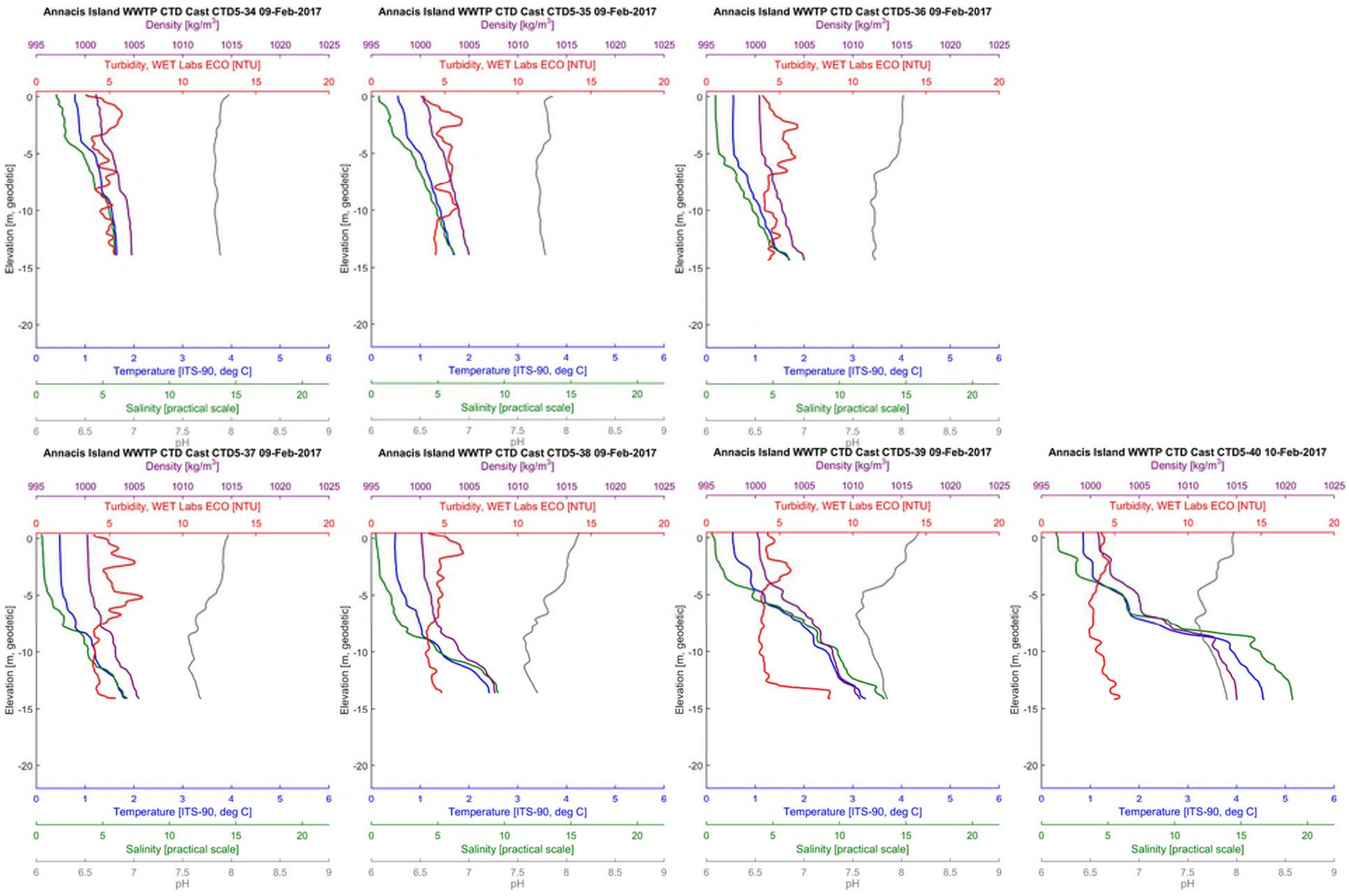


*Figure 37: CTD profiles measured at CTD5 on 9 February 2017*

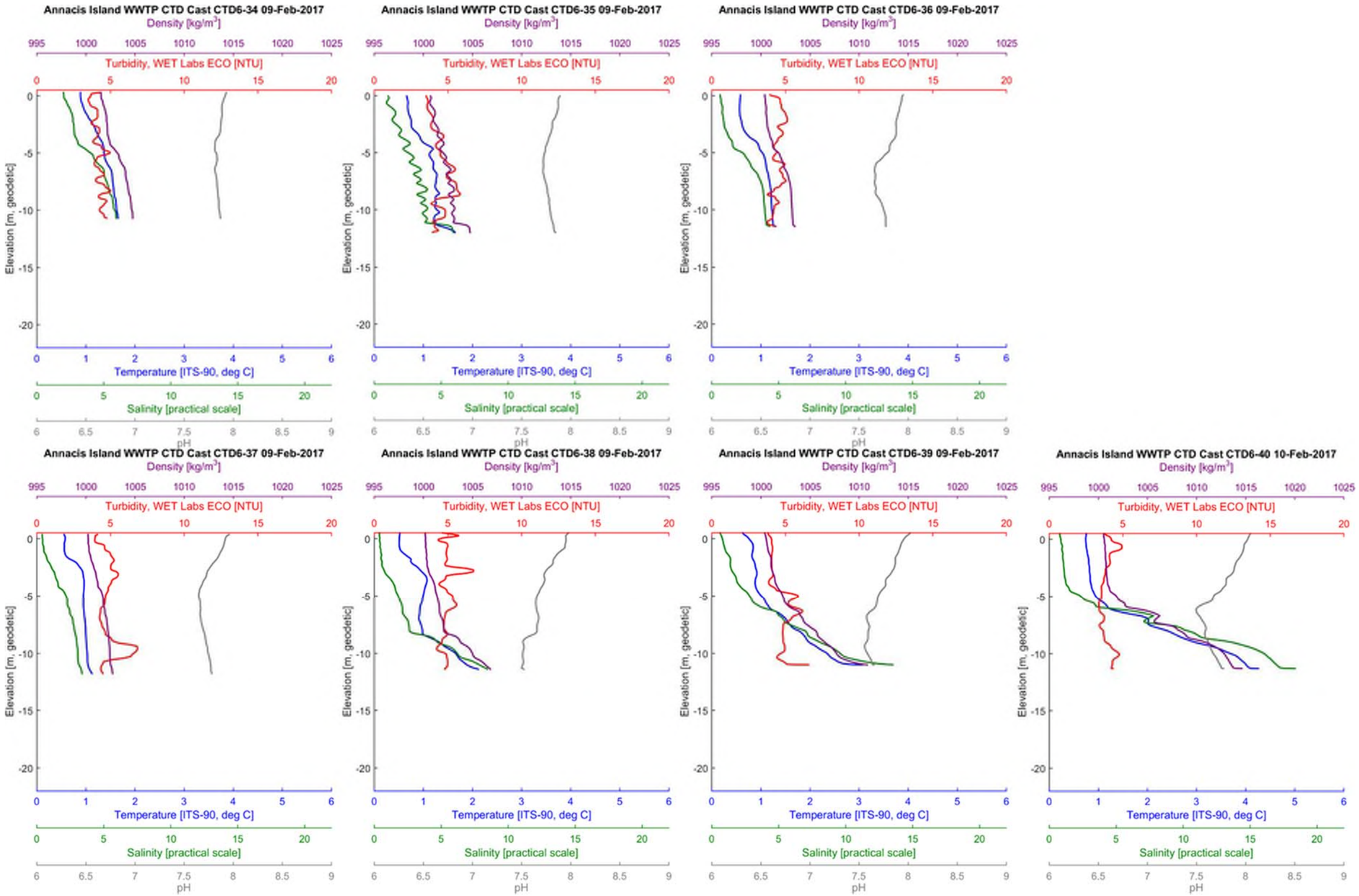


*Figure 38: CTD profiles measured at CTD6 on 9 February 2017*

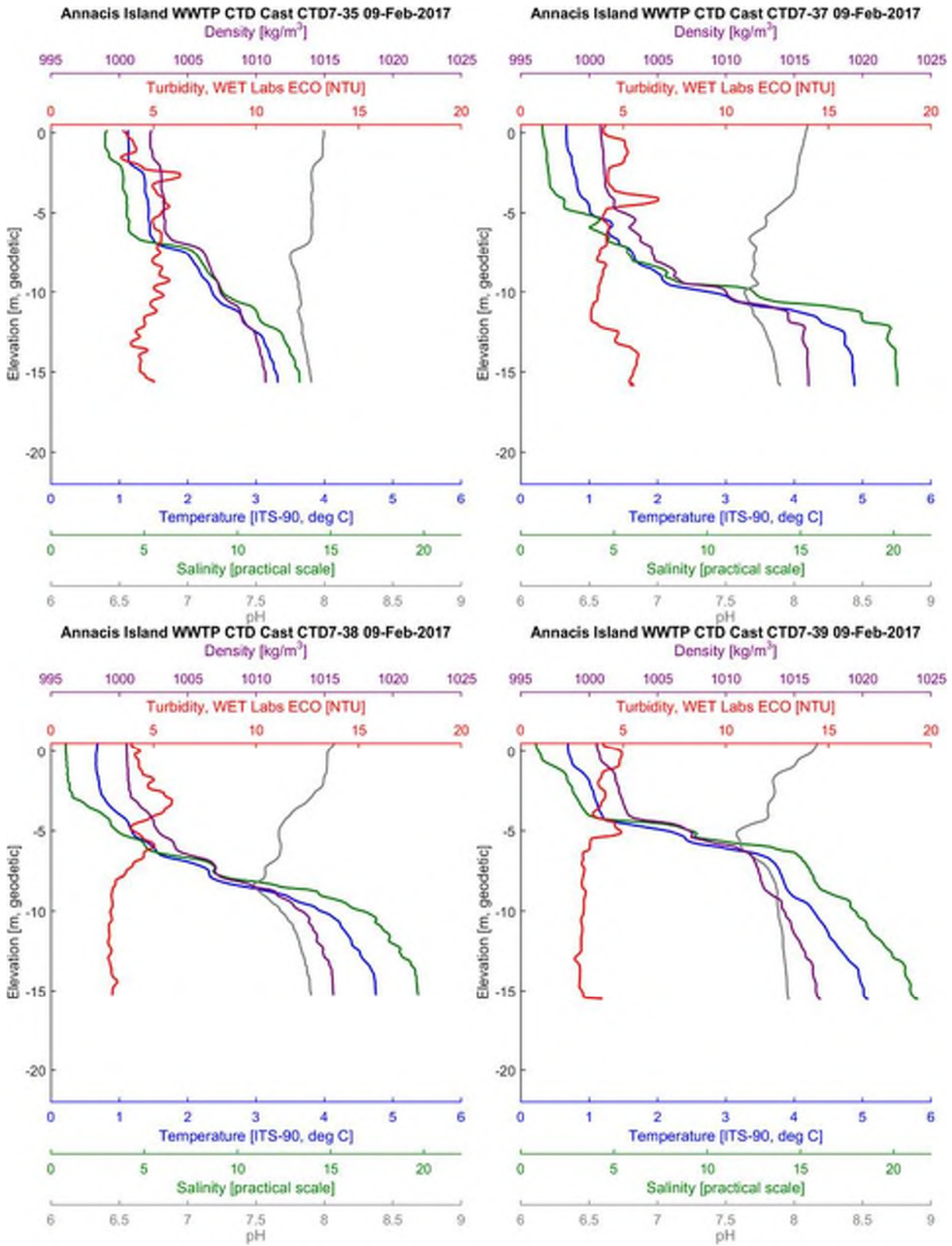


*Figure 39: CTD profiles measured at CTD7 on 9 February 2017*

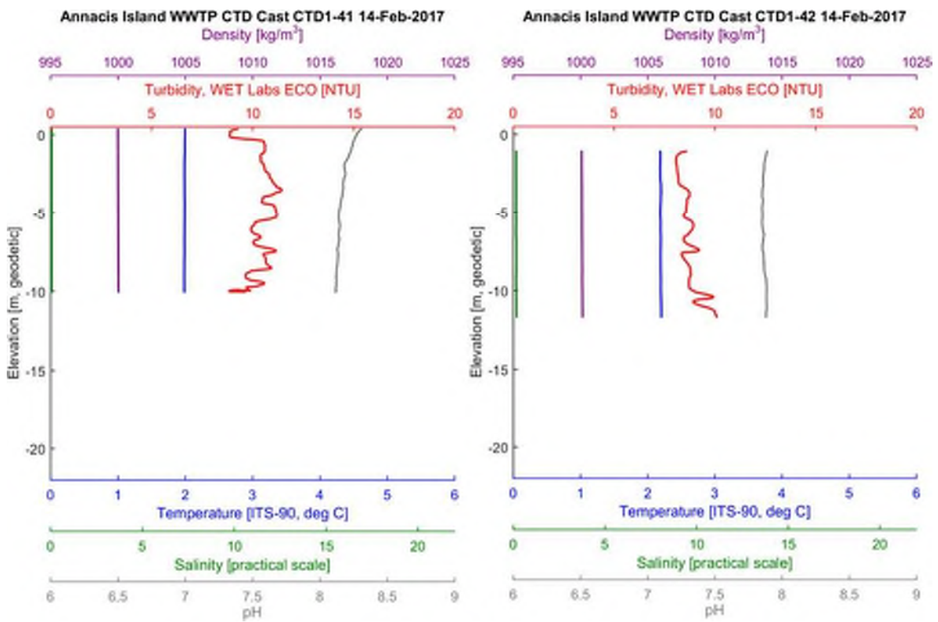


*Figure 40: CTD profiles measured at CTD1 on 14 February 2017*

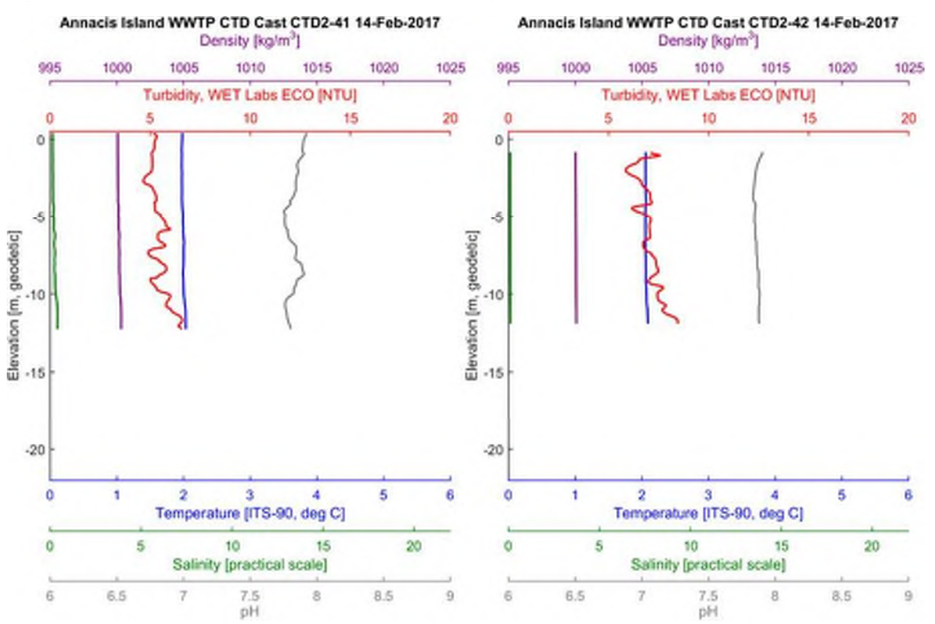


*Figure 41: CTD profiles measured at CTD2 on 14 February 2017*

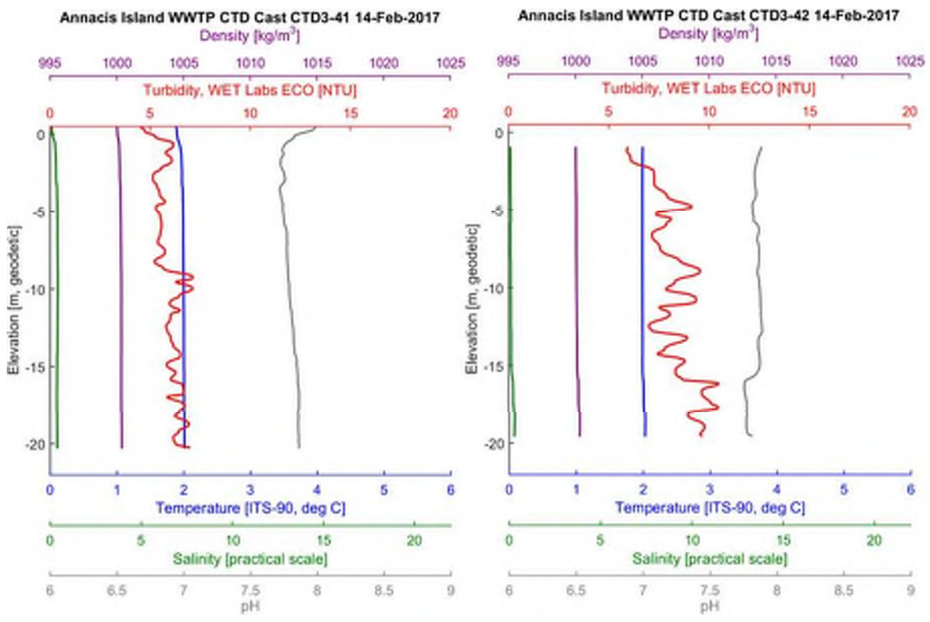


*Figure 42: CTD profiles measured at CTD3 on 14 February 2017*

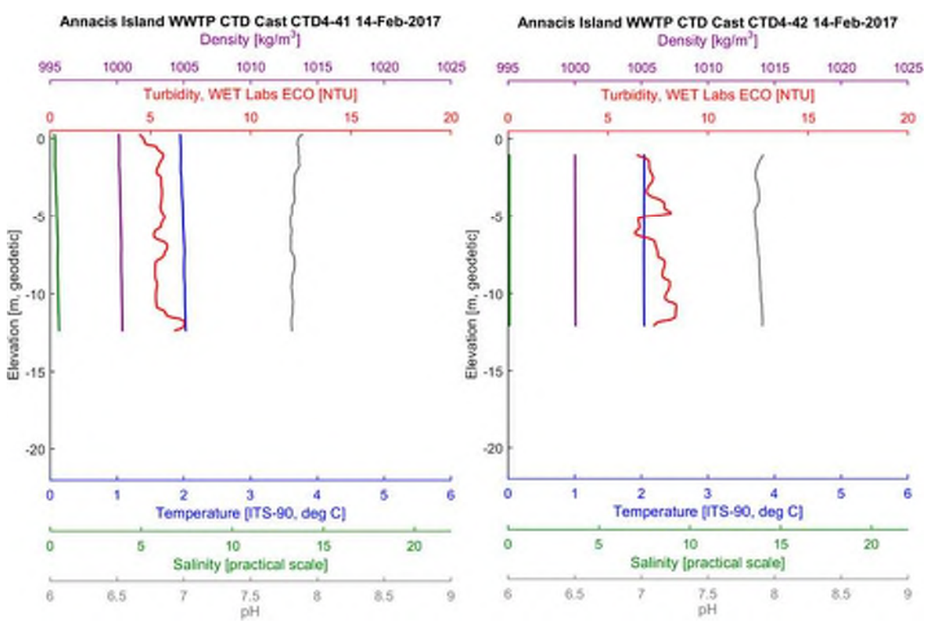


*Figure 43: CTD profiles measured at CTD4 on 14 February 2017*

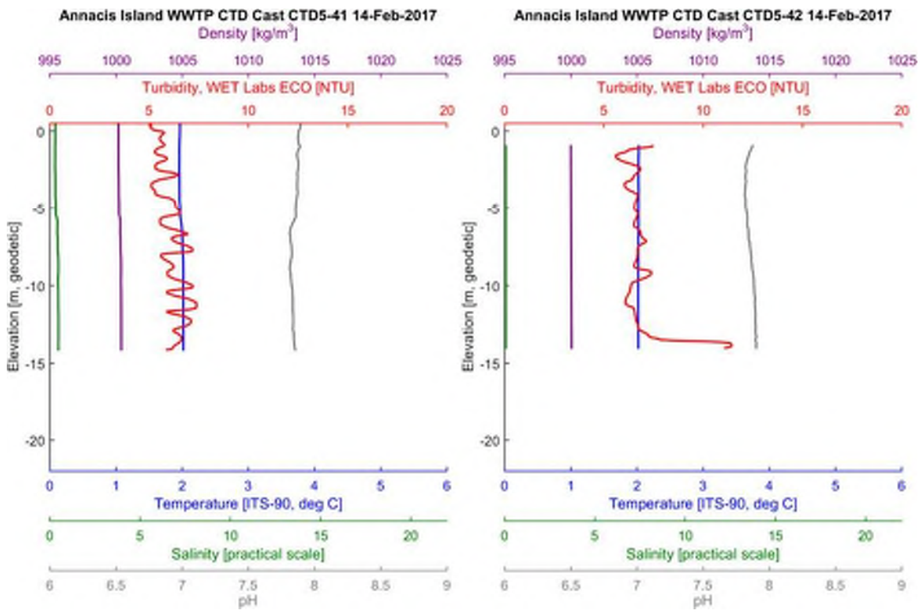


*Figure 44: CTD profiles measured at CTD5 on 14 February 2017*

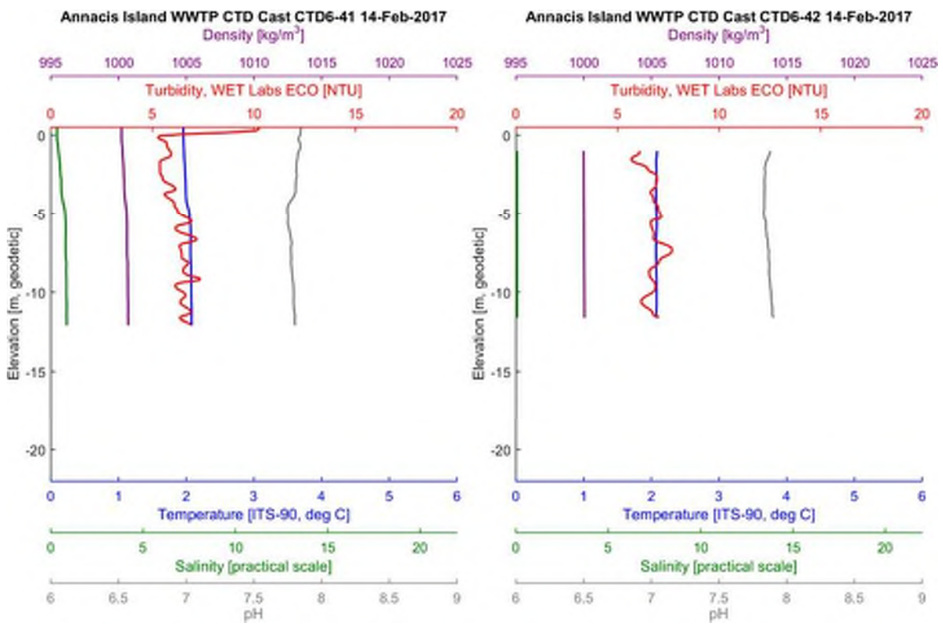


*Figure 45: CTD profiles measured at CTD6 on 14 February 2017*

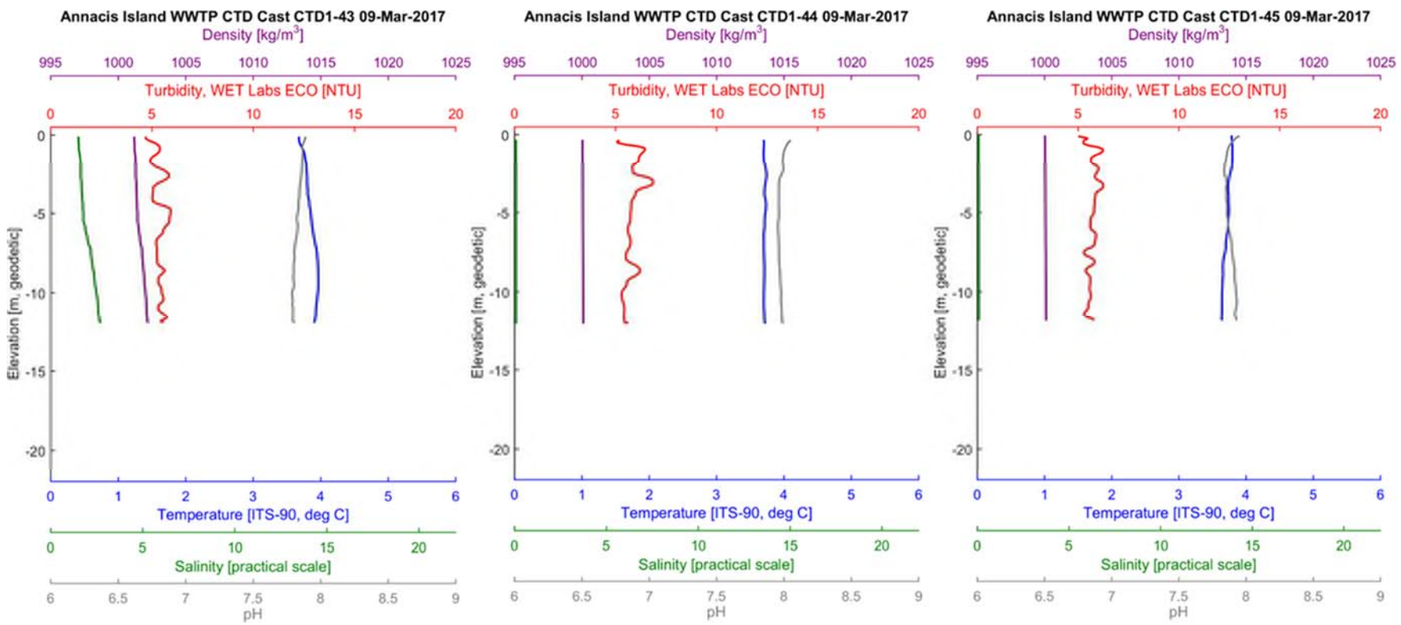


*Figure 46: CTD profiles measured at CTD1 on 9 March 2017*

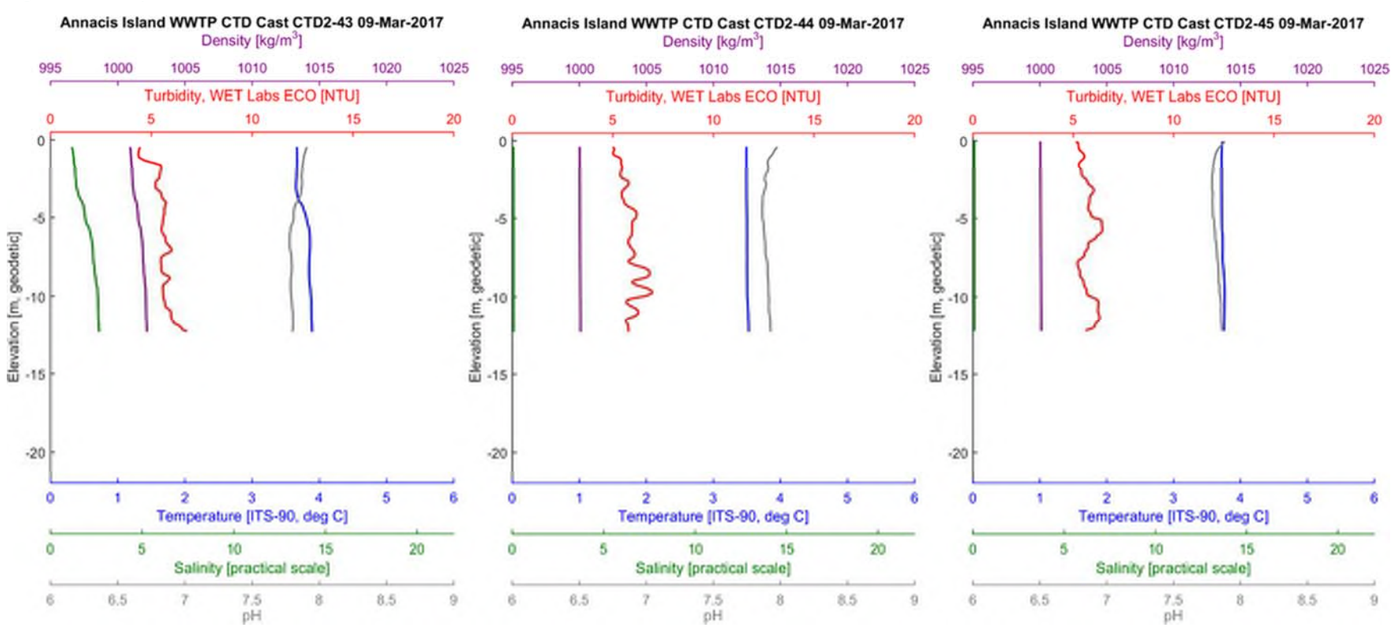


*Figure 47: CTD profiles measured at CTD2 on 9 March 2017*

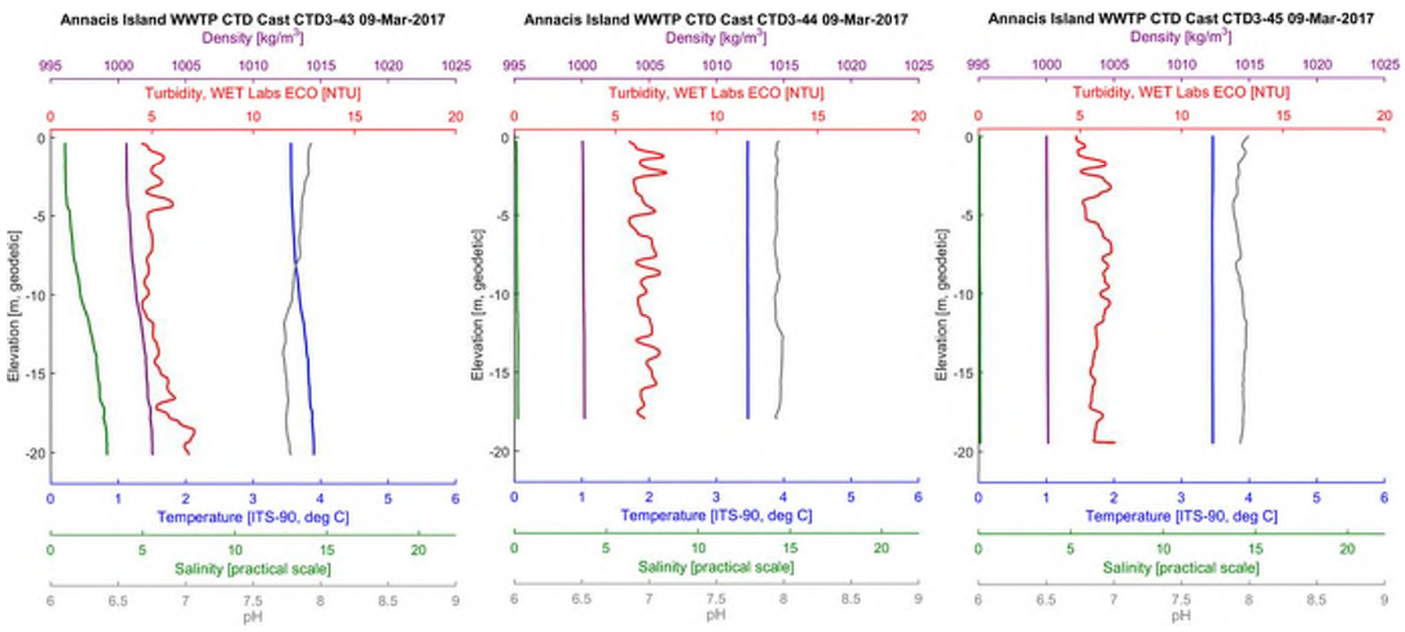


*Figure 48: CTD profiles measured at CTD3 on 9 March 2017*

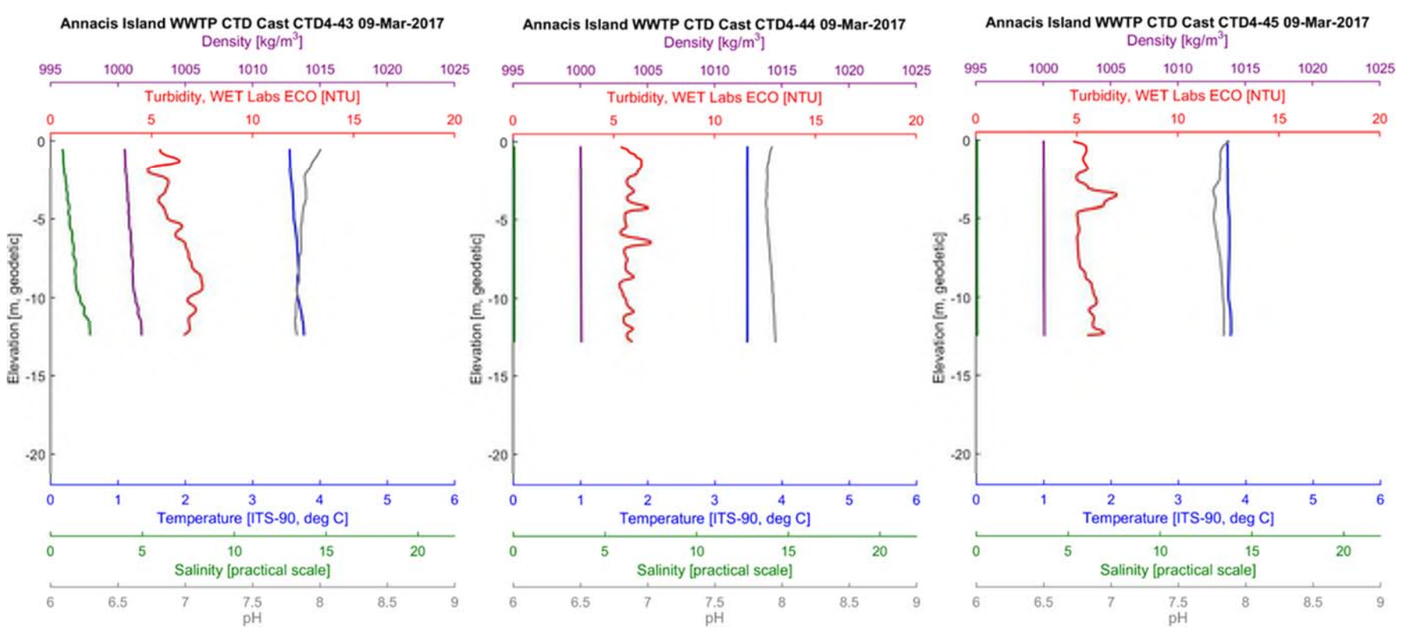


*Figure 49: CTD profiles measured at CTD4 on 9 March 2017*

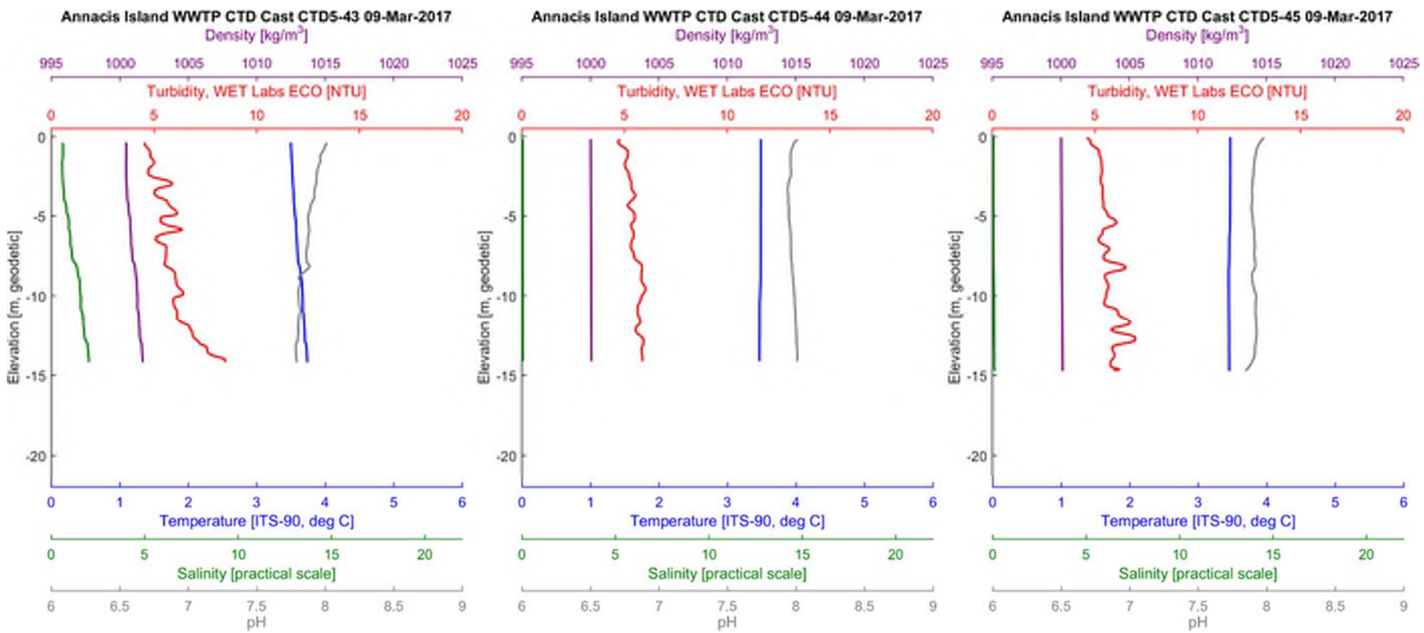


*Figure 50: CTD profiles measured at CTD5 on 9 March 2017*

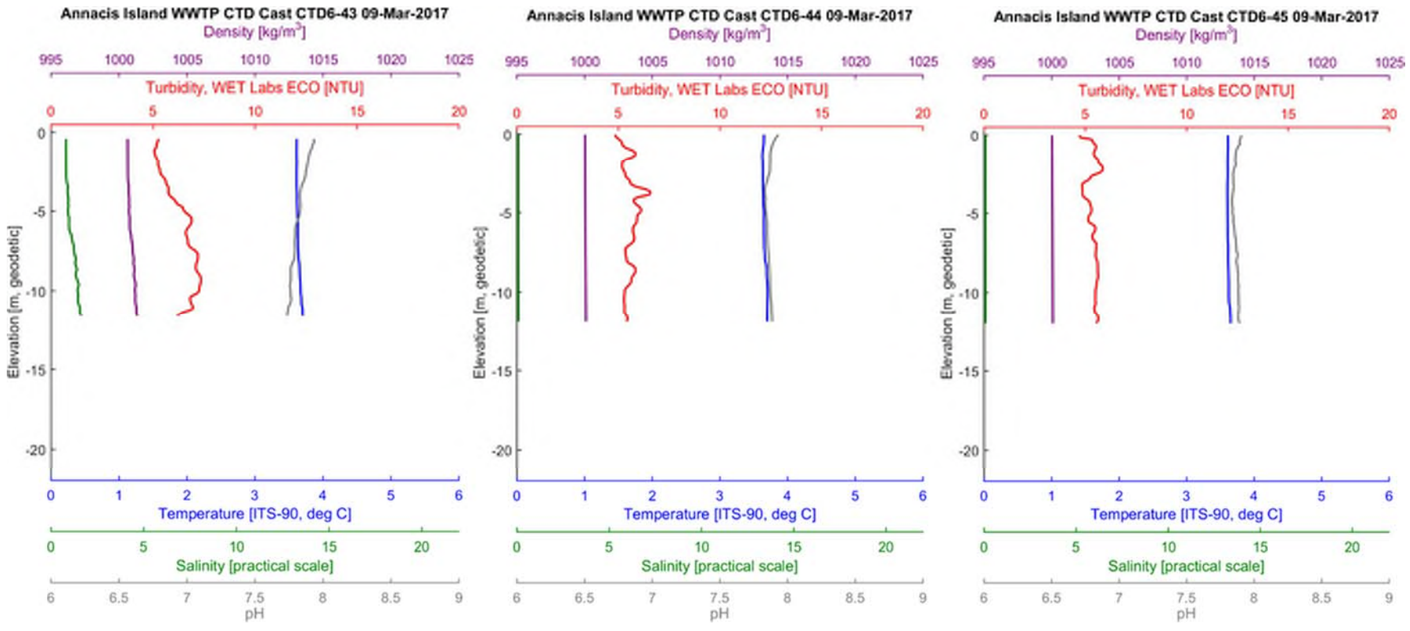


*Figure 51: CTD profiles measured at CTD6 on 9 March 2017*

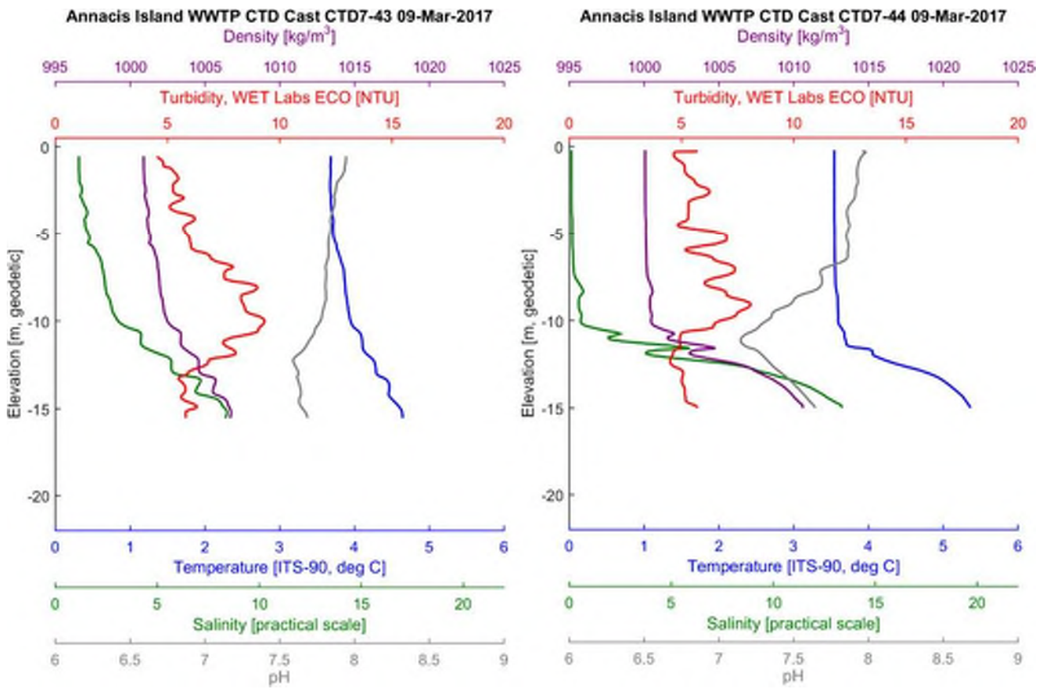


*Figure 52: CTD profiles measured at CTD7 on 9 March 2017*

o:\final\2015\3 proj\1525010 cdm_annacis island wwtp\1525010-083-r-rev1-703\app b\app b.docx

As a global, employee-owned organisation with over 50 years of experience, Golder Associates is driven by our purpose to engineer earth's development while preserving earth's integrity. We deliver solutions that help our clients achieve their sustainable development goals by providing a wide range of independent consulting, design and construction services in our specialist areas of earth, environment and energy.

For more information, visit golder.com


| | |
|---|---|
| Africa | + 27 11 254 4800 |
| Asia | + 86 21 6258 5522 |
| Australasia | + 61 3 8862 3500 |
| Europe | + 44 1628 851851 |
| North America | + 1 800 275 3281 |
| South America | + 56 2 2616 2000 |

solutions@golder.com
www.golder.com

**Golder Associates Ltd.**
**Suite 200 - 2920 Virtual Way**
**Vancouver, BC, V5M 0C4**
**Canada**
**T: +1 (604) 296 4200**


Golder Associates

# Attachment F

# Physical Model Study of The Annacis Island Outfall

This page intentionally left blank.

# PHYSICAL MODEL STUDY OF THE ANNACIS ISLAND OUTFALL

Final Report

Prepared by

Ishita Shrivastava, PhD student

E. Eric Adams, PhD PE, supervisor (eeadams@mit.edu)

MIT Department of Civil and Environmental Engineering

Cambridge, MA 02139

Prepared for

CDM Smith

75 State St #701

Boston, MA 02109

Attn: Bernadette Kolb (kolbBH@cdmsmith.com)

June 2017

(revised July 2017)

## Introduction and Summary

This report summarizes a physical model study of potential Tee diffuser designs for the Annacis Island WWTP. In the following we briefly describe the proposed outfalls, our tank, and how we used the tank to measure effluent dilution at the edge of the Initial Dilution Zone (IDZ) as defined in British Columbia's Municipal Wastewater Regulations. Results are presented in the final section, and are summarized below.

- Over the range tested, dilution generally decreases with increasing diffuser length. Thus a 240 m diffuser is more effective than a 300 m diffuser.
- Over the range tested, dilution decreases with increasing number of nozzles. Thus a 240 m diffuser with 24 nozzles is more effective than a 240 m diffuser with 48 nozzles.
- Over the range tested, dilution decreases with increasing effluent flow rate, holding discharge velocity constant. Thus dilution is lower for Stage VIII effluent flow conditions than for Stage V.
- Dilution decreases in the presence of ambient stratification.
- Minimum dilution is generally least at intermediate current speeds and increases somewhat as current speed increases or decreases.
- Flux average dilution exceeds minimum dilution by a factor of about 1.8.

## Annacis Island Outfall

We modeled three diffusers that could be used to discharge treated effluent from the Annacis Island WWTP to the Annieville Channel of the main arm of the Fraser River. The site is about 20 km upstream of the river mouth in British Columbia, and is characterized by reversing semi-diurnal tides with magnitudes up to about 1.4 m/s. While the estuary is generally fresh water at this location, occasionally a salt wedge is encountered (CDM Smith, 2016). The outfalls are being designed to handle increasing effluent flows in future years up to 18.9 $m^3/s$, under Stage V conditions, and 25.3 $m^3/s$ under later Stage VIII conditions.

The three diffuser alternatives are quite similar. The reference diffuser, which turns out to be the best performing of the three, has a length L = 240 m, and is oriented parallel to shore, approximately 180 m from the near bank where the water depth at low tide is about H = 10 m. As tested, the diffuser has 24 circular discharge ports, each with a diameter of 51 cm, rising one meter above the sediment-water interface and pointing in the offshore direction (making a "Tee" diffuser). Under Stage VIII conditions, all ports would be utilized, resulting in a discharge velocity through each port $u_o$ of about 5.2 m/s, and a nominal port spacing of 240 m/24 = 10 m. Under Stage V conditions, 25% of the ports would be blocked, leaving 18 ports, each with a discharge velocity of approximately 5.2 m/s. The nominal port spacing under these conditions would be 13.3 m. A second diffuser is similar to the reference diffuser except that it is 300 m long and is made up of 30 nozzles with diameters of 46 cm. Under Stage VIII conditions, all ports would be used yielding a nominal port spacing of 10 m and an exit velocity of about 5.2 m/s. A third diffuser is also similar to the reference diffuser, being 240 m long but having 48 nozzles. Under Stage VIII

conditions, all ports would be utilized, resulting in a discharge velocity through each port of about 5.2 m/s, and a nominal port spacing of 240 m/48 = 5 m.

Since we began testing, the design orifice velocity and associated orifice diameter have changed slightly. Hence the expected dilutions will change slightly. These changes are discussed below under the heading of Analysis.

The goal of this study was to quantify minimum and average dilution at the edge of the zone of initial dilution (IDZ) defined by a distance of 100 m from the outfall. Focus was on the maximum flow rates expected under Stage V and Stage VIII conditions (18.9 and 25.3 $m^3/s$ respectively), and on low tide (10 m), since these are the most conservative conditions, i.e., those expected to result in the lowest minimum dilutions. (An exception is during tests with stratification, where highest tide conditions (13 to 14 m) are considered because this is when salinity intrusion may be most likely.) Of particular interest was the effect on dilution of diffuser length, port spacing, ambient density stratification due to salinity intrusion, and ambient current speed.

**Facilities**

The tank is roughly 16 feet long, by 4 feet wide, by 2 feet deep (4.9 x 1.2 x 0.6 m) and made of clear plastic with 8020 aluminum framing. On the top is a carriage which can be towed by a computer driven motor to simulate an ambient current. (Note that the model diffuser is towed in a quiescent river rather than have the river flowing.) The carriage supports a horizontal false floor on wheels, traveling above the real (fixed) floor, which contains the diffuser and the manifold which feeds it. As indicated in Figure 2, the floor extends over most, but not all of the tank width with a gap of a few cm between the false floor and the tank edge. The discharge flow is delivered from a carboy mounted high on top of an adjacent tank. Head in the carboy can be maintained constant by inserting a glass tube in the otherwise sealed top of the carboy turning it into a Mariotte bottle (Fischer, et al., 1979). Discharge flow rate is gauged using a rotameter.

The nozzles are made of stainless steel tubing with precisely measured inside diameter, bent 90 degrees with sufficient radius of curvature so that the water discharges smoothly and horizontally. The nozzles are connected to the manifold, secured underneath the false floor, by Tygon tubing of equal lengths. The relatively large diameter of the manifold and the equal length feeder tubes guarantee uniform flow among the nozzles. The nozzles are securely mounted through holes in the false floor. They are positioned along a straight line, parallel to the (straight) shoreline, and they discharge horizontally in the offshore direction. Because tubing comes in discrete sizes, a different set of nozzles and different holes are required for each of the three diffuser designs. Figure 1 shows the setup and the IDZ boundary for one of the diffuser designs.

The carriage supports camera(s) and instrumentation (e.g., conductivity and fluorescence probes.) Even in the absence of ambient stratification, the wastewater discharge is positively buoyant due to temperature differences between the effluent and the receiving water of about 2 to 9$^oC$. This density difference is simulated by representing the real, positively buoyant, effluent discharging from nozzles near the seafloor, as a negatively buoyant discharge, created by adding salt to the

flow and discharging near the surface into fresh water. The density difference depends on both the water temperature (hence season) and the temperature difference. We have assumed a typical normalized density difference (ambient density minus discharge density divided by ambient density) in the field of $\Delta\rho_o/\rho = 0.0008$, corresponding to a discharge temperature difference in freshwater of about 6°C at an ambient water temperature of 15°C. Using a negatively buoyant salty jet has several advantages over a positively buoyant warm jet: i) the minimum dilution can be determined accurately by using conductivity probes to measure maximum salinity at the edge of the IDZ, since the background salinity is zero; ii) diffuser nozzles can be positioned more easily near the surface than near the bottom, since a finite riser height is required for a bottom mount (it is hard to make the nozzle "turn the corner" with a reasonable radius of curvature in very shallow water depth (4-5 cm)); and iii) conductivity or dye probes can be positioned more accurately near a rigid flat bottom than near a wavy surface. We have used this "upside down" approach in the past and it works well.

Most of the runs were conducted without stratification and used five conductivity probes (Thermo Scientific Orion Star A222) to record excess salinity and hence minimum dilution, $S_{min}$. The five probes were positioned along the boundary of the IDZ which was marked on the false floor for each diffuser design. The probes rested on the false floor and measured salinities approximately 1 cm from the bottom, in the model, or about 2-3 m below the surface in the field. Probe positions were previously determined from video images of dyed plumes. Following an experiment, the peak salinity, corresponding to the minimum dilution, was found by interpolation among the five probes. For higher ambient current speeds, video images of the dyed plume were also used to directly evaluate average dilution along the IDZ, using the definition $S_{ave} = u_{drift}HB/Q_o$, where $u_{drift}$ is the speed of the plume as it passes the IDZ boundary, H is the water depth, B is the plume width and $Q_o$ is the effluent flow rate. B and $u_{drift}$ were determined from videos of the dyed plume. Average dilution could generally only be determined for the two highest current speeds that produced an effluent plume that crossed the downstream boundary of the IDZ.

Vertical salinity profiles were measured during several tests, and confirmed that the salinity was nearly constant over the water depth which is consistent with the shallowness parameter $\phi = HL^{1/3}\Delta_o^{2/3}/(Q_o^{1/3}u_o)$ being around 0.2. Here $\Delta_o$ is the reduced gravity equal to $g\Delta\rho_o/\rho$. Adams (1982) found that the effluent plumes from a tee diffuser were well-mixed when $\phi < 0.3$.

While most tests were conducted in an unstratified ambient, one set was conducted with ambient stratification. In general, an arbitrary vertical profile of salinity can be established using a "two-tank" filling method (Hill, 2002). However, because of the shallow water depth in our tank, and the absence of definitive salinity profiles in the field, the goal was to use step-wise stratification consisting (in the real world) of a 5-m thick layer with salinity of 12 PSU overlain by an 8- to 9-m thick freshwater layer (total depth of 13 to 14 m). The moving carriage resulted in some mixing of the stratified ambient; measurements of stratification were taken before and after each test to determine this. For runs with ambient stratification, both the discharge and the ambient contain salt, so Rhodamine WT dye was added to the discharge, and minimum dilution was determined by fluorescence measured with a calibrated fluorescence probe (Turner Designs Cyclops 7). The

fluorescence probe measured concentrations about 4 cm above the false floor in the model, or 2.7 m above the bottom in the field.

**Model scaling and other considerations**

In a scale model, lengths, velocities, flow rates, times, and values of reduced gravity ($\Delta=g\Delta\rho/\rho$) must be chosen to honor dynamic, geometric and kinematic similitude between model and prototype. If we define $L_r$, $U_r$, $Q_r$, $T_r$, and $\Delta_r$ as the ratios of lengths, velocities, flow rates, times and density differences in the field to the lab, geometric similitude means that all lengths scale as $L_r$ (i.e., no distortion), kinematic similitude means that $L_r = U_rT_r$ (distance equals velocity times time in both model and prototype) and $U_r^2 = \Delta_r L_r$, which means that the densimetric Froude number is the same in lab as in the field.

Another dimensionless parameter of interest is the jet Reynolds number, $Re = u_oD_o/\nu$ where $u_o$ is the jet exit velocity, $D_o$ is the initial jet diameter, and $\nu$ is the kinematic viscosity of water. Assuming viscosity is the same in model and prototype, $Re_r = U_rL_r = L_r^{3/2}\Delta_r^{1/2}$. Clearly equivalent Re cannot be maintained in a reduced scale model, but results should be insensitive to Re if the jet is turbulent, which requires that Re be approximately 1500 or greater (Ungate, 1974). In order to achieve adequate values of Re in our finite-size tank, we used a value of $\Delta_r = 1/8$. This means that density differences in the model were eight times greater than in the field (e.g., the discharge density difference in the field of $\Delta\rho_o/\rho = 0.0008$ became 0.0064 in the model).

The area of interest is depicted schematically in the plan view of Figure 2, and includes the near shoreline, the diffuser, and the IDZ. Important dimensions include the diffuser length L, the port spacing $\ell$, the distance from the shoreline to the diffuser $X_s$, and the offshore distance between the diffuser and far wall W.

**Tests**

Tests were conducted in two phases: a set of confirmatory tests and a set of sensitivity tests.

***Phase 1*** (Confirmation tests): These consisted of several runs with a simpler model (not a direct replica of Annacis Is.) of a tee diffuser designed to test the validity of three of the modeling assumptions. These include:

1) Effect of $\Delta_r$. Most "Froude scale" models use a density ratio of $\Delta_r = 1$. Tests were conducted with a larger length diffuser (to achieve adequate Re) and different density ratios and corresponding length ratios to see if there was any change in observed dilution. The tests confirmed that the density scaling was satisfactory.

2) Treatment of $X_s$ (see Figure 2). Based on prior discussion, the actual distance from the shoreline to the diffuser is about 180 meters, and the bottom slopes over this distance from the shoreline to the diffuser. Adams et al. (1982) found that, for a quiescent ambient and uniform water depth, dilution decreased modestly as the normalized shoreline separation $X_s/L$ decreased. In the present

study, several tests were conducted in a current. Results of these tests showed that dilution was insensitive to $X_s$ for values of $X_s/L > 0.15$, where Xs is interpreted as the equivalent shoreline separation in water of constant depth. Thus all of our tests were conducted with $X_s/L > 0.3$. The lesser effect of shoreline separation on dilution in a current, versus under quiescent conditions, is likely due to the fact that in a current, more of the entrainment is from the offshore side of the diffuser.

3) Effect of W (see Figure 2). The offshore boundary of the model is fairly close to the IDZ, and conceivably could affect the results. However, experiments conducted with W/L equal to 0.80, 1.05, and 1.35 showed no significant difference, providing confidence in the model results (most of which were conducted with W/L = 0.84 or above). One explanation for the relative insensitivity to W/L is that the floor of the carriage does not extend to the far wall, allowing some of the dense, previously mixed effluent to "fall off the cliff" before it reaches the far wall, thus preventing build-up that would influence subsequent near field mixing.

***Phase 2*** (Basic sensitivity tests): As indicated in Table 1, five sets of tests were conducted. Each set consisted of a diffuser design with a given discharge flow rate, ambient stratification, and water depth, and operating in four (or in one set five) ambient current speeds, making a total of 21 runs. Many runs also included up to 6 replicates. The dimensions of the parameters listed in Table 1 are all at field scale, but one can uncover the laboratory dimensions using the length scale $L_r$ provided in the right-hand column, and the above scaling relationships described above. We note that, due to the relatively shallow water depth, a return current is generated when the carriage is towed. The ambient velocities reported are the effective velocities seen by the diffuser (in the field). These are equal to the towing speed plus the speed of the return current (as determined from videos of the dyed plume) converted from laboratory values to the field using the velocity ratio $U_r$.

The step-wise stratification in the real world with 5 m thick bottom layer with salinity of 12 PSU and 8.3 m thick fresh water layer (water depth of 13.3 m) scales (with $L_r = 272$ and $\Delta_r = 1/8$) to a step-wise stratification in the tank with a 1.8 cm thick fresh water layer over a 3.1 cm thick bottom layer with salinity of 96 PSU. The density difference between the warm, positively buoyant wastewater discharge and the bottom layer with salinity of 12 PSU (in the real world) is simulated by discharging salt water with salinity of about 103 PSU into the freshwater layer in the tank.

For the tests with ambient stratification, the tank was first filled with a salt water layer (salinity = 96 PSU) such that the water level was 3.1 cm above the false floor. The fresh water layer of 1.8 cm was then added using a splash plate to minimize mixing between the two layers. However, due to shallow depths of the two layers, there was some mixing and the resulting salinity profile, near the surface, was approximately linear, which actually better represents conditions in the Fraser River. Salinity measurements were taken at three different depths (0.4, 1.5 and 2.1 cm below the surface) and were extrapolated to the bottom by balancing the amount of fresh and salt water to the idealized two-layer profile. Figure 3 shows the salinity measurements and the extrapolation to the bottom for one test. The extrapolated salinity profile was linear over the top 3.5 cm, with salinity of about 28 PSU at the top to salinity of about 60 at a depth of 3.5 cm. The bottom 1.5 cm had the desired salinity of 96 PSU. This corresponds to a 4.1 m thick fresh water layer at the top of a 9.3 m layer with linear salinity profile going from 4.5 PSU to 8.5 PSU.

Table 2 lists the minimum dilution (as an average of replicates when more than one test was run) measured at the edge of the IDZ (based on maximum measured salinity or concentration), the average dilution at the edge of the IDZ (based on video images of the dyed plume), and the ratio of the two. The minimum dilutions are plotted in Figure 4 against the ambient current speed. For the tests in un-stratified ambient, "error" bars on some of the points reflect the range of dilutions from replicate runs. For the runs with ambient stratification, the error bars reflect the uncertainty in the fluorescence calibration. The fitted lines plotted with the data for the un-stratified tests reflect the dilution equation described below (Eq. 1)

The following conclusions can be drawn from Figure 4 and Table 2.

- Over the range tested, dilution generally decreases with increasing diffuser length (Set 4 with a length of 300 m performs worse than Set 1 with a length of 240 m). This is in accordance with other diffuser studies we have looked at recently (Shrivastava and Adams, 2017), and may be due to the fact that each individual jet in a longer diffuser, with similar port spacing, delivers somewhat less offshore momentum reducing the trajectory length and hence the dilution.
- Over the range tested, dilution decreases with increasing number of nozzles (Set 3 with 48 nozzles performs worse than Set 1 with a 24 nozzles). This is also not surprising, and is likely due to the increase in jet interference. When there are more nozzles, more closely spaced, the jets run into each other sooner, reducing dilution.
- Over the range tested, dilution decreases with increasing effluent flow rate (Set 1 with Stage VIII flows has lower dilution than Set 2 with Stage V flows). This confirms our assumption that high effluent flow is a worst case condition.
- Dilution decreases with ambient stratification (Set 5 with stratification) performs worse than Set 1 with no stratification) despite the greater water depth (13.3 m versus 10 m). This is likely because the plume is trapped, restricting the effective depth over which the jet can mix with ambient water.
- Minimum dilution is generally least at intermediate current speeds and increases somewhat as current speed increases or decreases. The minimum dilution at intermediate current speed has been observed in other diffuser studies, and could reflect the fact that the intermediate current speed corresponds to conditions when the diffuser momentum and ambient momentum are comparable, as seen in the momentum ratio $m_r$ described in the following section. Seo et al. (2001) suggested "when the crossflow momentum becomes stronger than the discharge momentum, i.e., $m_r > 1$, the crossflow begins to overcome the blocking effect of the effluent plume, tending to be entrained into the effluent plume." The blocking effect is the result of a region of high pressure caused by the ambient current and diffuser flow which leads to dilution lower than $S_o$ at small values of $m_r$ (Adams, 1982).
- Flux-average dilution exceeds minimum dilution by a factor of about 1.8 which is reasonably independent of current speed, diffuser length, nozzle spacing or discharge flow rate.

**Analysis**

Based on the minimum dilution measurements for Phase 2 tests as well as previously reported experiments with tee diffusers in a crossflow (Shrivastava and Adams, 2017), an equation was developed to describe the effect of various non-dimensional variables on the minimum dilution at the edge of the IDZ.

$$\frac{S_0}{S_{min}} = 0.8\left[1 + 0.08(L/H)^{3/4}(\ell/H)^{-0.28}\,\mathrm{sech}\{0.87\log_{10}(m_r)\}\right] \quad (1)$$

Here $S_0 = (HLu_0/(2Q_0))^{1/2}$ is the dilution of a tee diffuser in quiescent ambient (Adams, 1982), $\ell$ is the nominal port spacing and $m_r = u_a^2HL/(u_0Q_0)$ is the momentum ratio, a parameter which characterizes the effect of ambient current momentum relative to the momentum of the ambient current. The predicted dilutions using Eq. (1) for the four sets of tests in un-stratified ambient are shown in the four lines in Figure 4.

Eq. (1) was also "inverted" to compute the effective depth (H*) over which plumes, mixing in a stratified ambient, receive the minimum dilutions $S_{min}$ that were observed. With the ideal step-wise stratification, the diffuser plume could be expected to be trapped in the bottom layer which is 5 m deep, while for the observed salinity profiles, which were closer to linear, a value of H* somewhat greater than 5 m might be expected, due to the fact that the actual profile is already partly mixed (compared to the idealize step stratification). For the smallest current, the measured dilution is higher than the other cases. This is reflected in the value of H* which is 8.9 m for $u_a$ = 0.07 m/s and is higher than the other runs which have mixing depths between 4 and 6 m.

As noted above, the design conditions have changed somewhat since the experiments were conducted. In particular, the port velocity $u_o$ has been decreased, necessitating a corresponding increase in the port diameter $D_o$, such that the overall flow rate $Q_o$ remains constant. From Eq. (1) it can be seen that an increase/decrease in $u_o$ of 10% would result in an increase/decrease in $S_{min}$ of 4 to 6 %. It can be noted that a 10% change in $u_o$ results in a 5% change in $S_o$. $u_o$ also affects the value of $m_r$ which contributes to the 1% change (increase or decrease depending on the ambient current) in $S_{min}$.

**Table 1: Phase 2 tests conditions (parameter being varied listed in parentheses)**

| Set | Runs | L (m) | n | $Q_o$ ($m^3/s$) | Stratification | H (m) | $u_a$ (m/s) | $L_r$ |
|---|---|---|---|---|---|---|---|---|
| 1 | 1-4 | 240 | 24 | 25.3 | No | 10 | 0.07, 0.22, 0.52, 1.13 | 272 |
| 2 | 5-8 | 240 | 18 | **18.9** | No | 10 | 0.07, 0.22, 0.52, 1.13 | 272 |
| 3 | 9-13 | 240 | **48** | 25.3 | No | 10 | 0.06, 0.21, 0.48, 0.63, 1.05 | 225 |
| 4 | 14-17 | **300** | 30 | 25.3 | No | 10 | 0.07, 0.22, 0.52, 1.13 | 245 |
| 5 | 18-21 | 240 | 24 | 25.3 | **Yes** | 13.3 | 0.07, 0.22, 0.52, 1.13 | 272 |

**Table 2: Phase 2 results**

| Set | $u_a$ (m/s) | $S_{min}$ | $S_{ave}$ | $S_{ave}/S_{min}$ |
|---|---|---|---|---|
| 1-Base Case | 0.07 | 13.2 | | |
| 1-Base Case | 0.22 | 10.6 | | |
| 1-Base Case | 0.52 | 12.4 | 23.8 | 1.9 |
| 1-Base Case | 1.13 | 15.7 | 27.6 | 1.8 |
| 2-Stage V flow | 0.07 | 18.9 | | |
| 2-Stage V flow | 0.22 | 11.3 | | |
| 2-Stage V flow | 0.52 | 16.5 | | |
| 2-Stage V flow | 1.13 | 13.5 | | |
| 3- Reduced port spacing | 0.06 | 11.2 | | |
| 3- Reduced port spacing | 0.21 | 9.0 | | |
| 3- Reduced port spacing | 0.48 | 10.2 | 19.6 | 1.9 |
| 3- Reduced port spacing | 0.63 | 11.1 | | |
| 3- Red port space | 1.05 | 12.9 | 21.8 | 1.7 |
| 4-Longer diffuser | 0.07 | 14.1 | | |
| 4-Longer diffuser | 0.22 | 9.9 | | |
| 4-Longer diffuser | 0.52 | 10.1 | 17.7 | 1.8 |
| 4-Longer diffuser | 1.13 | 13.8 | 24.7 | 1.8 |
| 5-Stratification | 0.07 | 11.4 | | |
| 5-Stratification | 0.22 | 5.7 | | |
| 5-Stratification | 0.52 | 7.7 | | |
| 5-Stratification | 1.13 | 8.3 | | |

**References**

Adams, E. (1982). "Dilution analysis for unidirectional diffusers", *J. Hydraulics Division, ASCE* 108(HY3): 327-342.

Adams, E., Skamarock, W., and Nothaft, R. (1982). "Shoreline Effects on the Mixing of a Tee Diffuser". *J. Hydraulics Division, ASCE* 108(HYl0): 1232-1238.

CDM Smith Canada, "Multiport diffuser design and initial dilution modeling, Annacis Island WWTP Transient mitigation and outfall project", report prepared for Metro Vancouver, July 29, 2016.

Fischer, H., List J., Koh R., Imberger J., and Brooks N. (1979). *Mixing in Inland and Coastal Waters*. Academic Press, San Diego, CA.

Hill, D. F. (2002). "General density gradient in general domains: the 'two tank' method revisited". *Exp. Fluids., 32(4), 434-440.*

Seo, I. W., Kim, H. S., Yu, D., & Kim, D. S. (2001). "Performance of Tee Diffusers in Shallow Water with Crossflow" *J. Hydraulic Engineering*, 127 (1): 53-61.

Shrivastava, I., and Adams, E. (2017). "Dilution from shallow water outfalls: a review of historical data". Manuscript in preparation.

Ungate, C.D. (1974). "Temperature reduction in a submerged vertical jet in the laminar-turbulent transition", SM thesis, Dept. of Civil and Environmental Engineering, M.I.T., Cambridge, MA

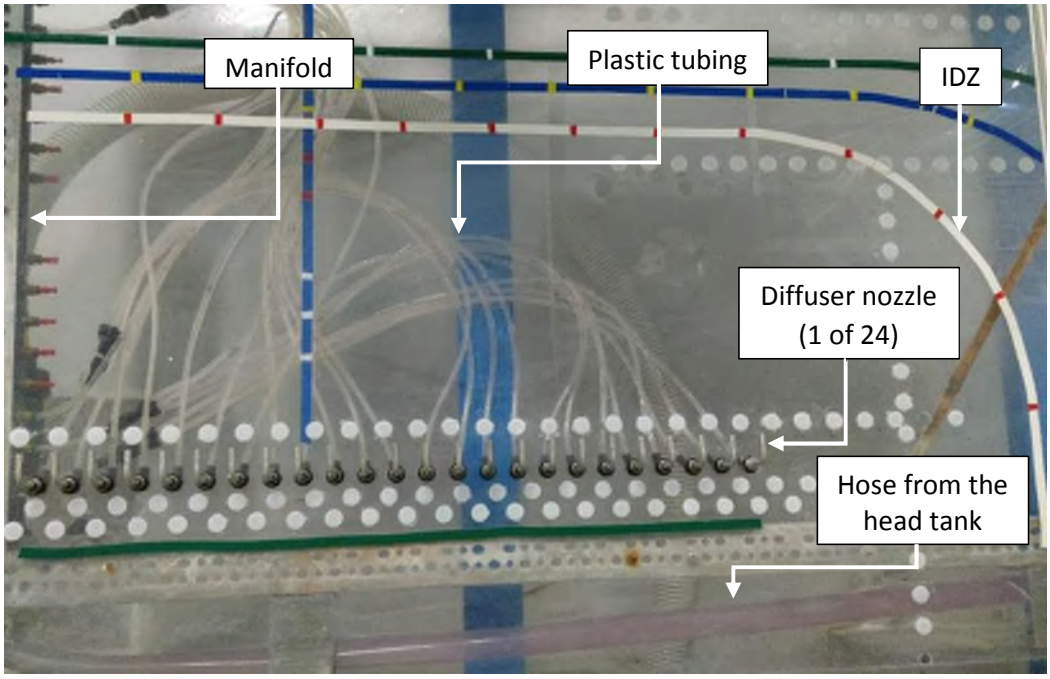


**Figure 1: Picture of the model diffuser and IDZ boundary. The diffuser is towed to the left, simulating a current to the right. The IDZ boundary is marked on the model floor in white with red markers. The manifold, supplying effluent through plastic tubing to the individual nozzles, is located to the left. The effluent is supplied from the head tank to the manifold by the hose seen at the bottom of the picture.**

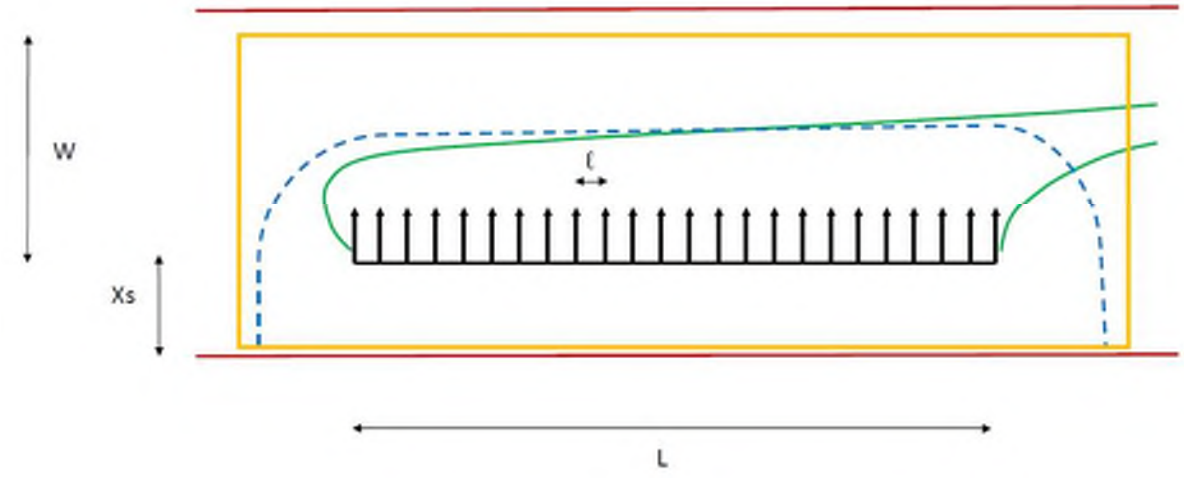


**Figure 2: Sketch of the model (not to scale). The diffuser is being towed to the left, simulating a current from left to right. Model boundaries are shown in red, the plume is shown in green, the false floor is shown in orange, and the IDZ is shown in dashed blue.**

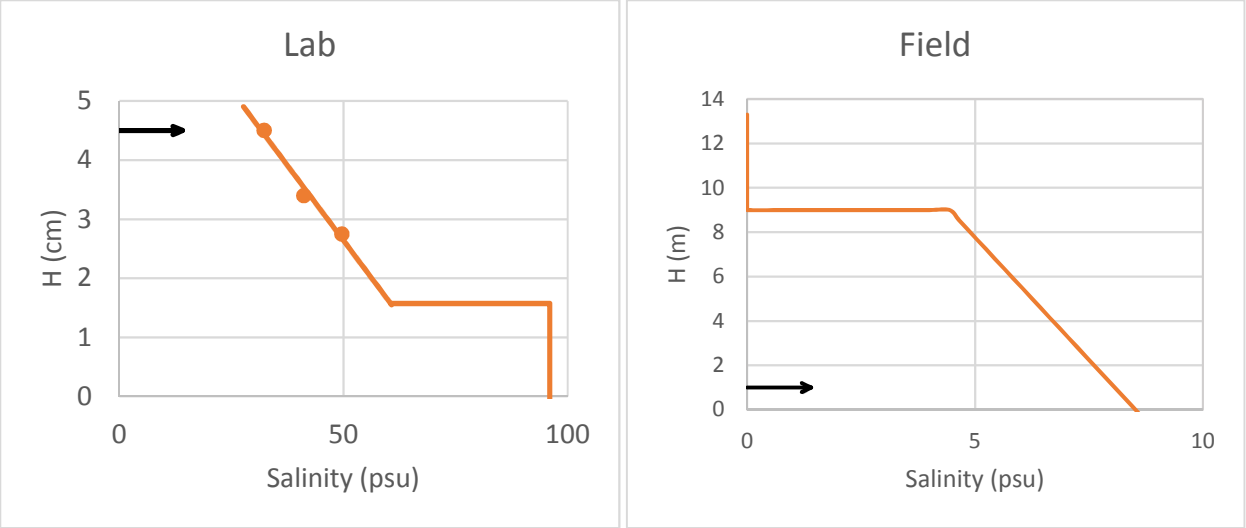


**Figure 3: Observed salinity profile in the lab (left); corresponding salinity profile in the field (right). The arrows show discharge elevation.**

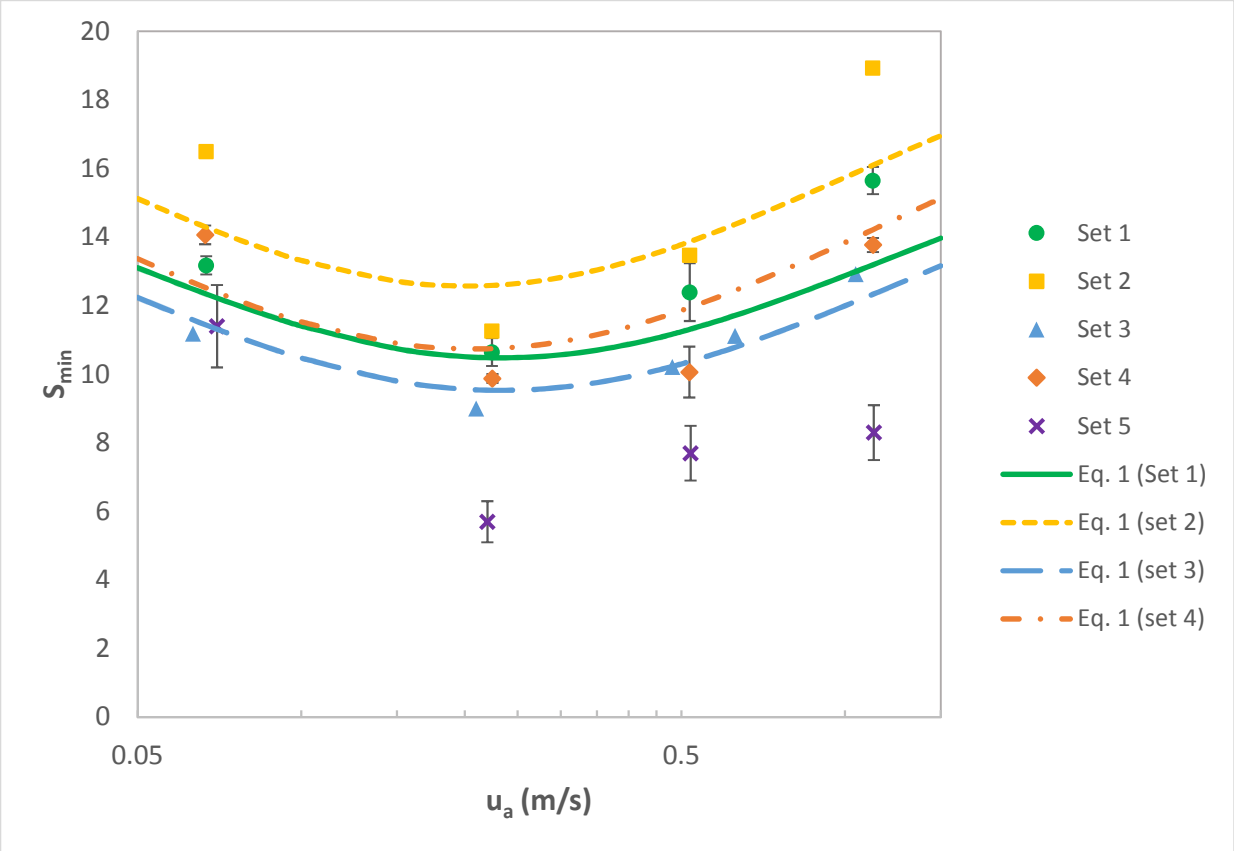


**Figure 4: Measured minimum dilution (symbols) versus $u_a$. "Error bars" for un-stratified tests reflect range of measured dilutions in replicates. Error bars for stratified tests reflect uncertainty in fluorescence calibration. Lines are predicted dilution from Eq. (1) for the un-stratified tests.**

# Attachment G

# Tetra Tech Far-Field Modelling Report

This page intentionally left blank.

# Hydrodynamic and Plume Modelling for the Annacis Island Outfall

PRESENTED TO

**CDM Smith Canada Ltd.**

JANUARY 23, 2018
ISSUED FOR USE
FILE: 704-TRN.WTRM03039-01

Tetra Tech Canada Inc.
Suite 1000 – 10th Floor, 885 Dunsmuir Street
Vancouver, BC V6C 1N5 CANADA
Tel 604.685.0275 Fax 604.684.6241

This page intentionally left blank.

# TABLE OF CONTENTS

## LIST OF TABLES IN TEXT



## LIST OF FIGURES IN TEXT

# APPENDIX SECTIONS

## APPENDICES

## LIMITATIONS OF REPORT

This report and its contents are intended for the sole use of CDM Smith and their agents. Tetra Tech Canada Inc. (Tetra Tech) does not accept any responsibility for the accuracy of any of the data, the analysis, or the recommendations contained or referenced in the report when the report is used or relied upon by any Party other than CDM Smith, or for any Project other than the proposed development at the subject site. Any such unauthorized use of this report is at the sole risk of the user. Use of this document is subject to the Limitations on the Use of this Document attached in the Appendix or Contractual Terms and Conditions executed by both parties.

# 1.0 INTRODUCTION

In 2015, Metro Vancouver retained CDM Smith Canada LLC.to design a new, larger capacity outfall to be situated in the Fraser River, downstream of the Alex Fraser Bridge, for the Annacis Island Wastewater Treatment Plant. CDM Smith leads the design/EIR team, and engaged Tetra Tech Canada Inc. (Tetra Tech) to conduct numerical modelling of the far-field dispersion properties of the proposed new outfall. This report describes the numerical modelling that was conducted and the data products that were generated to enable CDM Smith and Golder Consultants Ltd. to forecast the performance of the new diffuser with respect to dilutions achieved in the receiving environment.

The required data products were generated by coupling Tetra Tech's in-house three-dimensional model of the Fraser River with the UM3 PLUMES model developed by the US EPA. The coupling was implemented by integrating the UM3 model code into the compiled H3D code, so that the two models could communicate continuously, with a time-step of about 6 seconds.

Because of the large effect that local circulation has on diffuser performance, this report provides an overview of the circulation in the Lower Fraser River in Section 1.0. Section 2 describes the three-dimensional hydrodynamic model H3D, including its validation as well as a discussion of the flow features that the model generates. Section 3.0 describes the UM3 model and the integration of UM3 into H3D, as well as examples of model results. Section 4.0 describes the data products provided to CDM Smith.

## 1.1 Circulation in the Lower Fraser River

### 1.1.1 Hydrodynamics

The lower reach of the Fraser River between Sand Heads at the river mouth and Douglas Island at the confluence with the Pitt River approximately 45 km upstream (Figure 1.1) is a tidally-influenced estuary where freshwater runoff collected in the catchment of the Fraser River Basin mixes and interacts with saline water intruding from the Strait of Georgia. The hydrodynamics of the river in the lower reach is governed by complex processes that involve interaction between varying water level and salinity at the river mouth in the Strait of Georgia and the river flow at the upstream end. In addition, the Fraser River transports a significant amount of sediment; while some portions remain in suspension and are discharged into the Strait directly, a large amount settles to the bottom, of which some become re-mobilized from scouring due to high local current speeds: the balance of sedimentation and scouring action continuously sculpts and changes the geometry and bathymetry of the river. The presence of the sediment, moreover, gives rise to the varying frictional effects imparted to the river flow as a result of the morphological evolution of the bed with time.

### 1.1.2 Salt Wedge

The salt wedge in the Fraser River is a cyclical semi-diurnal intrusion of saltwater under the fresh river water on top, a feature typical of coastal estuaries. The term wedge refers to the wedge shape of the saltwater-freshwater interface that forms as the salt wedge moves up the river: the leading edge is location at the river bottom, with most of the water column above occupied by fresh water. Further downstream, salt water is found all the way from the river bed to the water surface, giving rise to the wedge shape. The upstream extent of the wedge varies depending on the stage of the tide and the river flow rate. The leading edge of the salt wedge ranges from Sand Heads at the river's mouth to past the trifurcation near Pattullo Bridge, 35 km upstream of the mouth. The salt wedge advances and retreats in synchronization with the rise and fall of the water level due to tide. In addition, the position of the salt wedge varies as a result of changes in river flow; the higher the river flow, the less upstream the salt wedge advances. Figures 1.1 and 1.2 are the surface and profile view, respectively, of the modelled salinity in the salt wedge at high tide on November 13, 2011 at 10 am. Figures 1.3 and 1.4, respectively, illustrate the surface and profile view of the modelled salinity at the preceding lower low water, 6 hours earlier at 2 am on November 13, 2011. These figures were generated by the three-dimensional circulation model H3D, discussed in Section 2.0, and used for the far-field simulations conducted for this report.

The longitudinal section (Figure 1.2) shows the salinity distribution over the reach from Sand Heads to the Alex Fraser Bridge. The observed water level and its fluctuation at New Westminster is shown in the inset graph in Figure 1.1. Figures 1.1 – 1.4 illustrate the large range of salinities and water levels that can occur in the river on a daily basis.

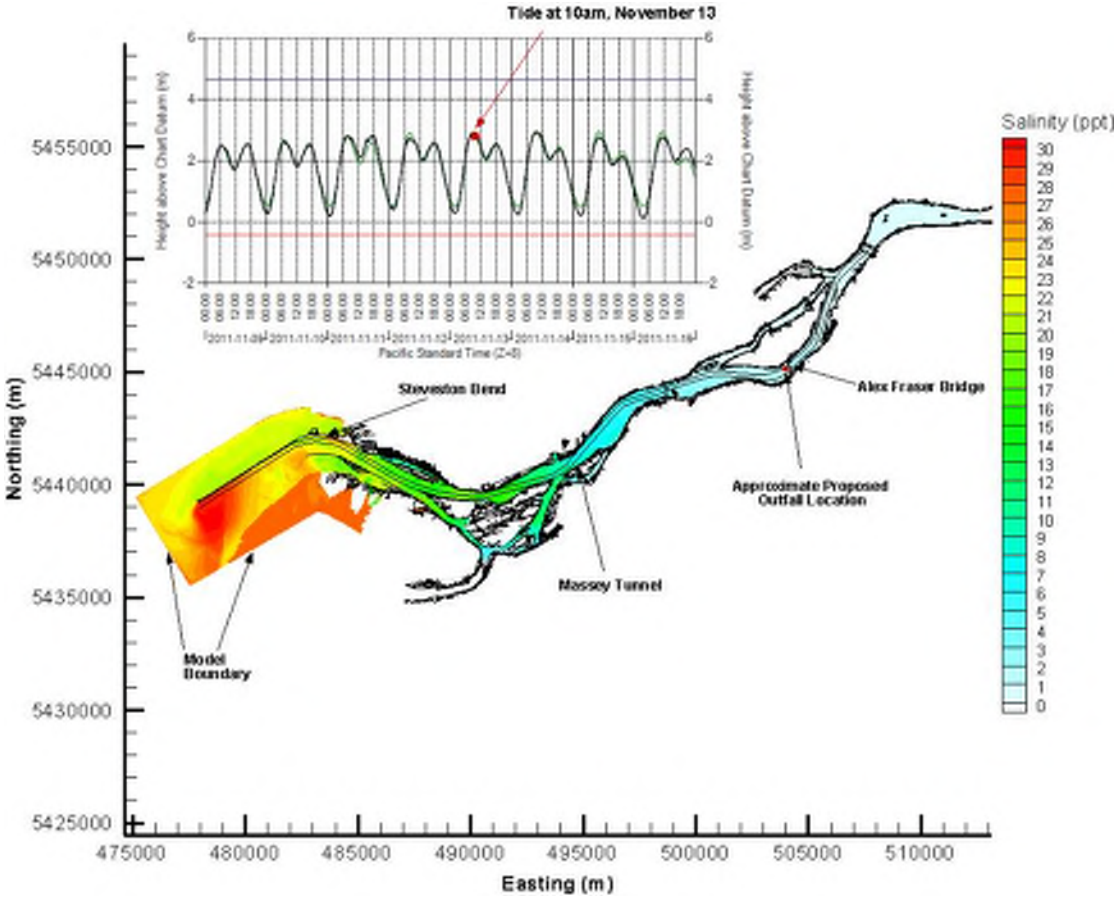


**Figure 1.1: Surface Salinity Contours at High Tide in the Fraser River (Nov 13, 2011 @ 10 am)**

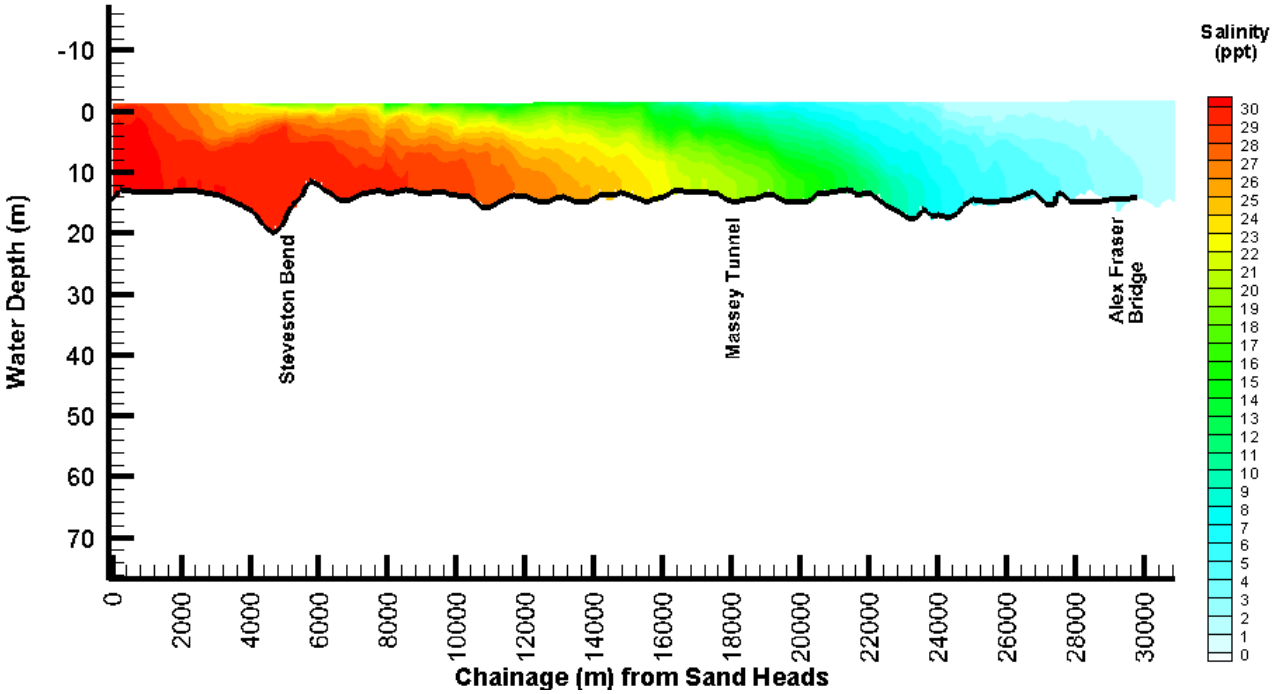


**Figure 1.2: Longitudinal Salinity Contours at High Tide along the Fraser River (Nov 13, 2011 @ 10 am)**

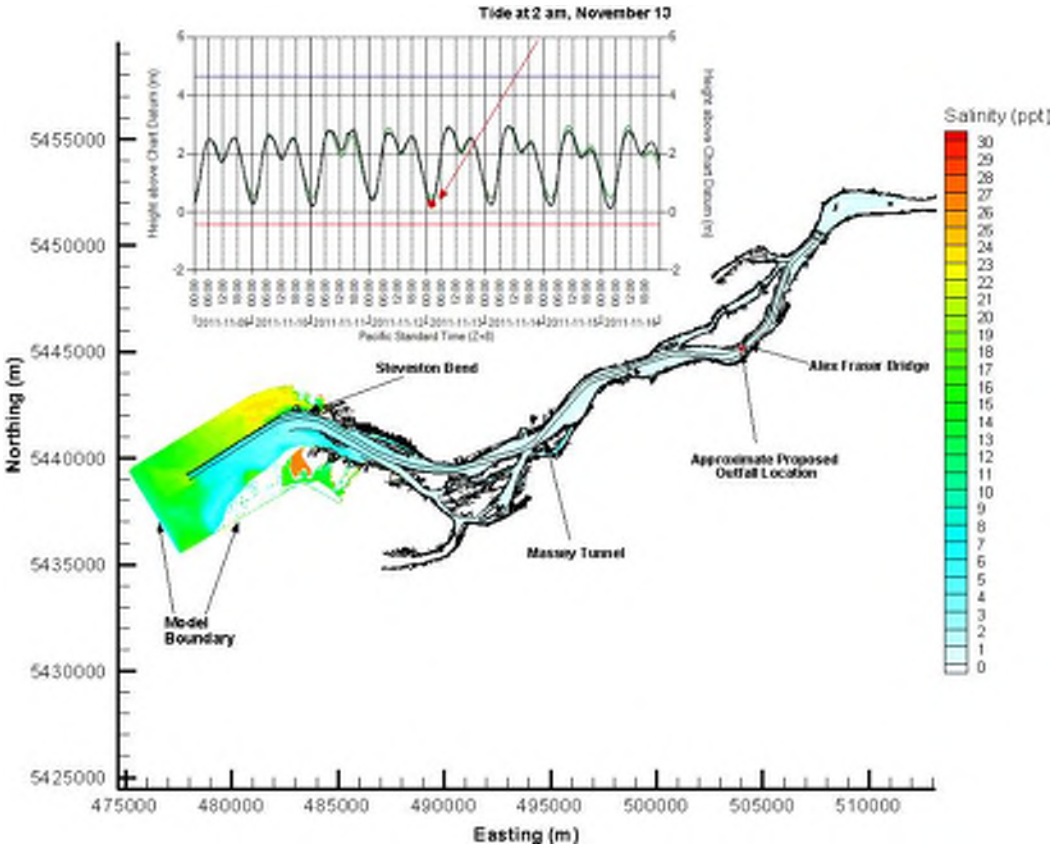


**Figure 1.3: Surface Salinity Contours at Low Tide in the Fraser River (Nov 13, 2011 @ 3 am)**

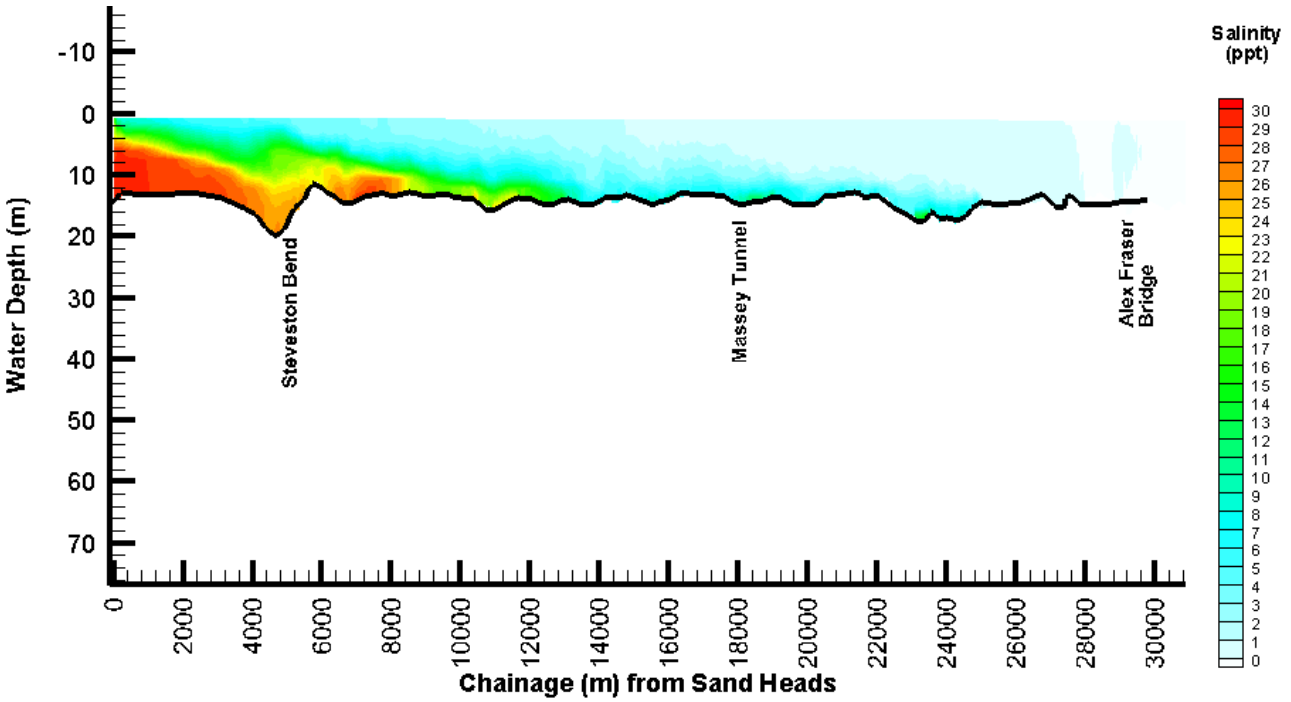


**Figure 1.4: Longitudinal Salinity Contours at Low Tide along the Fraser River (Nov 13, 2011 @ 2 am)**

# 2.0 HYDRODYNAMIC MODELLING

## 2.1 Hydrodynamic Circulation Model

A detailed technical description of H3D is attached in Appendix A. The following is a brief summary.

H3D is a three-dimensional time-stepping numerical model which computes the three components of velocity (u,v,w) on a rectilinear or curvilinear grid (the Fraser River model is a curvilinear grid model) in three dimensions (x,y,z), as well as scalar fields such as salinity, temperature and contaminant concentrations. The model uses the Arakawa C-grid (Arakawa and Lamb, 1977) in space, and uses a two level semi-implicit scheme in the time domain.

H3D is an implementation of the numerical model developed by Backhaus (1983; 1985) which has had numerous applications to the European continental shelf, (Duwe et al., 1983; Backhaus and Meir Reimer, 1983), Arctic waters (Kampf and Backhaus, 1999; Backhaus and Kampf, 1999) and deep estuarine waters, (Stronach et al., 1993). Locally, H3D has been used to model the temperature structure of Okanagan Lake (Stronach et al., 2002), the transport of scalar contaminants in Okanagan Lake, (Wang and Stronach, 2005), sediment movement and scour / deposition in the Fraser River, circulation and wave propagation in Seymour and Capilano dams, and salinity movement in the lower Fraser River. H3D forms the basis of the model developed by Saucier and co-workers for the Gulf of St. Lawrence (Saucier et al., 2003), and has been applied to the Gulf of Mexico (Rego et al., 2010).

## 2.2 Model Grids

Simulation of detailed hydrodynamics in the Fraser River requires detailed information in the Strait of Georgia as well, since the Strait of Georgia is the source of tidal forcing in the river and the source of the salt water that drives the tidally-varying salt wedge. For this study, a large-scale Strait of Georgia hydrodynamic model provides information to the higher-resolution Fraser River model. This procedure is called model nesting and the configuration is shown in Figure 2.1.

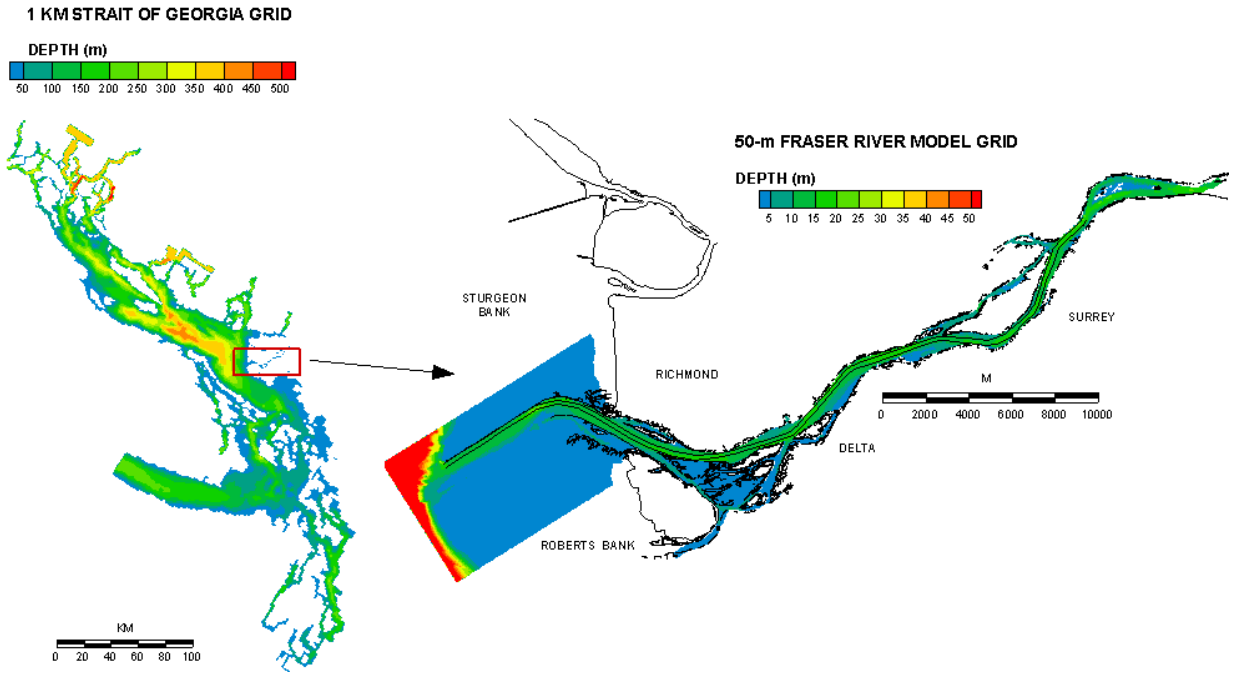


**Figure 2.1: Model Nesting of Strait of Georgia and Fraser River Grids**

The investigation of the hydrodynamics near the outfall location is done with a nominally 50-m resolution curvilinear model that spans the lower 41 km of the Fraser River, from Sand Heads to the Port Mann Bridge. The model uses 50-m resolution in the along-channel direction, and 20-m in the cross-channel direction. This 50-m resolution model is in turn embedded within a 1-km rectilinear resolution model of the entire Strait of Georgia and Juan de Fuca Strait (SOG). The river model has 1.5-m thick layers in the upper 21 m, resulting in 9-12 active layers in most locations in the model, depending on the tide.

Both models simulate tidal, wind-driven and density-driven currents. Water level, velocity components and any scalar quantities output from the Strait of Georgia model are passed to the Fraser River model along the common boundary between the two models, and are used to drive the Fraser River model. The fine-grid implementation for the Fraser River enables the simulation of the details of the effect of small-scale spatial variability in shorelines, depths and structures in the river, such as the Alex Fraser Bridge piers.

The 1-km SOG model is driven by wind on the water surface and by density and tidal conditions along its open boundaries, which border the northern entrance to the Strait of Georgia and the western entrance to Juan de Fuca Strait. The SOG model includes a coarse representation of the Fraser River, extending upstream to km 41, with separate channels for the North Arm, the South Arm and Canoe Pass. At km 41, upstream of all salt wedge penetration, the model is dynamically coupled to a one-dimensional model of the Fraser River, extending to Hope.

The 50-m lower Fraser River model is driven at its upstream end by a flow boundary condition provided by the same dynamically-coupled one-dimensional model of the Fraser River that was also used for the 1-km model. At the

downstream end, water levels and density profiles are obtained from the 1-km SOG model, spatially interpolated from those cells of the 1-km SOG model that correspond to the boundaries of the lower Fraser model.

## 2.3 Model Validation

To gain confidence in a numerical model's capability to correctly simulate circulation patterns, the model must be validated against observations. A typical model validation involves comparison of observed and modelled parameters such as water level, currents, salinity and sedimentation pattern. The H3D model used in this study was validated as part of the Delta Farmers Climate Change Study (TetraTech, 2016). In that study, H3D was validated against water level recorded at New Westminster, against salinity data collected by a sensor mounted at 2 m depth from a floating platform installed at a water intake near 8081 River Road, Delta and maintained by the Corporation of Delta, and against visual observation of surface current patterns in the area. The intake at 8081 River Road is a readily accessible data set, and close to the proposed outfall. However, detailed evaluation of the complex salinity movements around this intake have demonstrated that this measurement point is subject to considerable un-predicable fluctuations, and hence is somewhat challenging as a validation data set.

The year 2011 was chosen for the model validation because bathymetry data was collected from a bank-to-bank survey that year, enabling the construction on an accurate bathymetry grid for the 50-m Fraser River model. Thus, the Fraser River flow rate in 2011 was used to drive the upstream boundary of the river model. The flow rate at the upstream boundary of the model is the combination of the flow rate at Hope and the estimated runoffs that report to the river downstream of Hope and upstream of the Port Mann Bridge, notably the Harrison River based on monthly ratios to the Fraser at Hope flows. Figure 2.2 shows the river flow rate at Hope in 2011.

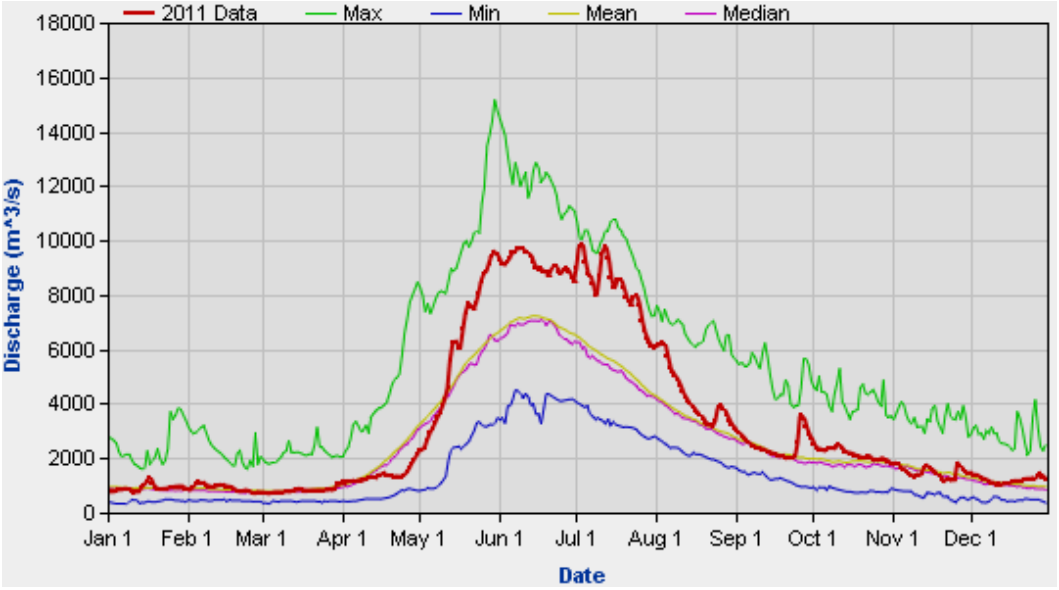


**Figure 2.2: Fraser River Flow Rate at Hope in 2011**

### 2.3.1 Water Level and Salinity

Figure 2.3 shows a comparison of salinity between observed and modelled values from November 3rd to 23rd 2011, at a depth of 2 m. Also included in the figure are observed and modelled water levels for the same time period. Black lines show modelled values and red lines show observed values. Since the conductivity sensor cuts off at 5,500 μS/cm, the model results were similarly cut-off to facilitate comparison.

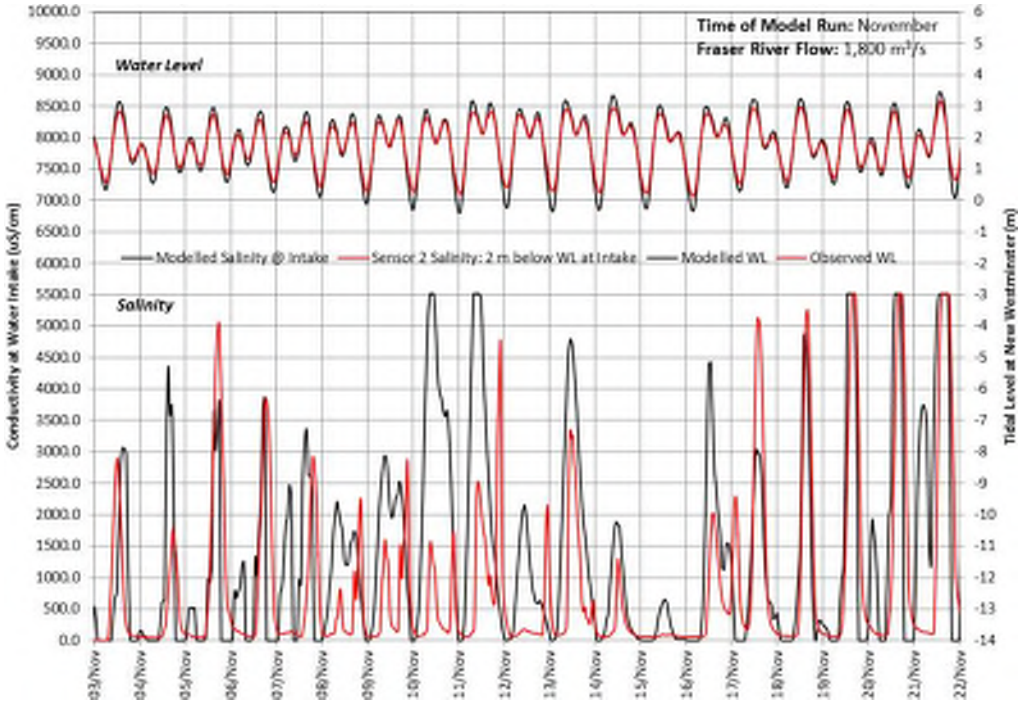


**Figure 2.3: Comparison of Observed and Modelled Water Level and Salinity in the Fraser River near the Delta Farmers Water Intake**

The model performs well with respect to water level. The disagreement in level for periods of low water arises because of uncertainty in the friction parameter, which in turn depends of the conditions of the river bed; the knowledge regarding the relationship between friction and river bed conditions is complex and is a topic of ongoing research and improvement. The model generally performs well, predicting the timing of salinity peaks on a daily time scale. However, the magnitude of the salinity peaks is less-well reproduced. For example, the model almost always predicts an elevation of salinity during high tides when river flow is comparatively lower and water level in the river higher (for example, on November 10$^{th}$); however, the sensor at the intake did not always detect such a salinity signal. There are two reasons for this level of disagreement. First, lower salinities than predicted are correlated with local large rainfall events, not captured in the model. Second, the water intake is situated in a shallow area where complex processes controlling the differential movement of salty and fresh water contribute to the observed high variability and, sometimes, unpredictability in salinity at the intake.

The effect of the flow processes in the vicinity of the intake can be appreciated by considering Figure 2.4, showing the map of salinity and currents at the 2-m depth, on Nov 11 at 7 am, where the modelled result appears to deviate the most from the observed value. It can be seen that there is a high degree of spatial variability in the salinity field (at 2 m depth) in the vicinity of the intake. Salinity can vary from 3.5 ppt (4,500 μS/cm) to more than 5.0 ppt (6,500 μS/cm) near the intake in a matter of metres.

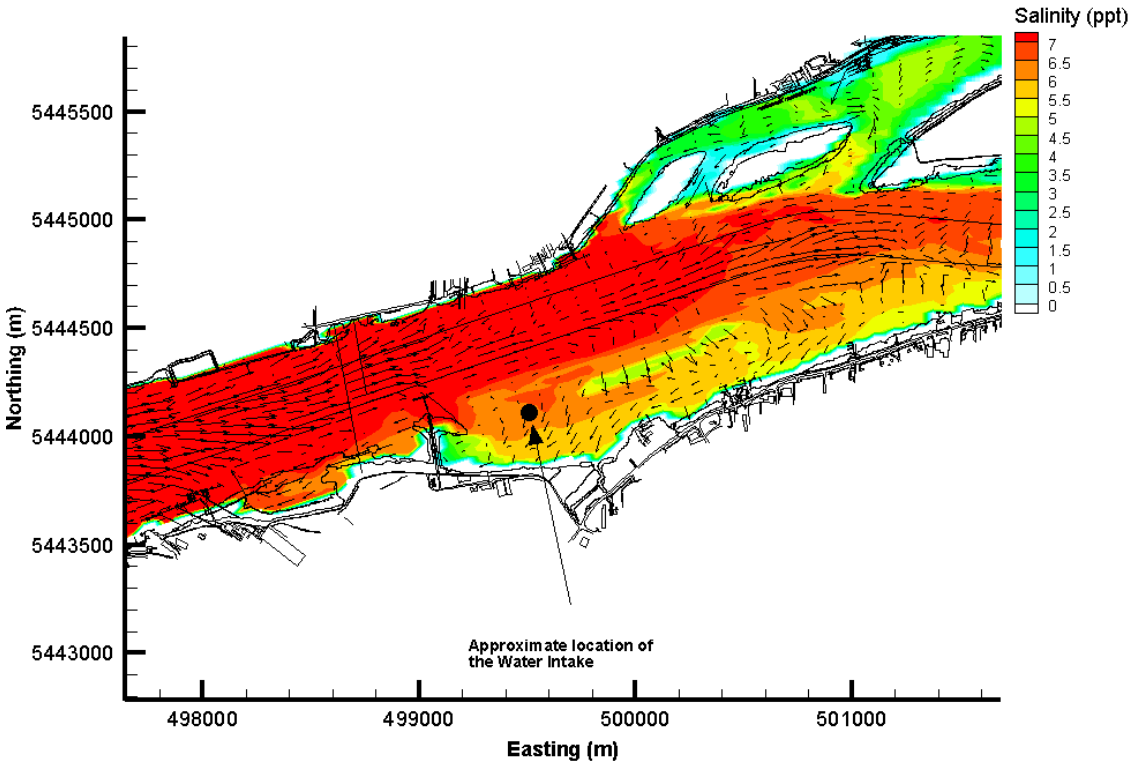


**Figure 2.4: Snapshot of Salinity Contour at Depth of 2m on November 11 at 7 am**

### 2.3.2 Surface Circulation Patterns

The Annacis Island outfall is located immediately downstream of the Alex Fraser Bridge where the river width significantly decreases at the two bridge abutments located on the south and north banks of the river. Upstream and downstream of the abutments, the river width increases. A satellite photo from Google Earth indicates a prominent circulation feature at this location that was also reproduced in the model: an anti-clockwise gyre is typically observed downstream of the south abutment during a falling tide when water level is decreasing. Figure 2.5 is a Google image of the area taken on June 4th, 2015 at 4 pm.


**Figure 2.5: Google Earth Image of Fraser River near Annacis Island Outfall on June 4, 2015 at 4 pm**

The figure shows a clear difference in light reflection from the water in the middle of the river than that near the south shore. Deducing from this observation, there appears to be a separation front downstream of the south bridge abutment, and it is likely a consequence of the difference in flow speed and direction between the two regions north and south of the separation front. Figure 2.6 shows the same aerial photo, but overlaid with the results from a fine grid model at the same tide stage as the aerial photo for comparison. The arrows are the surface current vectors.

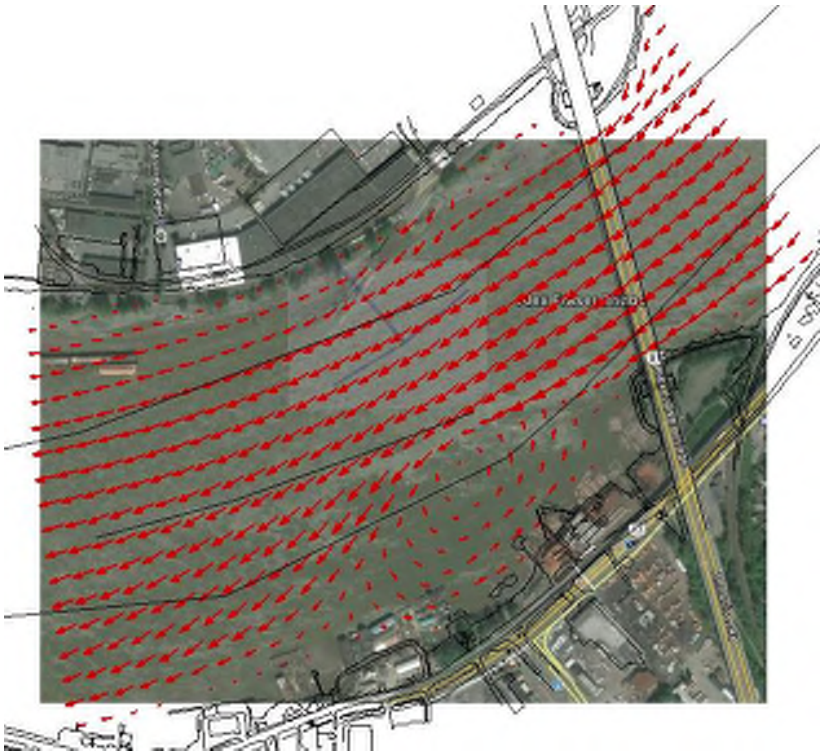

**Figure 2.6: Google Earth Image overlaid with Modelled Surface Current Results from the Fine Grid Model**

The model simulates an anti-clockwise gyre (a rotating circulation feature also known as a vortex) downstream of the south abutment, with the separation front coinciding with the one shown in the aerial photo. Also, the model simulates a smaller clockwise eddy downstream of the north abutment, which will be relevant for the proposed diffuser performance.

## 2.4 Changes to H3D for the Annacis Island Outfall Simulations

In order to improve the accuracy of H3D, particularly at periods of the year when the Hope flow was relatively low, the effect of the Harrison River was upgraded from a previous assumption that the Harrison flow was 10% of the Fraser River at Hope flow, to a monthly varying ratio of Harrison flow to Fraser at Hope, based on values developed by Seaconsult (1996), and summarized below.

### Table 2.1: Monthly ratio of Harrison River flow to Fraser River at Hope flow

| Month | Ratio $Q_{Harrison}$ / $Q_{Fraser\ at\ Hope}$ |
|---|---|
| January | 0.36 |
| February | 0.33 |
| March | 0.33 |
| April | 0.19 |

**Table 2.1: Monthly ratio of Harrison River flow to Fraser River at Hope flow**

| Month | Ratio $Q_{Harrison}$ / $Q_{Fraser\ at\ Hope}$ |
|---|---|
| May | 0.11 |
| June | 0.14 |
| July | 0.19 |
| August | 0.25 |
| September | 0.25 |
| October | 024 |
| November | 0.35 |
| December | 0.41 |

Source: Seaconsult (1996)

Additionally, the horizontal eddy viscosity and diffusivity parameters were reduced by a factor of 7, in order to better simulate the timing of the presence/absence of the toe of the salt wedge with respect to the phase of the tide, using salinity data collected by Golder Associates for comparison to the model.

## 2.5 Modelled Hydrodynamic Circulation Patterns

The hydrodynamic model results showed the effects that the tidal oscillation and river flow have on the local circulation near the outfall location in the Fraser River. In this section, the circulation pattern at various stages of the tide will be presented. The model results presented herein were based on river discharge of approximately 2,000 m3/s (Figure 2.2), on October 26th, 2011. The observed water elevation with respect to chart datum on that day is shown in Figure 2.7 below.

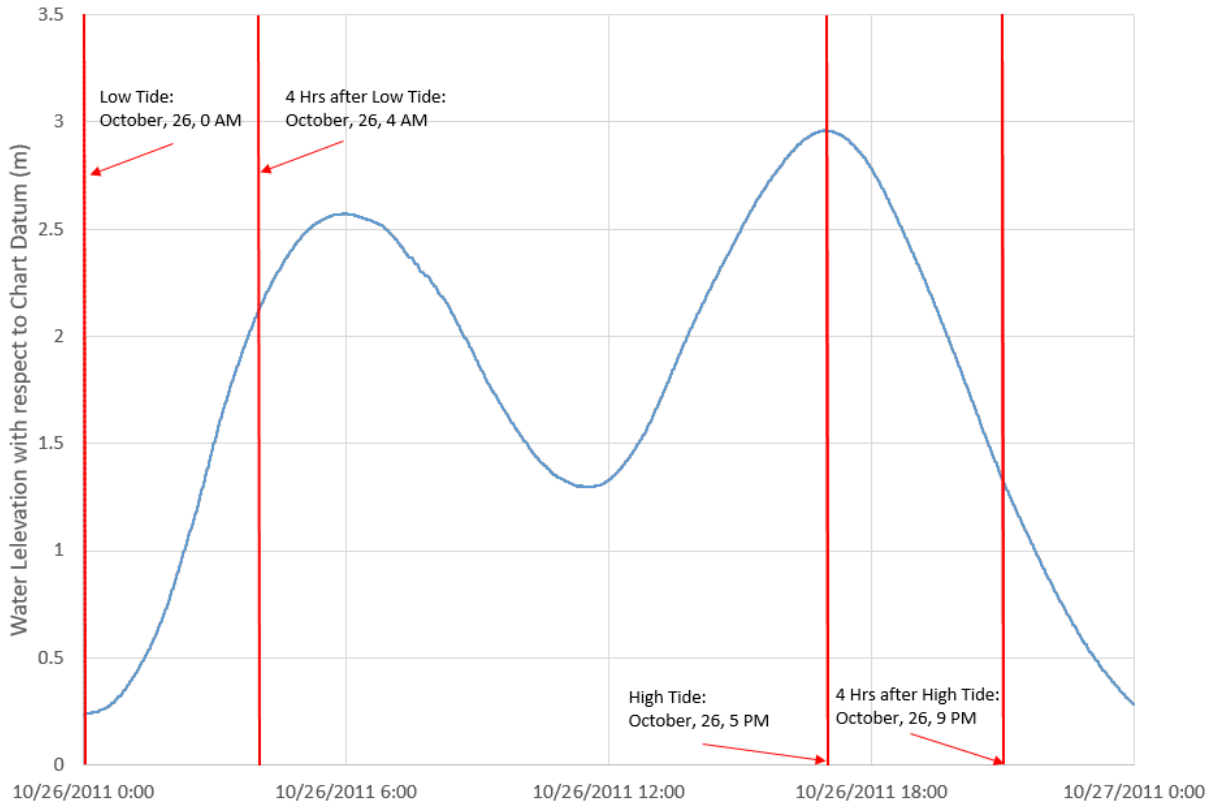


**Figure 2.7: Observed Water Elevation with respect to Chart Datum at New Westminster**

Note that the model results presented below are specific for the flow rate of 2,000 $m^3/s$. The circulation pattern in the river, given the same tide range, changes gradually with the river discharge. The low river flow case is presented here because it is during such conditions that one may expect the lowest dilutions. However both modelling results and dye studies for the existing diffuser, presented in Section 3, show that this concern is unfounded: the diffuser performs well under all but the most adverse tidal and river flow conditions.

### 2.5.1 Surface Current Maps at the Project Site

The proposed location of the outfall is in the Main Arm of the Fraser River, approximately 28-29 km upstream from the river mouth. In general, given a constant river flow rate, the local current speed in the lower reach is heavily modulated by the tidal fluctuations in the Strait of Georgia. Water elevation in the lower reach of the Fraser River follows a similar tidal pattern as in the Strait, but with diminishing amplitude in the upstream direction. The surface current is the slowest roughly 1 hour after high water, and fastest roughly 4-5 hours after high water, during the ebb tide. The water current reverses in direction and flows upstream at the outfall location during flood tides at lower and moderate river flows. However, during high river flow periods (freshet, for example), the current maintains its downstream flow direction during nearly all tidal stages, including the flood tide.

Figures 2.8 and 2.9 below show the modelled surface currents when the river discharge at Hope is 2,000 $m^3/s$, a relatively low river discharge which allows several complex current patterns to develop in the river. Figure 2.8 shows the surface current pattern at high tide and approximately 3hours after high tide (ebb tide. Figure 2.9 illustrates the surface current pattern at low tide, and approximately 4-hours after low tide (flood tide). The colour contours indicates the current speed and the arrows are vectors showing the direction of the flow. For clarity, all vectors are the same length, and the location of the diffuser is represented by the purple lines in the figures.

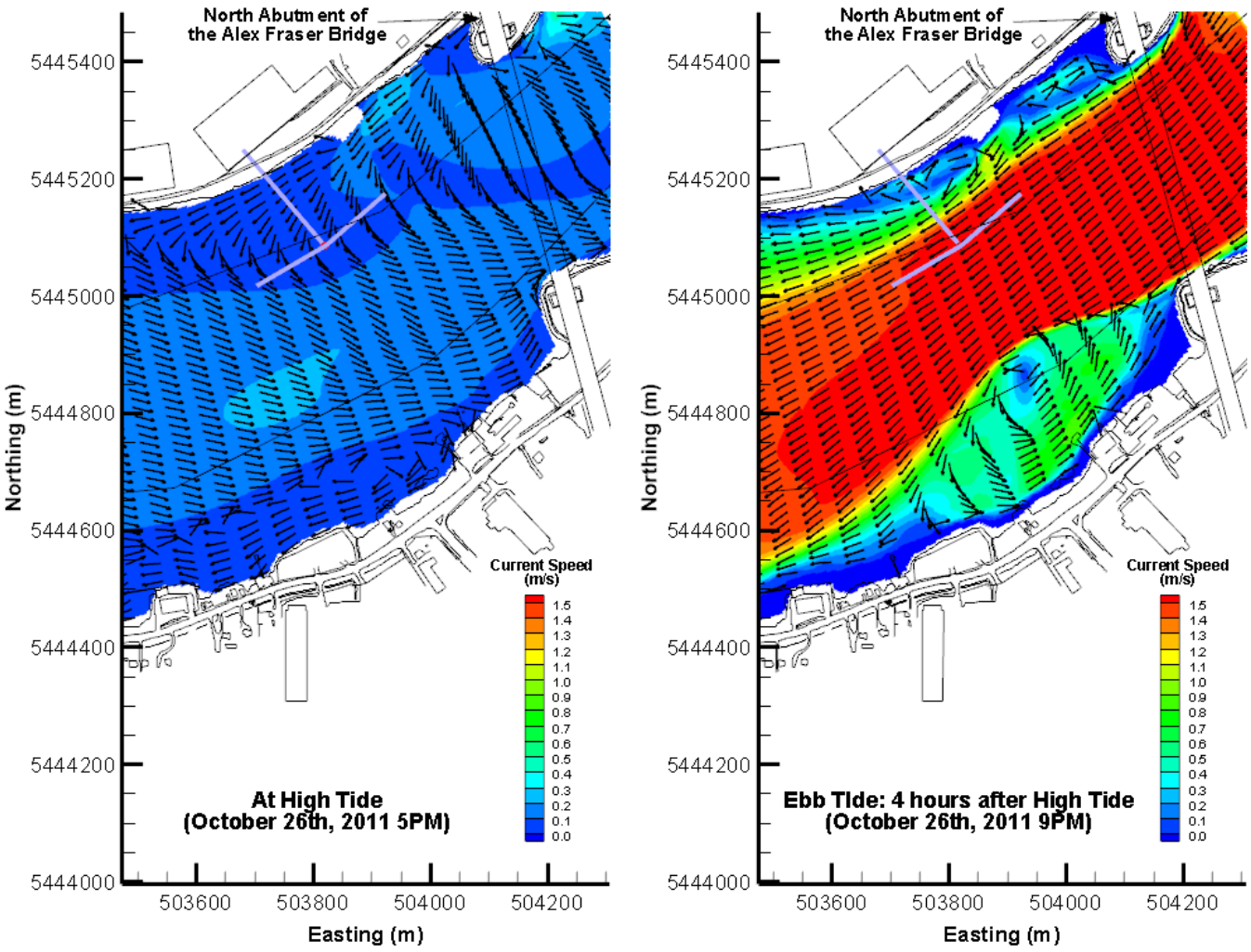


**Figure 2.8: Modelled Near-Field Surface Current near Outfall Location at High Tide and 4 Hours after High Tide on October 26th, 2011 (River Discharge Rate = 2,000 $m^3/s$)**

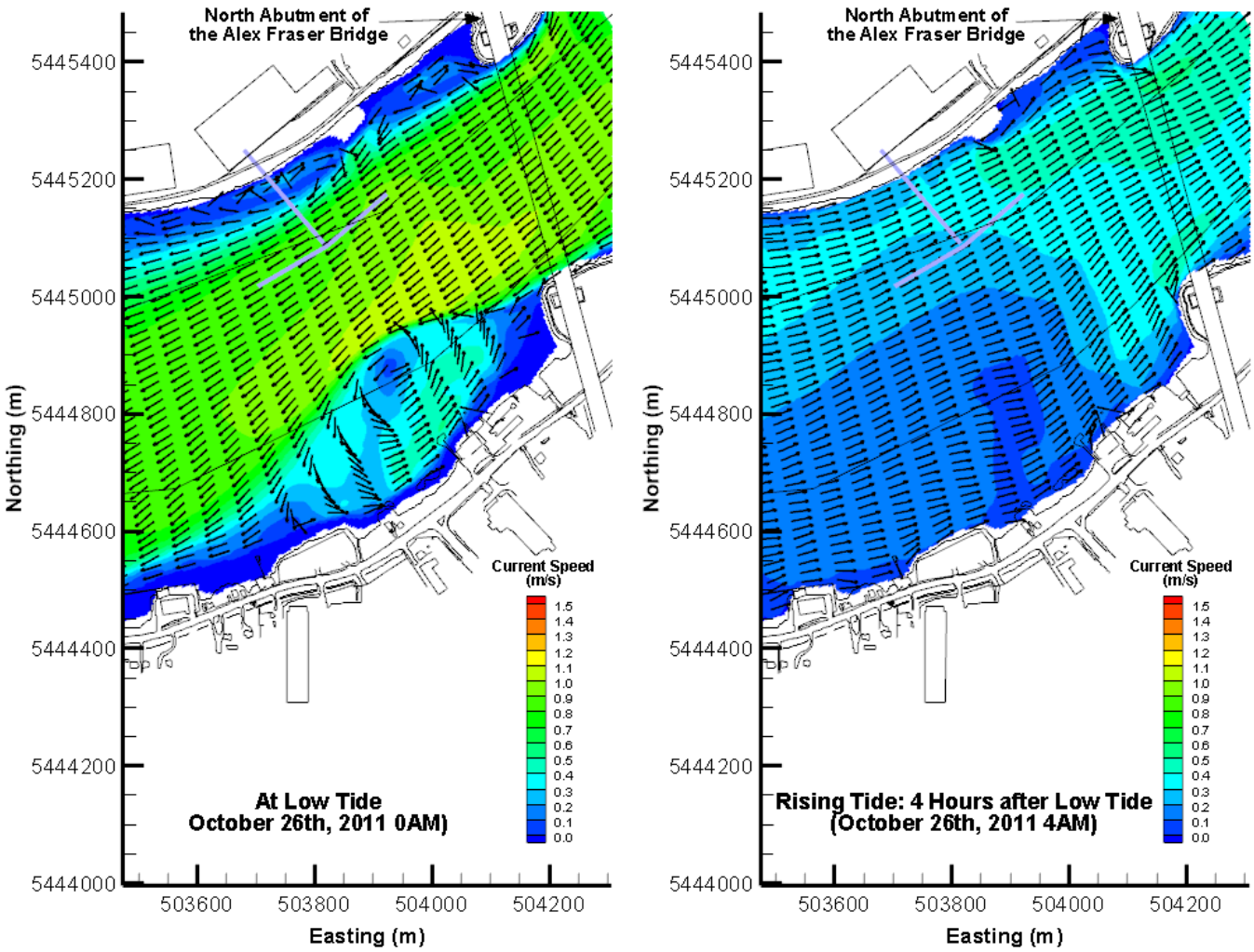


**Figure 2.9: Modelled Near-Field Surface Current near Outfall Location at Low Tide and 3-4 Hours after Low Tide on October 26th, 2011 (River Discharge Rate = 2,000 $m^3/s$)**

The model results indicate that an anti-clockwise gyre forms on the south side of the river, downstream of the Alex Fraser Bridge, during ebb conditions when the local current is fast, regardless of the Fraser River discharge rate. Relevant to the outfall performance, a smaller, clockwise gyre also forms downstream of the north bridge abutment during high river velocity conditions, (Figure 2.8 right panel, Figure 2.9, left panel). At high tide, flows are generally slow, and reversal in flow direction in the vicinity of the proposed diffuser occurs shortly afterward (Figure 2.8 left panel).

The timing of the flow reversal depends on the river discharge: the larger the river discharge, the later in the tidal cycle the flow reversal occurs. Flow reversal disappears altogether during the freshet period when the river discharge is sufficiently high.

### 2.5.2 Surface Current in the Lower Fraser River 0-7 km from the Project Site

The surface current patterns in the Lower Fraser River 0-7km downstream (between Tilbury Island and Alex Fraser Bridge) from the project site at various tidal stages, which correspond to the same time shown in Figure 2.8 and Figure 2.9, are illustrated in Figure 2.10 and Figure 2.11. The colour contours indicates the current speed and the arrows are vectors showing the direction of the flow. Also indicated in the figures are the chainage distance from the river mouth, represented by the red lines.

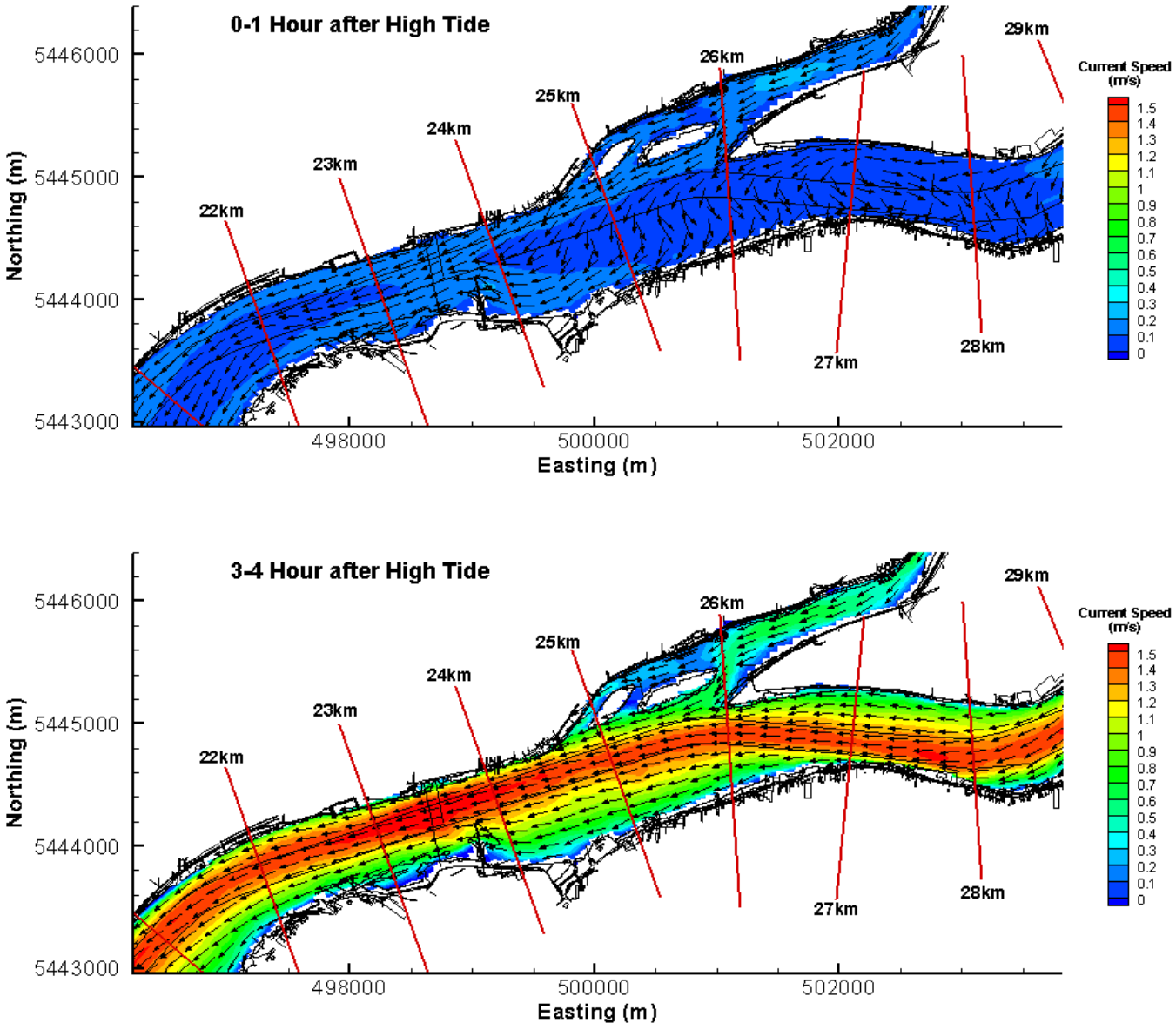


**Figure 2.10: Modelled Surface Current in the Lower Fraser River between Tilbury Island and Alex Fraser Bridge at High Tide and 3-4 Hours after High Tide (River Discharge Rate = 2,000 $m^3/s$)**

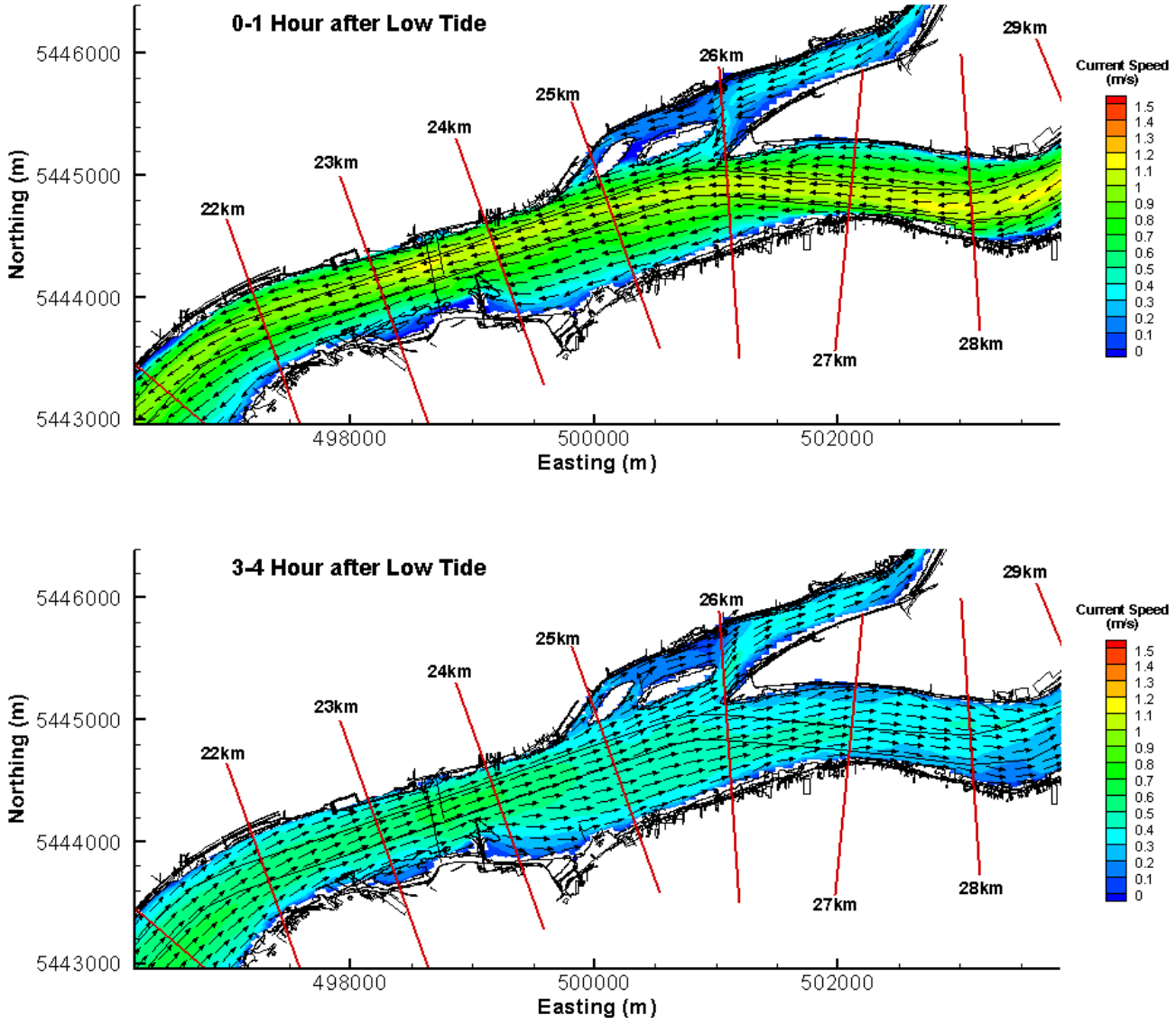


**Figure 2.11: Modelled Surface Current in the Lower Fraser River between Tilbury Island and Alex Fraser Bridge at Low Tide and 3-4 Hours after Low Tide (River Discharge Rate = 2,000 $m^3/s$)**

The far field flow demonstrates the similar tidal varying pattern as the near field flow as shown in Figure 2.8 and Figure 2.9. One prominent feature in the far field flow is that the strongest current is often found in the central portion of the channel, where the deepest, dredged depths are found, and that the slower regions are highly correlated with shallow platforms along the river.

## Sub-surface Currents

The pattern of the sub-surface currents in the lower reach of the Fraser River can be different from that of the surface currents. The upstream intrusion of the salt wedge from the Strait of Georgia as well as the presence of the apparent scour hole, the St. Mungo Hole, which was formed after the construction of the Alex Fraser Bridge and its two bridge two bridge abutments (Ron Suderman, Public Works and Government Services Canada, personal

communication, 2015) near the proposed outfall likely further complicate the circulation pattern in the area. A series of cross-sectional current plots is shown below to illustrate the sub-surface current pattern in the area. Figure 2.12 shows the bathymetry near the proposed outfall and the cross-sectional line along which the current plots are being drawn. Also shown in the figure is the location of the proposed outfall and the St. Mungo Hole.

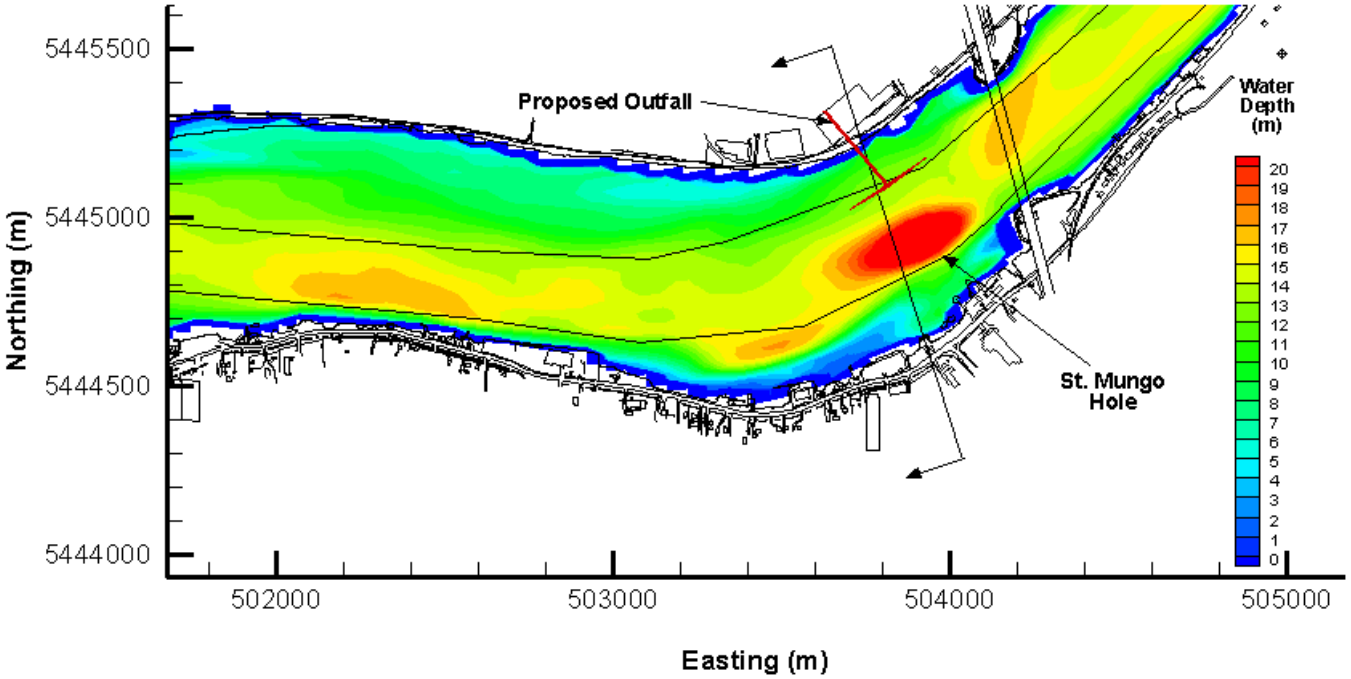


**Figure 2.12: Bathymetry near the Proposed Outfall, the Cross-Sectional Line for Current Plots**

### 2.5.3 Cross Sections Near the Annacis Diffuser

Figure 2.13 shows the flow pattern along the cross section at high tide and 3-4 hours after high tide, while Figure 2.14 illustrates the cross-sectional flow pattern at low tide and 3-4 hours after low tide. Also shown in these figures is the approximate location of the proposed diffuser. The blue colours indicate downstream flow (into the page), whereas yellow colours indicate upstream flow (out of page). The arrows are vectors indicating the cross-channel and vertical components of the current. A reference vector is provided in the figures for the speed scale. Note the diffuser is situated about 200 m from the right bank of the river.

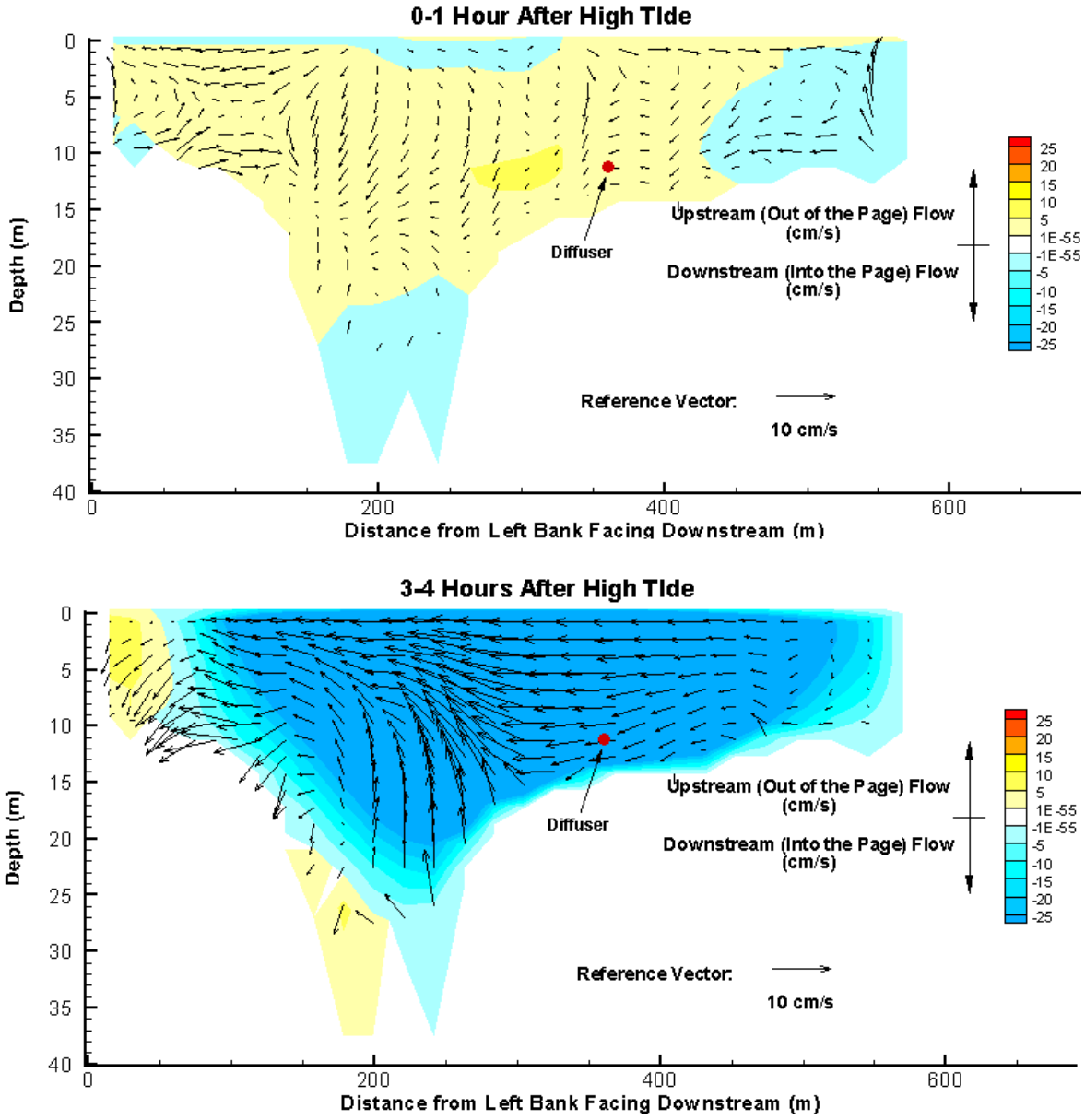


**Figure 2.13: Cross-Sectional Circulation Pattern at High Tide and 3-4Hours after High Tide**

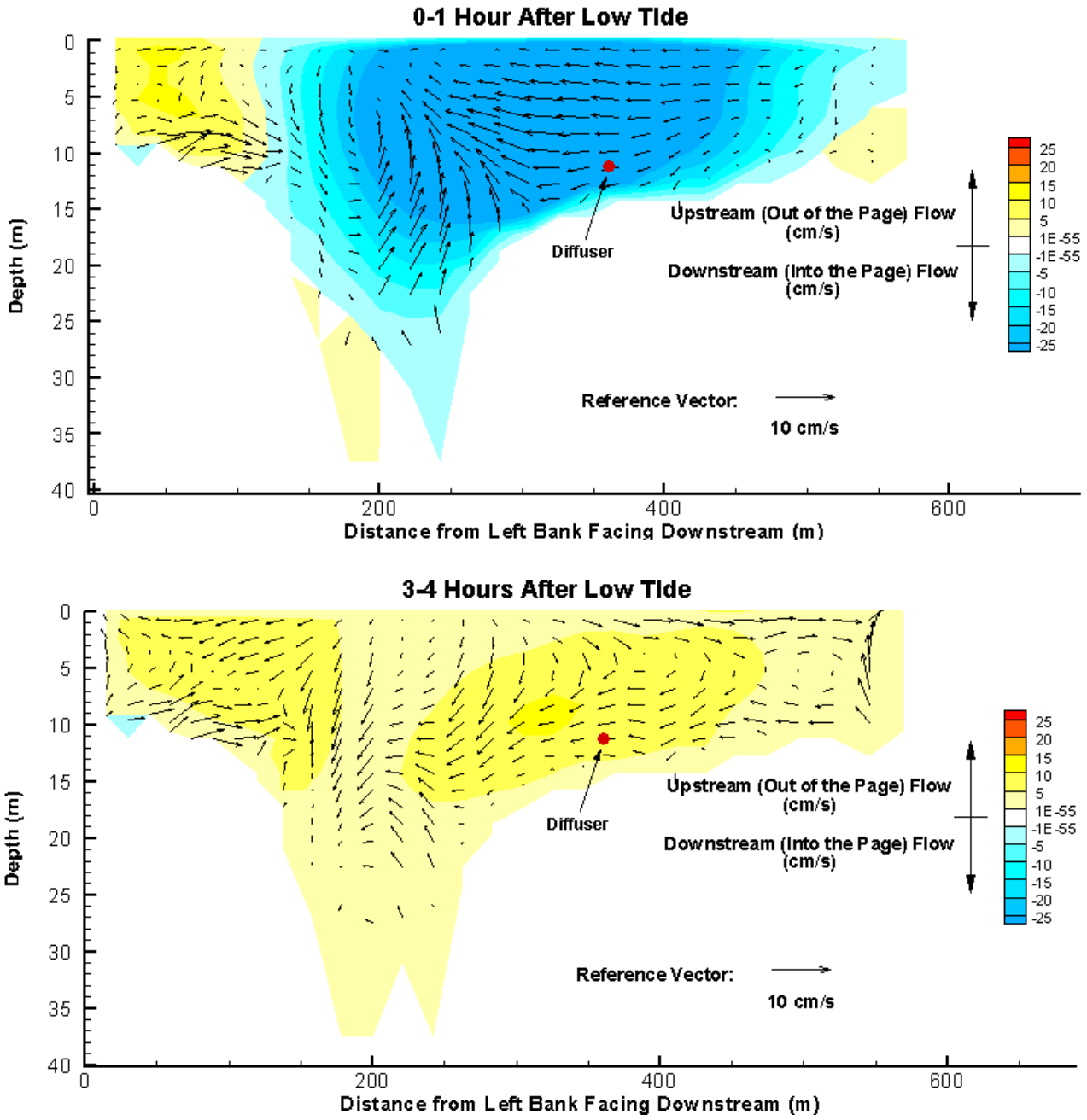


**Figure 2.14: Cross-Sectional Circulation Pattern at Low Tide and 3-4 Hours after Low Tide**

These two figures show clearly that the gyre near the south shore (bottom panel of Figure 2.13 and the top panel in Figure 2.14) of the river effects the entire water column. Also shown is that there is a significant vertical component in the current, especially near the St. Mungo Hole where upwelling appears prominent during the time when the main part of the river is flowing downstream. On the north side of the river, formation of a re-circulation cell is shown in Figure 2.14, with onshore flow near the top and return offshore flow near the bottom.

## 2.6 Modelled Time Periods for Annacis Simulations

### 2.6.1 Task 1 – Salinity Predictions using Historical Low River Flows

CDM Smith required simulations using the lowest possible river flows to estimate maximum density differences and stratification at the site for diffuser design purposes. Tetra Tech simulated the typical low flow months of January through April where river inputs were chosen from the historical minimum flows on each day. The time series of the lowest flow for each day can be read off the blue line in Figure 2.15. The resultant run had the lowest realistic river velocities and farthest upstream travel of the salt wedge. Data was provided to CDM Smith as discussed in Section 4.0.

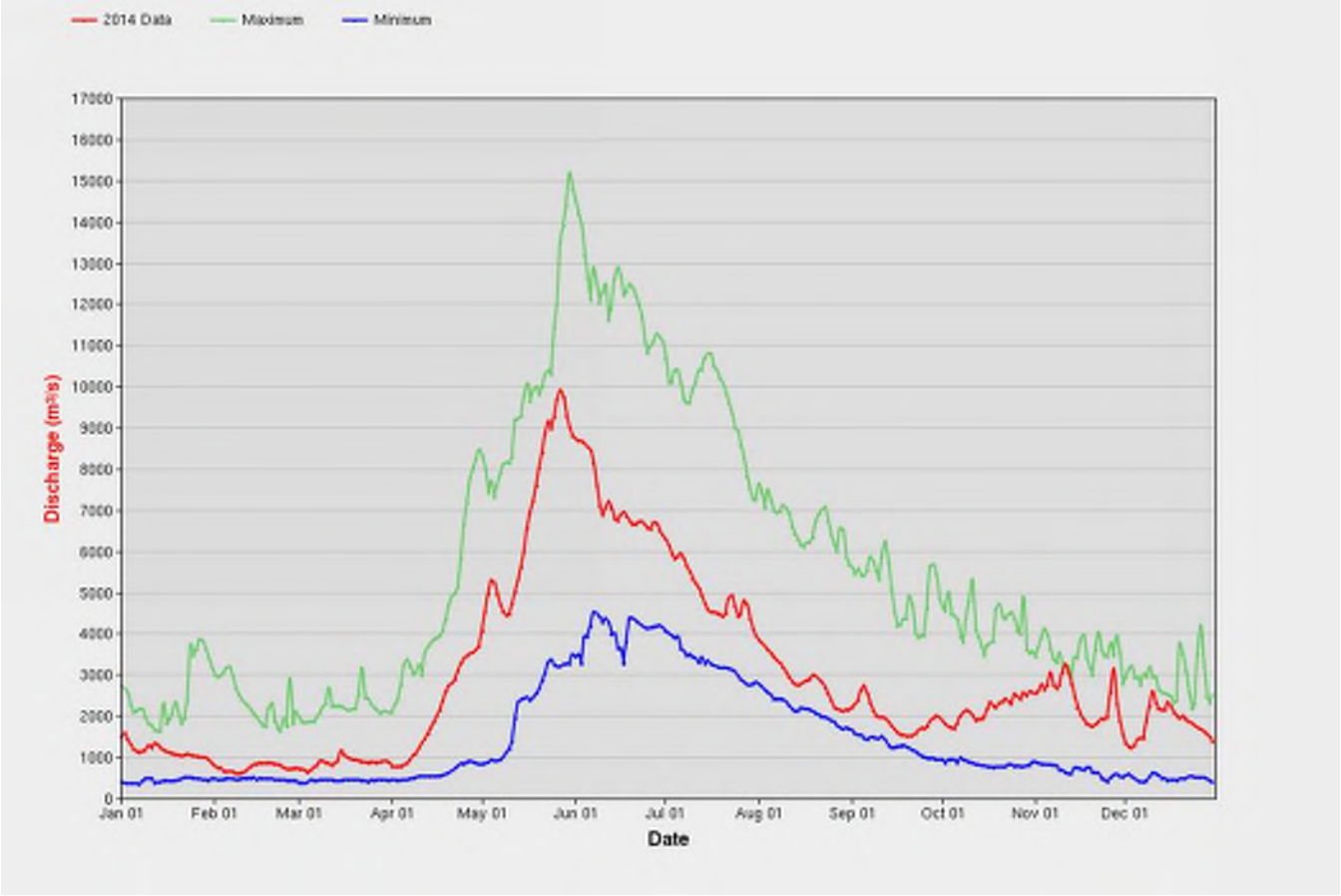


**Figure 2.15: Fraser River Discharge Flow Rate at Hope in 2014 (Red Line) and Historical Minimum (Blue Line) and Maximum (Green Line) Daily Discharge Flow Rates for Each Calendar Day Recorded between 1912 and 2017**

### 2.6.2 Task 2 – Salinity Predictions, 2014 Observed Low River Flows

Simulations with observed river flows during a low-flow time period were used to develop an understanding of the frequency of occurrence for the movement of the salt wedge at the project site, particularly at very low Fraser River discharge rates when measurement data are lacking . This task provided predictions of salinity with realistic historical river inputs, shown in Figure 2.15. The months of January through March 2014 were used because this date range had the lowest river flow in the past decade. The model set up included observed river flows at Hope and measured tides during the period.

### 2.6.3 Task 3 – Far Field, 2013 Full Year Simulation

Task 3 was a year-long simulation to evaluate diffuser performance over a wide variety of conditions, including potential background buildup and realistic combinations of river flow and tidal variability. The year 2013 (Figure 2.16) was used for this task, with observed river flows for 2013 instead of synthetic hydrology.

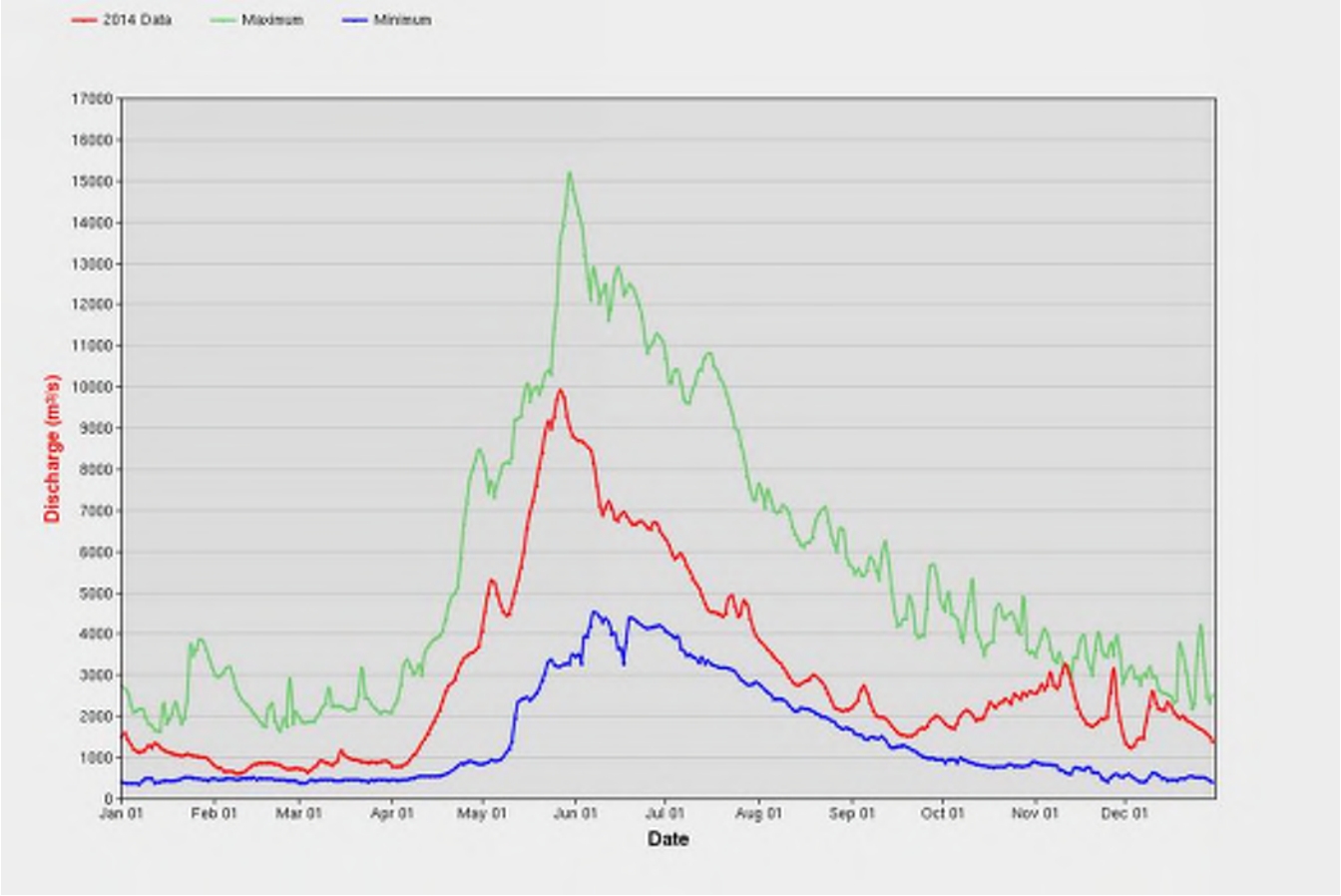


**Figure 2.16: Fraser River Discharge Flow Rate at Hope in 2013 (Red Line) and Historical Minimum and Maximum Daily Discharge Flow Rates for Each Calendar Day Recorded between 1912 and 2017**

# 3.0 PLUME MODELLING

## 3.1 Methods

### 3.1.1 Description of UM3 Model

Tetra Tech used the USEPA's UM3 model, embedded in the three-dimensional hydrodynamic model H3D, to simulate the behaviour of the proposed outfall in the Fraser River near Annacis Island. The UM3 model, developed and distributed by the US Environmental Protection Agency, is an accepted standard for determining environmental impacts from effluent discharge through an outfall.

For outfall assessments, the PLUMES UM3 code was integrated into H3D such that the simulated time-varying properties of velocity and density could have the appropriate influence on near-field plume behaviour, and the far-field behaviour could be simulated in a realistic manner. The UM3 mode, either earlier versions or the version contained in Visual Plumes, is valid in the near-field when boundary effects such as contact with the river bed or the water surface do not occur within the near-field, and when the river dynamics do not cause significant recirculation in the receiving environment.

The existing Fraser River H3D model resolution is relatively coarse (20x50 m) in order to simulate the entire river. Since a typical point of interest for dilution modelling is 100 m from the outfall, this grid resolution is not suitable for near-field modelling. Near-field dilution was simulated both by Tetra Tech and CDM Smith using Visual Plumes software, which is related to, but not identical to, the UM3 code used in H3D. For Stage 2, initial dilution under stratified conditions, CDM used CORMIX2

The salient difference between the far-field, long-term three dimensional approach (H3D-PLUMES) and the near-field approach (Visual Plumes or CORMIX only) is the possibility of building up a background concentration of effluent in the three-dimensional model of the river, reducing diffuser effectiveness regardless of near-field hydraulic performance. Additionally, it is doubtful if there is any other way to incorporate the complex flow patterns that occur in the river in the vicinity of the proposed outfall at high tide, low river flow conditions other than by the use of a three-dimensional numerical model.

The UM3 model source code was made available to Tetra Tech in the Pascal programming language by its author Dr. Water Frick, formerly of the USEPA. Tetra Tech incorporated the UM3 ‘kernel’ into H3D, and further modified it for Annacis to better handle the along-flow diffuser port configuration and the horizontal travel of jets and plumes from individual ports. There remain differences between the Pascal code and that within the Visual Plumes software. Some specific capabilities of each model version are compared in Table 3.1. One notes that the UM3 in H3D model meets or exceeds all capabilities identified in the first column, except that crossflow entrainment is somewhat simplified compared to Visual Plumes. This level of simplification is justified by the relatively simple trajectories that occur when the proposed Annacis diffuser discharges into the Fraser River.

### Table 3.1: Comparison of Model Capabilities

| Model Capability | Visual Plumes | UM3 Pascal Code | UM3 in H3D |
|---|---|---|---|
| Vertical Resolution | Constrained by input data | Constrained by input data | Simulated in detail |
| Temporal Resolution | Single time | Single time | Long-term |
| Horizontal dimensions Available | 2 | 1 | 2 |
| Handling of diffuser pipe angle | No | Yes | Yes |
| Handling of diffuser port angle | Yes | No | Yes |
| Crossflow Entrainment Terms | Yes | No | Simplified |
| Background Buildup of Effluent | Manually Calculated or with use of ‘Tidal Buildup’ feature | Manually Calculated | Included in detail |
| Handling of Surface and Bottom Interaction | Simulation continues after bottoming | Simulation ends | Modified to avoid premature model stops |

Most of the capabilities of Visual Plumes have been reproduced in UM3 embedded in H3D, with the exception that crossflow entrainment has been simplified. The presence of a crossflow is a given factor in the Annacis diffuser design, which points a jet directly across the river perpendicular to the flow direction. Since the plume deflection due to cross-flow is relatively simple, i.e., it conforms relatively quickly and monotonically to the along channel river flow, the simplified crossflow entrainment method implemented in H3D is adequate for the modelling described here.

The path of the plume in the horizontal is calculated in Visual Plumes such that the direction of diffuser ports and flow direction correctly interact. However, the length and orientation of the diffuser pipe is greatly simplified in the Visual Plumes results, and the behaviour of a diffuser pipe parallel with the direction of the river is poorly simulated. The Pascal version of theUM3 source code cannot orient the ports relative to the current, and only incorporates the

diffuser pipe angle in the calculation of an 'effective port spacing' which is less than the actual port spacing if the flow is primarily along the pipe. The UM3 model included in H3D was modified for this project so that it separates the directional components of jet or plume's horizontal velocity, and combines them individually with the ambient velocity components in a ratio specified by the calculated dilution. This method allows the effluent from each individual port to travel independently in a trajectory that eventually converges appropriately with the local ambient flow.

The UM3 model (the Pascal code version) by default stops calculation when the edge of the plume intersects the bottom or the surface. In Visual Plumes, calculation continues after the edge hits bottom, but ends if the plume centreline hits bottom. The UM3 model embedded in H3D uses the same approach as Visual Plumes, but also applies it to intersecting the water surface. This setting would have a biasing effect on UM3's internal calculation of dilution since the surface area available for entrainment would be over-estimated, but as described later, only the trajectory and diameter of the plume are required by H3D. The individual plume dilution result is not required because H3D uses the mass flux of discharged contaminant for its dilution calculations.

Note that the code also allows the plume trajectory to stop if the plume becomes trapped, i.e., for a rising plume, it will general cease its upward motion and form a waste field at a depth where the plume density is the same as the ambient. The Fraser River is relatively shallow, so that generally trapping does not occur, instead the plume top or bottom intersects either the surface or the river bed, respectively. This condition will be referred to as the termination point in this report.

Within the combined H3D-UM3 system, the following is a typical sequence of calculations:

1. After the velocity and density fields in H3D are updated from one timestep to the succeeding timestep, the UM3 subroutine is called.

2. UM3 updates its internal copy of the velocity and density fields, from the updated H3D velocity and fields.

3. UM3 then compute a separate plume trajectory for each diffuser port, terminating, as discussed above, when the plume centreline intersects either the top or bottom of the water column. Although the UM3 code embedded in H3D retains the ability to trap plumes at intermediate depths, the plume from the Annacis Island Outfall never appeared to trap at depths within the water column, likely because of the strong effluent flow rates and shallowness of the river. The condition when the plume centreline intersects the top or bottom of the water column is referred to, in this report, as the plume termination point.

4. UM3 then evaluates, on a diffuser port by diffuser port basis, the number of H3D cells that the trajectory intersects at its termination point, considering the location of the plume centreline and the radius of the plume. Typically, many cells in the vertical are intersected by the plume, and between one and three cells in plan view are intersected. UM3 then updates the effluent concentration field in each H3D cell identified as being contacted by the plume at its termination point by distributing the portion mass discharged in the current timestep across all grid cells identified as being plume termination cells.

This effluent concentration field, often expressed as dilutions, was then used for all far-field diffuser evaluations described in the following sections.

### 3.1.2 Integration of UM3 Model within Hydrodynamic Model

As implemented for the Annacis Project, the task of the near-field model is to simulate jet and plume processes and place effluent in a realistic horizontal and vertical position, i.e., computational cells, in the far-field model.

The discharge at 2xADWF (the compliance flow of 14.75 $m^3/s$, which was held constant through the year-long simulation) was used for this simulation. Modelled scalar concentrations (effluent concentration, temperature and salinity) were constantly updated based on flows from the diffuser mixing with the ambient. Table 3.2 summarizes the Effluent and outfall properties used in this simulation.

**Table 3.2: Effluent and Outfall Properties**

| Parameter | Annacis Outfall |
|---|---|
| Effluent Flow Rate ($m^3/s$) | 0.82 per port, 14.7 total |
| Effluent Salinity (ppt) | 0 |
| Effluent Temperature (°C) | 13 |
| Effluent Dye Concentration (-) | 1.0 |
| Effluent Density (g/L) | 999.38 |
| Modelled Location (UTM) | Six model cells, evenly spaced between UTM (503714, 5445043) and (503941, 5445177) |
| Discharge Depth (m) | Variable with tide, but at an elevation ~1m above bottom |
| Number of Ports | 18 |
| Port Spacing | 13.33 |
| Port Diameter (m) | 0.5 (at specified flow rate) |

The results of the UM3 model include horizontal travel in two dimensions, vertical position at the end of the simulation, plume diameter, and dilution. The 18 ports of the diffuser were simulated separately, and were distributed over six model cells representing 240 metres of diffuser length.

Modelled dye concentration can be converted to dilution, a quantity which facilitates prediction of mixing processes in general. Dilution is the quantity provided as a deliverable in this modelling study. Dilution is the ratio of effluent to background water in a mixture, and can be calculated from known concentrations using the following equation:

$$D = \frac{C_{effluent}}{C_{in\ situ}}$$

This equation is valid when there is a background concentration of zero, which is the case in the modelling study.

## 3.2 Maps and Sections of Plume Trajectory

Examples of four distinct plume behaviours are discussed in this section using example maps and sections (Figure 3.1 and Figure 3.2) from the far-field hydrodynamic model.

The top left panel in Figures 3.1 and 3.2 shows a map view of the lowest dilution in the water column. The proposed diffuser is shown as a blue line in the plan view; the red dots show the location of the existing diffuser. The 100-m dilution zone around the diffuser is shown as a blue oval. The centre panel in both figures shows a longitudinal section along a dynamic path in the river, which ensures that the contour plot illustrates the lowest dilution at each lateral cross-section along the river. Dilutions greater than 100:1 are not resolved by the colour scale. The bottom panel indicates the respective tidal stage at the time of the presented model results in Figure 3.1 and Figure 3.2.

### 3.2.1 Downstream Travel – High Velocity

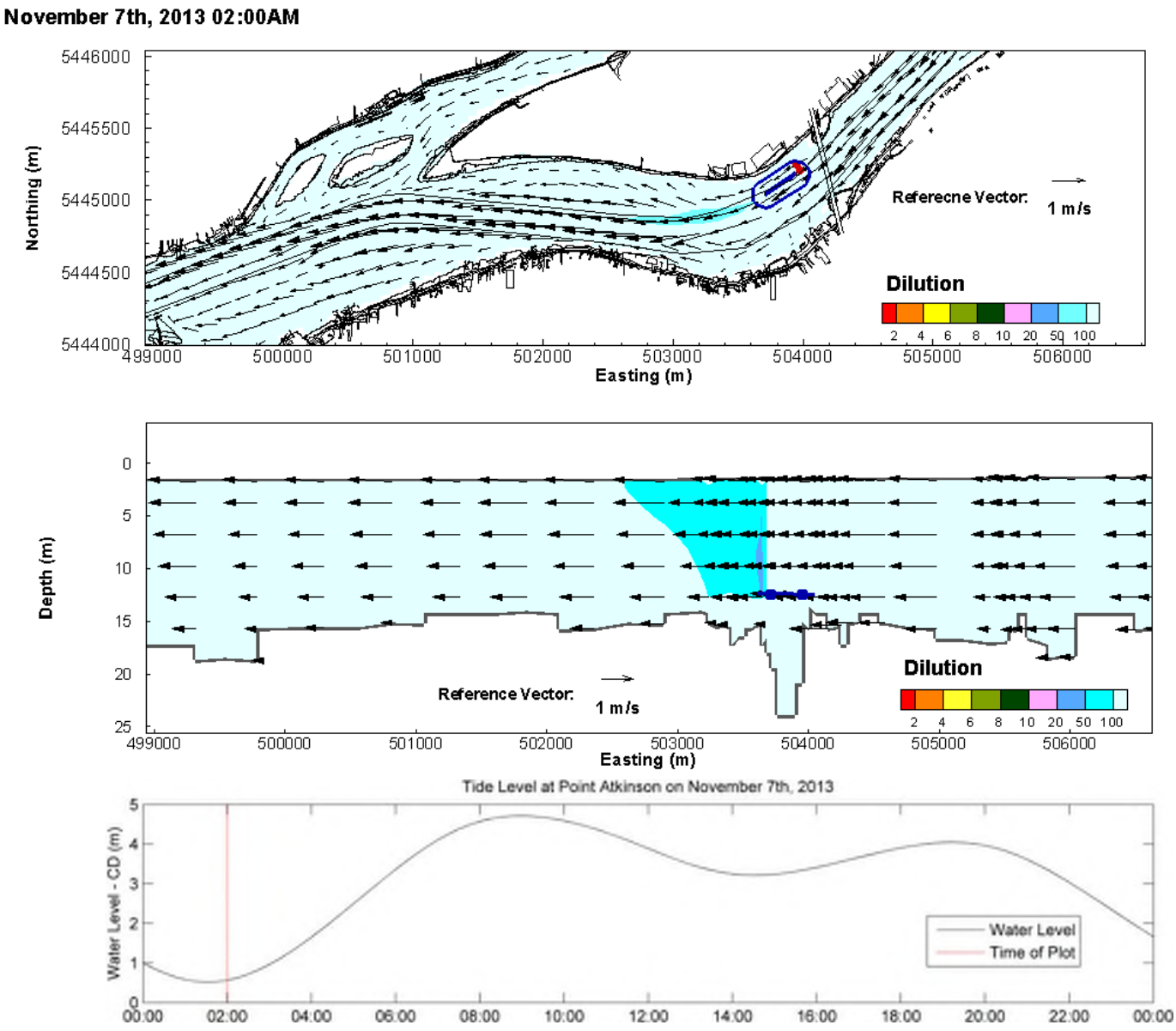


**Figure 3.1: Plan View and Longitudinal Section of Plume – Downstream Travel on November 7th, 2013 2AM**

In Figure 3.1, river currents flow downstream at high velocity as the tide approaches low water. The plume travels directly downstream from a starting point one model cell offset from the diffuser, as determined by the UM3 sub-model. Dilution is mostly well over 50:1 at a point 100 metres downstream of the diffuser. In this case, dilution is better than 20:1 at all locations. The results show that the plume is well diluted vertically throughout most of the water column.

### 3.2.2 Upstream Travel – High Velocity

**November 7th, 2013 08:00AM**

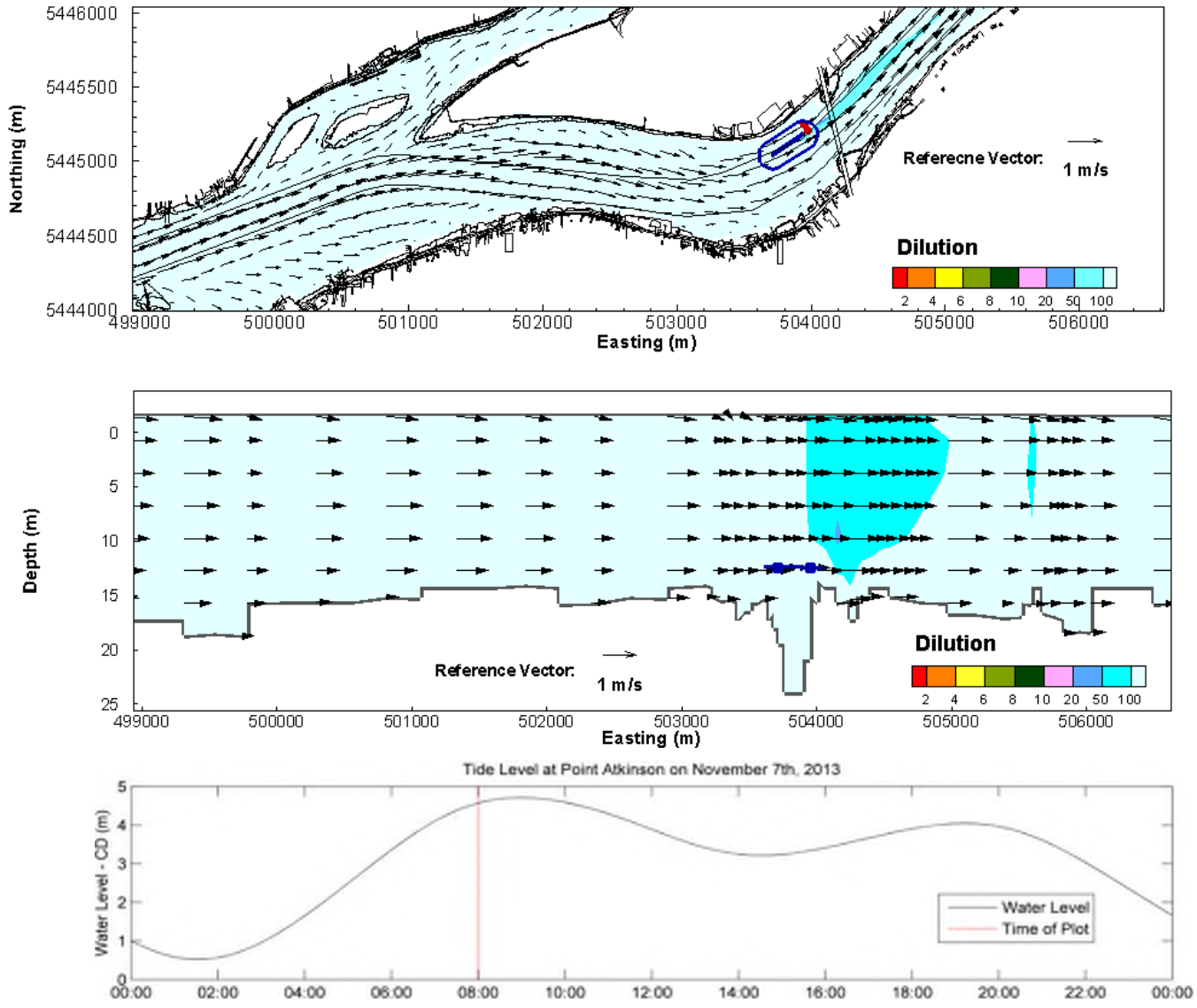


**Figure 3.2: Map, Cross-Section and Longitudinal Section of Plume – Upstream Travel on November 7th, 2013 8 AM**

The maps and sections in Figure 3.2 show a period of flow reversal as high tide approaches, with the plume travelling directly upstream. The lowest dilution on the map is over 40:1. The centre panel shows a longitudinal section along a dynamic path in the river, the path selected so that the minimum dilution at each cross-section of the river is shown. Similar to the downstream travel case, the results show, in the upstream travel case, that the plume is well diluted vertically throughout most of the water column.

Appendix B provides a complete set of hourly Figures for November 7, 2013. These figures are selected to firstly illustrate the distribution of effluent during the poorest performance of the diffuser (November 7, 2100) as well as the return to acceptable conditions between one and two hours later.

## 3.3 Comparison of Plumes-H3D Results with Seaconsult Maps

The 1997 Seaconsult report involved detailed dye studies of the existing Annacis Island diffuser. Although flow rates and diffuser design differ from the present study, the observations of the far-field behaviour of the effluent provide a useful check on this report's model results.

Figure 3.3 shows an example of a narrow plume headed downriver at high dilution, similar to that shown in Figure 3.1. The day of the model simulation shown in the Seaconsult map was November 22nd, 1995, and the corresponding discharge rate of Fraser River at Hope on that day was 2,480 $m^3/s$.

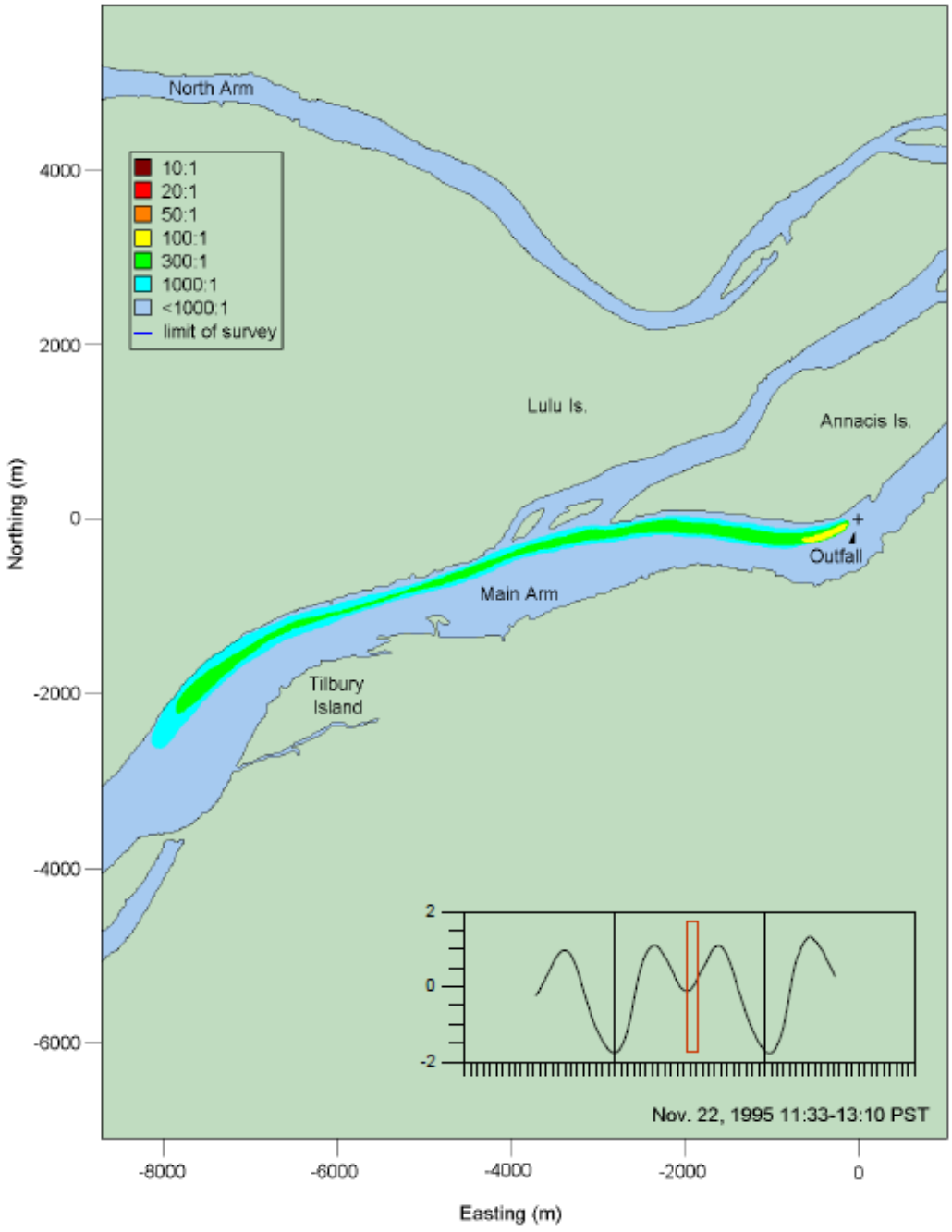


**Figure 3.3: Reproduced from Seaconsult (1997) Figure 5.51**

Figure 3.4 shows an example of a narrow plume headed upriver at high dilution, with many similarities (narrow elongated configuration, high dilutions generally greater than 50:1) to the plume in Figure 3.2. Similar to Figure 3.3, the day of the model simulation shown in the Seaconsult map was November 22nd, 1995, and the corresponding discharge rate of Fraser River at Hope on that day was 2,480 $m^3/s$.

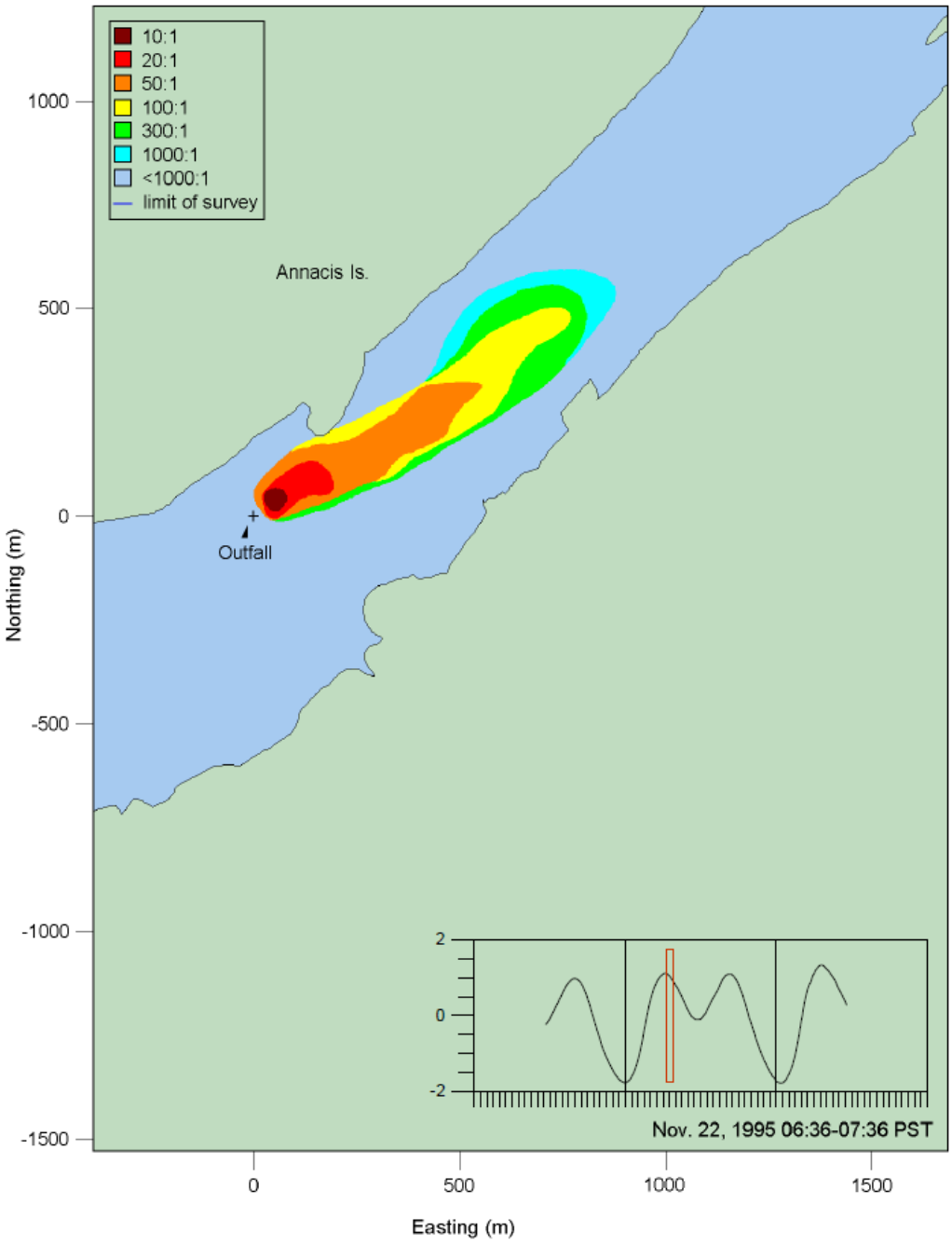


**Figure 3.4: Reproduced from Seaconsult (1997) Figure 5.56**

As described in the text deliverables to CDM Smith, there are also infrequent, short periods of effluent buildup during high tide, low river discharge conditions.

# 4.0 DESCRIPTION OF DELIVERABLES

Tetra Tech provided model output to CDM Smith in detailed text-based formats covering spatial and temporal variability in effluent concentration.

CDM Smith Canada Ltd. contracted with Tetra Tech Canada Inc. to employ their existing hydrodynamic model H3D of the Lower Fraser River to assist with the following project goals:

- Predict a reasonable worse case salinity for use in hydraulic calculations to quantify the need for significant head to discharge effluent when salt is present at the project site,
- Provide information on salinity at the project site to further aid in understanding its presence, magnitude and vertical profile, and
- Simulate the far-field mixing of AIWWTP effluent through a proposed diffuser over calendar year 2013 to provide input into:

    1. Background buildup that is part of the prediction of concentrations at the edge of the IDZ where background buildup represents typical tidal return flow concentrations for evaluating compliance with maximum (95$^{th}$ percentile) and 30-day average (calendar month average) water quality guidelines and objectives.
    2. The Stage 2 EIS assessment of potential impacts from the discharge at identified sensitive receptors located outside the IDZ.

## 4.1 Tasks 1 and 2 - Hydrodynamic Deliverables

Time series output from the Fraser River H3D model at three locations was provided for water speed and direction, salinity, and temperature at all depths at the three locations shown in Figure 4.1. For Task 1, results from the year with the historical lowest daily flows was provided. For Task 2, four months in the year 2014 were simulated, covering conditions during realistic, but low river flows.

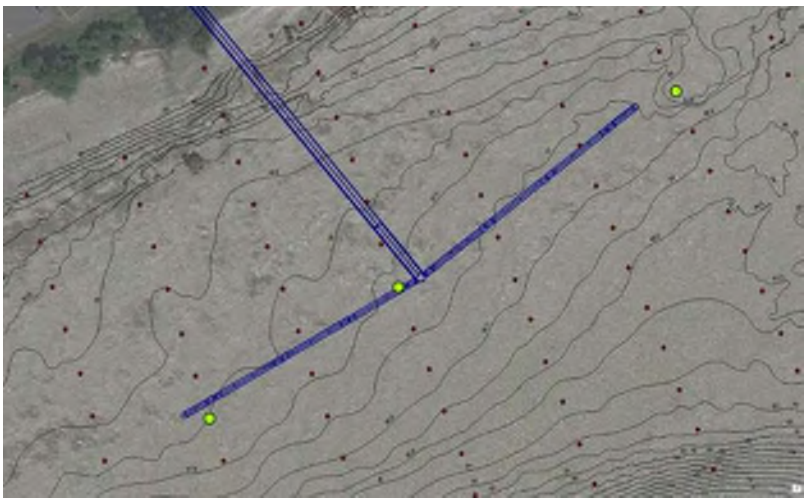

**Figure 4.1: Time Series Output Locations for Task 2**

## 4.2 Task 3 – Dilution Deliverables

### 4.2.1 Vertically Averaged and Lowest Dilution at Cross-Sections

The year-long 2013 model simulation was summarized at sections across the river located specific distances from the diffuser endpoints. Specific radii of interest are shown relative to the model grid in Figure 4.2 with dashed lines. The diffuser pipe is represented by a solid blue line. Individual grid cells are shown in light grey linework. Cross sections (shown in solid lines) were extracted 200 metres (red), 500 metres (purple) and 1000 metres (orange) downstream of the downstream end of the diffuser and 200 metres upstream of the upstream end of the diffuser.

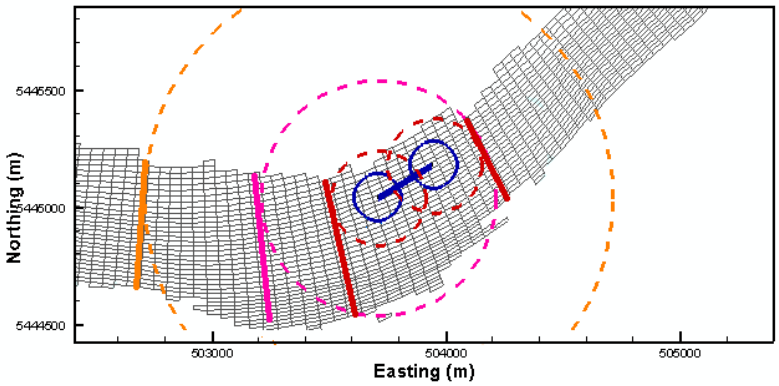


**Figure 4.2: Distances to Cross-Section Output Summary**

The lowest dilution along each entire cross-section was found for each hour, and reported in terms of horizontal and vertical location. The vertical average concentration was then calculated at each point along each cross-section, and the maximum taken across the cross-section and reported separately.

### 4.2.2 Counts Below 10:1 Dilution Outside of IDZ

The initial dilution zone (IDZ) is a 100 metre radius circle from the point of discharge. In the case of the Annacis diffuser, circles are drawn at the upstream and downstream ends of the diffuser pipe and the area between them is also included in the IDZ (Figure 4.2). There are also river width criterion when defining an IDZ, but these are not relevant to this design. The dilution of interest in this design is 10:1.

Tetra Tech analyzed the year-long model simulation for locations outside of the IDZ envelope that were lower (worse) than 10:1 dilution in each hour, and reported the location and dilution achieved in a time series text file. Separate files were produced for exceedances north of the diffuser centreline and south of the diffuser.

# 5.0 ANALYSIS

The near-field to far-field coupling described above has limitations. To date, no single hydrodynamic model has been able to simultaneously represent the turbulence of the initial mixing process as well as the general, large-scale circulation typifying the receiving environment. Consequently, various model approximations are required to provide a practical estimate of the performance of a new diffuser. In this case, the near-field model, UM3, does not function well when limited by the proximity to the bottom or water surface; that is its numerically-modelled plume diameter expands faster than it would in the real world. In the real world, and if the plume were not restrained by top and bottom boundaries, the plume diameter would grow at a rate governed by entrainment processes and by the plume diameter, which determines the area available for entrainment. Since the UM3 implementation in H3D does not adjust the amount of surface available for entrainment, thereby allowing it to be overestimated, the plume acquires the ambient velocity quicker that it would in the real world. Thus, the UM3 plume does not travel as far before it releases its effluent to the H3D model as it would in reality, leading to higher modelled concentrations of effluent. Thus, the modelling reported here likely provides a somewhat conservative (i.e., low) estimate of dilution. For this reason, effluent momentum may continue across the river farther than UM3 simulates, particularly when ambient currents are low. The overestimate of effluent concentration will be greatest when ambient velocities are small, such as at low flow, high tide slack conditions. The UM3-H3D coupling provides reasonable results at distance from the diffuser (as one would expect from a far-field model), but likely represents higher concentrations than are

present at certain low velocity tidal conditions both within the IDZ (where far-field models are not representative) and the region immediately adjacent to it.

# 6.0 CLOSURE

We trust this document meets your present requirements. If you have any questions or comments, please contact the undersigned.

Respectfully submitted,
Tetra Tech Canada Inc.

Prepared by:
Justin Rogers M.Sc.
Oceanographer – Christchurch
Direct Line: +64 3 336.5441
Justin.Rogers@coffey.com

Prepared and Peer-Reviewed by:
Albert Tsz Yeung Leung, M.A.Sc., P.Eng., P.E.
Hydrotechnical Engineer
Direct Line: 778.945.5730
Albert.Leung@tetratech.com

Senior-Reviewed by:
Jim Stronach, Ph.D., P.Eng.
Manager and Physical Oceanographer, Water and Marine Engineering
Direct Line: 778.945.5849
Jim.Stronach@tetratech.com

JR/AL/JS/tak

# REFERENCES

TetraTech 2016. Final Report – Modelling Effects of Climate Change and Dredging on the Availability of Irrigation Water for Delta Farmers. Report prepared by TetraTech Canada Inc. for the Delta Farmers Institute. 59 pp.

Seaconsult, 1997. Annacis Island Wastewater Treatment Plant Pre-Discharge Monitoring Dilution/Dispersion Study. Report prepared for the Greater Vancouver Sewerage and Drainage District.

# APPENDIX A

## H3D TECHNICAL DESCRIPTION

# APPENDIX A:
# H3D TECHNICAL DESCRIPTION

## 1.0 INTRODUCTION

H3D is an implementation of the numerical model developed by Backhaus (1983; 1985) which has had numerous applications to the European continental shelf, (Duwe et al., 1983; Backhaus and Meir Reimer, 1983), Arctic waters (Kampf and Backhaus, 1999; Backhaus and Kampf, 1999) and deep estuarine waters, (Stronach et al., 1993). H3D forms the basis of the model developed by Saucier and co-workers for the Gulf of St. Lawrence (Saucier et al., 2003), and has been applied to the Gulf of Mexico (Rego et al., 2010). In British Columbia, H3D has been used to model the temperature structure of Okanagan Lake (Stronach et al., 2002), the transport of scalar contaminants in Okanagan Lake, (Wang and Stronach, 2005), sediment movement and scour / deposition in the Fraser River, circulation and wave propagation in Seymour and Capilano dams, and salinity movement in the lower Fraser River.

## 2.0 THEORETICAL BASIS

H3D is a three-dimensional time-stepping numerical model which computes the three components of velocity (u,v,w) on a regular grid in three dimensions (x,y,z), as well as scalar fields such as temperature and contaminant concentrations. The model uses the Arakawa C-grid (Arakawa and Lamb, 1977) in space, and uses a two level semi-implicit scheme in the time domain. H3D bears many similarities to the well-known Princeton Ocean Model (POM) (Blumberg and Mellor, 1987) in terms of the equations it solves, but differs in how the time-domain aspects are implemented. H3D uses a semi-implicit scheme, allowing relatively large time steps, and does not separately solve the internal and external models as POM does. It also uses a considerably simpler turbulence scheme in the vertical. These considerations combined allow H3D to execute complex problems relatively quickly.

The equations to be solved are:

Mass Conservation:

$$\frac{\partial u}{\partial x}+\frac{\partial v}{\partial y}+\frac{\partial w}{\partial z}=0 \qquad \text{(A1)}$$

At the end of each time step, equation (A1) is used to diagnostically determine the vertical component of velocity *(w)* once the two horizontal components of velocity (*u* and *v*) have been calculated by the model.

X-directed momentum:

$$\frac{\partial u}{\partial t}+u\frac{\partial u}{\partial x}+v\frac{\partial u}{\partial y}+w\frac{\partial u}{\partial z}+g\frac{\partial \eta}{\partial x}+\frac{1}{\rho_o}\frac{\partial}{\partial x}\int_z^\eta(\rho_w-\rho_o)gdz-fv-\frac{\partial}{\partial x}A_H\frac{\partial u}{\partial x}-\frac{\partial}{\partial y}A_H\frac{\partial u}{\partial y}-\frac{\partial}{\partial z}A_V\frac{\partial u}{\partial z}=0 \qquad \text{(A2)}$$

Y-directed momentum:

$$\frac{\partial v}{\partial t}+u\frac{\partial v}{\partial x}+v\frac{\partial v}{\partial y}+w\frac{\partial v}{\partial z}+g\frac{\partial \eta}{\partial y}+\frac{1}{\rho_o}\frac{\partial}{\partial y}\int_z^\eta(\rho_w-\rho_o)gdz+fu-\frac{\partial}{\partial x}A_H\frac{\partial v}{\partial x}-\frac{\partial}{\partial y}A_H\frac{\partial v}{\partial y}-\frac{\partial}{\partial z}A_V\frac{\partial v}{\partial z}=0 \qquad \text{(A3)}$$

Water surface elevation determined from the vertically-integrated continuity equation:

$$\frac{\partial \eta}{\partial t} = -\frac{\partial}{\partial x}\int_{-H}^{\eta} u dz - \frac{\partial}{\partial y}\int_{-H}^{\eta} v dz. \quad \text{(A4)}$$

The effect of wind forcing introduced by means of the surface wind-stress boundary condition:

$$\left(A_V \frac{\partial u}{\partial z}, A_V \frac{\partial v}{\partial z}\right)_{z=\eta} = \frac{\rho_a}{\rho_w} C_{D,\,air} \vec{U}_{wind} \left|\vec{U}_{wind}\right|. \quad \text{(A5)}$$

The effect of bottom friction introduced by the bottom boundary condition:

$$\left(A_V \frac{\partial u}{\partial z}, A_V \frac{\partial v}{\partial z}\right)_{z=-H} = K_{bottom} \vec{U}_{bottom} \left|\vec{U}_{bottom}\right|. \quad \text{(A6)}$$

The bottom friction coefficient is usually understood to apply to currents at an elevation of one metre above the bottom. The bottom-most vector in H3D will, in general, be at a different elevation, i.e., at the midpoint of the lowest computational cell. H3D uses the 'law of the wall' to estimate the flow velocity at one metre above the bottom from the modelled near-bottom velocity.

The evolution of scalars, such as salinity, temperature, or suspended sediment, is given by the scalar transport/diffusion equation:

$$\frac{\partial S}{\partial t} + u\frac{\partial S}{\partial x} + v\frac{\partial S}{\partial y} + w\frac{\partial S}{\partial z} \frac{\partial}{\partial x} N_H \frac{\partial S}{\partial x} - \frac{\partial}{\partial y} N_H \frac{\partial S}{\partial y} - \frac{\partial}{\partial z} N_V \frac{\partial S}{\partial z} = Q\,. \quad \text{(A7)}$$

In the above equations:

*u(x,y,z,t)*: component of velocity in the *x* direction;

*v(x,y,z,t)*: component of velocity in the *y* direction;

*w(x,y,z,t)*: component of velocity in the *z* direction;

*S(x,y,z,t)*: scalar concentration;

*Q(x,y,z,t)*: source term for each scalar species

*f*: Coriolis parameter, determined by the earth's rotation and the local latitude;

$A_H\left(\partial u/\partial x, \partial u/\partial y, \partial v/\partial x, \partial v/\partial y\right)$: horizontal eddy viscosity;

$A_V\ \left(\partial u/\partial z, \partial v/\partial z, \partial \rho_{water}/\partial z\right)$: vertical eddy viscosity;

$N_H$: horizontal eddy diffusivity;

$N_V\ \left(\partial u/\partial z, \partial v/\partial z, \partial \rho_{water}/\partial z\right)$: vertical eddy diffusivity;

$C_{D,air}$: drag coefficient at the air-water interface;

$C_{D,bottom}$: drag coefficient at the water/sea bottom interface;

$\rho_a$: density of air;

$\rho_w(x,y,z,t)$ : density of water;

$\rho_o$ : reference density of water;

$\eta(x,y,t)$: water surface elevation;

$H(x,y)$ : local depth of water.

The above equations are formally integrated over the small volumes defined by the computational grid, and a set of algebraic equations results, for which an appropriate time-stepping methodology must be found. Backhaus (1983, 1985) presents such a procedure, referred to as a semi-implicit method. The spatially-discretized version of the continuity equation is written as:

$$\eta^{(1)} = \eta^{(0)} - \alpha\frac{\Delta t}{\Delta l}(\delta_x U^{(1)} + \delta_y V^{(1)}) - (1-\alpha)\frac{\Delta t}{\Delta l}(\delta_x U^{(0)} + \delta_y V^{(0)}) \quad \text{(A8)}$$

where superscript *(0)* and *(1)* refer to the present and the advanced time, $\delta_x$ and $\delta_y$ are spatial differencing operators, and *U* and *V* are vertically integrated velocities. The factor α represents an implicit weighting, which must be greater than 0.5 for numerical stability. $U^{(0)}$ and $V^{(0)}$ are known at the start of each computational cycle. $U^{(1)}$, and similarly $V^{(1)}$, can be expressed as:

$$U^{(1)} = U^{(0)} - g\alpha\Delta t\eta_x^{(1)} - g(1-\alpha)\Delta t\eta_x^{(0)} + \Delta tX^{(0)} \quad \text{(A9)}$$

where $X^{(0)}$ symbolically represents all other terms in the equation of motion for the u- or v-component, which are evaluated at time level *(0)*: Coriolis force, internal pressure gradients, non-linear terms, and top and bottom stresses,*)*. When these expressions are substituted into the continuity equation (A4), after some further manipulations, there results an elliptic equation for $\delta_{i,k}$, the change in water level over one time step at grid cell *i,k* (respectively the *y* and *x* directions):

$$\delta_{i,k} - (ce\delta_{i,k+1} + cw\delta_{i,k-1} + cn\delta_{i-1,k} + cs\delta_{i+1,k}) = Z_{i,k} \quad \text{(A10)}$$

where *ce*, *cw*, *cn*, and *cs* are coefficients depending on local depths and the weighting factor (α), and $Z_{i,k}$ represents the sum of the divergence formed from velocities at time level *(0)* plus a weighted sum of adjacent water levels at time level *(0).*

Once equation (A10) is solved for $\delta_{i,k}$, the water level can be updated:

$$\eta_{i,k}^{(1)} = \eta_{i,k}^{(0)} + \delta_{i,k} \quad \text{(A11)}$$

and equation (A9) can be completed.

At the end of each time step, volume conservation is used to diagnostically compute the vertical velocity *w(j,i,k)* from the two horizontal components *u* and *v*.

## 2.1 Vertical Grid Geometry

In the vertical, the levels near the surface are typically closely spaced to assist with resolving near-surface dynamics. In addition, the model is capable of dealing with relatively large excursions in overall water level as the water level rises and falls in response to varying inflows and outflows, by allowing the number of near-surface layers to change as the water level varies. That is, as water levels rise in a particular cell, successive layers above the original layer are turned on and become part of the computational mesh. Similarly, as water levels fall, layers are turned off. This procedure has proven to be quite robust, and allows for any reasonable vertical resolution in near-surface waters. When modelling thin river plumes in areas of large tidal range, the variable number of layers approach allows for much better control over vertical resolution than does the σ-coordinate method.

In addition to tides, the model is able to capture the important response, in terms of enhanced currents and vertical mixing, to wind-driven events. This is achieved by applying wind stress to each surface grid point on each time step. Vertical mixing in the model then re-distributes this horizontal momentum throughout the water column. Similarly, heat flux through the water surface is re-distributed by turbulence and currents in temperature simulations.

## 2.2 Turbulence Closure

Turbulence modelling is important in determining the correct distribution of velocity and scalars in the model. The diffusion coefficients for momentum ($A_H$ and $A_V$) and scalars ($N_H$ and $N_V$) at each computational cell are dependent on the level of turbulence at that point. H3D uses a shear-dependent turbulence formulation in the horizontal, (Smagorinsky, 1963). The basic form is:

$$A_H = A_{H0}\, dx\, dy \sqrt{\left(\frac{du}{dx}\right)^2 + \left(\frac{dv}{dy}\right)^2 + \frac{1}{2}\left(\frac{\partial v}{\partial x} + \frac{\partial u}{\partial y}\right)^2} \qquad \text{(A12)}$$

The parameter $A_{H0}$ is a dimensionless tuning variable, and experience has shown it to lie in the range of 0.1 to 1.0 for most water bodies such as rivers, lakes and estuaries.

A shear and stratification dependent formulation, the Level 2 model of Mellor and Yamada (1982), is used for the vertical eddy diffusivity. The basic theory for the vertical viscosity formulation is taken from an early paper, Mellor and Durbin (1975). The evaluation of length scale is based on a methodology presented in Mellor and Yamada (1982).

For scalars, both horizontal and vertical eddy diffusivity are taken to be similar to their eddy viscosity counterparts, but scaled by a fixed ratio from the eddy viscosity values. Different ratios are used for the horizontal and vertical diffusivities. If data is available for calibration, these ratios can be adjusted based on comparisons between modelled and observed data. Otherwise, standard values based on experience with similar previously modelled water bodies are used.

## 2.3 Scalar Transport

The scalar transport equation implements a form of the flux-corrected algorithm (Zalesak, 1979), in which all fluxes through the sides of each computational cell are first calculated using a second-order method. Although generally more accurate than a first order method, second order flux calculations can sometimes lead to unwanted high frequency oscillations in the numerical solution. To determine if such a situation is developing, the model examines each cell to see if the computed second order flux would cause a local minimum or maximum to develop. If so, then all fluxes into or out of that cell are replaced by first order fluxes, and the calculation is completed. As noted, the method is not a strict implementation of the Zalesak method, but is much faster and achieves very good performance with respect to propagation of a Gaussian distribution through a computational mesh. It does not propagate box-car distributions as well as the full Zalesak method, but achieves realistic simulations of the advection of scalars in lakes, rivers and estuaries, which is the goal of the model. This scheme as implemented is thus a good tradeoff between precision and execution time, important since in many situations, where more than one scalar is involved, the transport-diffusion algorithm can take up more than half the execution time.

## 2.4 Heat Flux at the Air-Water Interface

The contribution of heat flux to the evolution of the water temperature field can be schematized as:

$$\frac{dT}{dt} = \frac{\Delta Q}{\rho * c_p * h}$$

where $\Delta Q$ is the net heat flux per unit area retained in a particular layer, $\rho$ is the density of water, $c_p$ is the heat capacity of water and $h$ is the layer thickness.

Heat flux at the air-water interface incorporates the following terms:

$Q_{in}$: incident short wave radiation. Generally, this is not known from direct observations and is estimated from the cloud cover and opacity observations at nearby stations, a theoretical calculation of radiation at the top of the atmosphere based on the geometry of the earth/sun system, and an empirical adjustment based on radiation measurements at Vancouver Airport and UBC respectively for the period 1974-1977. This procedure has worked well for many water bodies, notably Okanagan Lake and the waters of the north coast of British Columbia, in terms of allowing H3D to reproduce the observed temperature distributions in space and time. Values for albedo as a function of solar height are taken from Kondratyev (1972).

$Q_{back}$: net long wave radiation, calculated according to Gill (1982), involving the usual fourth power dependence on temperature, a factor of 0.985 to allow for the non-black body behaviour of the ocean, a factor depending on vapor pressure to allow for losses due to back radiation from moisture in the air, and a factor representing backscatter from clouds.

$Q_L$ and $Q_H$: latent and sensible heat flux. Latent heat flux ($Q_L$) is the heat carried away by the process of evaporation of water. Sensible heat flux ($Q_S$) is driven by the air-water temperature difference and is similar to conduction, but assisted by turbulence in the air. Latent and sensible heat flux is described by:

$$Q_L = 1.32e^{-3} * L * windspeed * (q_{obs} - q_{sat}) * latent\_factor$$

$$Q_S = 1.46e^{-3} * \rho_{air} * \ c_p * windspeed * (T_{air} - T_{water}) * sensible\_factor$$

Where $q_{obs}$ and $q_{sat}$ are the observed and saturated specific humidities, $T_{air}$ and $T_{water}$ are the air and water temperatures, $L$ is the latent heat of evaporation of water, and $c_p$ is the heat capacity of water. '*latent_factor*' and '*sensible_factor*' are scaling factors introduced to account for local factors, and can be adjusted, when needed, to achieve better calibration of the model. Typically, the only adjustment is that *Sensible_factor* is doubled when the air temperature is less than the water or ice surface temperature to account for increased turbulence in an unstable air column.

Light absorption in the water column. As light passes through the water column it is absorbed and the absorbed energy is a component of the energy balance that drives water temperature. H3D assumes that light attenuation follows an exponential decay law:

$$E(z) = E(z_0) * e^{-k*(z-z_0)}$$

The model computes the energy at the top and bottom of each layer and the difference is applied to the general heat equation in that layer. The extinction coefficient ($k$) is related to the Secci depth ($D_s$) by

$$k = \frac{2.1}{D_s}$$

Temperature is treated like any other scalar as far as advection and diffusion are concerned. Heat flux at the water-sediment interface is not currently included in H3D.

# 3.0 VALIDATION

Three validations are discussed below.

## 3.1 Strait of Georgia/Point Atkinson Tide: Wave Propagation

A fundamental concern with a circulation model such as H3D is how well it propagates waves, the carriers of information through the system. Figure A-1 presents results of a simulation of tides in the Strait of Georgia and Juan de Fuca Strait, with tidal elevations prescribed at the entrance to Juan de Fuca Strait and at a section north of Texada Island in the Strait of Georgia. The complex dynamics of the northern passes, such as Discovery Passage and Seymour Narrows, are thus avoided, allowing a test of H3D's wave propagation capabilities. The figure plots the modelled water level at Point Atkinson in red, and the observed water level in black. There is nearly perfect agreement, with the slight difference resulting from small storm surge events. This validation demonstrates that the selection of grid schematization (Arakawa C-grid) and the semi-implicit time-stepping approach have produced a system than can accurately propagate information through a water body.

## 3.2 Okanagan Lake Temperature Profiles

Obtaining good reproduction of the seasonally–evolving temperate structure of a lake indicates that the heat flux across the air-water interface is accurately parameterized and that the transport-diffusive processes operating in the water column are also accurately reproduced by the model. Figure A-2 presents a comparison of observed and computed temperature profiles at the northern end of Okanagan Lake near Vernon, in April, August, October and December of 1997. The agreement is very good as the model reproduced the transition from a well-mixed condition in the spring to the development of a strong thermocline in the summer, the deepening of the upper layer during the fall cooling period, and a return to isothermal conditions in winter. There is little doubt that H3D can compute accurate temperature distributions in water bodies, as long as adequate meteorological data is available. For this simulation, the meteorological data was obtained from Penticton Airport: winds, rotated to follow the thalweg of the valley; cloud cover, air temperature and relative humidity.

## 3.3 Thermistor Response: Okanagan Lake

Okanagan Lake is subject to significant fluctuations in the vertical thermal structure during the summer stratified period. Figure A-3 shows a temperature time-series at a site on the north side of the William R. Bennett Bridge which exhibits significant temperature excursions at periods of about 60 hours, or 2.5 days. Figure A-4 shows the modelled time series of temperature at three selected depths, 51 m, 21 m and 9 m. The occurrence and magnitude of the temperature fluctuations is generally predicted by the model, but the reproduction is not perfect: the occurrence and timing of the temperature events is quite good, but the modelled peaks appear to be generally somewhat broader in time. It was found that there were considerable differences in the simulated behaviour depending on whether winds at Kelowna Airport, which is situated in a side-valley, were included in the model or not. It is also clear that H3D can generally reproduce internal seiches in a lake, as long as adequate spatial resolution is used. This is particularly apparent when the coherent internal waves that propagate up and down the lake are examined in a longitudinal section, illustrated in two snapshots from a model simulation of such an event in Figure A-5.

# REFERENCES

Arakawa, A. and V.R. Lamb. 1977. Computational design of the basic dynamical processes of the UCLA general circulation model. Methods in Computational Physics, 17, 173-263.

Backhaus, J.O. 1983. A semi-implicit scheme for the shallow water equations for applications to shelf sea modelling. Continental Shelf Research, 2, 243-254.

Backhaus, J.O. and E. Meir-Reimer. 1983. On seasonal circulation patterns in the North Sea. In: North Sea Dynamics, J. Sundermann and W. Lenz, editors. Springerr-Verlag, Heidelberg, pp 63-84.

Backhaus, J.O., and J. Kampf, 1999. Simulation of sub-mesoscale oceanic convection and ice-ocean interactions in the Greenland Sea. Deep Sea Research Part II: Topical Studies in Oceanography, 46, 1427-1455.

Backhaus, J.O., 1985. A three-dimensional model for the simulation of shelf-sea dynamics. Deutsche Hydrographische Zeitschrift, 38, 165-187.

Blumberg, A. F. and G. L. Mellor, A description of a three-dimensional coastal ocean circulation model, In Three-Dimensional Coastal Ocean Models, N. S. Heaps, editor. American Geophysical Union, Washington, DC, 1987, pp 1-16.

Duwe, K.C., R.R. Hewer, and J.O. Backhaus. 1983. Results of a semi-implicit two-step method for the simulation of markedly non-linear flow in coastal seas. Continental Shelf Research, 2, 255-274.

Friehe C.A. and K.F. Schmitt,1976. Parameterization of air-sea interface fluxes of sensible heat and moisture by the bulk aerodynamic formulas. Journal of Physical Oceanography. 76:801-805.

Kampf, J. and J.O Backhaus, 1999. Ice-ocean interactions during shallow convection under conditions of steady winds: three-dimensional numerical studies. Deep Sea Research Part II: Topical Studies in Oceanography, 46, 1335-1355.

Kondratyev, K.Y., 1972. Radiation Processes in the Atmosphere, WMO No. 309,.

Mellor, G.L. and P.A. Durbin. 1975. The structure and dynamics of the ocean surface mixed layer. Journal of Physical Oceanography, 5, 718-728.

Mellor, G.L. and T. Yamada. 1982. Development of a turbulence closure model for geophysical fluid problems. Reviews of Geophysics and Space Physics, 20, 851-875.

Nezhikhovskiy, R.A. 1964. Coefficients of roughness of bottom surface of slush-ice cover. Soviet Hydrology: Selected Papers, 2, 127-150.

Rego, J.L., E. Meselhe, J. Stronach and E. Habib. Numerical Modeling of the Mississippi-Atchafalaya Rivers' Sediment Transport and Fate: Considerations for Diversion Scenarios. Journal of Coastal Research, 26, 212-229.

Saucier, F.J.; F. Roy, D. Gilbert, P. Pellerin and H. Ritchie. 2003. The formationof water masses and sea ice in the Gulf of St. Lawrence. Journal of Geophysical Research, 108 (C8): 3269–3289.

Smagorinsky, J. 1963. General circulation experiments with primitive equations I. The basic experiment. Monthly Weather Review, 91, 91-164.

Stronach, J.A., J.O. Backhaus, and T.S. Murty. 1993. An update on the numerical simulation of oceanographic processes in the waters between Vancouver Island and the mainland: the G8 model. Oceanography and Marine Biology: an Annual Review, 31, 1-86.

Stronach, J.A., R.P. Mulligan, H. Soderholm, R. Draho, D Degen. 2002. Okanagan Lake Limnology: Helping to Improve Water Quality and Safety. Innovation, Journal of the Association of Professional Engineers and Geoscientists of B.C. November 2002.

Wang, E and J.A. Stronach. 2005. Summerland Water Intake Feasibility Study. In “Water – Our Limiting Resource”, Proceedings of a conference held in Kelowna Feb 23-25, 2005. BC Branch, Canadian Water Resources Association. pp. 256 – 269.

Zalesak, S.T. 1979. Fully multidimensional flux-corrected transport algorithms for fluids. Journal of Computational Physics, 31, 335-362.

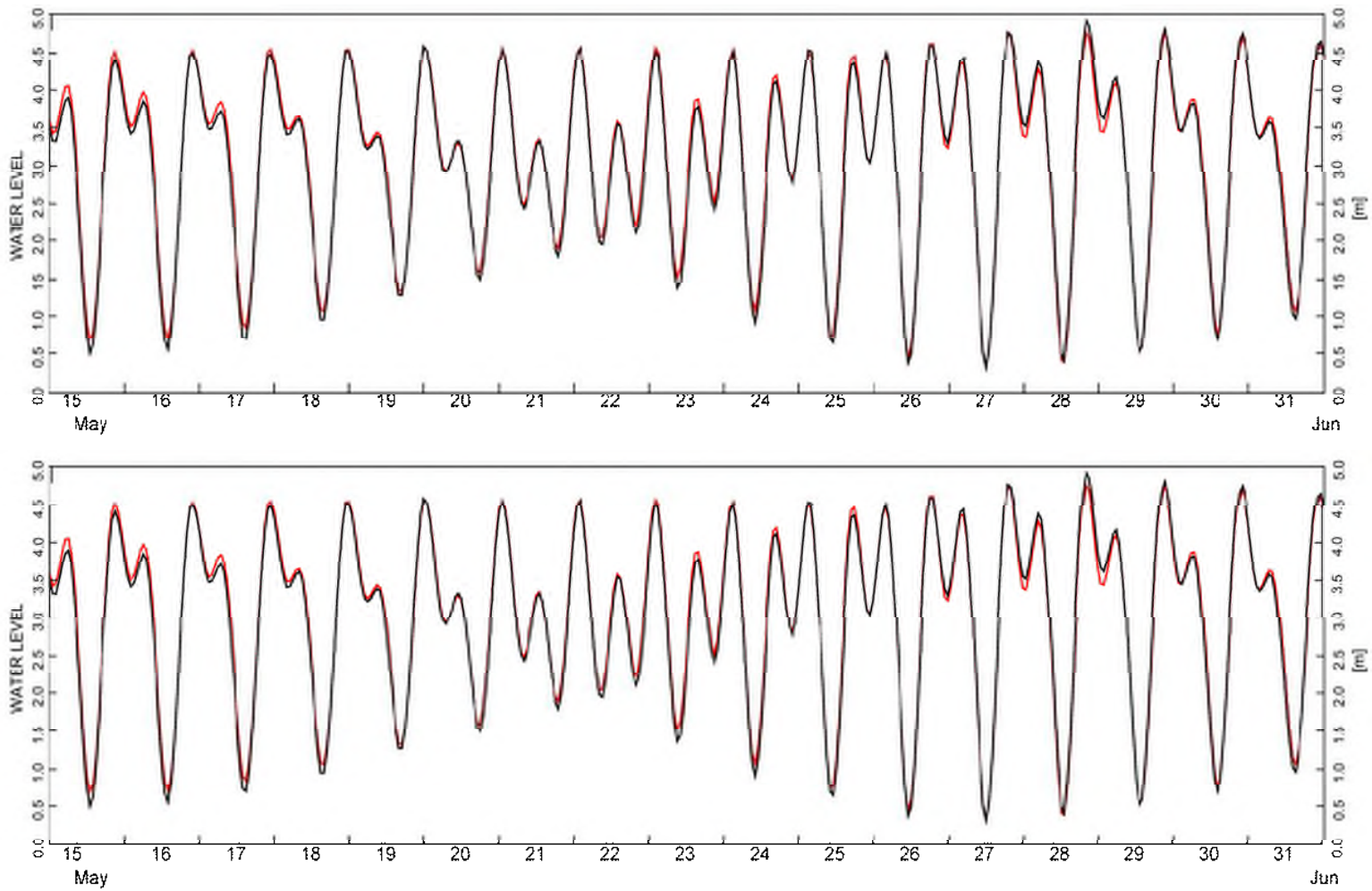


## LEGEND

- Black lines represent observed profiles
- Red lines represent modelled profiles

NOTES

STATUS

CLIENT

-

TETRA TECH

# H3D TECHNICAL DESCRIPTION

## H3D Validation
## Tidal Reproduction

| PROJECT NO. | DWN | CKD | APVD | REV |
|---|---|---|---|---|
| V132 | JMR | JAS | JAS | 001 |

| OFFICE | DATE |
|---|---|
| EBA-VANC | March 2015 |

**Figure A-1**

L:\src\H3D\Documentation\Tech Description 2013\Figures\TtEBA\FigureA1.docx

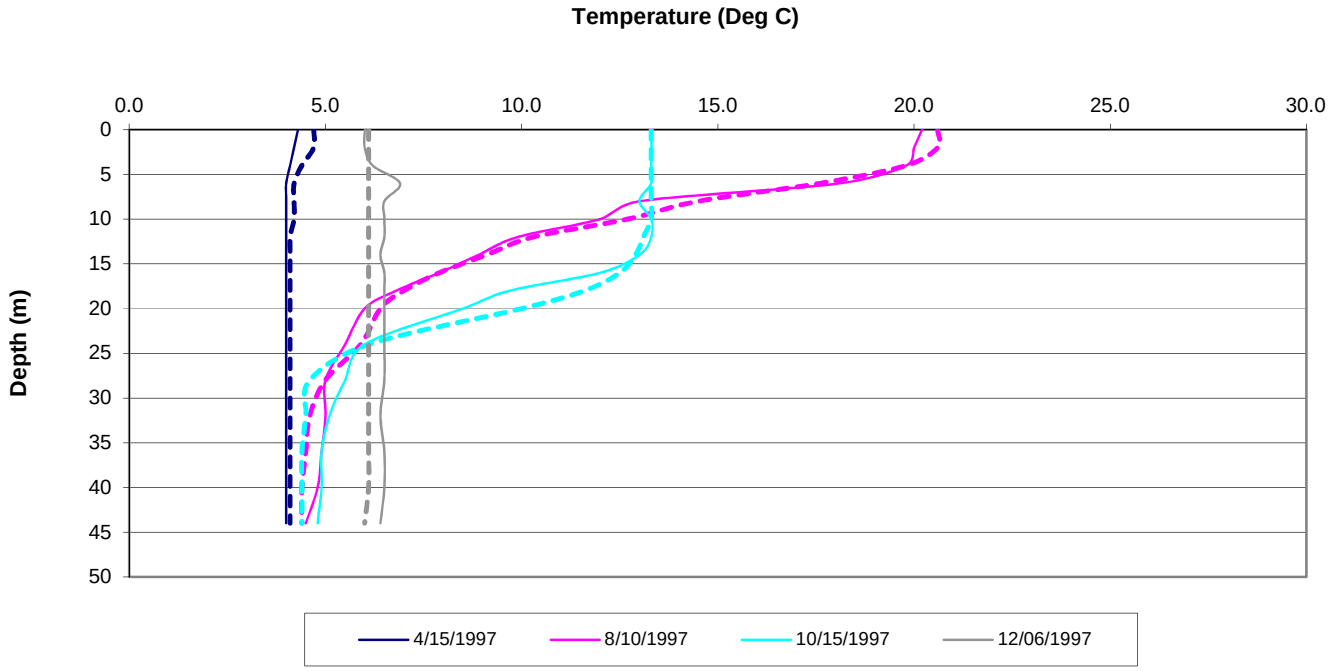


## LEGEND

- Solid lines represent observed profiles
- Dashed lines represent modelled profiles

NOTES

STATUS

CLIENT

-

TETRA TECH

# H3D TECHNICAL DESCRIPTION

## H3D Validation
## Comparison of Observed and Modelled Temperature Profiles at Vernon

| PROJECT NO. | DWN | CKD | APVD | REV |
|---|---|---|---|---|
| V132 | JMR | JAS | JAS | 001 |

| OFFICE | DATE |
|---|---|
| EBA-VANC | March 2015 |

**Figure A-2**

L:\src\H3D\Documentation\Tech Description 2013\Figures\TtEBA\FigureA2.docx

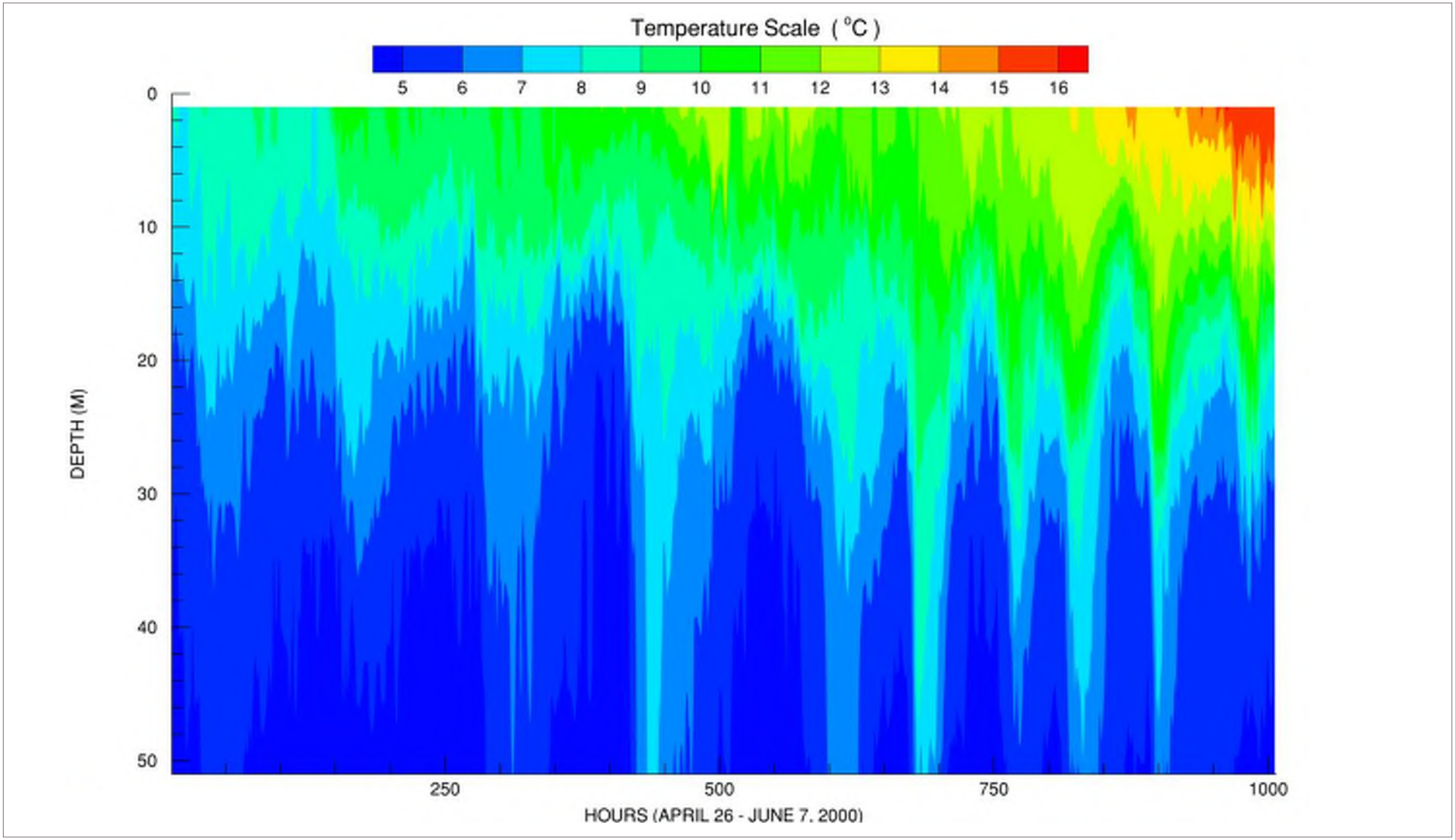


**LEGEND**

NOTES

STATUS
ISSUED FOR USE

CLIENT
-

# H3D TECHNICAL DESCRIPTION

## H3D VALIDATION
## SEICHES IN OKANAGAN LAKE (OBSERVED DATA)

TETRA TECH

| PROJECT NO. | DWN | CKD | APVD | REV |
|---|---|---|---|---|
| V132 | JMR | JAS | JAS | 0 |

| OFFICE | DATE |
|---|---|
| EBA-VANC | March 2015 |

**Figure A-3**

\\eba.local\corp\Vancouver\Engineering\V132\Users\Local\src\H3D\Documentation\Tech Description 2013\Figures\TtEBA\figureA3.doc

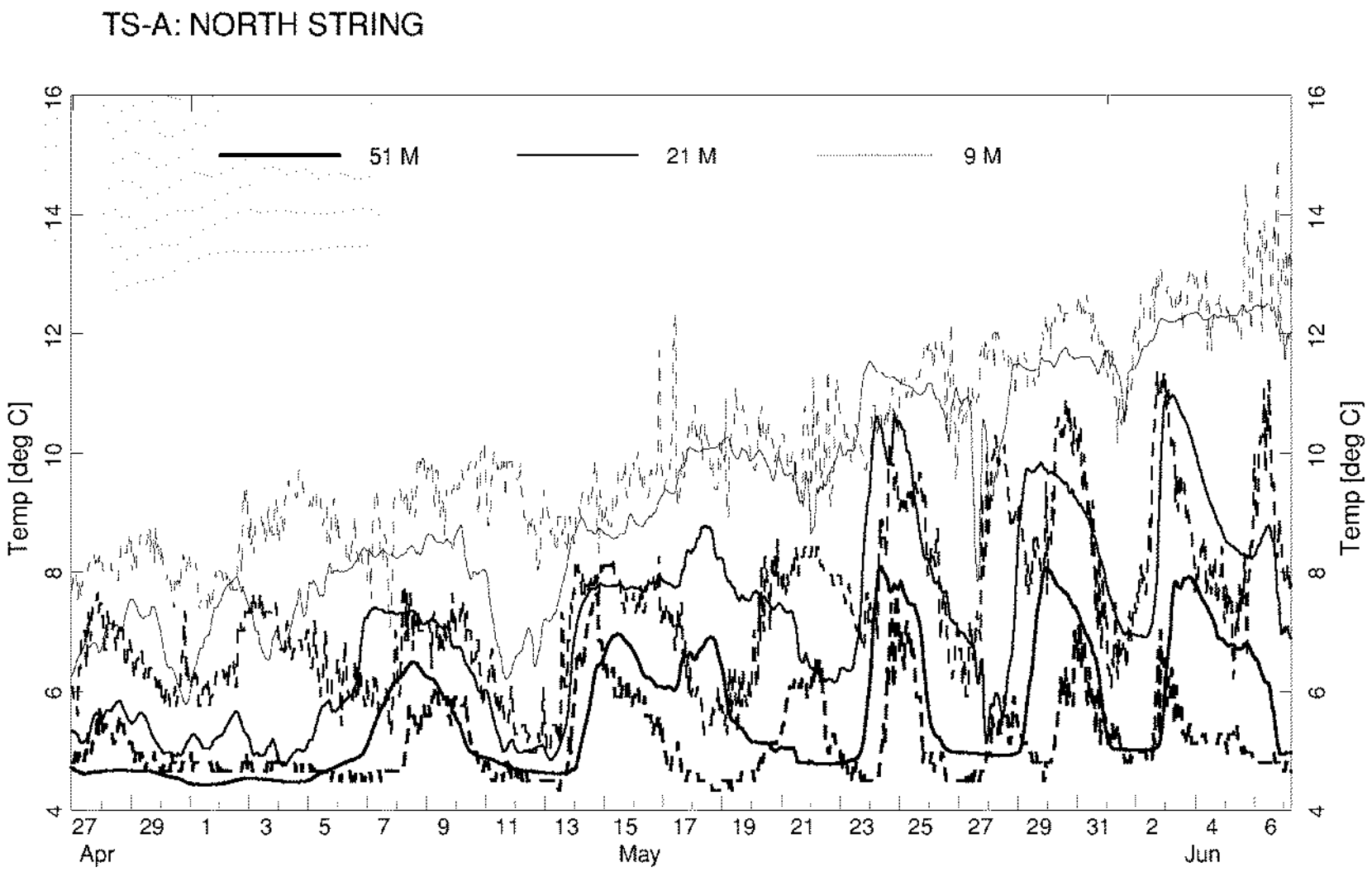


**LEGEND**

Dashed Lines: Observed Temperature
Solid Lines: Modelled Temperature

**NOTES**

**STATUS**
ISSUED FOR USE

**CLIENT**
-

**H3D TECHNICAL DESCRIPTION**

**H3D VALIDATION**
**INTERNAL SEICHE DYNAMICS**
**OKANAGAN LAKE**

TETRA TECH

| PROJECT NO. | DWN | CKD | APVD | REV |
|---|---|---|---|---|
| V132 | JMR | JAS | JAS | 0 |

| OFFICE | DATE |
|---|---|
| EBA-VANC | Marhc 2015 |

**Figure A-4**

\\eba.local\corp\Vancouver\Engineering\V132\Users\Local\src\H3D\Documentation\Tech Description 2013\Figures\TtEBA\figureA4.doc

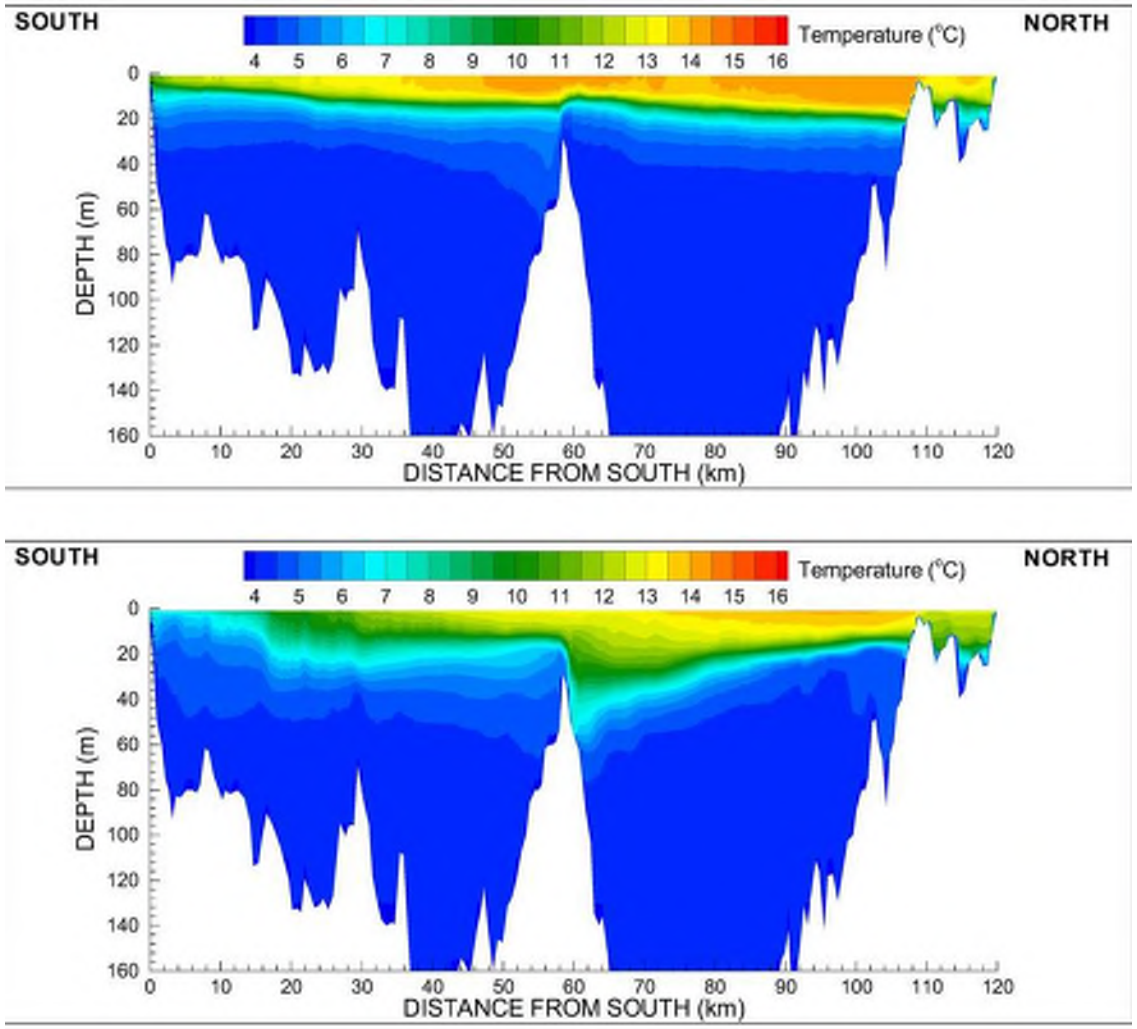


**LEGEND**

**NOTES**

**STATUS**
ISSUED FOR USE

**CLIENT**
-

# H3D TECHNICAL DESCRIPTION

## H3D VALIDATION
## INTERNAL SEICHE DYNAMICS
## OKANAGAN LAKE

TETRA TECH

| PROJECT NO. | DWN | CKD | APVD | REV |
|---|---|---|---|---|
| V132 | JMR | JAS | JAS | JAS |

| OFFICE | DATE |
|---|---|
| EBA-VANC | March 2015 |

**Figure A-5**

# APPENDIX B

## 24 TECPLOT FIGURES ON NOVEMBER 7, 2013

The following 24 figures provide hourly maps and longitudinal section of the effluent plume, in the same format as Figures 3.1 and 3.2, These figures are selected to firstly illustrate the distribution of effluent during the day of poorest performance of the diffuser (November 7, 2013) as well as the return to acceptable conditions between one and two hours later.

**2013 11 07 0000**

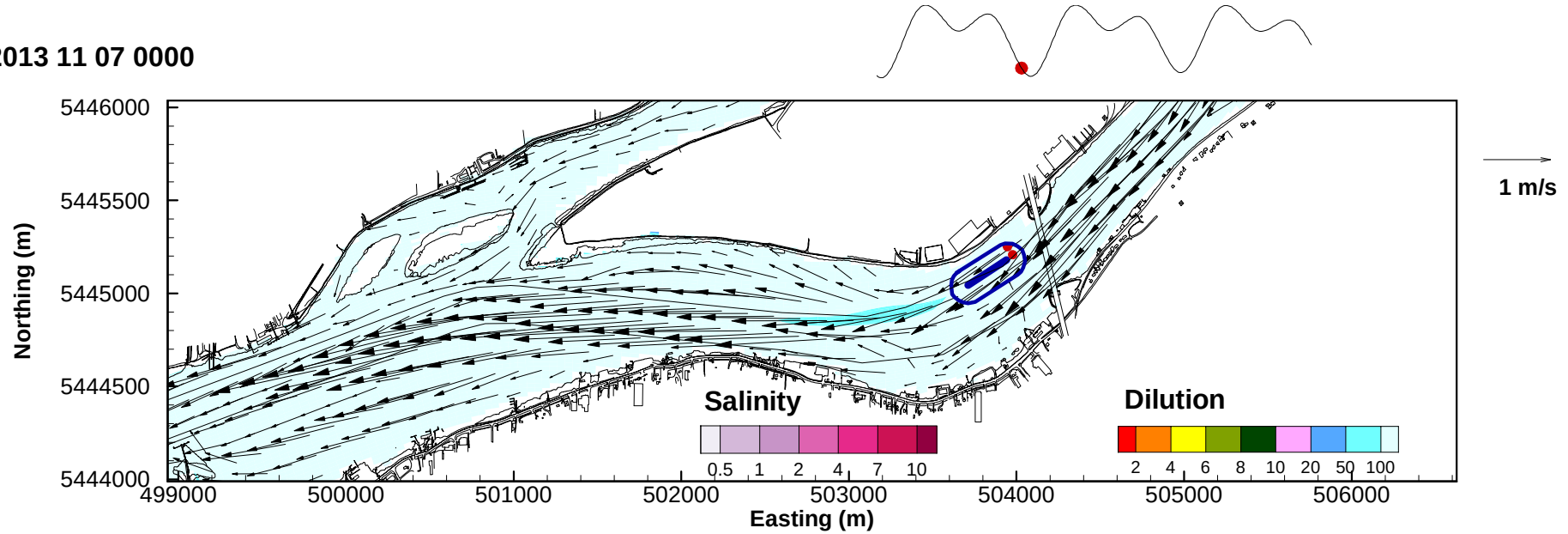


**2013 11 07 0000**

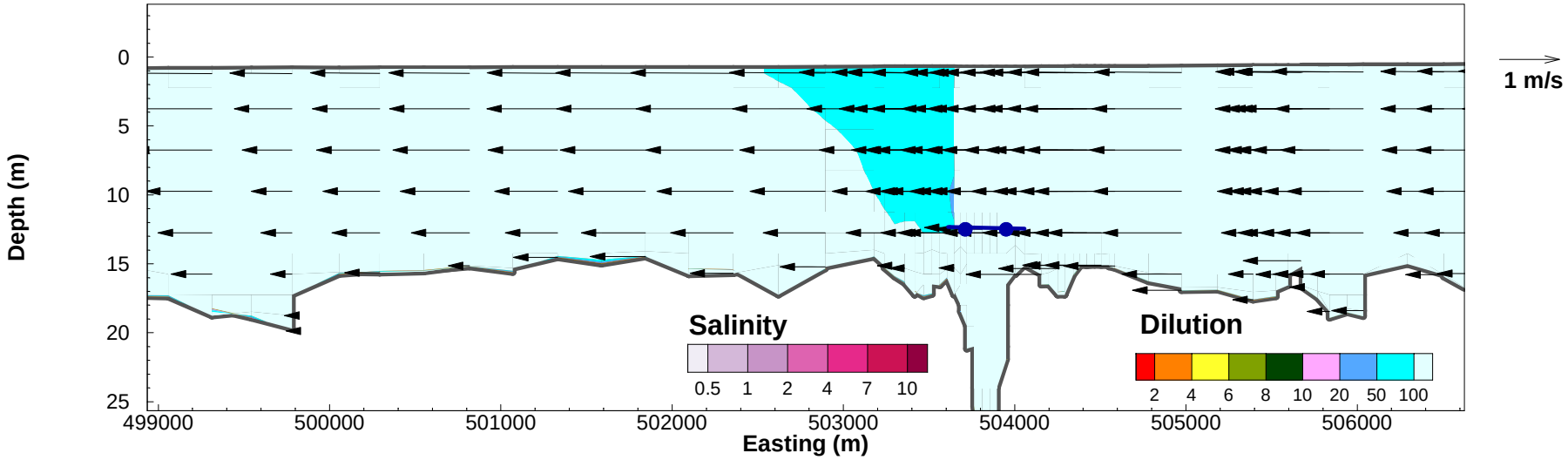


**NOTES**

**Original Run: 02_2013_Nov_Dec**

STATUS
ISSUED FOR USE

CLIENT

CDM Smith

TETRA TECH

**ANNACIS OUTFALL SIMULATION**

**Plan View Minimum Dilution**
**Section View Minimum Dilution**
**Annacis Effluent @14.7 $m^3/s$**

| PROJECT NO. | DWN | CKD | APVD | REV |
|---|---|---|---|---|
| WTRM03039 | AH | JAS | JAS | 0 |

| OFFICE | DATE |
|---|---|
| Tetra Tech Canada - VAN | 18 Sept 2017 |

**Figure B-1**

**2013 11 07 0100**

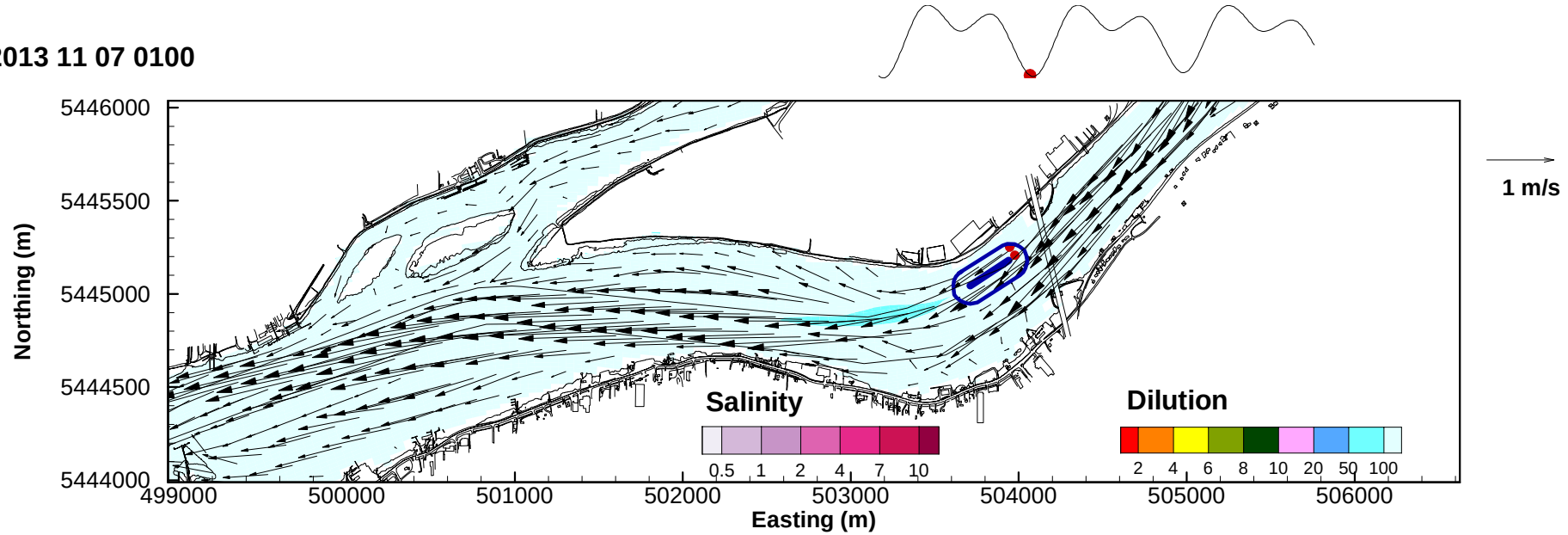


**2013 11 07 0100**

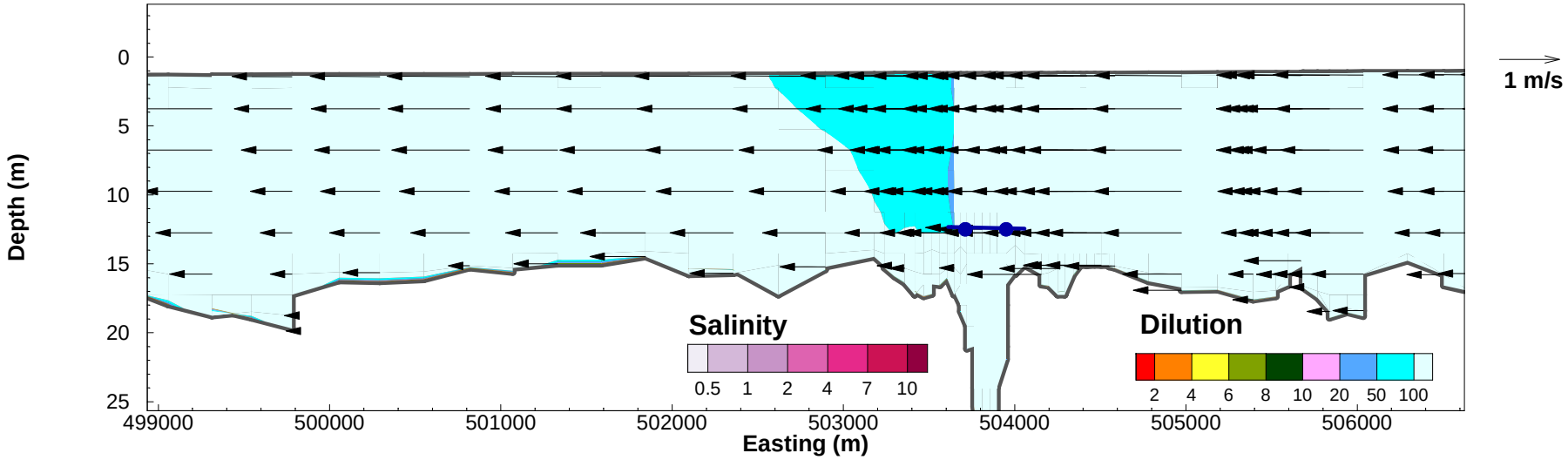


**NOTES**

**Original Run: 02_2013_Nov_Dec**

CLIENT

CDM Smith

TETRA TECH

**ANNACIS OUTFALL SIMULATION**

**Plan View Minimum Dilution**
**Section View Minimum Dilution**
**Annacis Effluent @14.7 $m^3/s$**

| PROJECT NO. | DWN | CKD | APVD | REV |
|---|---|---|---|---|
| WTRM03039 | AH | JAS | JAS | 0 |

| OFFICE | DATE |
|---|---|
| Tetra Tech Canada - VAN | 18 Sept 2017 |

**Figure B-2**

STATUS
ISSUED FOR USE

**2013 11 07 0200**

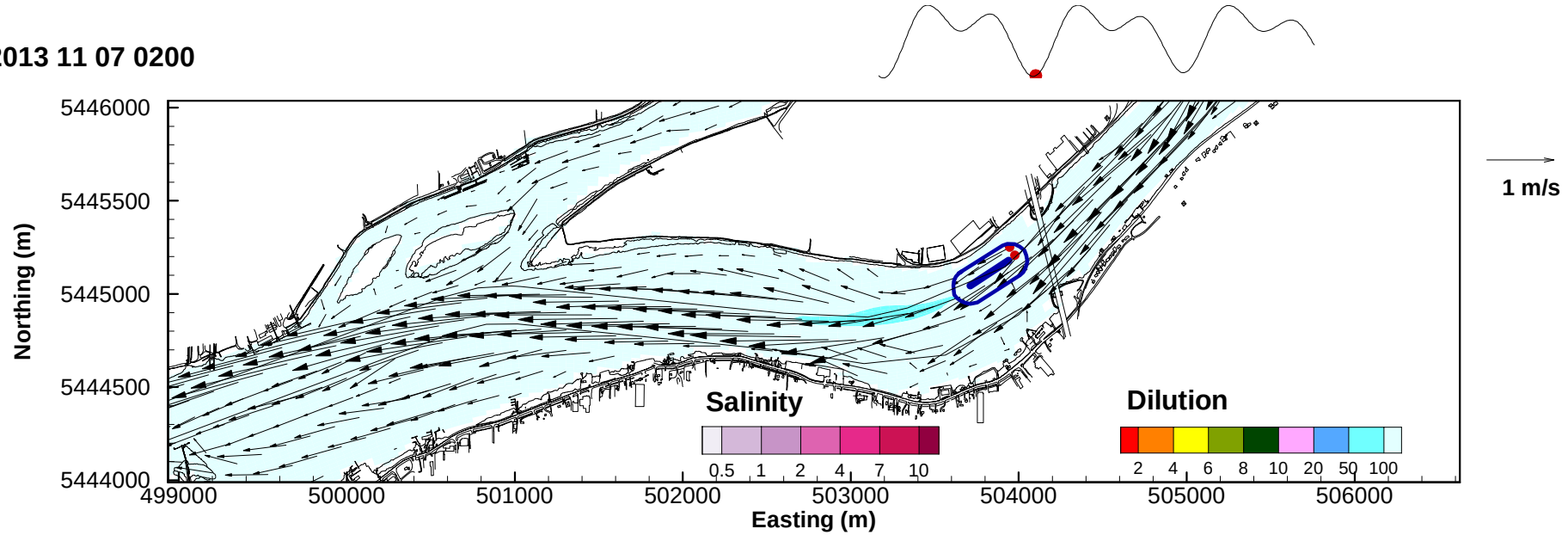


**2013 11 07 0200**

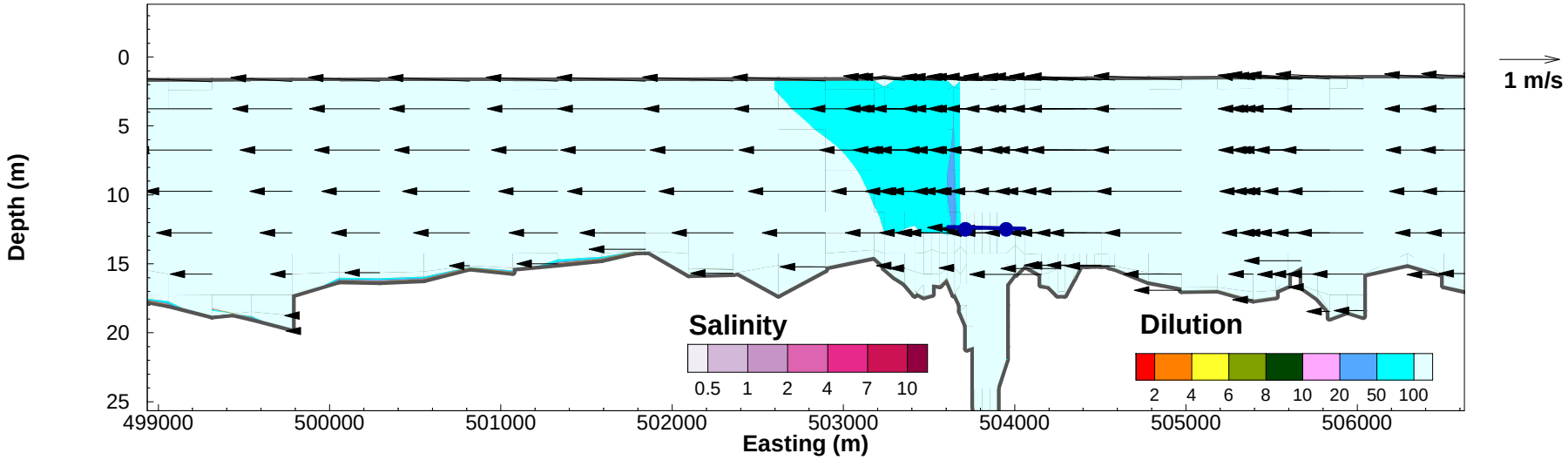


**NOTES**

**Original Run: 02_2013_Nov_Dec**

CLIENT

CDM Smith

TETRA TECH

STATUS
ISSUED FOR USE

**ANNACIS OUTFALL SIMULATION**

**Plan View Minimum Dilution**
**Section View Minimum Dilution**
**Annacis Effluent @14.7 $m^3/s$**

| PROJECT NO. | DWN | CKD | APVD | REV |
|---|---|---|---|---|
| WTRM03039 | AH | JAS | JAS | 0 |

| OFFICE | DATE |
|---|---|
| Tetra Tech Canada - VAN | 18 Sept 2017 |

**Figure B-3**

**2013 11 07 0300**

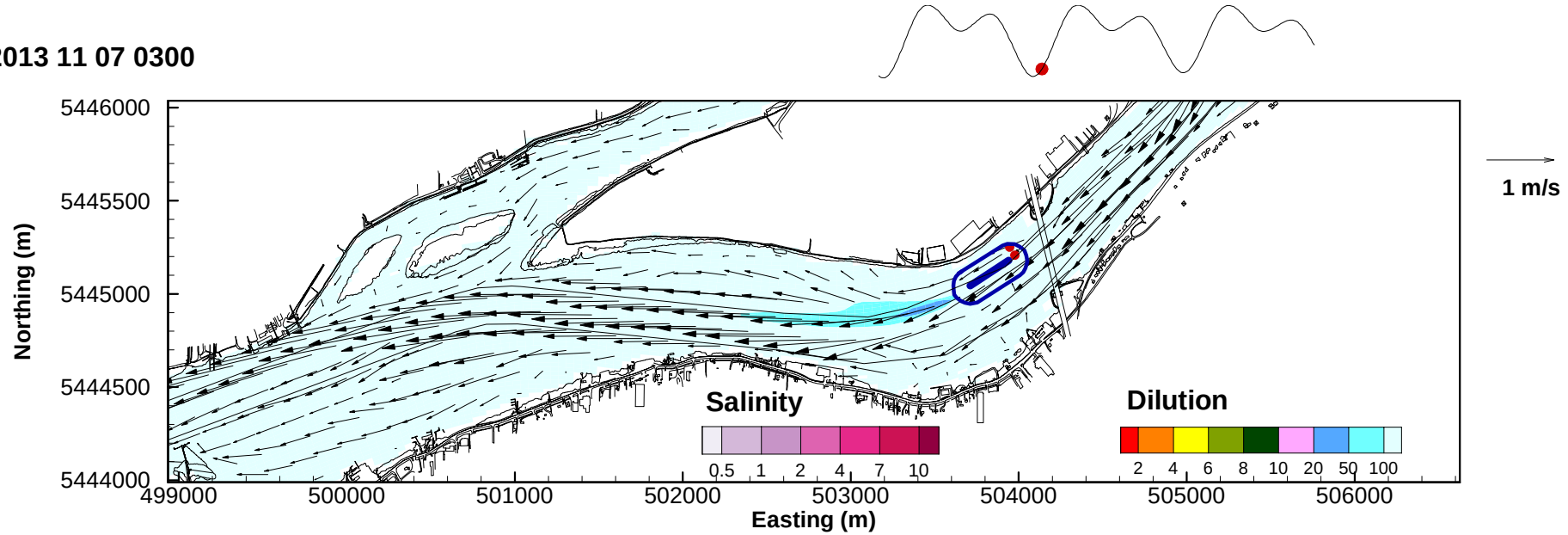


**2013 11 07 0300**

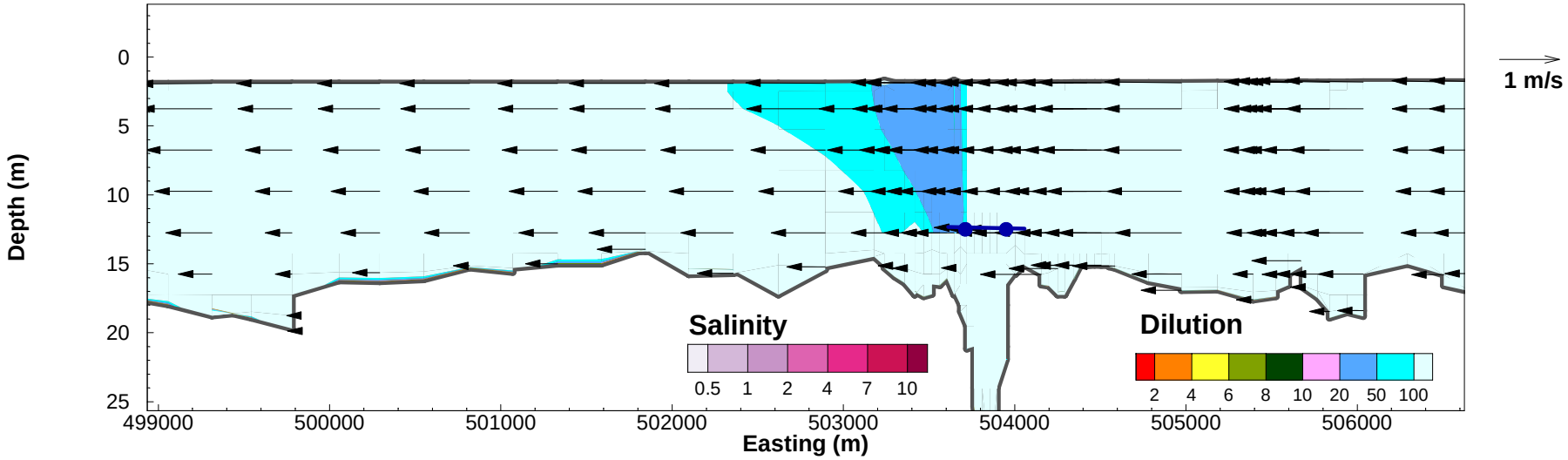


**NOTES**

**Original Run: 02_2013_Nov_Dec**

STATUS
ISSUED FOR USE

CLIENT

CDM Smith

TETRA TECH

**ANNACIS OUTFALL SIMULATION**

**Plan View Minimum Dilution**
**Section View Minimum Dilution**
**Annacis Effluent @14.7 $m^3/s$**

| PROJECT NO. | DWN | CKD | APVD | REV |
|---|---|---|---|---|
| WTRM03039 | AH | JAS | JAS | 0 |

| OFFICE | DATE |
|---|---|
| Tetra Tech Canada - VAN | 18 Sept 2017 |

**Figure B-4**

**2013 11 07 0400**

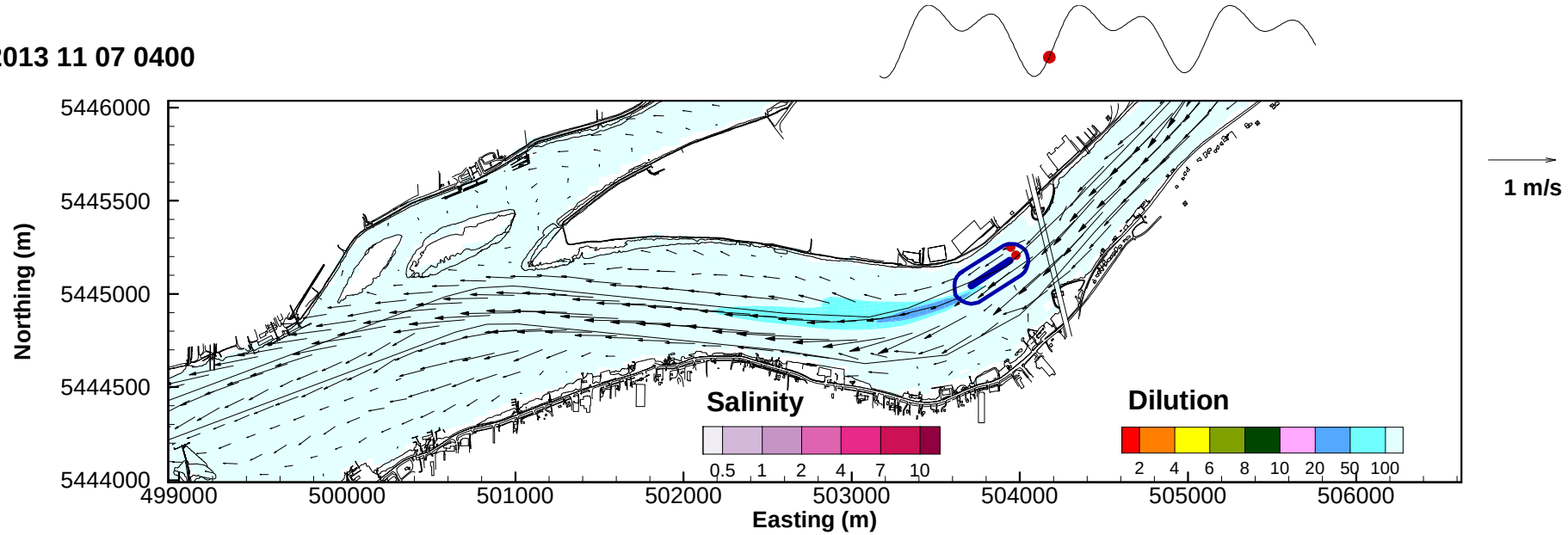


**2013 11 07 0400**

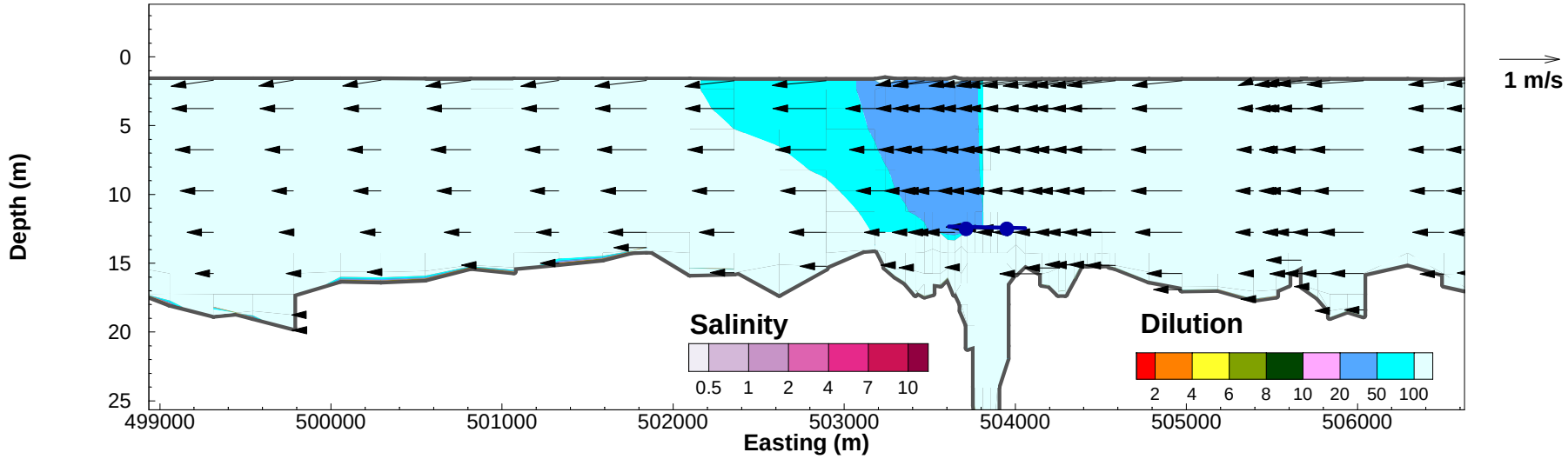


**NOTES**

**Original Run: 02_2013_Nov_Dec**

STATUS
ISSUED FOR USE

CLIENT

CDM Smith

TETRA TECH

**ANNACIS OUTFALL SIMULATION**

**Plan View Minimum Dilution**
**Section View Minimum Dilution**
**Annacis Effluent @14.7 $m^3/s$**

| PROJECT NO. | DWN | CKD | APVD | REV |
|---|---|---|---|---|
| WTRM03039 | AH | JAS | JAS | 0 |

OFFICE: Tetra Tech Canada - VAN
DATE: 18 Sept 2017

**Figure B-5**

2013 11 07 0500

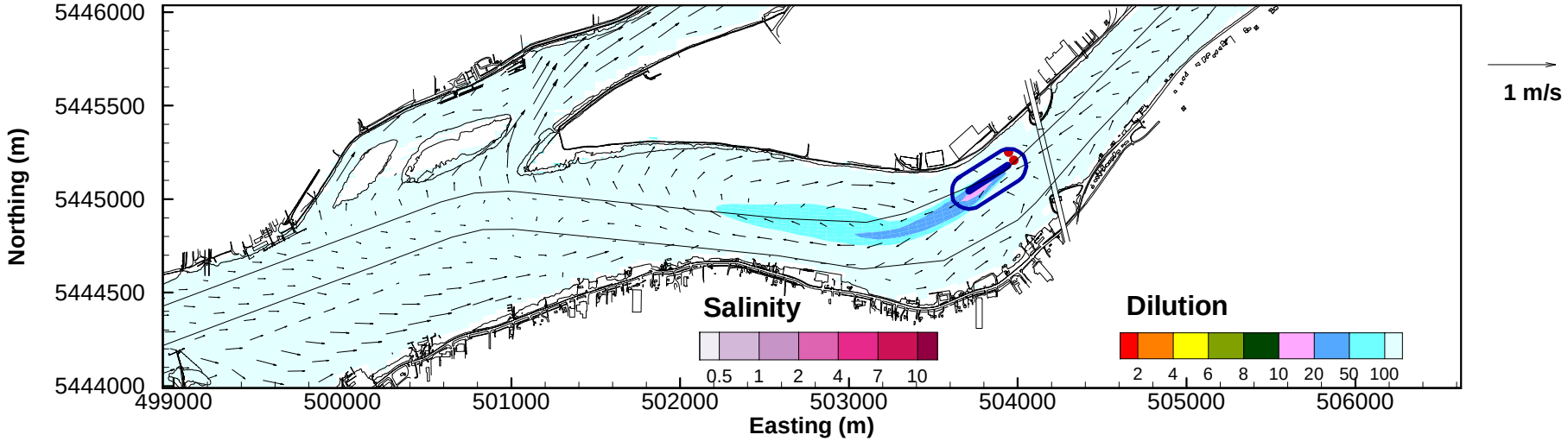


2013 11 07 0500

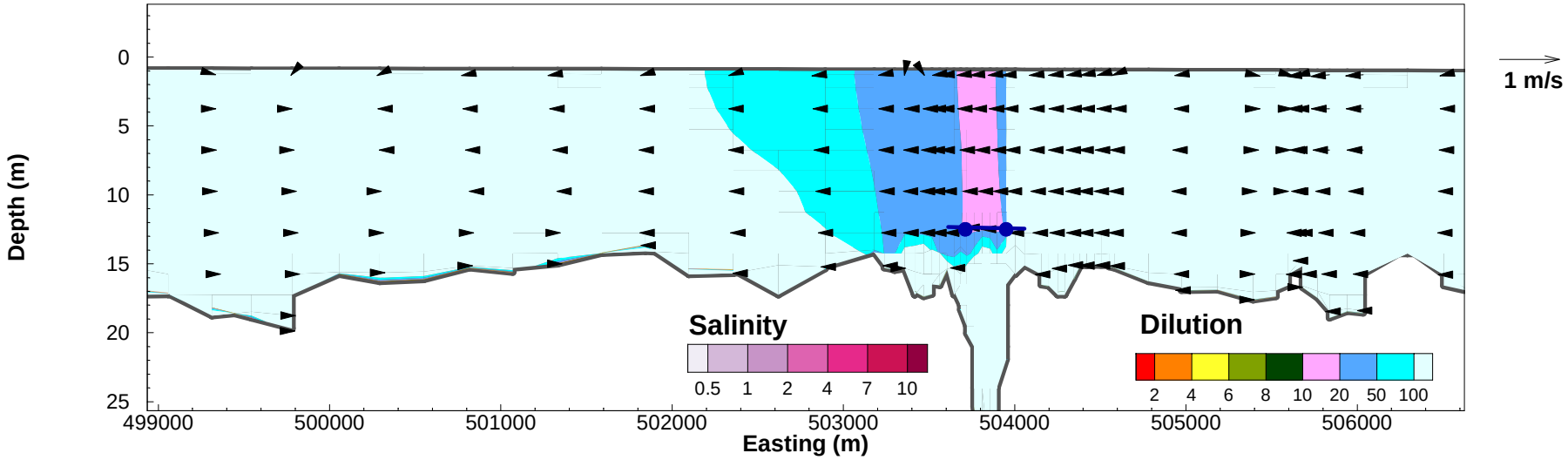


**NOTES**

**Original Run: 02_2013_Nov_Dec**

STATUS
ISSUED FOR USE

CLIENT

CDM Smith

TETRA TECH

**ANNACIS OUTFALL SIMULATION**

**Plan View Minimum Dilution**
**Section View Minimum Dilution**
**Annacis Effluent @14.7 $m^3/s$**

| PROJECT NO. | DWN | CKD | APVD | REV |
|---|---|---|---|---|
| WTRM03039 | AH | JAS | JAS | 0 |

OFFICE: Tetra Tech Canada - VAN
DATE: 18 Sept 2017

**Figure B-6**

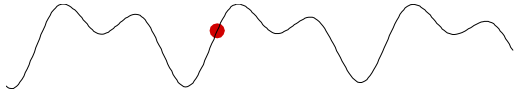

**2013 11 07 0600**

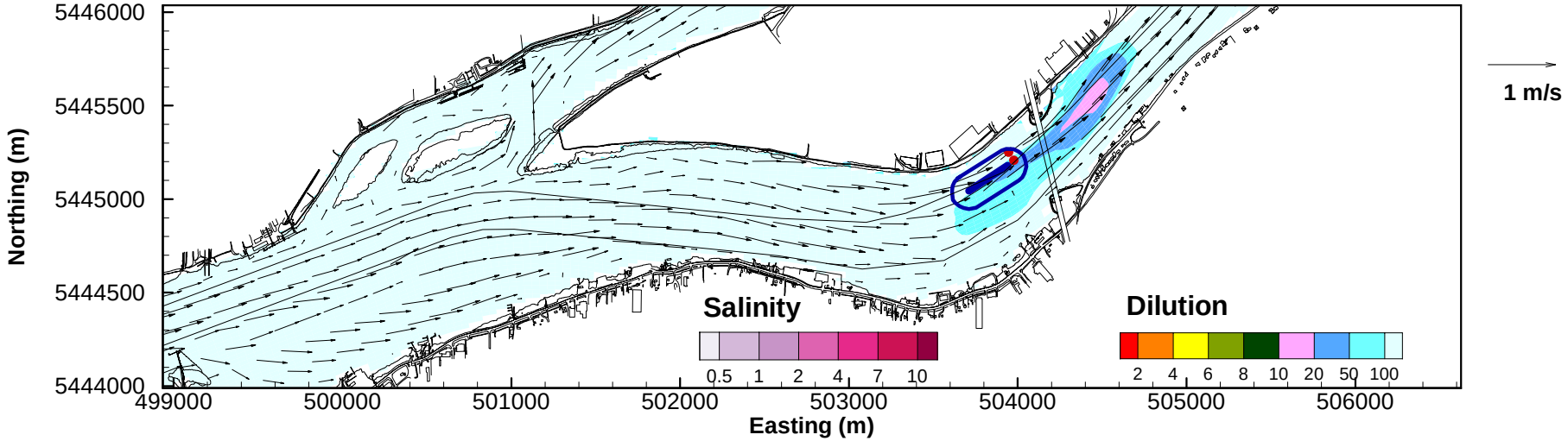


**2013 11 07 0600**

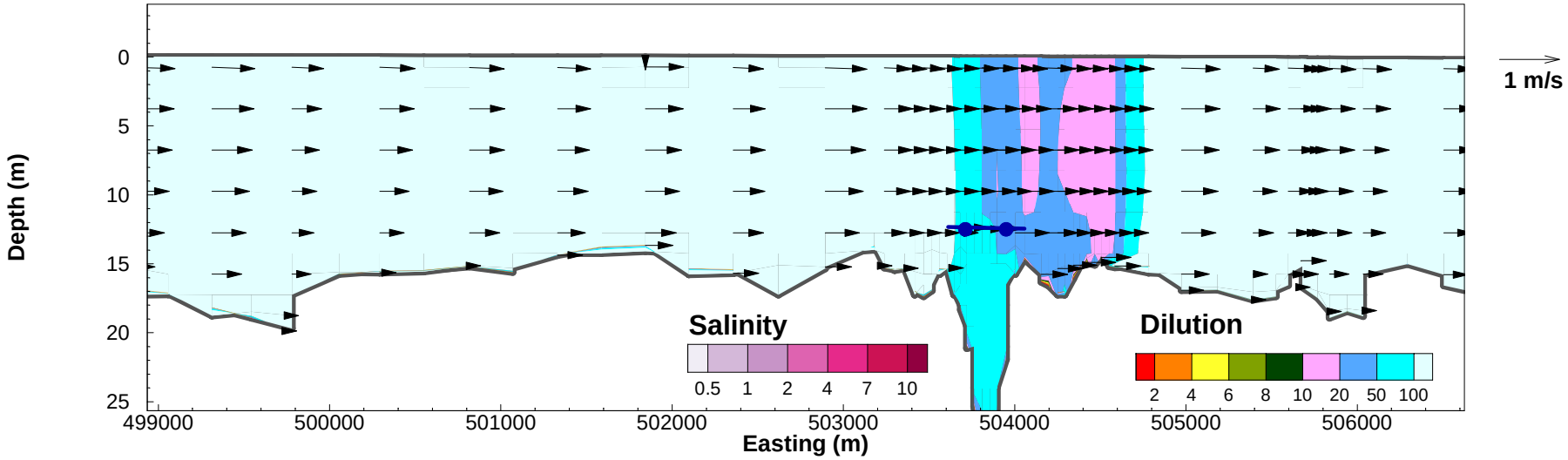


**NOTES**

**Original Run: 02_2013_Nov_Dec**

STATUS
ISSUED FOR USE

CLIENT

CDM Smith

TETRA TECH

**ANNACIS OUTFALL SIMULATION**

**Plan View Minimum Dilution**
**Section View Minimum Dilution**
**Annacis Effluent @14.7 $m^3/s$**

| PROJECT NO. | DWN | CKD | APVD | REV |
|---|---|---|---|---|
| WTRM03039 | AH | JAS | JAS | 0 |

| OFFICE | DATE |
|---|---|
| Tetra Tech Canada - VAN | 18 Sept 2017 |

**Figure B-7**

2013 11 07 0700

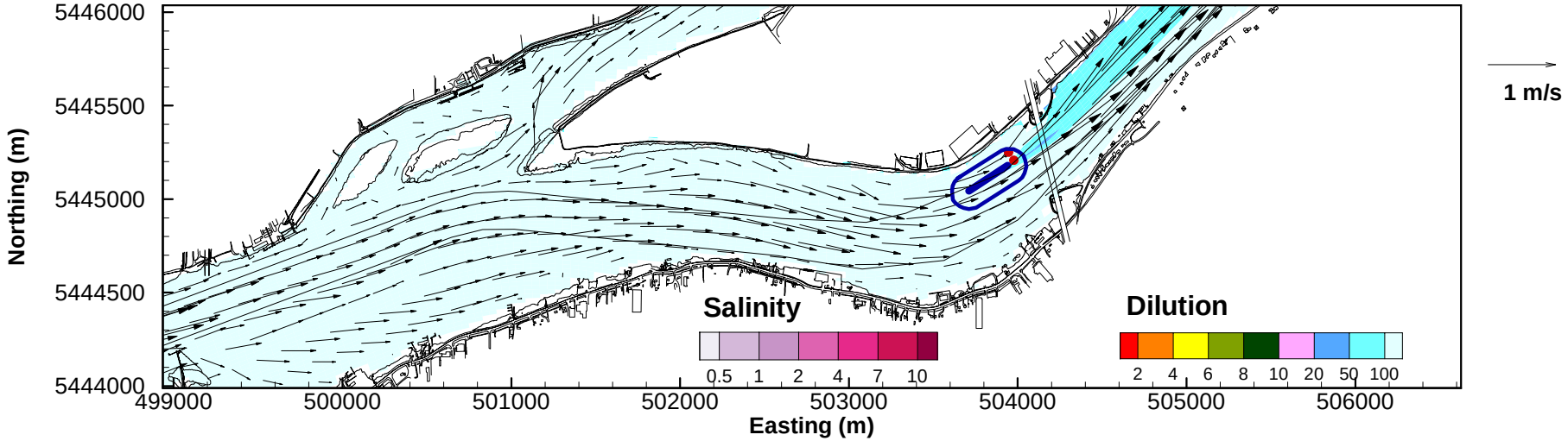


2013 11 07 0700

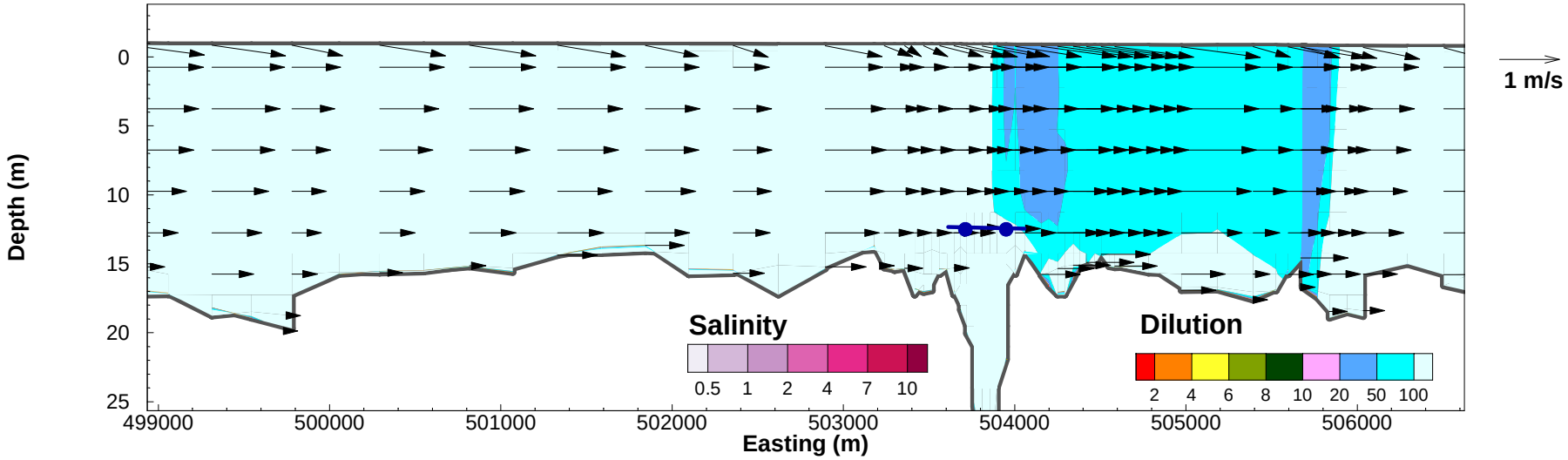


**NOTES**

**Original Run: 02_2013_Nov_Dec**

CLIENT

CDM Smith

TETRA TECH

STATUS
ISSUED FOR USE

# ANNACIS OUTFALL SIMULATION

## Plan View Minimum Dilution
## Section View Minimum Dilution
## Annacis Effluent @14.7 $m^3/s$

| PROJECT NO. | DWN | CKD | APVD | REV |
|---|---|---|---|---|
| WTRM03039 | AH | JAS | JAS | 0 |

| OFFICE | DATE |
|---|---|
| Tetra Tech Canada - VAN | 18 Sept 2017 |

**Figure B-8**

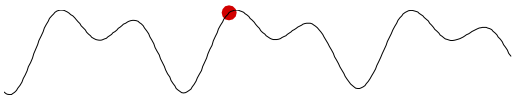

**2013 11 07 0800**

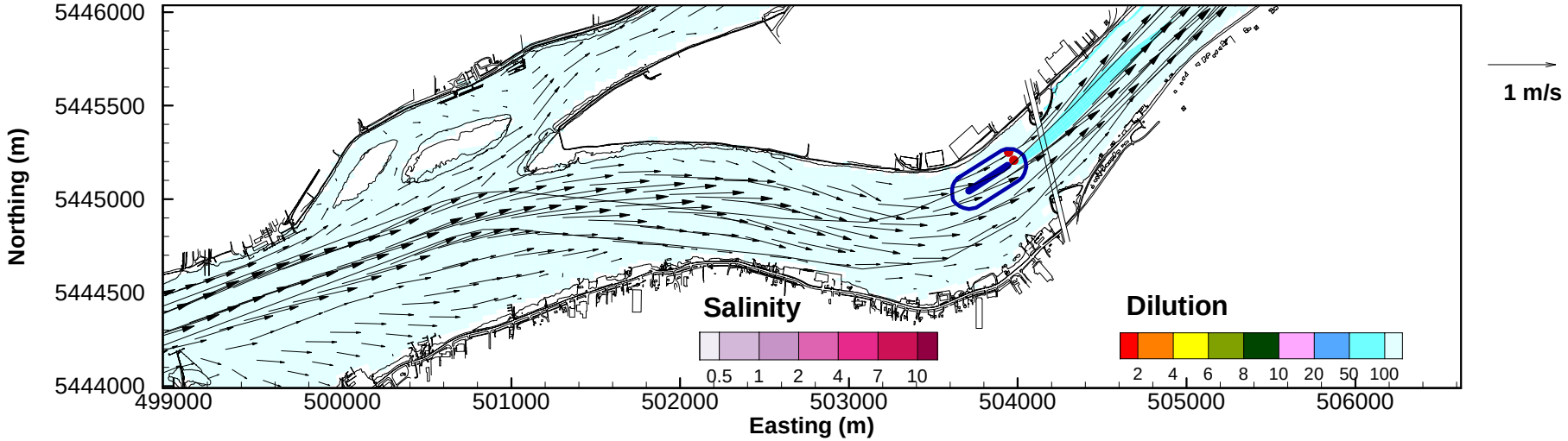


**2013 11 07 0800**

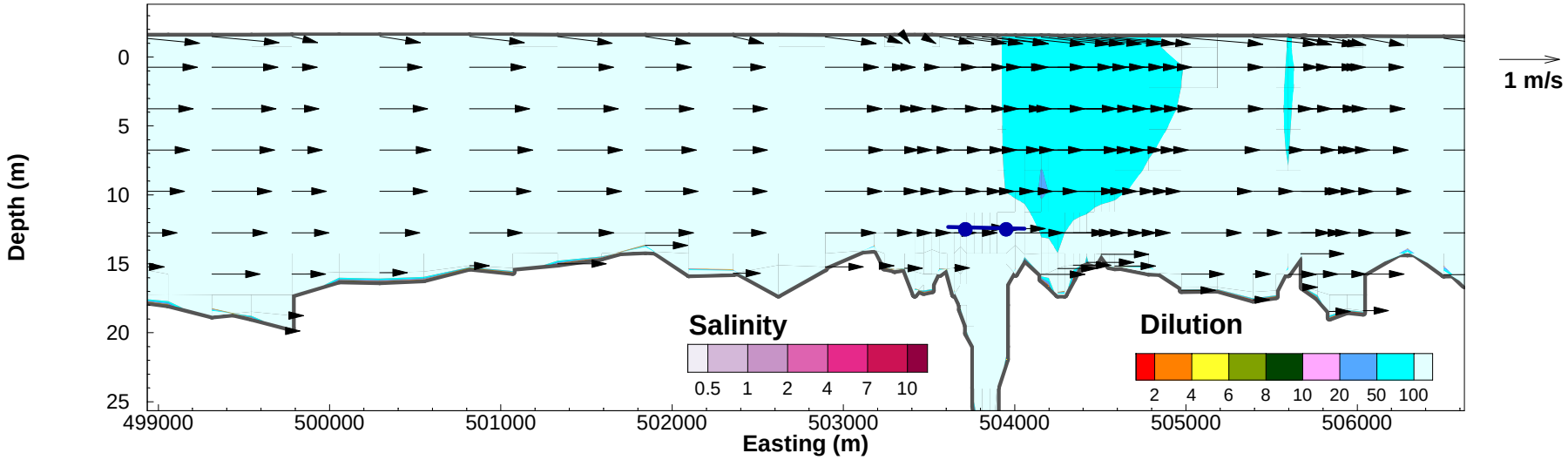


**NOTES**

**Original Run: 02_2013_Nov_Dec**

STATUS
ISSUED FOR USE

CLIENT

CDM Smith

TETRA TECH

**ANNACIS OUTFALL SIMULATION**

**Plan View Minimum Dilution**
**Section View Minimum Dilution**
**Annacis Effluent @14.7 $m^3/s$**

| PROJECT NO. | DWN | CKD | APVD | REV |
|---|---|---|---|---|
| WTRM03039 | AH | JAS | JAS | 0 |

| OFFICE | DATE |
|---|---|
| Tetra Tech Canada - VAN | 18 Sept 2017 |

**Figure B-9**

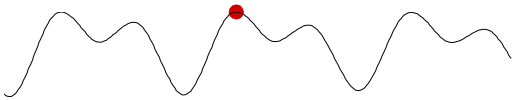

**2013 11 07 0900**

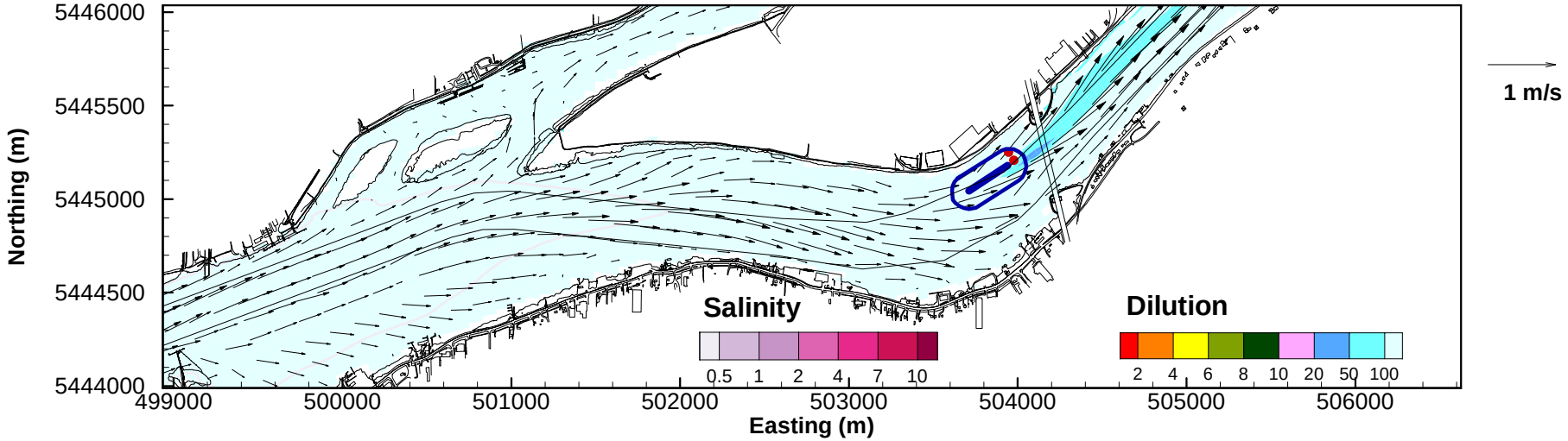


**2013 11 07 0900**

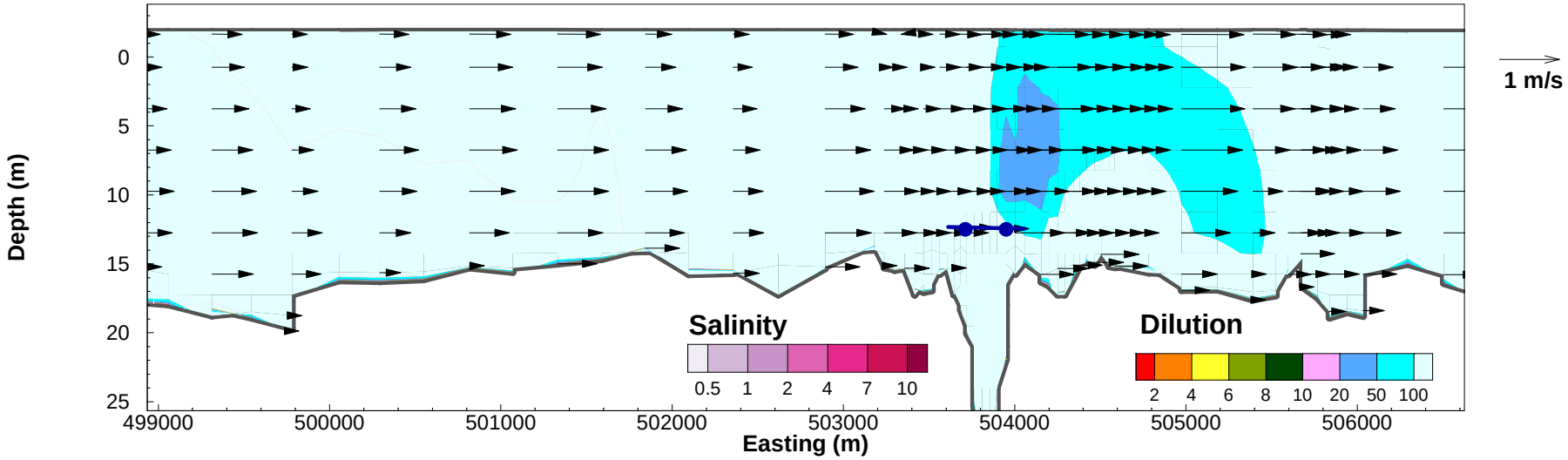


**NOTES**

**Original Run: 02_2013_Nov_Dec**

CLIENT

CDM Smith

TETRA TECH

STATUS
ISSUED FOR USE

**ANNACIS OUTFALL SIMULATION**

**Plan View Minimum Dilution**
**Section View Minimum Dilution**
**Annacis Effluent @14.7 $m^3/s$**

| PROJECT NO. | DWN | CKD | APVD | REV |
|---|---|---|---|---|
| WTRM03039 | AH | JAS | JAS | 0 |

OFFICE: Tetra Tech Canada - VAN
DATE: 18 Sept 2017

**Figure B-10**

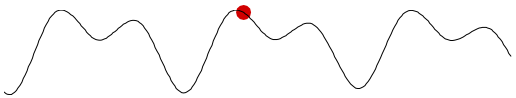

2013 11 07 1000

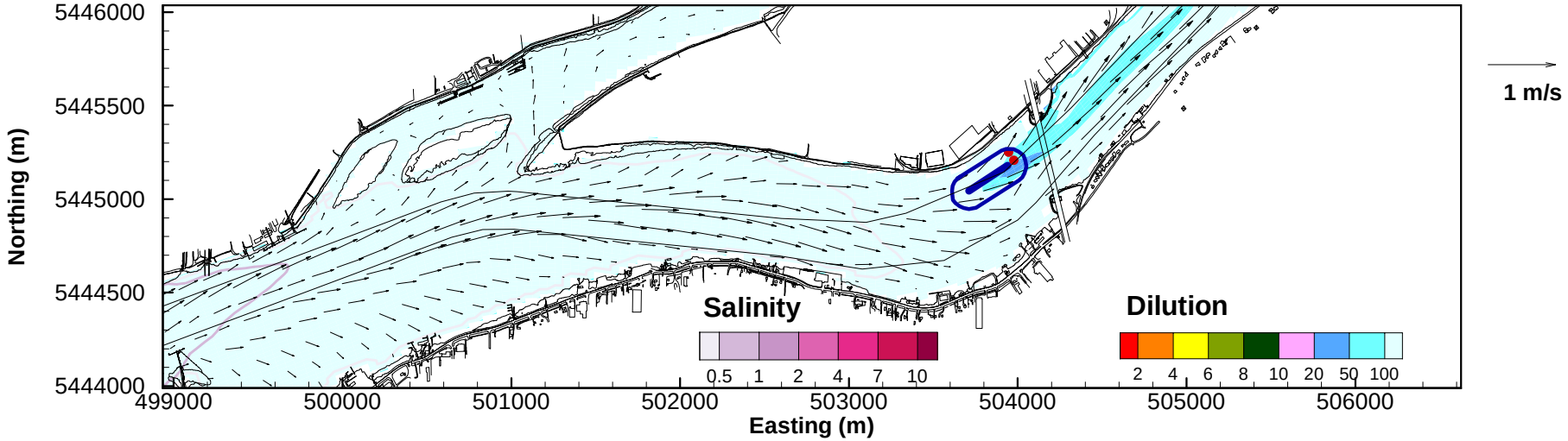


2013 11 07 1000

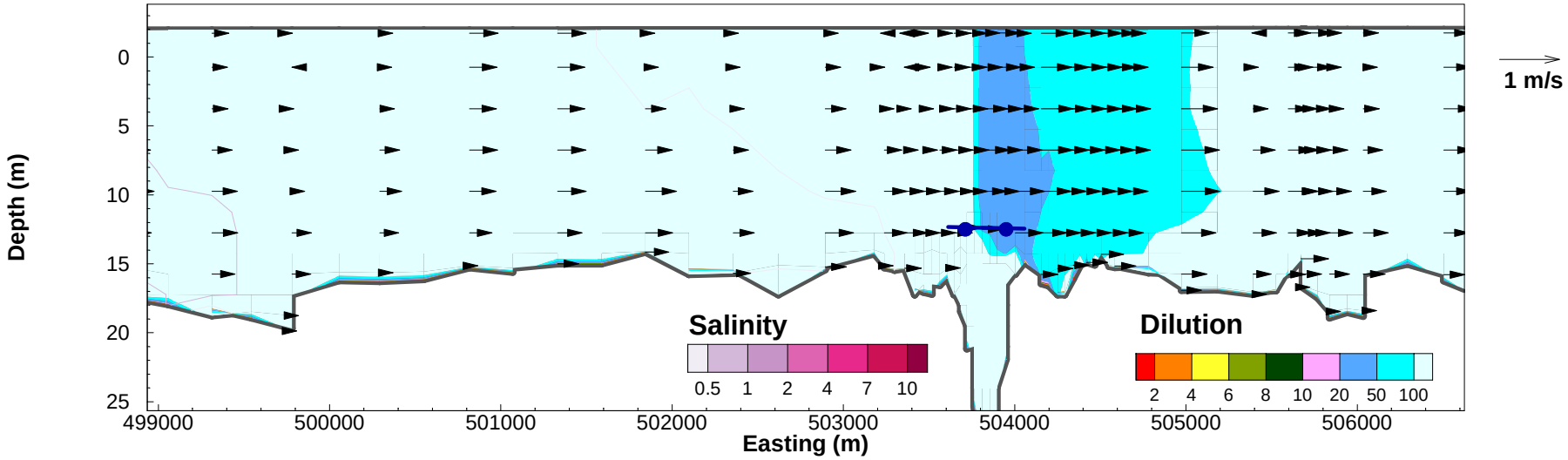


**NOTES**

**Original Run: 02_2013_Nov_Dec**

STATUS
ISSUED FOR USE

CLIENT

CDM Smith

TETRA TECH

# ANNACIS OUTFALL SIMULATION

## Plan View Minimum Dilution
## Section View Minimum Dilution
## Annacis Effluent @14.7 $m^3/s$

| PROJECT NO. | DWN | CKD | APVD | REV |
|---|---|---|---|---|
| WTRM03039 | AH | JAS | JAS | 0 |

| OFFICE | DATE |
|---|---|
| Tetra Tech Canada - VAN | 18 Sept 2017 |

**Figure B-11**

2013 11 07 1100

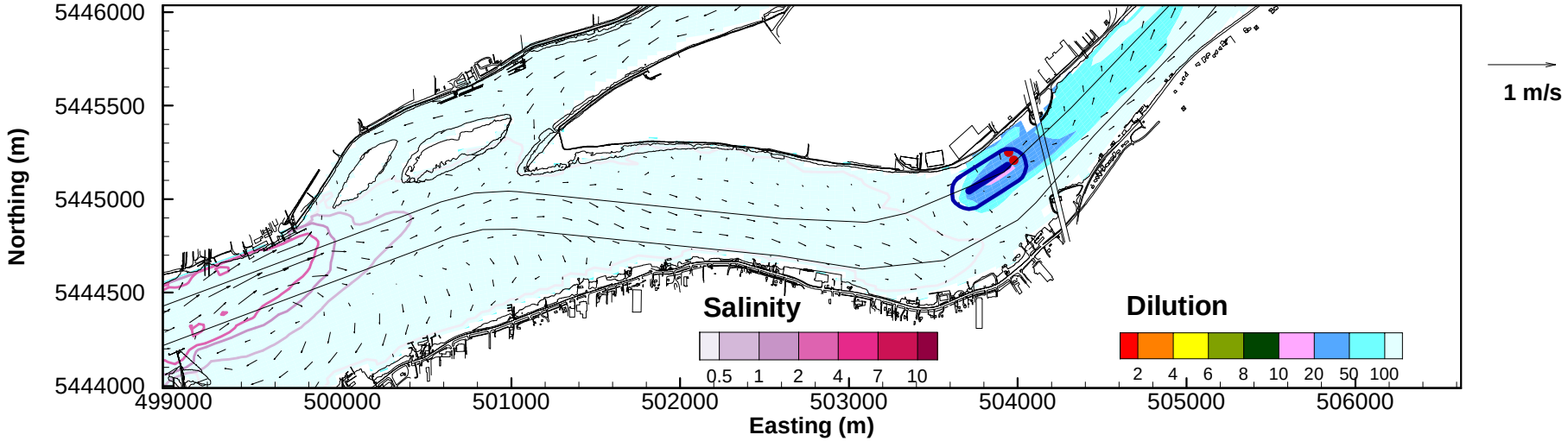


2013 11 07 1100

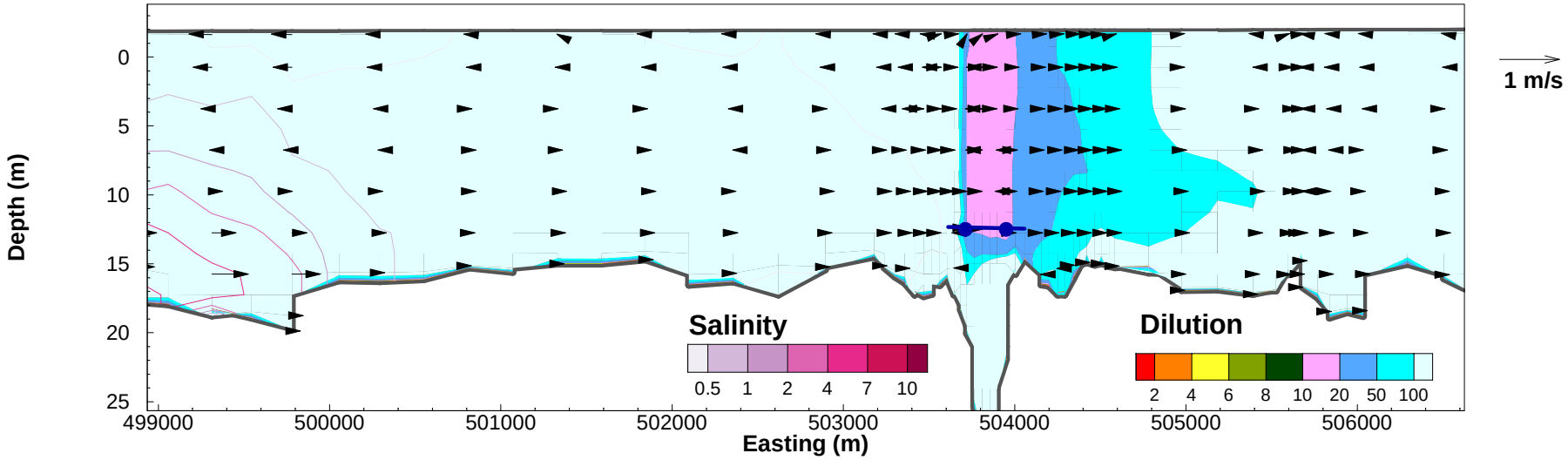


**NOTES**

**Original Run: 02_2013_Nov_Dec**

STATUS
ISSUED FOR USE

CLIENT

CDM Smith

TETRA TECH

**ANNACIS OUTFALL SIMULATION**

**Plan View Minimum Dilution**
**Section View Minimum Dilution**
**Annacis Effluent @14.7 $m^3/s$**

| PROJECT NO. | DWN | CKD | APVD | REV |
|---|---|---|---|---|
| WTRM03039 | AH | JAS | JAS | 0 |

OFFICE: Tetra Tech Canada - VAN
DATE: 18 Sept 2017

**Figure B-12**

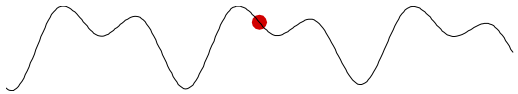

2013 11 07 1200

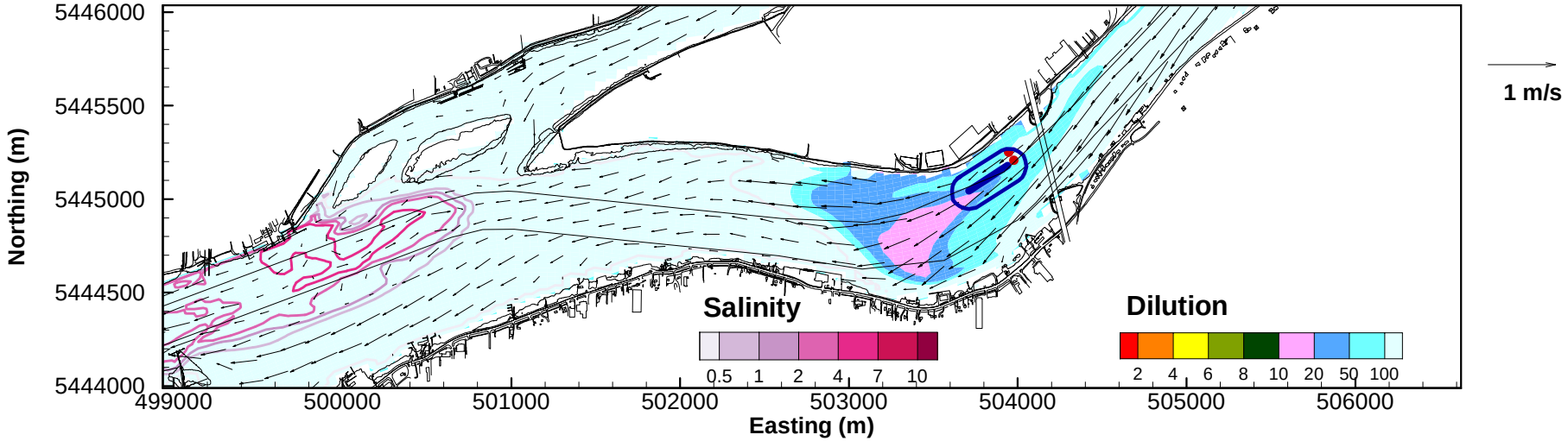


2013 11 07 1200

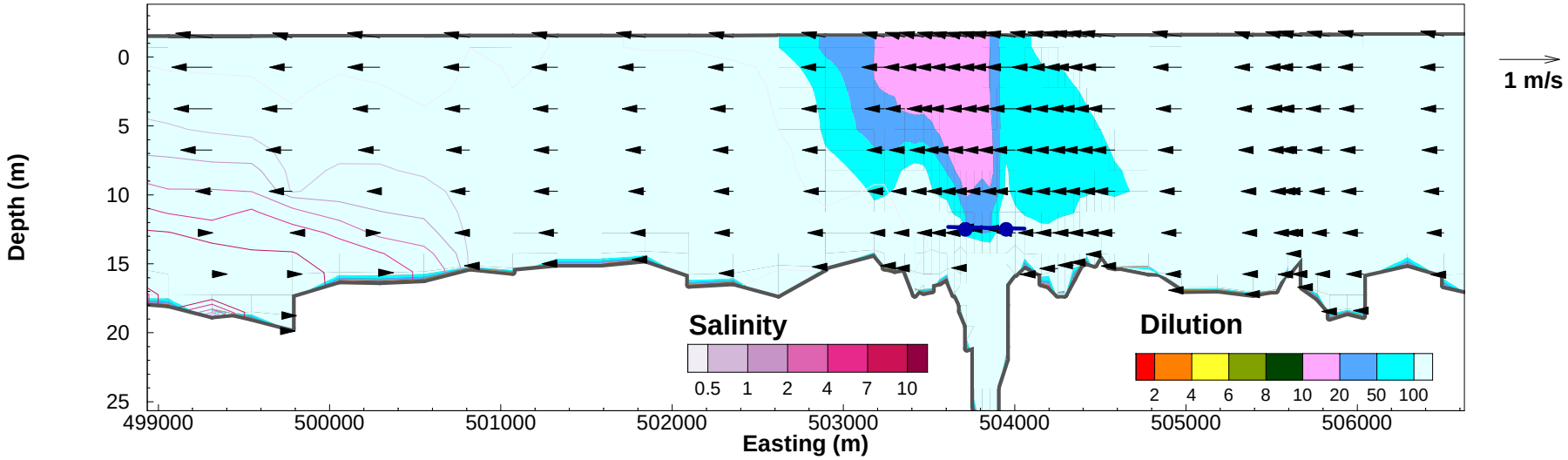


**NOTES**

**Original Run: 02_2013_Nov_Dec**

STATUS
ISSUED FOR USE

CLIENT

CDM Smith

TETRA TECH

**ANNACIS OUTFALL SIMULATION**

**Plan View Minimum Dilution**
**Section View Minimum Dilution**
**Annacis Effluent @14.7 $m^3/s$**

| PROJECT NO. | DWN | CKD | APVD | REV |
|---|---|---|---|---|
| WTRM03039 | AH | JAS | JAS | 0 |

OFFICE: Tetra Tech Canada - VAN
DATE: 18 Sept 2017

**Figure B-13**

**2013 11 07 1300**

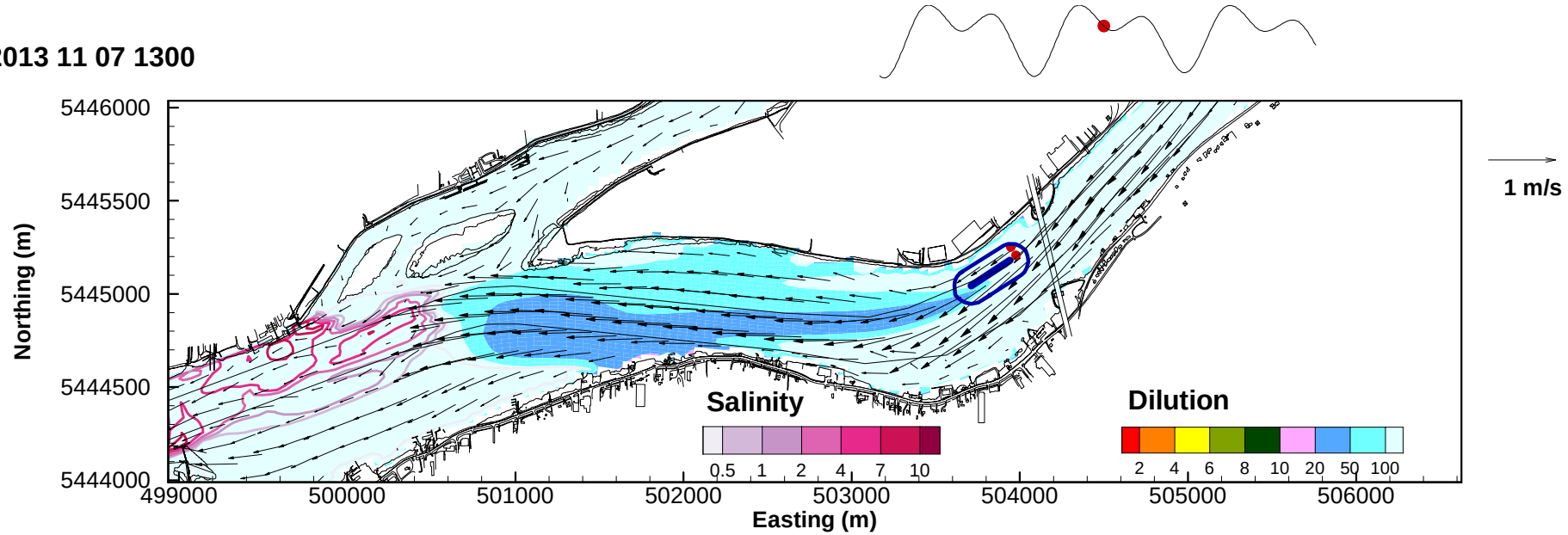


**2013 11 07 1300**

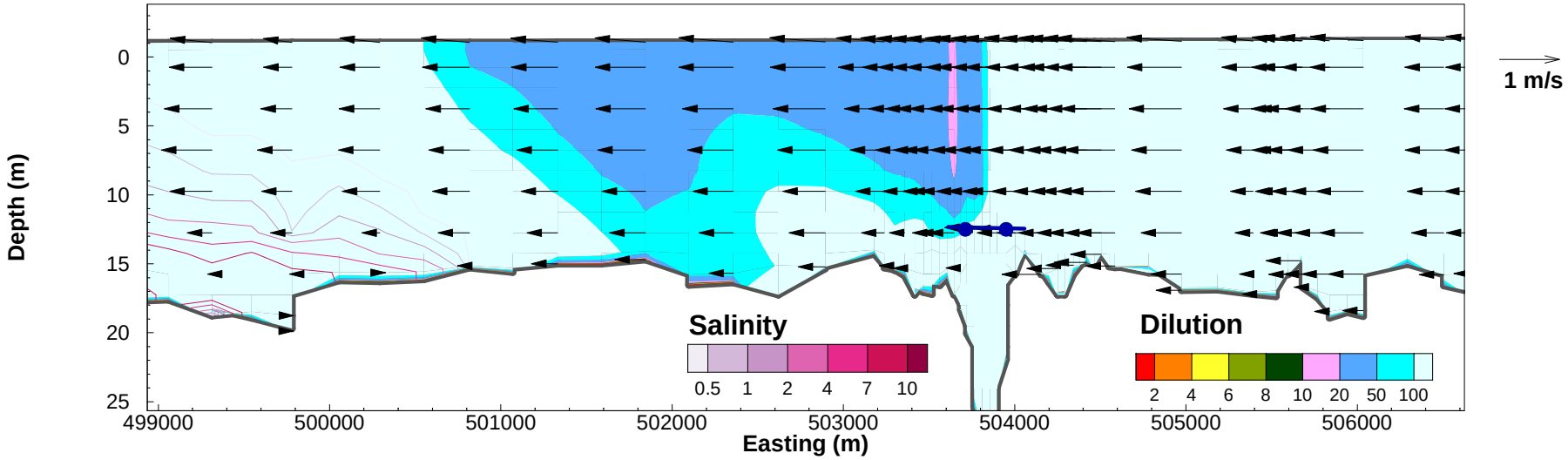


**NOTES**

**Original Run: 02_2013_Nov_Dec**

CLIENT

CDM Smith

TETRA TECH

STATUS
ISSUED FOR USE

**ANNACIS OUTFALL SIMULATION**

**Plan View Minimum Dilution**
**Section View Minimum Dilution**
**Annacis Effluent @14.7 $m^3/s$**

| PROJECT NO. | DWN | CKD | APVD | REV |
|---|---|---|---|---|
| WTRM03039 | AH | JAS | JAS | 0 |

| OFFICE | DATE |
|---|---|
| Tetra Tech Canada - VAN | 18 Sept 2017 |

**Figure B-14**

**2013 11 07 1400**

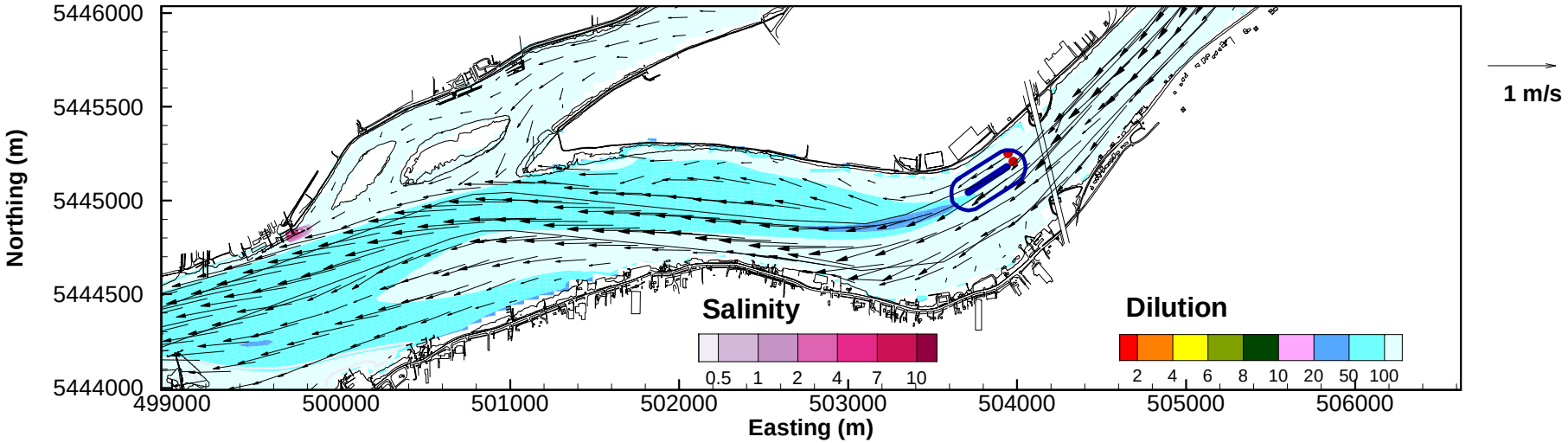


**2013 11 07 1400**

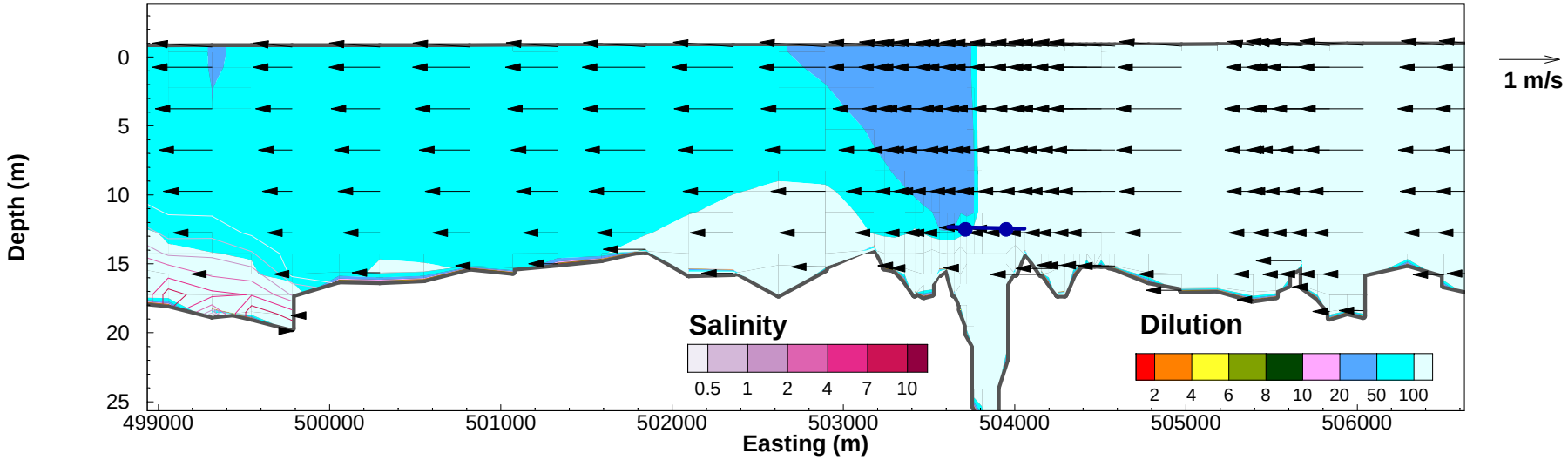


**NOTES**

**Original Run: 02_2013_Nov_Dec**

CLIENT

CDM Smith

TETRA TECH

STATUS
ISSUED FOR USE

**ANNACIS OUTFALL SIMULATION**

**Plan View Minimum Dilution**
**Section View Minimum Dilution**
**Annacis Effluent @14.7 $m^3/s$**

| PROJECT NO. | DWN | CKD | APVD | REV |
|---|---|---|---|---|
| WTRM03039 | AH | JAS | JAS | 0 |

| OFFICE | DATE |
|---|---|
| Tetra Tech Canada - VAN | 18 Sept 2017 |

**Figure B-15**

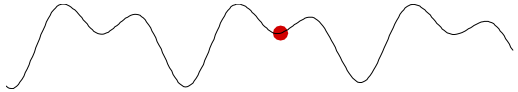

2013 11 07 1500

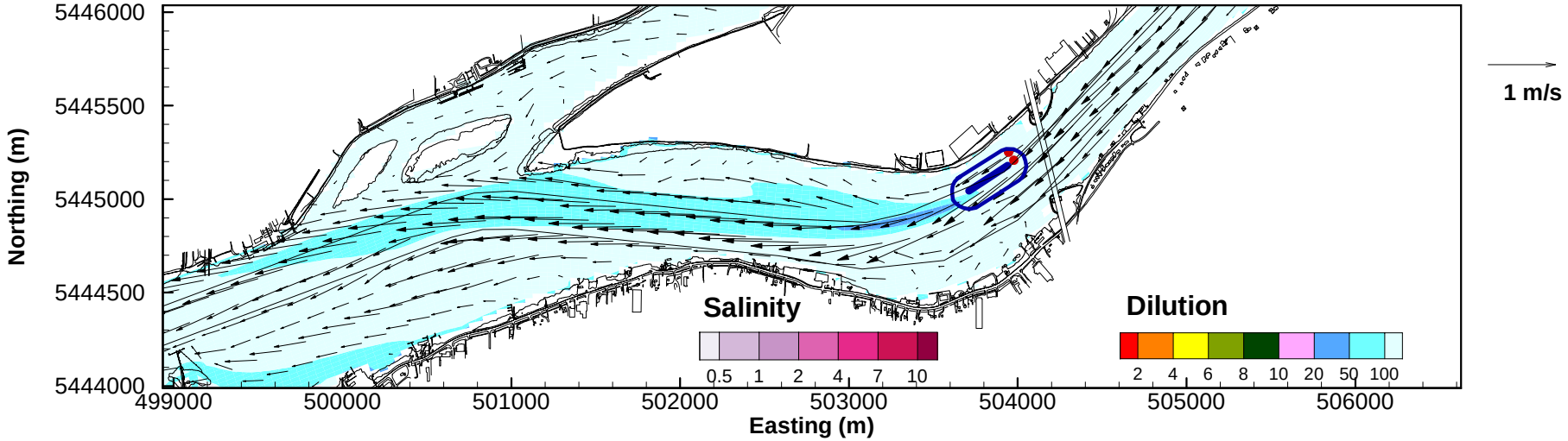


2013 11 07 1500

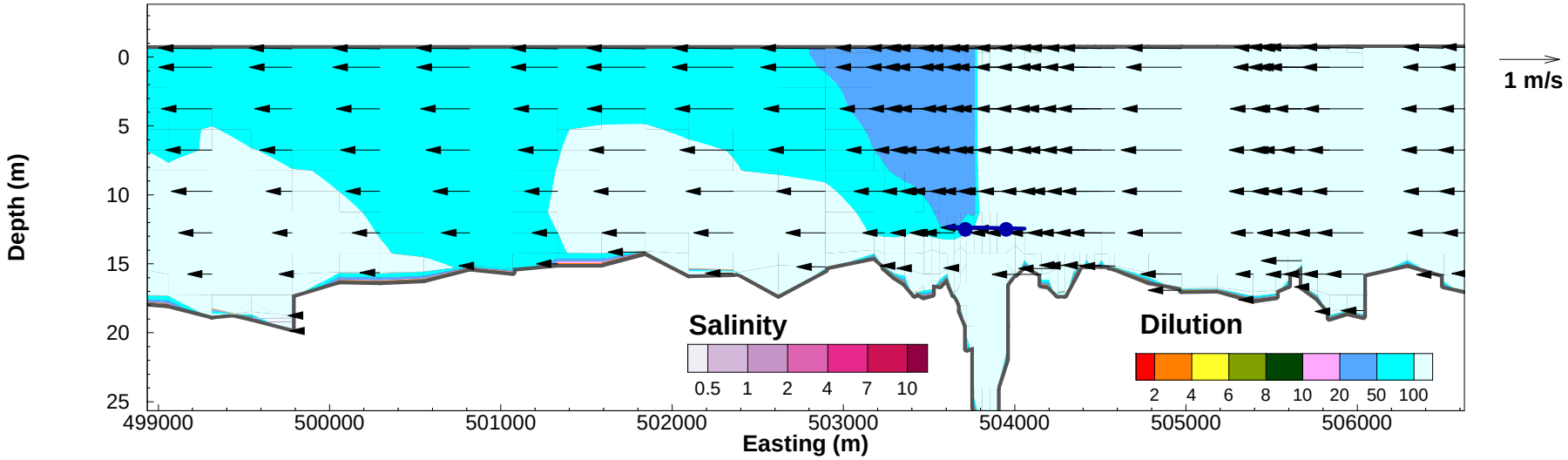


**NOTES**

**Original Run: 02_2013_Nov_Dec**

CLIENT

CDM Smith

TETRA TECH

STATUS
ISSUED FOR USE

**ANNACIS OUTFALL SIMULATION**

**Plan View Minimum Dilution**
**Section View Minimum Dilution**
**Annacis Effluent @14.7 $m^3/s$**

| PROJECT NO. | DWN | CKD | APVD | REV |
|---|---|---|---|---|
| WTRM03039 | AH | JAS | JAS | 0 |

| OFFICE | DATE |
|---|---|
| Tetra Tech Canada - VAN | 18 Sept 2017 |

**Figure B-16**

**2013 11 07 1600**

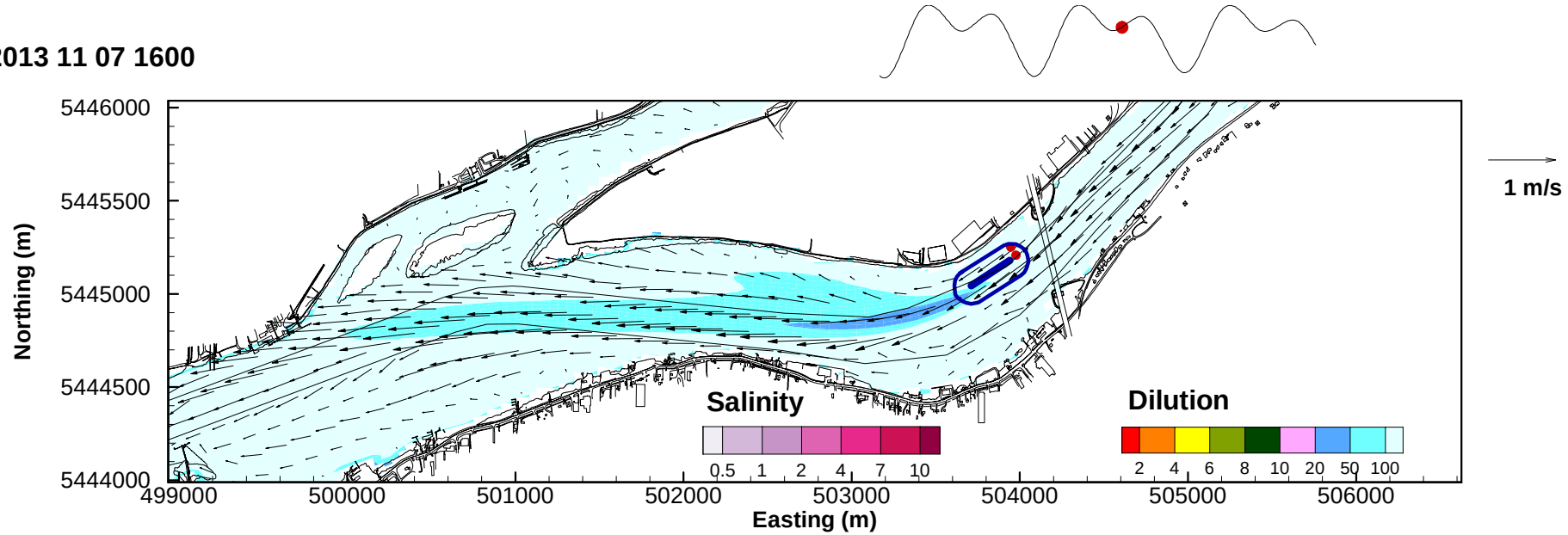


**2013 11 07 1600**

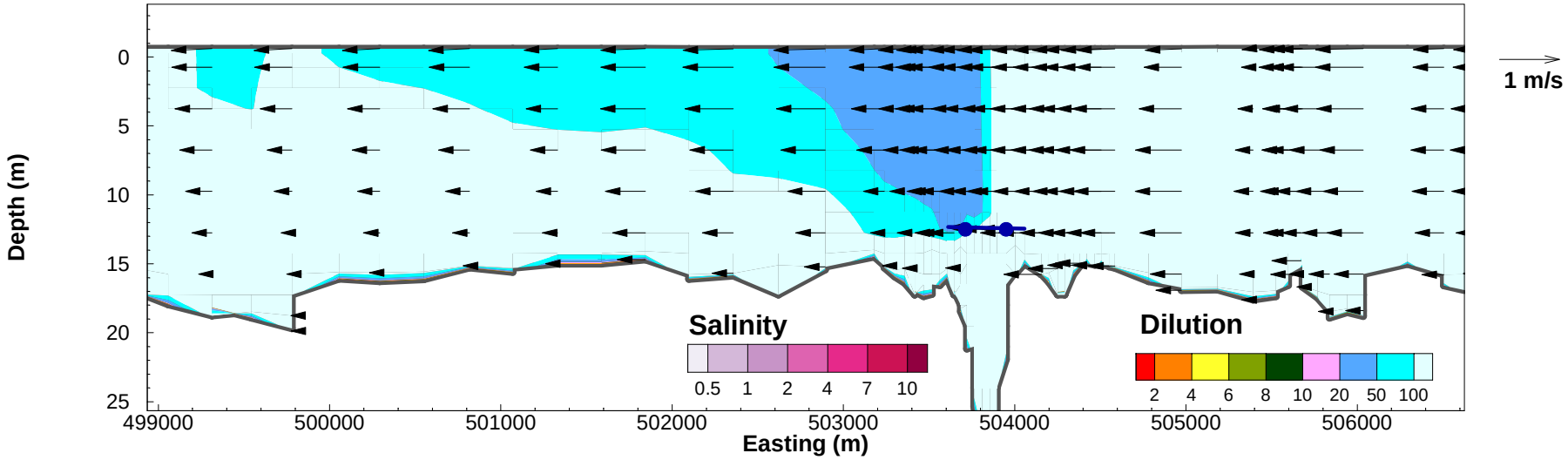


**NOTES**

**Original Run: 02_2013_Nov_Dec**

CLIENT

CDM Smith

TETRA TECH

STATUS
ISSUED FOR USE

**ANNACIS OUTFALL SIMULATION**

**Plan View Minimum Dilution**
**Section View Minimum Dilution**
**Annacis Effluent @14.7 $m^3/s$**

| PROJECT NO. | DWN | CKD | APVD | REV |
|---|---|---|---|---|
| WTRM03039 | AH | JAS | JAS | 0 |

OFFICE: Tetra Tech Canada - VAN
DATE: 18 Sept 2017

**Figure B-17**

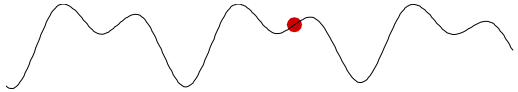

**2013 11 07 1700**

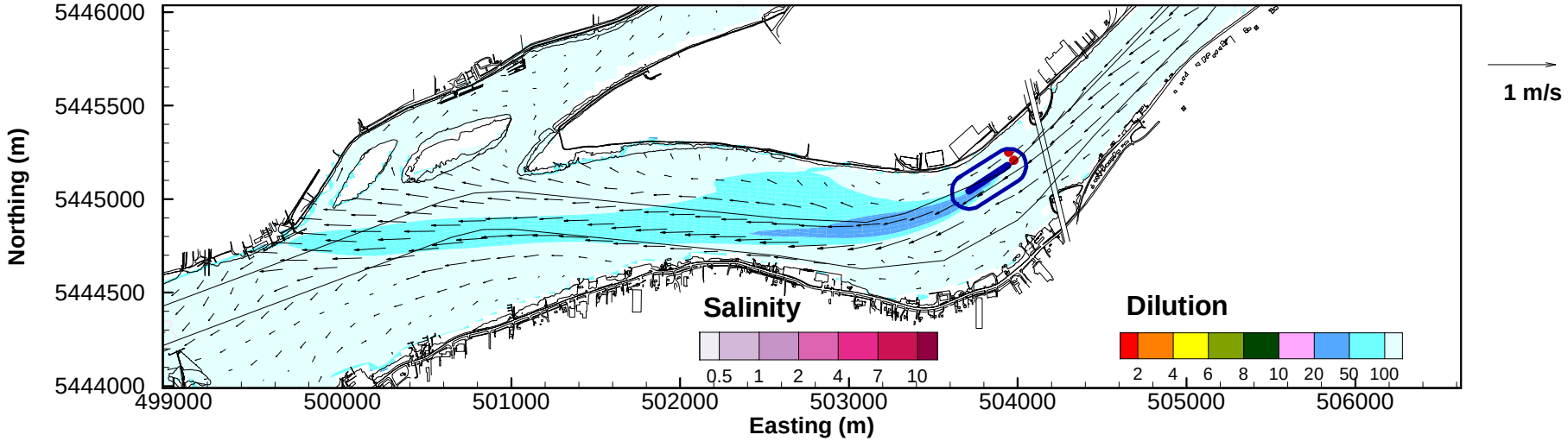


**2013 11 07 1700**

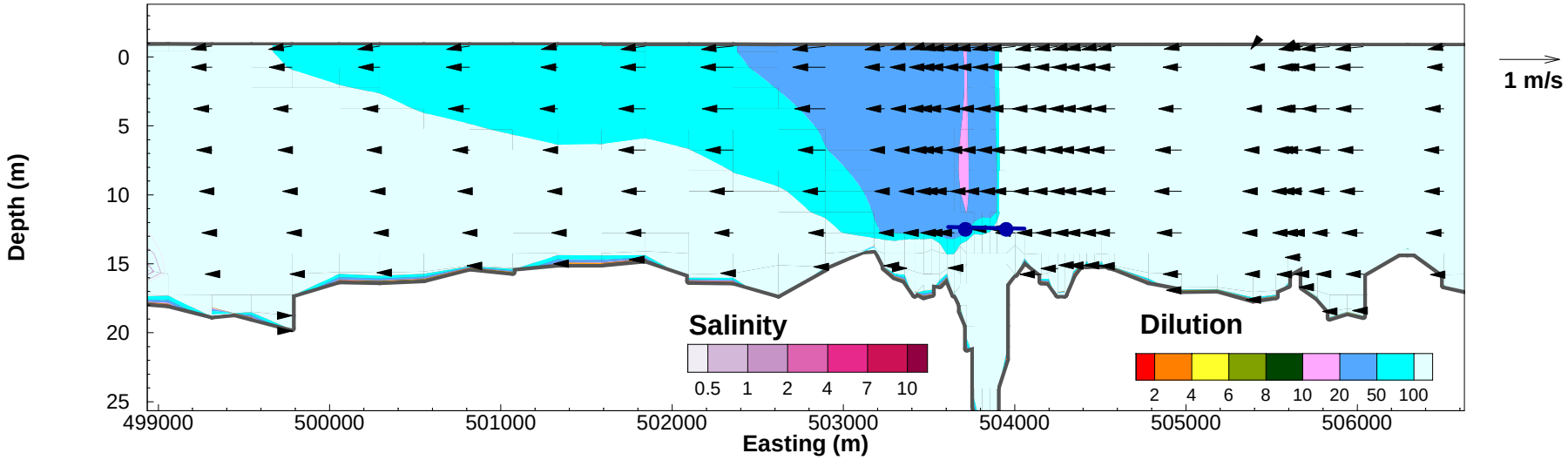


**NOTES**

**Original Run: 02_2013_Nov_Dec**

CLIENT

CDM Smith

TETRA TECH

STATUS
ISSUED FOR USE

**ANNACIS OUTFALL SIMULATION**

**Plan View Minimum Dilution**
**Section View Minimum Dilution**
**Annacis Effluent @14.7 $m^3/s$**

| PROJECT NO. | DWN | CKD | APVD | REV |
|---|---|---|---|---|
| WTRM03039 | AH | JAS | JAS | 0 |

| OFFICE | DATE |
|---|---|
| Tetra Tech Canada - VAN | 18 Sept 2017 |

**Figure B-18**

**2013 11 07 1800**

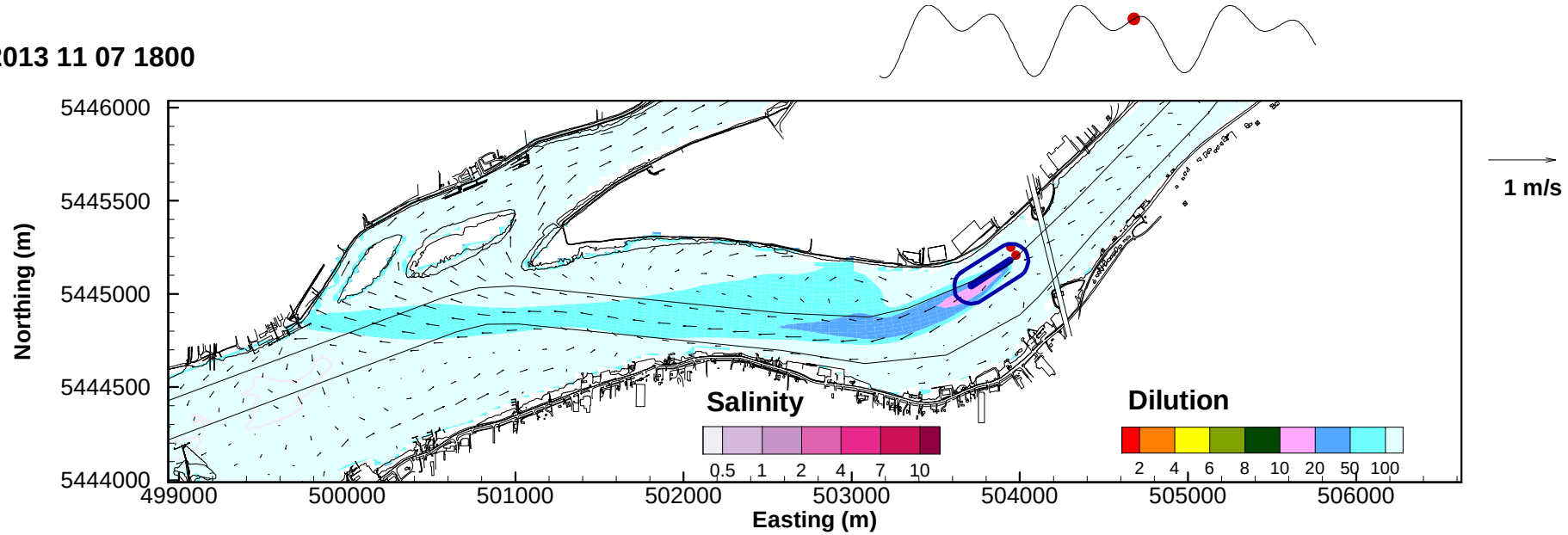


**2013 11 07 1800**

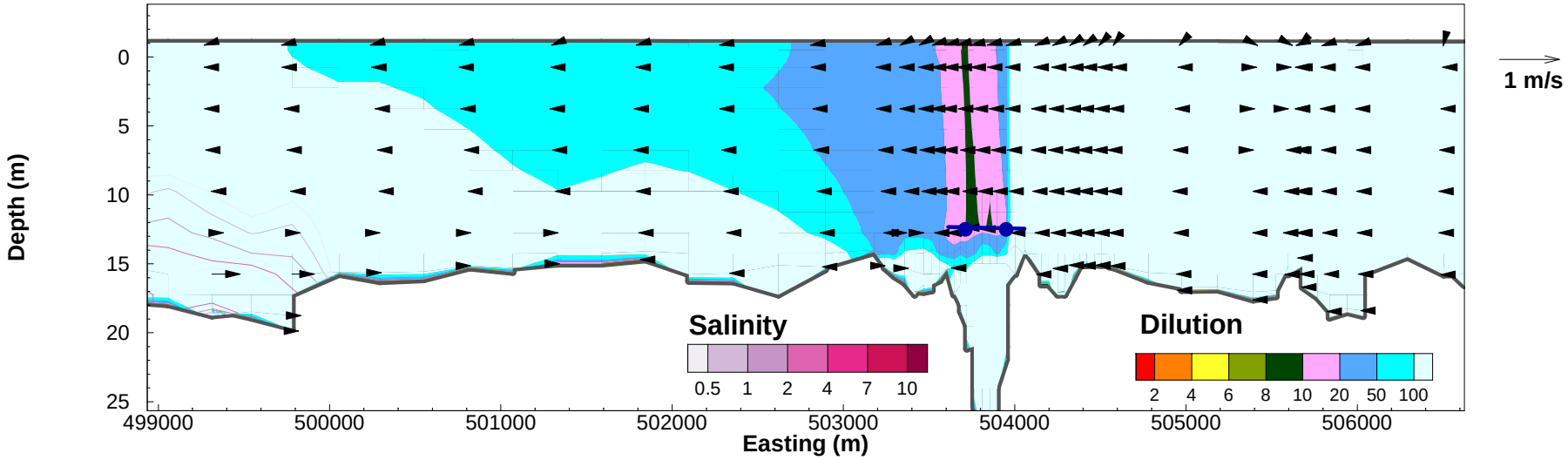


**NOTES**

**Original Run: 02_2013_Nov_Dec**

STATUS
ISSUED FOR USE

CLIENT

CDM Smith

TETRA TECH

**ANNACIS OUTFALL SIMULATION**

**Plan View Minimum Dilution**
**Section View Minimum Dilution**
**Annacis Effluent @14.7 $m^3/s$**

| PROJECT NO. | DWN | CKD | APVD | REV |
|---|---|---|---|---|
| WTRM03039 | AH | JAS | JAS | 0 |

| OFFICE | DATE |
|---|---|
| Tetra Tech Canada - VAN | 18 Sept 2017 |

**Figure B-19**

**2013 11 07 1900**

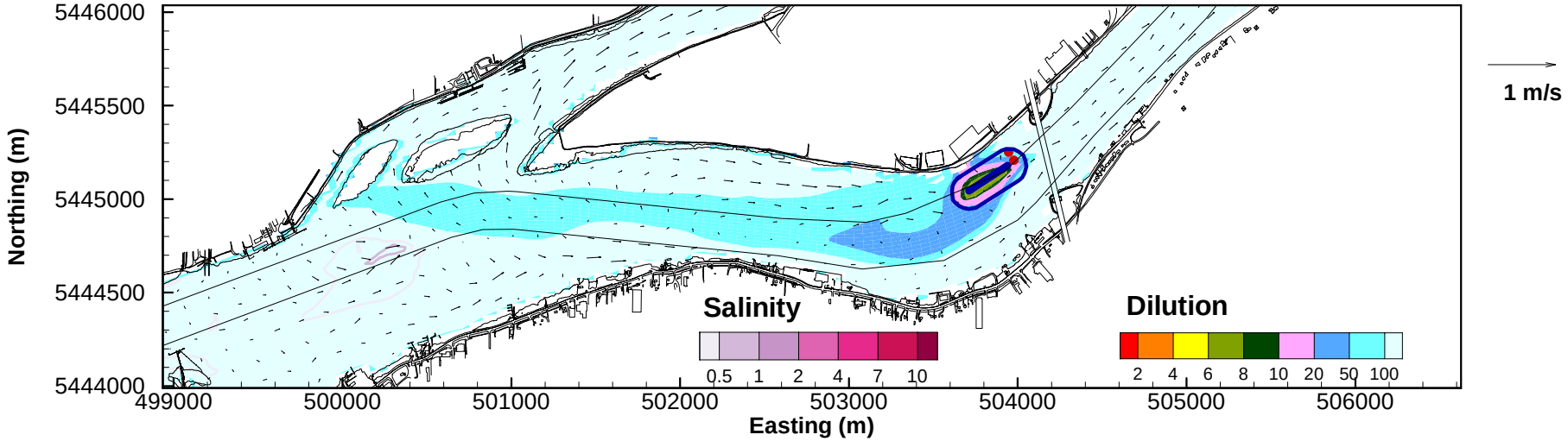


**2013 11 07 1900**

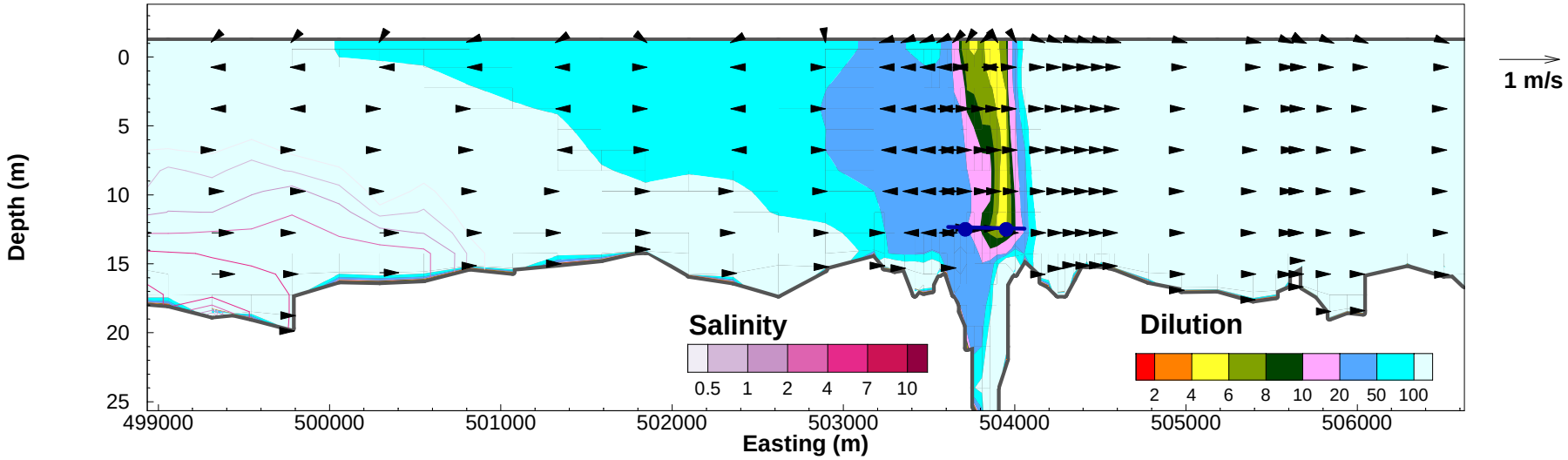


**NOTES**

**Original Run: 02_2013_Nov_Dec**

STATUS
ISSUED FOR USE

CLIENT

CDM Smith

TETRA TECH

**ANNACIS OUTFALL SIMULATION**

**Plan View Minimum Dilution**
**Section View Minimum Dilution**
**Annacis Effluent @14.7 $m^3/s$**

| PROJECT NO. | DWN | CKD | APVD | REV |
|---|---|---|---|---|
| WTRM03039 | AH | JAS | JAS | 0 |

OFFICE: Tetra Tech Canada - VAN
DATE: 18 Sept 2017

**Figure B-20**

2013 11 07 2000

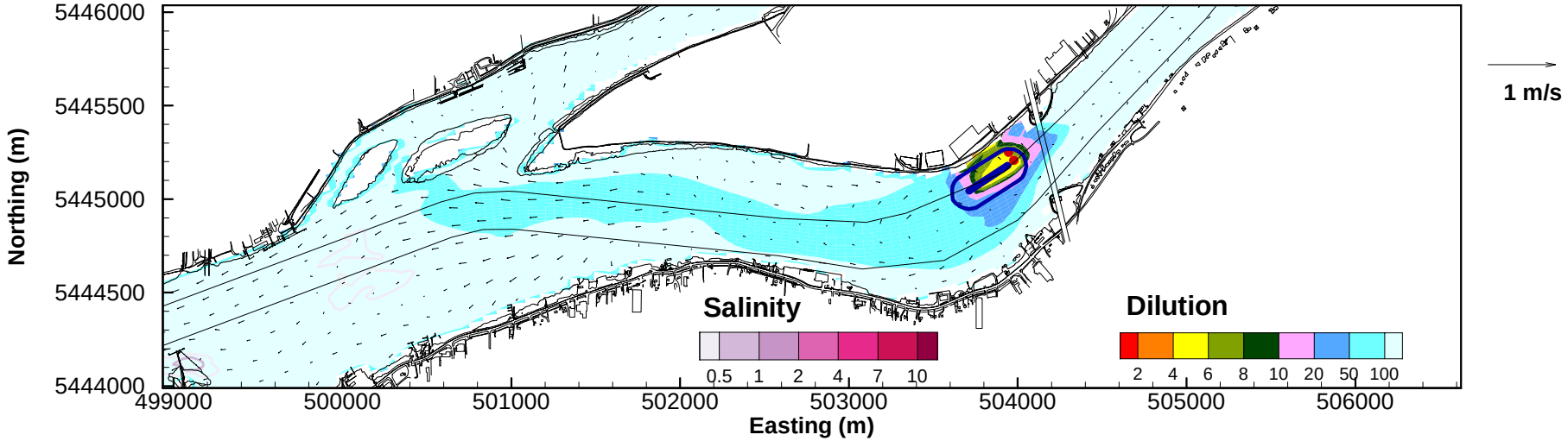


2013 11 07 2000

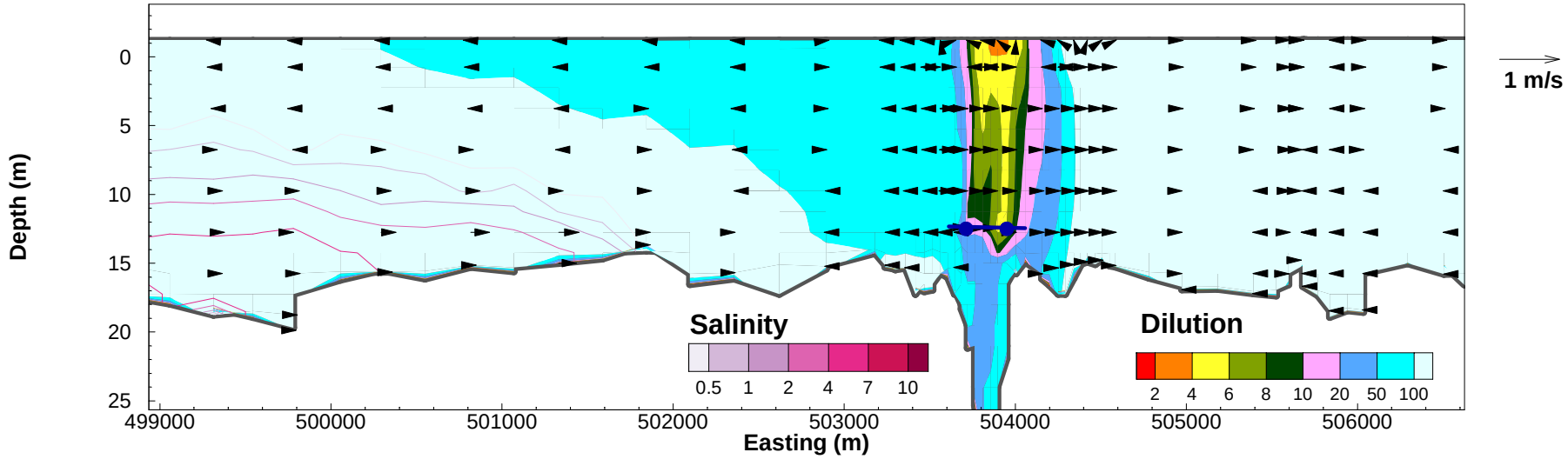


**NOTES**

**Original Run: 02_2013_Nov_Dec**

STATUS
ISSUED FOR USE

CLIENT

CDM Smith

TETRA TECH

**ANNACIS OUTFALL SIMULATION**

**Plan View Minimum Dilution**
**Section View Minimum Dilution**
**Annacis Effluent @14.7 $m^3/s$**

| PROJECT NO. | DWN | CKD | APVD | REV |
|---|---|---|---|---|
| WTRM03039 | AH | JAS | JAS | 0 |

| OFFICE | DATE |
|---|---|
| Tetra Tech Canada - VAN | 18 Sept 2017 |

**Figure B-21**

**2013 11 07 2100**

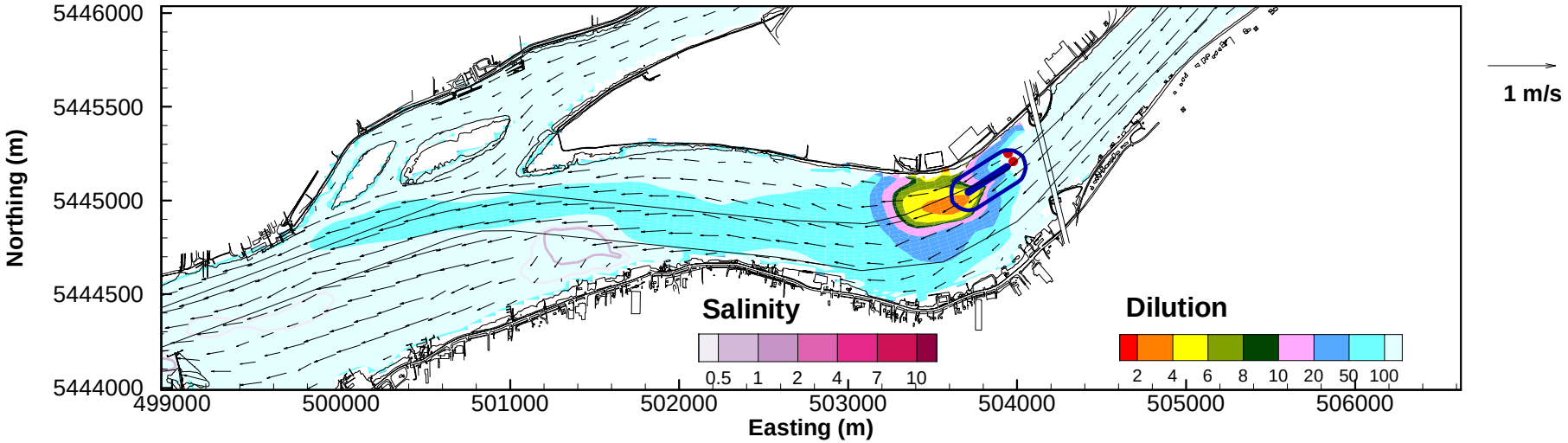


**2013 11 07 2100**

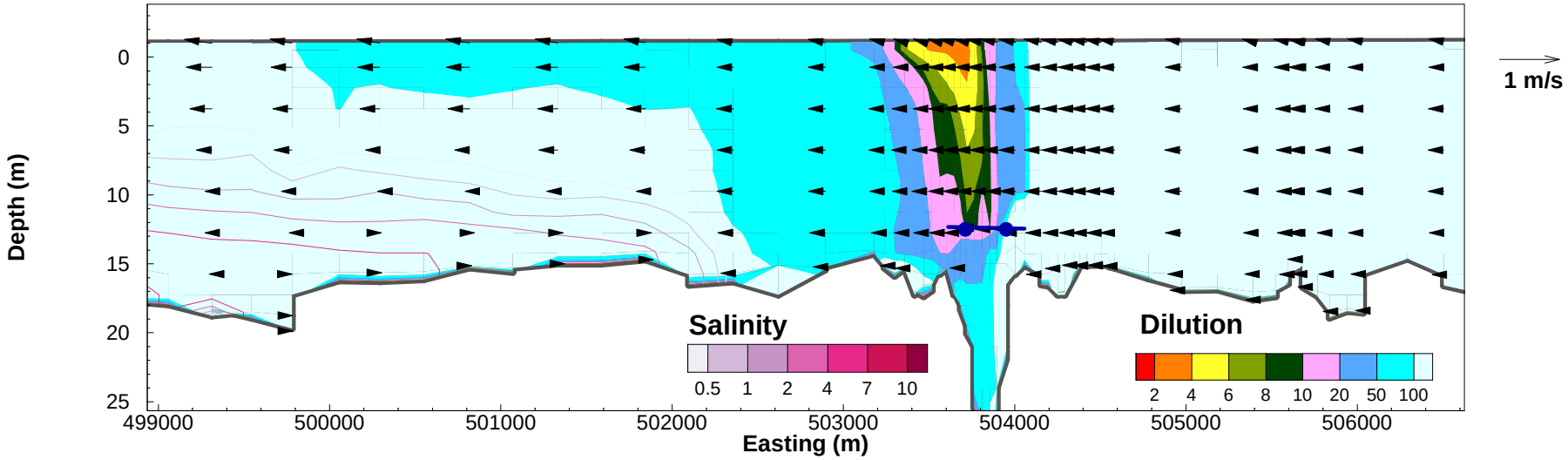


**NOTES**

**Original Run: 02_2013_Nov_Dec**

CLIENT

CDM Smith

TETRA TECH

STATUS
ISSUED FOR USE

**ANNACIS OUTFALL SIMULATION**

**Plan View Minimum Dilution**
**Section View Minimum Dilution**
**Annacis Effluent @14.7 $m^3/s$**

| PROJECT NO. | DWN | CKD | APVD | REV |
|---|---|---|---|---|
| WTRM03039 | AH | JAS | JAS | 0 |

OFFICE: Tetra Tech Canada - VAN
DATE: 18 Sept 2017

**Figure B-22**

**2013 11 07 2200**

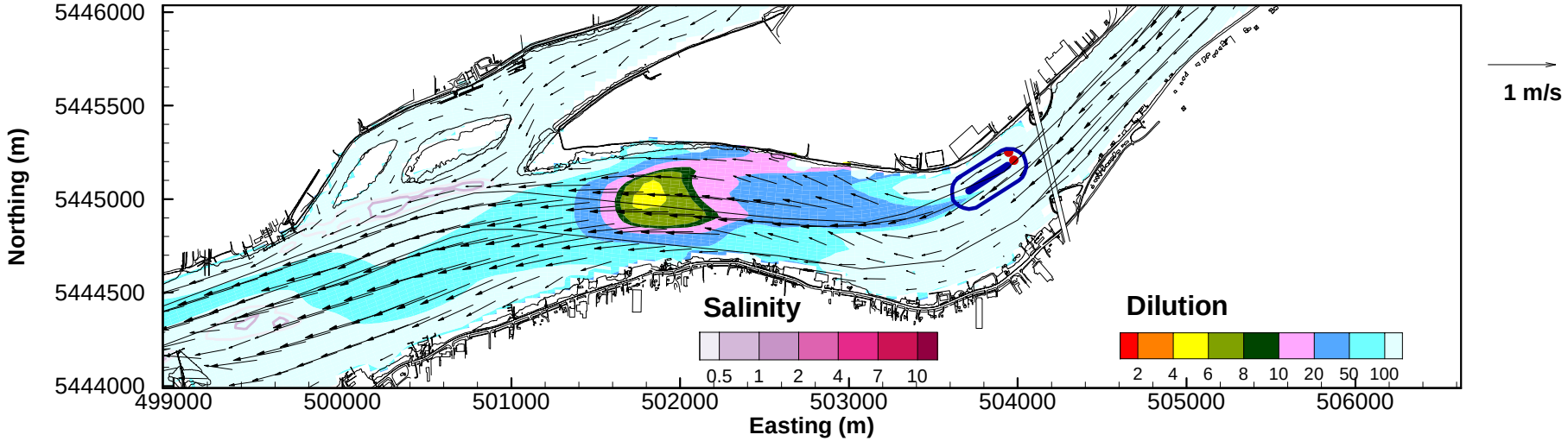


**2013 11 07 2200**

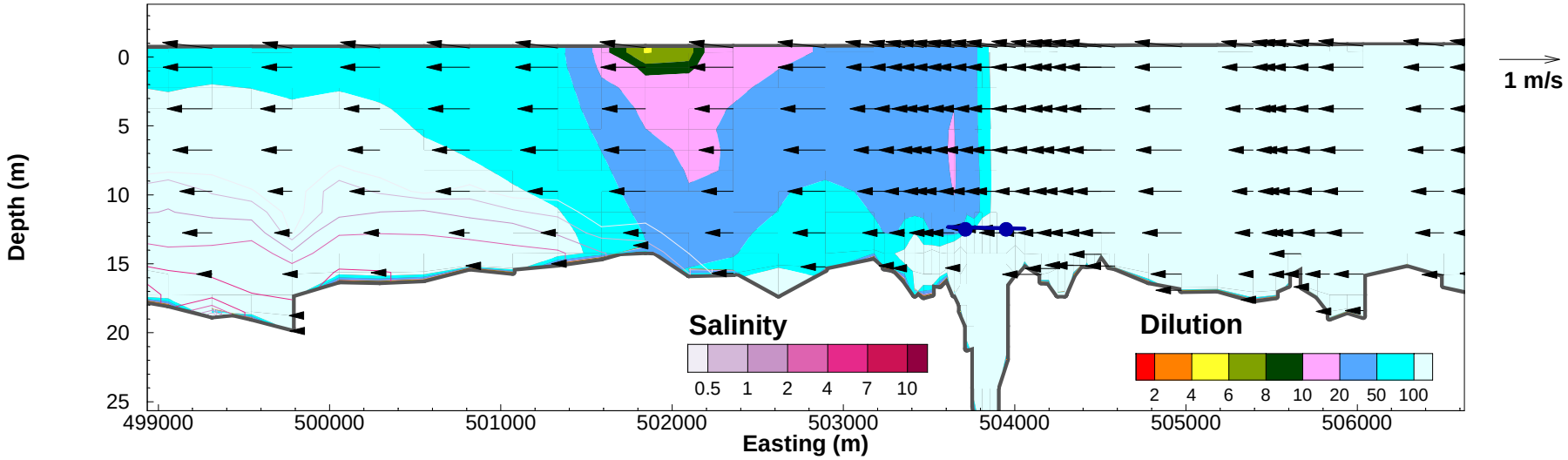


**NOTES**

**Original Run: 02_2013_Nov_Dec**

CLIENT

CDM Smith

TETRA TECH

STATUS
ISSUED FOR USE

**ANNACIS OUTFALL SIMULATION**

**Plan View Minimum Dilution**
**Section View Minimum Dilution**
**Annacis Effluent @14.7 $m^3/s$**

| PROJECT NO. | DWN | CKD | APVD | REV |
|---|---|---|---|---|
| WTRM03039 | AH | JAS | JAS | 0 |

| OFFICE | DATE |
|---|---|
| Tetra Tech Canada - VAN | 18 Sept 2017 |

**Figure B-23**

**2013 11 07 2300**

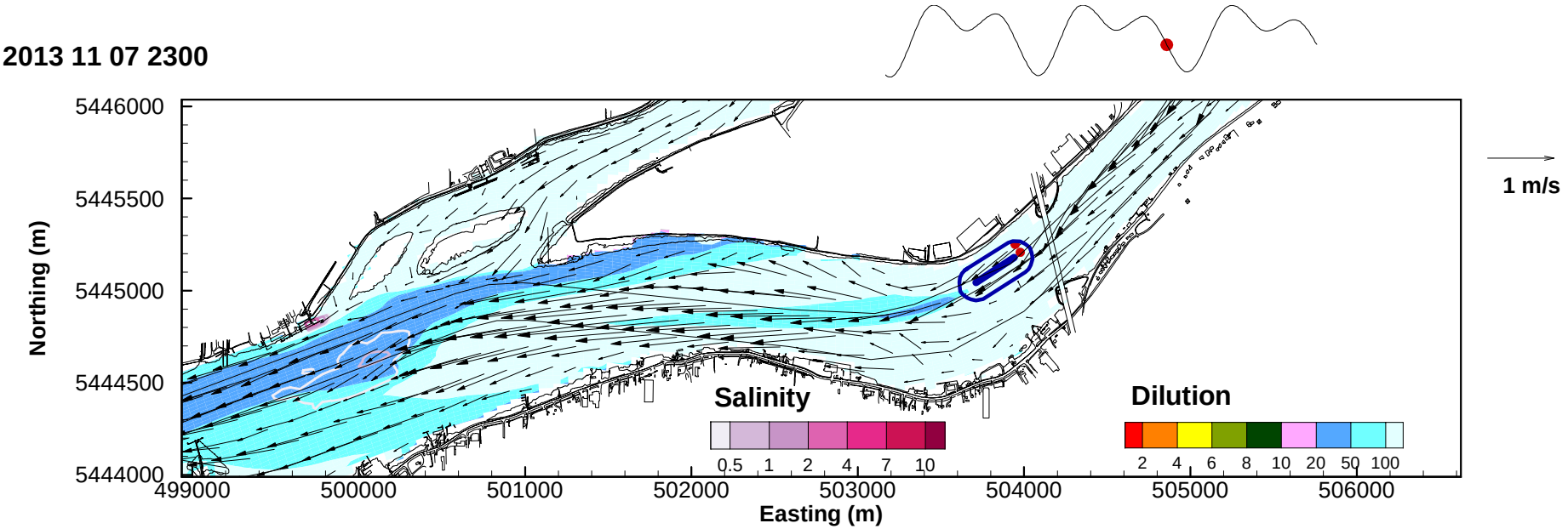


**2013 11 07 2300**

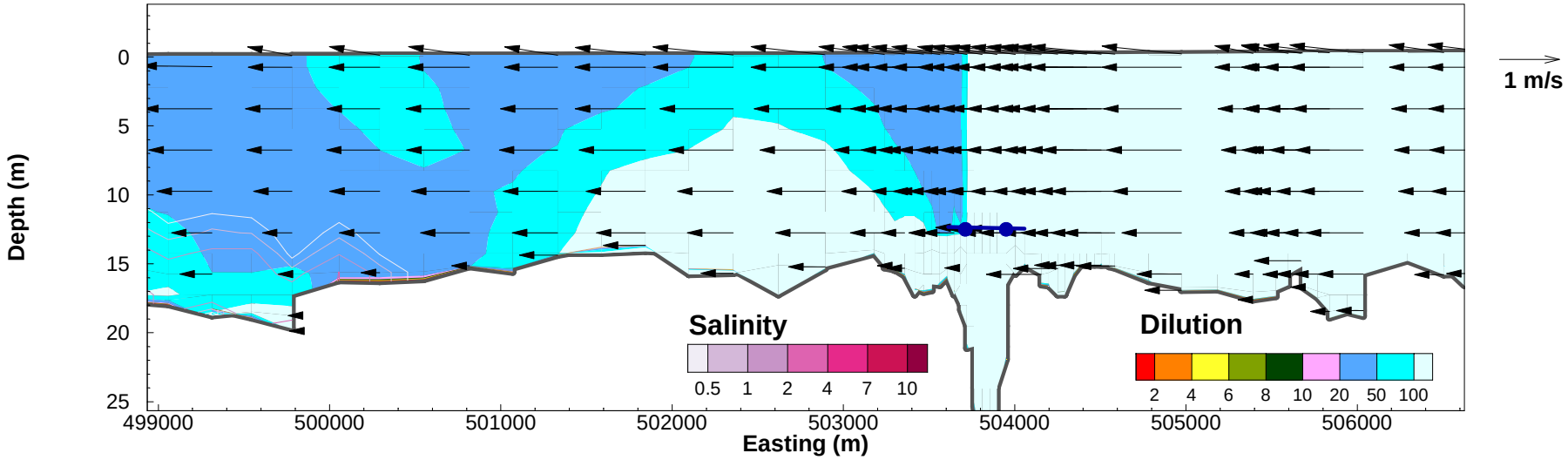


**NOTES**

**Original Run: 02_2013_Nov_Dec**

STATUS
ISSUED FOR USE

CLIENT

CDM Smith

TETRA TECH

**ANNACIS OUTFALL SIMULATION**

**Plan View Minimum Dilution**
**Section View Minimum Dilution**
**Annacis Effluent @14.7 $m^3/s$**

| PROJECT NO. | DWN | CKD | APVD | REV |
|---|---|---|---|---|
| WTRM03039 | AH | JAS | JAS | 0 |

| OFFICE | DATE |
|---|---|
| Tetra Tech Canada - VAN | 18 Sept 2017 |

**Figure B-24**

# APPENDIX C

## TETRA TECH'S LIMITATIONS ON THE USE OF THIS DOCUMENT

# LIMITATIONS ON USE OF THIS DOCUMENT

## HYDROTECHNICAL

### 1.1 USE OF DOCUMENT AND OWNERSHIP

This document pertains to a specific site, a specific development, and a specific scope of work. The document may include plans, drawings, profiles and other supporting documents that collectively constitute the document (the "Professional Document").

The Professional Document is intended for the sole use of TETRA TECH's Client (the "Client") as specifically identified in the TETRA TECH Services Agreement or other Contractual Agreement entered into with the Client (either of which is termed the "Contract" herein). TETRA TECH does not accept any responsibility for the accuracy of any of the data, analyses, recommendations or other contents of the Professional Document when it is used or relied upon by any party other than the Client, unless authorized in writing by TETRA TECH.

Any unauthorized use of the Professional Document is at the sole risk of the user. TETRA TECH accepts no responsibility whatsoever for any loss or damage where such loss or damage is alleged to be or, is in fact, caused by the unauthorized use of the Professional Document.

Where TETRA TECH has expressly authorized the use of the Professional Document by a third party (an "Authorized Party"), consideration for such authorization is the Authorized Party's acceptance of these Limitations on Use of this Document as well as any limitations on liability contained in the Contract with the Client (all of which is collectively termed the "Limitations on Liability"). The Authorized Party should carefully review both these Limitations on Use of this Document and the Contract prior to making any use of the Professional Document. Any use made of the Professional Document by an Authorized Party constitutes the Authorized Party's express acceptance of, and agreement to, the Limitations on Liability.

The Professional Document and any other form or type of data or documents generated by TETRA TECH during the performance of the work are TETRA TECH's professional work product and shall remain the copyright property of TETRA TECH.

The Professional Document is subject to copyright and shall not be reproduced either wholly or in part without the prior, written permission of TETRA TECH. Additional copies of the Document, if required, may be obtained upon request.

### 1.2 ALTERNATIVE DOCUMENT FORMAT

Where TETRA TECH submits electronic file and/or hard copy versions of the Professional Document or any drawings or other project-related documents and deliverables (collectively termed TETRA TECH's "Instruments of Professional Service"), only the signed and/or sealed versions shall be considered final. The original signed and/or sealed electronic file and/or hard copy version archived by TETRA TECH shall be deemed to be the original. TETRA TECH will archive a protected digital copy of the original signed and/or sealed version for a period of 10 years.

Both electronic file and/or hard copy versions of TETRA TECH's Instruments of Professional Service shall not, under any circumstances, be altered by any party except TETRA TECH. TETRA TECH's Instruments of Professional Service will be used only and exactly as submitted by TETRA TECH.

Electronic files submitted by TETRA TECH have been prepared and submitted using specific software and hardware systems. TETRA TECH makes no representation about the compatibility of these files with the Client's current or future software and hardware systems.

### 1.3 STANDARD OF CARE

Services performed by TETRA TECH for the Professional Document have been conducted in accordance with the Contract, in a manner consistent with the level of skill ordinarily exercised by members of the profession currently practicing under similar conditions in the jurisdiction in which the services are provided. Professional judgment has been applied in developing the conclusions and/or recommendations provided in this Professional Document. No warranty or guarantee, express or implied, is made concerning the test results, comments, recommendations, or any other portion of the Professional Document.

If any error or omission is detected by the Client or an Authorized Party, the error or omission must be immediately brought to the attention of TETRA TECH.

### 1.4 DISCLOSURE OF INFORMATION BY CLIENT

The Client acknowledges that it has fully cooperated with TETRA TECH with respect to the provision of all available information on the past, present, and proposed conditions on the site, including historical information respecting the use of the site. The Client further acknowledges that in order for TETRA TECH to properly provide the services contracted for in the Contract, TETRA TECH has relied upon the Client with respect to both the full disclosure and accuracy of any such information.

### 1.5 INFORMATION PROVIDED TO TETRA TECH BY OTHERS

During the performance of the work and the preparation of this Professional Document, TETRA TECH may have relied on information provided by third parties other than the Client.

While TETRA TECH endeavours to verify the accuracy of such information, TETRA TECH accepts no responsibility for the accuracy or the reliability of such information even where inaccurate or unreliable information impacts any recommendations, design or other deliverables and causes the Client or an Authorized Party loss or damage.

### 1.6 GENERAL LIMITATIONS OF DOCUMENT

This Professional Document is based solely on the conditions presented and the data available to TETRA TECH at the time the data were collected in the field or gathered from available databases.

The Client, and any Authorized Party, acknowledges that the Professional Document is based on limited data and that the conclusions, opinions, and recommendations contained in the Professional Document are the result of the application of professional judgment to such limited data.

The Professional Document is not applicable to any other sites, nor should it be relied upon for types of development other than those to which it refers. Any variation from the site conditions present, or variation in assumed conditions which might form the basis of design or recommendations as outlined in this report, at or on the development proposed as of the date of the Professional Document requires a supplementary exploration, investigation, and assessment.

TETRA TECH is neither qualified to, nor is it making, any recommendations with respect to the purchase, sale, investment or development of the property, the decisions on which are the sole responsibility of the Client.

### 1.7 ENVIRONMENTAL AND REGULATORY ISSUES

Unless expressly agreed to in the Services Agreement, TETRA TECH was not retained to investigate, address or consider, and has not investigated, addressed or considered any environmental or regulatory issues associated with the project.

### 1.8 LEVEL OF RISK

It is incumbent upon the Client and any Authorized Party, to be knowledgeable of the level of risk that has been incorporated into the project design, in consideration of the level of the hydrotechnical information that was reasonably acquired to facilitate completion of the design.

This page intentionally left blank.

# Attachment H

# Summary of Model Inputs and Results

This page intentionally left blank.

| Flow Classification | Percent of Time Ambient Flow Occurs | Density Profile | Percent of Time Profile Occurs | Depth (m) | Percent of Time Depth Occurs | Effluent Flow ($m^3/s$) | Percent of Time Effluent Flow Occurs | Ambient Current Speed (m/s) | Percent of Time Current Speed Occurs | Flux-Averaged Initial Dilution | Probability of Occurrence |
|---|---|---|---|---|---|---|---|---|---|---|---|
| 1501<Q<2000 | 12.6% | SALINE | 3% | 14.5 | 50% | 14.75 | 100% | 0.07 | 9.8% | 12.79 | 0.02% |
| 801<Q<1500 | 29.8% | SALINE | 20% | 14.5 | 50% | 14.75 | 100% | 0.07 | 9.8% | 13.10 | 0.29% |
| Q<800 | 9.8% | SALINE | 39% | 14.5 | 50% | 14.75 | 100% | 0.07 | 9.8% | 13.10 | 0.19% |
| Q<800 | 9.8% | SALINE | 39% | 14.5 | 50% | 14.75 | 100% | 0.37 | 41.4% | 13.60 | 0.79% |
| Q<800 | 9.8% | SALINE | 39% | 10.9 | 50% | 14.75 | 100% | 0.07 | 9.8% | 14.87 | 0.19% |
| 801<Q<1500 | 29.8% | SALINE | 20% | 14.5 | 50% | 14.75 | 100% | 0.37 | 41.4% | 16.10 | 1.21% |
| 1501<Q<2000 | 12.6% | SALINE | 3% | 14.5 | 50% | 14.75 | 100% | 0.37 | 41.4% | 17.20 | 0.07% |
| Q<800 | 9.8% | SALINE | 39% | 14.5 | 50% | 14.75 | 100% | 0.90 | 40.5% | 17.40 | 0.77% |
| 801<Q<1500 | 29.8% | SALINE | 20% | 14.5 | 50% | 14.75 | 100% | 0.90 | 40.5% | 17.70 | 1.18% |
| 1501<Q<2000 | 12.6% | SALINE | 3% | 14.5 | 50% | 14.75 | 100% | 0.90 | 40.5% | 18.30 | 0.07% |
| 801<Q<1500 | 29.8% | SALINE | 20% | 14.5 | 50% | 14.75 | 100% | 1.30 | 8.3% | 18.60 | 0.24% |
| Q<800 | 9.8% | SALINE | 39% | 14.5 | 50% | 14.75 | 100% | 1.30 | 8.3% | 18.70 | 0.16% |
| Q<800 | 9.8% | SALINE | 39% | 10.9 | 50% | 14.75 | 100% | 0.37 | 41.4% | 18.90 | 0.79% |
| 1501<Q<2000 | 12.6% | SALINE | 3% | 14.5 | 50% | 14.75 | 100% | 1.30 | 8.3% | 19.10 | 0.01% |
| Q<800 | 9.8% | SALINE | 39% | 10.9 | 50% | 14.75 | 100% | 0.90 | 40.5% | 20.10 | 0.77% |
| Q<800 | 9.8% | SALINE | 39% | 10.9 | 50% | 14.75 | 100% | 1.30 | 8.3% | 20.70 | 0.16% |
| 1501<Q<2000 | 12.6% | FRESH | 97% | 10.9 | 50% | 14.75 | 100% | 0.07 | 9.8% | 26.16 | 0.60% |
| 1501<Q<2000 | 12.6% | FRESH | 3% | 10.9 | 50% | 14.75 | 100% | 0.07 | 9.8% | 26.16 | 0.02% |
| 2001<Q<6000 | 37.1% | FRESH | 100% | 10.9 | 50% | 14.75 | 100% | 0.07 | 9.8% | 26.16 | 1.82% |
| 801<Q<1500 | 29.8% | FRESH | 80% | 10.9 | 50% | 14.75 | 100% | 0.07 | 9.8% | 26.16 | 1.18% |
| 801<Q<1500 | 29.8% | FRESH | 20% | 10.9 | 50% | 14.75 | 100% | 0.07 | 9.8% | 26.16 | 0.29% |
| Q<800 | 9.8% | FRESH | 61% | 10.9 | 50% | 14.75 | 100% | 0.07 | 9.8% | 26.16 | 0.29% |
| 1501<Q<2000 | 12.6% | FRESH | 97% | 10.9 | 50% | 14.75 | 100% | 0.37 | 41.4% | 26.59 | 2.53% |
| 1501<Q<2000 | 12.6% | FRESH | 3% | 10.9 | 50% | 14.75 | 100% | 0.37 | 41.4% | 26.59 | 0.07% |
| 2001<Q<6000 | 37.1% | FRESH | 100% | 10.9 | 50% | 14.75 | 100% | 0.37 | 41.4% | 26.59 | 7.67% |
| 801<Q<1500 | 29.8% | FRESH | 80% | 10.9 | 50% | 14.75 | 100% | 0.37 | 41.4% | 26.59 | 4.96% |
| 801<Q<1500 | 29.8% | FRESH | 20% | 10.9 | 50% | 14.75 | 100% | 0.37 | 41.4% | 26.59 | 1.21% |
| Q<800 | 9.8% | FRESH | 61% | 10.9 | 50% | 14.75 | 100% | 0.37 | 41.4% | 26.59 | 1.24% |
| Q>6001 | 10.7% | FRESH | 100% | 11.65 | 50% | 14.75 | 100% | 0.36 | 0.2% | 27.85 | 0.01% |
| 1501<Q<2000 | 12.6% | FRESH | 97% | 14.5 | 50% | 14.75 | 100% | 0.07 | 9.8% | 31.13 | 0.60% |
| 2001<Q<6000 | 37.1% | FRESH | 100% | 14.5 | 50% | 14.75 | 100% | 0.07 | 9.8% | 31.13 | 1.82% |
| 801<Q<1500 | 29.8% | FRESH | 80% | 14.5 | 50% | 14.75 | 100% | 0.07 | 9.8% | 31.13 | 1.18% |
| Q<800 | 9.8% | FRESH | 61% | 14.5 | 50% | 14.75 | 100% | 0.07 | 9.8% | 31.13 | 0.29% |
| 1501<Q<2000 | 12.6% | FRESH | 97% | 10.9 | 50% | 14.75 | 100% | 0.90 | 40.5% | 31.37 | 2.48% |
| 1501<Q<2000 | 12.6% | FRESH | 3% | 10.9 | 50% | 14.75 | 100% | 0.90 | 40.5% | 31.37 | 0.07% |
| 2001<Q<6000 | 37.1% | FRESH | 100% | 10.9 | 50% | 14.75 | 100% | 0.90 | 40.5% | 31.37 | 7.51% |
| 801<Q<1500 | 29.8% | FRESH | 80% | 10.9 | 50% | 14.75 | 100% | 0.90 | 40.5% | 31.37 | 4.86% |
| 801<Q<1500 | 29.8% | FRESH | 20% | 10.9 | 50% | 14.75 | 100% | 0.90 | 40.5% | 31.37 | 1.18% |
| Q<800 | 9.8% | FRESH | 61% | 10.9 | 50% | 14.75 | 100% | 0.90 | 40.5% | 31.37 | 1.21% |
| Q>6001 | 10.7% | FRESH | 100% | 14.5 | 50% | 14.75 | 100% | 0.36 | 0.2% | 32.83 | 0.01% |
| 1501<Q<2000 | 12.6% | FRESH | 97% | 14.5 | 50% | 14.75 | 100% | 0.37 | 41.4% | 32.98 | 2.53% |
| 2001<Q<6000 | 37.1% | FRESH | 100% | 14.5 | 50% | 14.75 | 100% | 0.37 | 41.4% | 32.98 | 7.67% |
| 801<Q<1500 | 29.8% | FRESH | 80% | 14.5 | 50% | 14.75 | 100% | 0.37 | 41.4% | 32.98 | 4.96% |
| Q<800 | 9.8% | FRESH | 61% | 14.5 | 50% | 14.75 | 100% | 0.37 | 41.4% | 32.98 | 1.24% |
| 1501<Q<2000 | 12.6% | FRESH | 97% | 10.9 | 50% | 14.75 | 100% | 1.30 | 8.3% | 33.39 | 0.51% |
| 1501<Q<2000 | 12.6% | FRESH | 3% | 10.9 | 50% | 14.75 | 100% | 1.30 | 8.3% | 33.39 | 0.01% |
| 2001<Q<6000 | 37.1% | FRESH | 100% | 10.9 | 50% | 14.75 | 100% | 1.30 | 8.3% | 33.39 | 1.54% |
| 801<Q<1500 | 29.8% | FRESH | 80% | 10.9 | 50% | 14.75 | 100% | 1.30 | 8.3% | 33.39 | 0.99% |
| 801<Q<1500 | 29.8% | FRESH | 20% | 10.9 | 50% | 14.75 | 100% | 1.30 | 8.3% | 33.39 | 0.24% |
| Q<800 | 9.8% | FRESH | 61% | 10.9 | 50% | 14.75 | 100% | 1.30 | 8.3% | 33.39 | 0.25% |
| Q>6001 | 10.7% | FRESH | 100% | 11.65 | 50% | 14.75 | 100% | 1.08 | 42.0% | 33.93 | 2.26% |
| Q>6001 | 10.7% | FRESH | 100% | 11.65 | 50% | 14.75 | 100% | 1.56 | 42.3% | 35.89 | 2.27% |
| Q>6001 | 10.7% | FRESH | 100% | 11.65 | 50% | 14.75 | 100% | 1.93 | 15.4% | 36.92 | 0.83% |
| 1501<Q<2000 | 12.6% | FRESH | 97% | 14.5 | 50% | 14.75 | 100% | 0.90 | 40.5% | 38.33 | 2.48% |
| 2001<Q<6000 | 37.1% | FRESH | 100% | 14.5 | 50% | 14.75 | 100% | 0.90 | 40.5% | 38.33 | 7.51% |
| 801<Q<1500 | 29.8% | FRESH | 80% | 14.5 | 50% | 14.75 | 100% | 0.90 | 40.5% | 38.33 | 4.86% |
| Q<800 | 9.8% | FRESH | 61% | 14.5 | 50% | 14.75 | 100% | 0.90 | 40.5% | 38.33 | 1.21% |
| Q>6001 | 10.7% | FRESH | 100% | 14.5 | 50% | 14.75 | 100% | 1.08 | 42.0% | 39.40 | 2.26% |
| 1501<Q<2000 | 12.6% | FRESH | 97% | 14.5 | 50% | 14.75 | 100% | 1.30 | 8.3% | 40.43 | 0.51% |
| 2001<Q<6000 | 37.1% | FRESH | 100% | 14.5 | 50% | 14.75 | 100% | 1.30 | 8.3% | 40.43 | 1.54% |
| 801<Q<1500 | 29.8% | FRESH | 80% | 14.5 | 50% | 14.75 | 100% | 1.30 | 8.3% | 40.43 | 0.99% |
| Q<800 | 9.8% | FRESH | 61% | 14.5 | 50% | 14.75 | 100% | 1.30 | 8.3% | 40.43 | 0.25% |
| Q>6001 | 10.7% | FRESH | 100% | 14.5 | 50% | 14.75 | 100% | 1.56 | 42.3% | 41.39 | 2.27% |
| Q>6001 | 10.7% | FRESH | 100% | 14.5 | 50% | 14.75 | 100% | 1.93 | 15.4% | 42.41 | 0.83% |

| Flow Classification | Percent of Time Ambient Flow Occurs | Density Profile | Percent of Time Profile Occurs | Depth (m) | Percent of Time Depth Occurs | Effluent Flow ($m^3/s$) | Percent of Time Effluent Flow Occurs | Ambient Current Speed (m/s) | Percent of Time Current Speed Occurs | Flux-Averaged Initial Dilution | Probability of Occurrence |
|---|---|---|---|---|---|---|---|---|---|---|---|
| 801<Q<1500 | 29.8% | SALINE | 19.6% | 14.5 | 50% | 18.90 | 1% | 0.07 | 9.8% | 11.85 | 0.003% |
| 1501<Q<2000 | 12.6% | SALINE | 2.6% | 14.5 | 50% | 18.90 | 1% | 0.07 | 9.8% | 12.51 | 0.000% |
| Q<800 | 9.8% | SALINE | 38.9% | 14.5 | 50% | 18.90 | 1% | 0.07 | 9.8% | 12.77 | 0.002% |
| 1501<Q<2000 | 12.6% | SALINE | 2.6% | 14.5 | 50% | 13.19 | 31% | 0.07 | 9.8% | 13.28 | 0.005% |
| Q<800 | 9.8% | SALINE | 38.9% | 14.5 | 50% | 13.19 | 31% | 0.07 | 9.8% | 13.29 | 0.058% |
| Q<800 | 9.8% | SALINE | 38.9% | 14.5 | 50% | 13.19 | 31% | 0.37 | 41.4% | 13.60 | 0.244% |
| 801<Q<1500 | 29.8% | SALINE | 19.6% | 14.5 | 50% | 13.19 | 31% | 0.07 | 9.8% | 13.79 | 0.089% |
| Q<800 | 9.8% | SALINE | 38.9% | 14.5 | 50% | 9.71 | 64% | 0.37 | 41.4% | 13.80 | 0.504% |
| Q<800 | 9.8% | SALINE | 38.9% | 14.5 | 50% | 18.90 | 1% | 0.37 | 41.4% | 13.80 | 0.008% |
| Q<800 | 9.8% | SALINE | 38.9% | 14.5 | 50% | 8.65 | 4% | 0.37 | 41.4% | 13.90 | 0.032% |
| Q<800 | 9.8% | SALINE | 38.9% | 14.5 | 50% | 9.71 | 64% | 0.07 | 9.8% | 14.23 | 0.119% |
| Q<800 | 9.8% | SALINE | 38.9% | 10.9 | 50% | 18.90 | 1% | 0.07 | 9.8% | 14.31 | 0.002% |
| Q<800 | 9.8% | SALINE | 38.9% | 14.5 | 50% | 8.65 | 4% | 0.07 | 9.8% | 14.39 | 0.007% |
| Q<800 | 9.8% | SALINE | 38.9% | 10.9 | 50% | 13.19 | 31% | 0.07 | 9.8% | 15.05 | 0.058% |
| 1501<Q<2000 | 12.6% | SALINE | 2.6% | 14.5 | 50% | 9.71 | 64% | 0.07 | 9.8% | 15.47 | 0.010% |
| 801<Q<1500 | 29.8% | SALINE | 19.6% | 14.5 | 50% | 9.71 | 64% | 0.07 | 9.8% | 15.54 | 0.183% |
| 801<Q<1500 | 29.8% | SALINE | 19.6% | 14.5 | 50% | 18.90 | 1% | 0.37 | 41.4% | 15.90 | 0.012% |
| 1501<Q<2000 | 12.6% | SALINE | 2.6% | 14.5 | 50% | 8.65 | 4% | 0.07 | 9.8% | 16.13 | 0.001% |
| 801<Q<1500 | 29.8% | SALINE | 19.6% | 14.5 | 50% | 8.65 | 4% | 0.37 | 41.4% | 16.20 | 0.048% |
| 801<Q<1500 | 29.8% | SALINE | 19.6% | 14.5 | 50% | 13.19 | 31% | 0.37 | 41.4% | 16.20 | 0.375% |
| 801<Q<1500 | 29.8% | SALINE | 19.6% | 14.5 | 50% | 9.71 | 64% | 0.37 | 41.4% | 16.30 | 0.774% |
| 801<Q<1500 | 29.8% | SALINE | 19.6% | 14.5 | 50% | 8.65 | 4% | 0.07 | 9.8% | 16.34 | 0.011% |
| 1501<Q<2000 | 12.6% | SALINE | 2.6% | 14.5 | 50% | 18.90 | 1% | 0.37 | 41.4% | 17.00 | 0.001% |
| Q<800 | 9.8% | SALINE | 38.9% | 14.5 | 50% | 18.90 | 1% | 0.90 | 40.5% | 17.20 | 0.008% |
| 801<Q<1500 | 29.8% | SALINE | 19.6% | 14.5 | 50% | 18.90 | 1% | 0.90 | 40.5% | 17.30 | 0.012% |
| 1501<Q<2000 | 12.6% | SALINE | 2.6% | 14.5 | 50% | 13.19 | 31% | 0.37 | 41.4% | 17.40 | 0.021% |
| Q<800 | 9.8% | SALINE | 38.9% | 14.5 | 50% | 13.19 | 31% | 0.90 | 40.5% | 17.50 | 0.239% |
| Q<800 | 9.8% | SALINE | 38.9% | 14.5 | 50% | 9.71 | 64% | 0.90 | 40.5% | 17.90 | 0.494% |
| 1501<Q<2000 | 12.6% | SALINE | 2.6% | 14.5 | 50% | 9.71 | 64% | 0.37 | 41.4% | 17.90 | 0.043% |
| Q<800 | 9.8% | SALINE | 38.9% | 14.5 | 50% | 8.65 | 4% | 0.90 | 40.5% | 18.00 | 0.031% |
| 1501<Q<2000 | 12.6% | SALINE | 2.6% | 14.5 | 50% | 8.65 | 4% | 0.37 | 41.4% | 18.00 | 0.003% |
| 801<Q<1500 | 29.8% | SALINE | 19.6% | 14.5 | 50% | 13.19 | 31% | 0.90 | 40.5% | 18.00 | 0.367% |
| 801<Q<1500 | 29.8% | SALINE | 19.6% | 14.5 | 50% | 18.90 | 1% | 1.30 | 8.3% | 18.30 | 0.002% |
| 801<Q<1500 | 29.8% | SALINE | 19.6% | 14.5 | 50% | 8.65 | 4% | 0.90 | 40.5% | 18.50 | 0.047% |
| 801<Q<1500 | 29.8% | SALINE | 19.6% | 14.5 | 50% | 9.71 | 64% | 0.90 | 40.5% | 18.50 | 0.758% |
| 1501<Q<2000 | 12.6% | SALINE | 2.6% | 14.5 | 50% | 13.19 | 31% | 0.90 | 40.5% | 18.60 | 0.021% |
| Q<800 | 9.8% | SALINE | 38.9% | 14.5 | 50% | 18.90 | 1% | 1.30 | 8.3% | 18.60 | 0.002% |
| Q<800 | 9.8% | SALINE | 38.9% | 10.9 | 50% | 18.90 | 1% | 0.37 | 41.4% | 18.60 | 0.008% |
| 1501<Q<2000 | 12.6% | SALINE | 2.6% | 14.5 | 50% | 18.90 | 1% | 1.30 | 8.3% | 18.70 | 0.000% |
| Q<800 | 9.8% | SALINE | 38.9% | 10.9 | 50% | 13.19 | 31% | 0.37 | 41.4% | 19.20 | 0.244% |
| 1501<Q<2000 | 12.6% | SALINE | 2.6% | 14.5 | 50% | 9.71 | 64% | 0.90 | 40.5% | 19.40 | 0.042% |
| Q<800 | 9.8% | SALINE | 38.9% | 14.5 | 50% | 13.19 | 31% | 1.30 | 8.3% | 19.40 | 0.049% |
| 1501<Q<2000 | 12.6% | SALINE | 2.6% | 14.5 | 50% | 8.65 | 4% | 0.90 | 40.5% | 19.60 | 0.003% |
| 801<Q<1500 | 29.8% | SALINE | 19.6% | 14.5 | 50% | 13.19 | 31% | 1.30 | 8.3% | 19.70 | 0.075% |
| Q<800 | 9.8% | SALINE | 38.9% | 10.9 | 50% | 9.71 | 64% | 0.37 | 41.4% | 19.80 | 0.504% |
| Q<800 | 9.8% | SALINE | 38.9% | 10.9 | 50% | 8.65 | 4% | 0.37 | 41.4% | 20.00 | 0.032% |
| 1501<Q<2000 | 12.6% | SALINE | 2.6% | 14.5 | 50% | 18.90 | 1% | 0.90 | 40.5% | 20.10 | 0.001% |
| 1501<Q<2000 | 12.6% | SALINE | 2.6% | 14.5 | 50% | 13.19 | 31% | 1.30 | 8.3% | 20.40 | 0.004% |
| Q<800 | 9.8% | SALINE | 38.9% | 10.9 | 50% | 13.19 | 31% | 0.90 | 40.5% | 20.40 | 0.239% |
| Q<800 | 9.8% | SALINE | 38.9% | 10.9 | 50% | 18.90 | 1% | 1.30 | 8.3% | 20.40 | 0.002% |
| Q<800 | 9.8% | SALINE | 38.9% | 10.9 | 50% | 9.71 | 64% | 0.90 | 40.5% | 21.20 | 0.494% |
| Q<800 | 9.8% | SALINE | 38.9% | 10.9 | 50% | 8.65 | 4% | 0.90 | 40.5% | 21.50 | 0.031% |
| Q<800 | 9.8% | SALINE | 38.9% | 10.9 | 50% | 18.90 | 1% | 0.90 | 40.5% | 22.10 | 0.008% |
| Q<800 | 9.8% | SALINE | 38.9% | 10.9 | 50% | 13.19 | 31% | 1.30 | 8.3% | 22.20 | 0.049% |
| Q<800 | 9.8% | SALINE | 38.9% | 14.5 | 50% | 9.71 | 64% | 1.30 | 8.3% | 22.30 | 0.101% |
| 801<Q<1500 | 29.8% | SALINE | 19.6% | 14.5 | 50% | 9.71 | 64% | 1.30 | 8.3% | 23.10 | 0.155% |
| Q<800 | 9.8% | SALINE | 38.9% | 14.5 | 50% | 8.65 | 4% | 1.30 | 8.3% | 23.60 | 0.006% |
| 1501<Q<2000 | 12.6% | SALINE | 2.6% | 14.5 | 50% | 9.71 | 64% | 1.30 | 8.3% | 24.30 | 0.009% |
| Q<800 | 9.8% | SALINE | 38.9% | 10.9 | 50% | 9.71 | 64% | 0.07 | 9.8% | 24.40 | 0.119% |
| 801<Q<1500 | 29.8% | SALINE | 19.6% | 14.5 | 50% | 8.65 | 4% | 1.30 | 8.3% | 24.40 | 0.010% |

| Flow Classification | Percent of Time Ambient Flow Occurs | Density Profile | Percent of Time Profile Occurs | Depth (m) | Percent of Time Depth Occurs | Effluent Flow ($m^3/s$) | Percent of Time Effluent Flow Occurs | Ambient Current Speed (m/s) | Percent of Time Current Speed Occurs | Flux-Averaged Initial Dilution | Probability of Occurrence |
|---|---|---|---|---|---|---|---|---|---|---|---|
| Q<800 | 9.8% | SALINE | 38.9% | 10.9 | 50% | 8.65 | 4% | 0.07 | 9.8% | 24.57 | 0.007% |
| Q<800 | 9.8% | FRESH | 61.1% | 10.9 | 50% | 18.90 | 1% | 0.37 | 41.4% | 24.61 | 0.012% |
| 801<Q<1500 | 29.8% | SALINE | 19.6% | 10.9 | 50% | 18.90 | 1% | 0.37 | 41.4% | 24.61 | 0.012% |
| 801<Q<1500 | 29.8% | FRESH | 80.4% | 10.9 | 50% | 18.90 | 1% | 0.37 | 41.4% | 24.61 | 0.050% |
| 1501<Q<2000 | 12.6% | SALINE | 2.6% | 10.9 | 50% | 18.90 | 1% | 0.37 | 41.4% | 24.61 | 0.001% |
| 1501<Q<2000 | 12.6% | FRESH | 97.4% | 10.9 | 50% | 18.90 | 1% | 0.37 | 41.4% | 24.61 | 0.025% |
| Q<800 | 9.8% | FRESH | 61.1% | 10.9 | 50% | 18.90 | 1% | 0.07 | 9.8% | 25.87 | 0.003% |
| 801<Q<1500 | 29.8% | SALINE | 19.6% | 10.9 | 50% | 18.90 | 1% | 0.07 | 9.8% | 25.87 | 0.003% |
| 801<Q<1500 | 29.8% | FRESH | 80.4% | 10.9 | 50% | 18.90 | 1% | 0.07 | 9.8% | 25.87 | 0.012% |
| 1501<Q<2000 | 12.6% | SALINE | 2.6% | 10.9 | 50% | 18.90 | 1% | 0.07 | 9.8% | 25.87 | 0.000% |
| 1501<Q<2000 | 12.6% | FRESH | 97.4% | 10.9 | 50% | 18.90 | 1% | 0.07 | 9.8% | 25.87 | 0.006% |
| 1501<Q<2000 | 12.6% | SALINE | 2.6% | 14.5 | 50% | 8.65 | 4% | 1.30 | 8.3% | 25.90 | 0.001% |
| Q<800 | 9.8% | FRESH | 61.1% | 10.9 | 50% | 13.19 | 31% | 0.07 | 9.8% | 26.42 | 0.091% |
| 801<Q<1500 | 29.8% | SALINE | 19.6% | 10.9 | 50% | 13.19 | 31% | 0.07 | 9.8% | 26.42 | 0.089% |
| 801<Q<1500 | 29.8% | FRESH | 80.4% | 10.9 | 50% | 13.19 | 31% | 0.07 | 9.8% | 26.42 | 0.364% |
| 1501<Q<2000 | 12.6% | SALINE | 2.6% | 10.9 | 50% | 13.19 | 31% | 0.07 | 9.8% | 26.42 | 0.005% |
| 1501<Q<2000 | 12.6% | FRESH | 97.4% | 10.9 | 50% | 13.19 | 31% | 0.07 | 9.8% | 26.42 | 0.186% |
| Q<800 | 9.8% | SALINE | 38.9% | 10.9 | 50% | 9.71 | 64% | 1.30 | 8.3% | 26.80 | 0.101% |
| 2001<Q<6000 | 37.1% | FRESH | 100% | 10.9 | 50% | 11.33 | 14% | 0.07 | 9.8% | 26.82 | 0.254% |
| 2001<Q<6000 | 37.1% | FRESH | 100% | 10.9 | 50% | 14.66 | 6% | 0.07 | 9.8% | 27.15 | 0.109% |
| Q<800 | 9.8% | FRESH | 61.1% | 10.9 | 50% | 9.71 | 64% | 0.07 | 9.8% | 27.31 | 0.188% |
| 801<Q<1500 | 29.8% | SALINE | 19.6% | 10.9 | 50% | 9.71 | 64% | 0.07 | 9.8% | 27.31 | 0.183% |
| 801<Q<1500 | 29.8% | FRESH | 80.4% | 10.9 | 50% | 9.71 | 64% | 0.07 | 9.8% | 27.31 | 0.752% |
| 1501<Q<2000 | 12.6% | SALINE | 2.6% | 10.9 | 50% | 9.71 | 64% | 0.07 | 9.8% | 27.31 | 0.010% |
| 1501<Q<2000 | 12.6% | FRESH | 97.4% | 10.9 | 50% | 9.71 | 64% | 0.07 | 9.8% | 27.31 | 0.384% |
| 2001<Q<6000 | 37.1% | FRESH | 100% | 10.9 | 50% | 14.66 | 6% | 0.37 | 41.4% | 27.36 | 0.460% |
| 2001<Q<6000 | 37.1% | FRESH | 100% | 10.9 | 50% | 9.18 | 72% | 0.07 | 9.8% | 27.52 | 1.308% |
| Q<800 | 9.8% | FRESH | 61.1% | 10.9 | 50% | 13.19 | 31% | 0.37 | 41.4% | 27.64 | 0.383% |
| 801<Q<1500 | 29.8% | SALINE | 19.6% | 10.9 | 50% | 13.19 | 31% | 0.37 | 41.4% | 27.64 | 0.375% |
| 801<Q<1500 | 29.8% | FRESH | 80.4% | 10.9 | 50% | 13.19 | 31% | 0.37 | 41.4% | 27.64 | 1.538% |
| 1501<Q<2000 | 12.6% | SALINE | 2.6% | 10.9 | 50% | 13.19 | 31% | 0.37 | 41.4% | 27.64 | 0.021% |
| 1501<Q<2000 | 12.6% | FRESH | 97.4% | 10.9 | 50% | 13.19 | 31% | 0.37 | 41.4% | 27.64 | 0.785% |
| Q<800 | 9.8% | FRESH | 61.1% | 10.9 | 50% | 8.65 | 4% | 0.07 | 9.8% | 27.74 | 0.012% |
| 801<Q<1500 | 29.8% | SALINE | 19.6% | 10.9 | 50% | 8.65 | 4% | 0.07 | 9.8% | 27.74 | 0.011% |
| 801<Q<1500 | 29.8% | FRESH | 80.4% | 10.9 | 50% | 8.65 | 4% | 0.07 | 9.8% | 27.74 | 0.047% |
| 1501<Q<2000 | 12.6% | SALINE | 2.6% | 10.9 | 50% | 8.65 | 4% | 0.07 | 9.8% | 27.74 | 0.001% |
| 1501<Q<2000 | 12.6% | FRESH | 97.4% | 10.9 | 50% | 8.65 | 4% | 0.07 | 9.8% | 27.74 | 0.024% |
| 2001<Q<6000 | 37.1% | FRESH | 100% | 10.9 | 50% | 7.74 | 8% | 0.07 | 9.8% | 28.20 | 0.145% |
| Q<800 | 9.8% | SALINE | 38.9% | 10.9 | 50% | 8.65 | 4% | 1.30 | 8.3% | 28.60 | 0.006% |
| Q<800 | 9.8% | FRESH | 61.1% | 10.9 | 50% | 18.90 | 1% | 0.90 | 40.5% | 28.87 | 0.012% |
| 801<Q<1500 | 29.8% | SALINE | 19.6% | 10.9 | 50% | 18.90 | 1% | 0.90 | 40.5% | 28.87 | 0.012% |
| 801<Q<1500 | 29.8% | FRESH | 80.4% | 10.9 | 50% | 18.90 | 1% | 0.90 | 40.5% | 28.87 | 0.049% |
| 1501<Q<2000 | 12.6% | SALINE | 2.6% | 10.9 | 50% | 18.90 | 1% | 0.90 | 40.5% | 28.87 | 0.001% |
| 1501<Q<2000 | 12.6% | FRESH | 97.4% | 10.9 | 50% | 18.90 | 1% | 0.90 | 40.5% | 28.87 | 0.025% |
| 2001<Q<6000 | 37.1% | FRESH | 100% | 10.9 | 50% | 11.33 | 14% | 0.37 | 41.4% | 29.16 | 1.074% |
| Q<800 | 9.8% | FRESH | 61.1% | 14.5 | 50% | 18.90 | 1% | 0.37 | 41.4% | 30.51 | 0.012% |
| 801<Q<1500 | 29.8% | FRESH | 80.4% | 14.5 | 50% | 18.90 | 1% | 0.37 | 41.4% | 30.51 | 0.050% |
| 1501<Q<2000 | 12.6% | FRESH | 97.4% | 14.5 | 50% | 18.90 | 1% | 0.37 | 41.4% | 30.51 | 0.025% |
| Q<800 | 9.8% | FRESH | 61.1% | 14.5 | 50% | 18.90 | 1% | 0.07 | 9.8% | 30.60 | 0.003% |
| 801<Q<1500 | 29.8% | FRESH | 80.4% | 14.5 | 50% | 18.90 | 1% | 0.07 | 9.8% | 30.60 | 0.012% |
| 1501<Q<2000 | 12.6% | FRESH | 97.4% | 14.5 | 50% | 18.90 | 1% | 0.07 | 9.8% | 30.60 | 0.006% |
| Q<800 | 9.8% | FRESH | 61.1% | 10.9 | 50% | 9.71 | 64% | 0.37 | 41.4% | 30.81 | 0.792% |
| 801<Q<1500 | 29.8% | SALINE | 19.6% | 10.9 | 50% | 9.71 | 64% | 0.37 | 41.4% | 30.81 | 0.774% |
| 801<Q<1500 | 29.8% | FRESH | 80.4% | 10.9 | 50% | 9.71 | 64% | 0.37 | 41.4% | 30.81 | 3.174% |
| 1501<Q<2000 | 12.6% | SALINE | 2.6% | 10.9 | 50% | 9.71 | 64% | 0.37 | 41.4% | 30.81 | 0.043% |
| 1501<Q<2000 | 12.6% | FRESH | 97.4% | 10.9 | 50% | 9.71 | 64% | 0.37 | 41.4% | 30.81 | 1.621% |
| Q>6001 | 10.7% | FRESH | 100% | 11.65 | 50% | 10.99 | 5% | 0.36 | 0.2% | 30.85 | 0.001% |
| Q<800 | 9.8% | FRESH | 61.1% | 10.9 | 50% | 18.90 | 1% | 1.30 | 8.3% | 30.86 | 0.002% |
| 801<Q<1500 | 29.8% | SALINE | 19.6% | 10.9 | 50% | 18.90 | 1% | 1.30 | 8.3% | 30.86 | 0.002% |
| 801<Q<1500 | 29.8% | FRESH | 80.4% | 10.9 | 50% | 18.90 | 1% | 1.30 | 8.3% | 30.86 | 0.010% |

| Flow Classification | Percent of Time Ambient Flow Occurs | Density Profile | Percent of Time Profile Occurs | Depth (m) | Percent of Time Depth Occurs | Effluent Flow ($m^3/s$) | Percent of Time Effluent Flow Occurs | Ambient Current Speed (m/s) | Percent of Time Current Speed Occurs | Flux-Averaged Initial Dilution | Probability of Occurrence |
|---|---|---|---|---|---|---|---|---|---|---|---|
| 1501<Q<2000 | 12.6% | SALINE | 2.6% | 10.9 | 50% | 18.90 | 1% | 1.30 | 8.3% | 30.86 | 0.000% |
| 1501<Q<2000 | 12.6% | FRESH | 97.4% | 10.9 | 50% | 18.90 | 1% | 1.30 | 8.3% | 30.86 | 0.005% |
| 2001<Q<6000 | 37.1% | FRESH | 100% | 10.9 | 50% | 9.18 | 72% | 0.37 | 41.4% | 31.45 | 5.523% |
| Q<800 | 9.8% | FRESH | 61.1% | 14.5 | 50% | 13.19 | 31% | 0.07 | 9.8% | 31.53 | 0.091% |
| 801<Q<1500 | 29.8% | FRESH | 80.4% | 14.5 | 50% | 13.19 | 31% | 0.07 | 9.8% | 31.53 | 0.364% |
| 1501<Q<2000 | 12.6% | FRESH | 97.4% | 14.5 | 50% | 13.19 | 31% | 0.07 | 9.8% | 31.53 | 0.186% |
| Q>6001 | 10.7% | FRESH | 100% | 11.65 | 50% | 9.93 | 19% | 0.36 | 0.2% | 31.97 | 0.002% |
| Q<800 | 9.8% | FRESH | 61.1% | 10.9 | 50% | 8.65 | 4% | 0.37 | 41.4% | 32.12 | 0.049% |
| 801<Q<1500 | 29.8% | SALINE | 19.6% | 10.9 | 50% | 8.65 | 4% | 0.37 | 41.4% | 32.12 | 0.048% |
| 801<Q<1500 | 29.8% | FRESH | 80.4% | 10.9 | 50% | 8.65 | 4% | 0.37 | 41.4% | 32.12 | 0.198% |
| 1501<Q<2000 | 12.6% | SALINE | 2.6% | 10.9 | 50% | 8.65 | 4% | 0.37 | 41.4% | 32.12 | 0.003% |
| 1501<Q<2000 | 12.6% | FRESH | 97.4% | 10.9 | 50% | 8.65 | 4% | 0.37 | 41.4% | 32.12 | 0.101% |
| 2001<Q<6000 | 37.1% | FRESH | 100% | 14.5 | 50% | 11.33 | 14% | 0.07 | 9.8% | 32.14 | 0.254% |
| 2001<Q<6000 | 37.1% | FRESH | 100% | 10.9 | 50% | 14.66 | 6% | 0.90 | 40.5% | 32.26 | 0.451% |
| 2001<Q<6000 | 37.1% | FRESH | 100% | 14.5 | 50% | 14.66 | 6% | 0.07 | 9.8% | 32.28 | 0.109% |
| Q<800 | 9.8% | FRESH | 61.1% | 10.9 | 50% | 13.19 | 31% | 0.90 | 40.5% | 32.62 | 0.376% |
| 801<Q<1500 | 29.8% | SALINE | 19.6% | 10.9 | 50% | 13.19 | 31% | 0.90 | 40.5% | 32.62 | 0.367% |
| 801<Q<1500 | 29.8% | FRESH | 80.4% | 10.9 | 50% | 13.19 | 31% | 0.90 | 40.5% | 32.62 | 1.506% |
| 1501<Q<2000 | 12.6% | SALINE | 2.6% | 10.9 | 50% | 13.19 | 31% | 0.90 | 40.5% | 32.62 | 0.021% |
| 1501<Q<2000 | 12.6% | FRESH | 97.4% | 10.9 | 50% | 13.19 | 31% | 0.90 | 40.5% | 32.62 | 0.769% |
| Q>6001 | 10.7% | FRESH | 100% | 11.65 | 50% | 9.32 | 66% | 0.36 | 0.2% | 32.71 | 0.009% |
| Q<800 | 9.8% | FRESH | 61.1% | 14.5 | 50% | 9.71 | 64% | 0.07 | 9.8% | 32.87 | 0.188% |
| 801<Q<1500 | 29.8% | FRESH | 80.4% | 14.5 | 50% | 9.71 | 64% | 0.07 | 9.8% | 32.87 | 0.752% |
| 1501<Q<2000 | 12.6% | FRESH | 97.4% | 14.5 | 50% | 9.71 | 64% | 0.07 | 9.8% | 32.87 | 0.384% |
| 2001<Q<6000 | 37.1% | FRESH | 100% | 14.5 | 50% | 9.18 | 72% | 0.07 | 9.8% | 33.16 | 1.308% |
| 2001<Q<6000 | 37.1% | FRESH | 100% | 10.9 | 50% | 7.74 | 8% | 0.37 | 41.4% | 33.44 | 0.614% |
| Q<800 | 9.8% | FRESH | 61.1% | 14.5 | 50% | 8.65 | 4% | 0.07 | 9.8% | 33.49 | 0.012% |
| 801<Q<1500 | 29.8% | FRESH | 80.4% | 14.5 | 50% | 8.65 | 4% | 0.07 | 9.8% | 33.49 | 0.047% |
| 1501<Q<2000 | 12.6% | FRESH | 97.4% | 14.5 | 50% | 8.65 | 4% | 0.07 | 9.8% | 33.49 | 0.024% |
| Q>6001 | 10.7% | FRESH | 100% | 11.65 | 50% | 8.72 | 10% | 0.36 | 0.2% | 33.49 | 0.001% |
| 2001<Q<6000 | 37.1% | FRESH | 100% | 14.5 | 50% | 14.66 | 6% | 0.37 | 41.4% | 33.93 | 0.460% |
| 2001<Q<6000 | 37.1% | FRESH | 100% | 14.5 | 50% | 7.74 | 8% | 0.07 | 9.8% | 34.16 | 0.145% |
| Q<800 | 9.8% | FRESH | 61.1% | 14.5 | 50% | 13.19 | 31% | 0.37 | 41.4% | 34.26 | 0.383% |
| 801<Q<1500 | 29.8% | FRESH | 80.4% | 14.5 | 50% | 13.19 | 31% | 0.37 | 41.4% | 34.26 | 1.538% |
| 1501<Q<2000 | 12.6% | FRESH | 97.4% | 14.5 | 50% | 13.19 | 31% | 0.37 | 41.4% | 34.26 | 0.785% |
| 2001<Q<6000 | 37.1% | FRESH | 100% | 10.9 | 50% | 14.66 | 6% | 1.30 | 8.3% | 34.36 | 0.092% |
| 2001<Q<6000 | 37.1% | FRESH | 100% | 10.9 | 50% | 11.33 | 14% | 0.90 | 40.5% | 34.38 | 1.052% |
| Q<800 | 9.8% | FRESH | 61.1% | 10.9 | 50% | 13.19 | 31% | 1.30 | 8.3% | 34.65 | 0.077% |
| 801<Q<1500 | 29.8% | SALINE | 19.6% | 10.9 | 50% | 13.19 | 31% | 1.30 | 8.3% | 34.65 | 0.075% |
| 801<Q<1500 | 29.8% | FRESH | 80.4% | 10.9 | 50% | 13.19 | 31% | 1.30 | 8.3% | 34.65 | 0.308% |
| 1501<Q<2000 | 12.6% | SALINE | 2.6% | 10.9 | 50% | 13.19 | 31% | 1.30 | 8.3% | 34.65 | 0.004% |
| 1501<Q<2000 | 12.6% | FRESH | 97.4% | 10.9 | 50% | 13.19 | 31% | 1.30 | 8.3% | 34.65 | 0.157% |
| Q<800 | 9.8% | FRESH | 61.1% | 14.5 | 50% | 18.90 | 1% | 0.90 | 40.5% | 35.45 | 0.012% |
| 801<Q<1500 | 29.8% | FRESH | 80.4% | 14.5 | 50% | 18.90 | 1% | 0.90 | 40.5% | 35.45 | 0.049% |
| 1501<Q<2000 | 12.6% | FRESH | 97.4% | 14.5 | 50% | 18.90 | 1% | 0.90 | 40.5% | 35.45 | 0.025% |
| 2001<Q<6000 | 37.1% | FRESH | 100% | 14.5 | 50% | 11.33 | 14% | 0.37 | 41.4% | 36.11 | 1.074% |
| Q<800 | 9.8% | FRESH | 61.1% | 10.9 | 50% | 9.71 | 64% | 0.90 | 40.5% | 36.22 | 0.776% |
| 801<Q<1500 | 29.8% | SALINE | 19.6% | 10.9 | 50% | 9.71 | 64% | 0.90 | 40.5% | 36.22 | 0.758% |
| 801<Q<1500 | 29.8% | FRESH | 80.4% | 10.9 | 50% | 9.71 | 64% | 0.90 | 40.5% | 36.22 | 3.110% |
| 1501<Q<2000 | 12.6% | SALINE | 2.6% | 10.9 | 50% | 9.71 | 64% | 0.90 | 40.5% | 36.22 | 0.042% |
| 1501<Q<2000 | 12.6% | FRESH | 97.4% | 10.9 | 50% | 9.71 | 64% | 0.90 | 40.5% | 36.22 | 1.588% |
| Q>6001 | 10.7% | FRESH | 100% | 14.5 | 50% | 10.99 | 5% | 0.36 | 0.2% | 36.32 | 0.001% |
| 2001<Q<6000 | 37.1% | FRESH | 100% | 10.9 | 50% | 11.33 | 14% | 1.30 | 8.3% | 36.42 | 0.215% |
| 2001<Q<6000 | 37.1% | FRESH | 100% | 10.9 | 50% | 9.18 | 72% | 0.90 | 40.5% | 36.92 | 5.410% |
| Q>6001 | 10.7% | FRESH | 100% | 11.65 | 50% | 10.99 | 5% | 1.08 | 42.0% | 37.43 | 0.113% |
| Q<800 | 9.8% | FRESH | 61.1% | 14.5 | 50% | 18.90 | 1% | 1.30 | 8.3% | 37.55 | 0.002% |
| 801<Q<1500 | 29.8% | FRESH | 80.4% | 14.5 | 50% | 18.90 | 1% | 1.30 | 8.3% | 37.55 | 0.010% |
| 1501<Q<2000 | 12.6% | FRESH | 97.4% | 14.5 | 50% | 18.90 | 1% | 1.30 | 8.3% | 37.55 | 0.005% |
| Q>6001 | 10.7% | FRESH | 100% | 14.5 | 50% | 9.93 | 19% | 0.36 | 0.2% | 37.61 | 0.002% |
| Q<800 | 9.8% | FRESH | 61.1% | 10.9 | 50% | 8.65 | 4% | 0.90 | 40.5% | 37.65 | 0.048% |

| Flow Classification | Percent of Time Ambient Flow Occurs | Density Profile | Percent of Time Profile Occurs | Depth (m) | Percent of Time Depth Occurs | Effluent Flow ($m^3/s$) | Percent of Time Effluent Flow Occurs | Ambient Current Speed (m/s) | Percent of Time Current Speed Occurs | Flux-Averaged Initial Dilution | Probability of Occurrence |
|---|---|---|---|---|---|---|---|---|---|---|---|
| 801<Q<1500 | 29.8% | SALINE | 19.6% | 10.9 | 50% | 8.65 | 4% | 0.90 | 40.5% | 37.65 | 0.047% |
| 801<Q<1500 | 29.8% | FRESH | 80.4% | 10.9 | 50% | 8.65 | 4% | 0.90 | 40.5% | 37.65 | 0.194% |
| 1501<Q<2000 | 12.6% | SALINE | 2.6% | 10.9 | 50% | 8.65 | 4% | 0.90 | 40.5% | 37.65 | 0.003% |
| 1501<Q<2000 | 12.6% | FRESH | 97.4% | 10.9 | 50% | 8.65 | 4% | 0.90 | 40.5% | 37.65 | 0.099% |
| Q<800 | 9.8% | FRESH | 61.1% | 14.5 | 50% | 9.71 | 64% | 0.37 | 41.4% | 38.09 | 0.792% |
| 801<Q<1500 | 29.8% | FRESH | 80.4% | 14.5 | 50% | 9.71 | 64% | 0.37 | 41.4% | 38.09 | 3.174% |
| 1501<Q<2000 | 12.6% | FRESH | 97.4% | 14.5 | 50% | 9.71 | 64% | 0.37 | 41.4% | 38.09 | 1.621% |
| Q<800 | 9.8% | FRESH | 61.1% | 10.9 | 50% | 9.71 | 64% | 1.30 | 8.3% | 38.25 | 0.159% |
| 801<Q<1500 | 29.8% | SALINE | 19.6% | 10.9 | 50% | 9.71 | 64% | 1.30 | 8.3% | 38.25 | 0.155% |
| 801<Q<1500 | 29.8% | FRESH | 80.4% | 10.9 | 50% | 9.71 | 64% | 1.30 | 8.3% | 38.25 | 0.636% |
| 1501<Q<2000 | 12.6% | SALINE | 2.6% | 10.9 | 50% | 9.71 | 64% | 1.30 | 8.3% | 38.25 | 0.009% |
| 1501<Q<2000 | 12.6% | FRESH | 97.4% | 10.9 | 50% | 9.71 | 64% | 1.30 | 8.3% | 38.25 | 0.325% |
| Q>6001 | 10.7% | FRESH | 100% | 14.5 | 50% | 9.32 | 66% | 0.36 | 0.2% | 38.45 | 0.009% |
| Q>6001 | 10.7% | FRESH | 100% | 11.65 | 50% | 9.93 | 19% | 1.08 | 42.0% | 38.67 | 0.429% |
| 2001<Q<6000 | 37.1% | FRESH | 100% | 14.5 | 50% | 9.18 | 72% | 0.37 | 41.4% | 38.84 | 5.523% |
| 2001<Q<6000 | 37.1% | FRESH | 100% | 10.9 | 50% | 9.18 | 72% | 1.30 | 8.3% | 38.94 | 1.107% |
| 2001<Q<6000 | 37.1% | FRESH | 100% | 10.9 | 50% | 7.74 | 8% | 0.90 | 40.5% | 39.05 | 0.601% |
| Q>6001 | 10.7% | FRESH | 100% | 14.5 | 50% | 8.72 | 10% | 0.36 | 0.2% | 39.35 | 0.001% |
| Q>6001 | 10.7% | FRESH | 100% | 11.65 | 50% | 10.99 | 5% | 1.56 | 42.3% | 39.36 | 0.114% |
| 2001<Q<6000 | 37.1% | FRESH | 100% | 14.5 | 50% | 14.66 | 6% | 0.90 | 40.5% | 39.45 | 0.451% |
| Q>6001 | 10.7% | FRESH | 100% | 11.65 | 50% | 9.32 | 66% | 1.08 | 42.0% | 39.47 | 1.490% |
| Q<800 | 9.8% | FRESH | 61.1% | 14.5 | 50% | 8.65 | 4% | 0.37 | 41.4% | 39.65 | 0.049% |
| 801<Q<1500 | 29.8% | FRESH | 80.4% | 14.5 | 50% | 8.65 | 4% | 0.37 | 41.4% | 39.65 | 0.198% |
| 1501<Q<2000 | 12.6% | FRESH | 97.4% | 14.5 | 50% | 8.65 | 4% | 0.37 | 41.4% | 39.65 | 0.101% |
| Q<800 | 9.8% | FRESH | 61.1% | 10.9 | 50% | 8.65 | 4% | 1.30 | 8.3% | 39.67 | 0.010% |
| 801<Q<1500 | 29.8% | SALINE | 19.6% | 10.9 | 50% | 8.65 | 4% | 1.30 | 8.3% | 39.67 | 0.010% |
| 801<Q<1500 | 29.8% | FRESH | 80.4% | 10.9 | 50% | 8.65 | 4% | 1.30 | 8.3% | 39.67 | 0.040% |
| 1501<Q<2000 | 12.6% | SALINE | 2.6% | 10.9 | 50% | 8.65 | 4% | 1.30 | 8.3% | 39.67 | 0.001% |
| 1501<Q<2000 | 12.6% | FRESH | 97.4% | 10.9 | 50% | 8.65 | 4% | 1.30 | 8.3% | 39.67 | 0.020% |
| Q<800 | 9.8% | FRESH | 61.1% | 14.5 | 50% | 13.19 | 31% | 0.90 | 40.5% | 39.77 | 0.376% |
| 801<Q<1500 | 29.8% | FRESH | 80.4% | 14.5 | 50% | 13.19 | 31% | 0.90 | 40.5% | 39.77 | 1.506% |
| 1501<Q<2000 | 12.6% | FRESH | 97.4% | 14.5 | 50% | 13.19 | 31% | 0.90 | 40.5% | 39.77 | 0.769% |
| Q>6001 | 10.7% | FRESH | 100% | 11.65 | 50% | 8.72 | 10% | 1.08 | 42.0% | 40.32 | 0.226% |
| Q>6001 | 10.7% | FRESH | 100% | 11.65 | 50% | 10.99 | 5% | 1.93 | 15.4% | 40.35 | 0.041% |
| Q>6001 | 10.7% | FRESH | 100% | 11.65 | 50% | 9.93 | 19% | 1.56 | 42.3% | 40.59 | 0.432% |
| 2001<Q<6000 | 37.1% | FRESH | 100% | 10.9 | 50% | 7.74 | 8% | 1.30 | 8.3% | 41.06 | 0.123% |
| 2001<Q<6000 | 37.1% | FRESH | 100% | 14.5 | 50% | 7.74 | 8% | 0.37 | 41.4% | 41.21 | 0.614% |
| Q>6001 | 10.7% | FRESH | 100% | 11.65 | 50% | 9.32 | 66% | 1.56 | 42.3% | 41.38 | 1.501% |
| Q>6001 | 10.7% | FRESH | 100% | 11.65 | 50% | 9.93 | 19% | 1.93 | 15.4% | 41.57 | 0.157% |
| 2001<Q<6000 | 37.1% | FRESH | 100% | 14.5 | 50% | 14.66 | 6% | 1.30 | 8.3% | 41.64 | 0.092% |
| 2001<Q<6000 | 37.1% | FRESH | 100% | 14.5 | 50% | 11.33 | 14% | 0.90 | 40.5% | 41.79 | 1.052% |
| Q<800 | 9.8% | FRESH | 61.1% | 14.5 | 50% | 13.19 | 31% | 1.30 | 8.3% | 41.87 | 0.077% |
| 801<Q<1500 | 29.8% | FRESH | 80.4% | 14.5 | 50% | 13.19 | 31% | 1.30 | 8.3% | 41.87 | 0.308% |
| 1501<Q<2000 | 12.6% | FRESH | 97.4% | 14.5 | 50% | 13.19 | 31% | 1.30 | 8.3% | 41.87 | 0.157% |
| Q>6001 | 10.7% | FRESH | 100% | 11.65 | 50% | 8.72 | 10% | 1.56 | 42.3% | 42.21 | 0.227% |
| Q>6001 | 10.7% | FRESH | 100% | 11.65 | 50% | 9.32 | 66% | 1.93 | 15.4% | 42.35 | 0.547% |
| Q>6001 | 10.7% | FRESH | 100% | 11.65 | 50% | 8.72 | 10% | 1.93 | 15.4% | 43.16 | 0.083% |
| Q>6001 | 10.7% | FRESH | 100% | 14.5 | 50% | 10.99 | 5% | 1.08 | 42.0% | 43.27 | 0.113% |
| 2001<Q<6000 | 37.1% | FRESH | 100% | 14.5 | 50% | 11.33 | 14% | 1.30 | 8.3% | 43.87 | 0.215% |
| Q<800 | 9.8% | FRESH | 61.1% | 14.5 | 50% | 9.71 | 64% | 0.90 | 40.5% | 43.90 | 0.776% |
| 801<Q<1500 | 29.8% | FRESH | 80.4% | 14.5 | 50% | 9.71 | 64% | 0.90 | 40.5% | 43.90 | 3.110% |
| 1501<Q<2000 | 12.6% | FRESH | 97.4% | 14.5 | 50% | 9.71 | 64% | 0.90 | 40.5% | 43.90 | 1.588% |
| Q>6001 | 10.7% | FRESH | 100% | 14.5 | 50% | 9.93 | 19% | 1.08 | 42.0% | 44.64 | 0.429% |
| 2001<Q<6000 | 37.1% | FRESH | 100% | 14.5 | 50% | 9.18 | 72% | 0.90 | 40.5% | 44.69 | 5.410% |
| Q>6001 | 10.7% | FRESH | 100% | 14.5 | 50% | 10.99 | 5% | 1.56 | 42.3% | 45.20 | 0.114% |
| Q>6001 | 10.7% | FRESH | 100% | 14.5 | 50% | 9.32 | 66% | 1.08 | 42.0% | 45.53 | 1.490% |
| Q<800 | 9.8% | FRESH | 61.1% | 14.5 | 50% | 8.65 | 4% | 0.90 | 40.5% | 45.53 | 0.048% |
| 801<Q<1500 | 29.8% | FRESH | 80.4% | 14.5 | 50% | 8.65 | 4% | 0.90 | 40.5% | 45.53 | 0.194% |
| 1501<Q<2000 | 12.6% | FRESH | 97.4% | 14.5 | 50% | 8.65 | 4% | 0.90 | 40.5% | 45.53 | 0.099% |
| Q<800 | 9.8% | FRESH | 61.1% | 14.5 | 50% | 9.71 | 64% | 1.30 | 8.3% | 45.95 | 0.159% |

| Flow Classification | Percent of Time Ambient Flow Occurs | Density Profile | Percent of Time Profile Occurs | Depth (m) | Percent of Time Depth Occurs | Effluent Flow ($m^3/s$) | Percent of Time Effluent Flow Occurs | Ambient Current Speed (m/s) | Percent of Time Current Speed Occurs | Flux-Averaged Initial Dilution | Probability of Occurrence |
|---|---|---|---|---|---|---|---|---|---|---|---|
| 801<Q<1500 | 29.8% | FRESH | 80.4% | 14.5 | 50% | 9.71 | 64% | 1.30 | 8.3% | 45.95 | 0.636% |
| 1501<Q<2000 | 12.6% | FRESH | 97.4% | 14.5 | 50% | 9.71 | 64% | 1.30 | 8.3% | 45.95 | 0.325% |
| Q>6001 | 10.7% | FRESH | 100% | 14.5 | 50% | 10.99 | 5% | 1.93 | 15.4% | 46.18 | 0.041% |
| Q>6001 | 10.7% | FRESH | 100% | 14.5 | 50% | 8.72 | 10% | 1.08 | 42.0% | 46.45 | 0.226% |
| Q>6001 | 10.7% | FRESH | 100% | 14.5 | 50% | 9.93 | 19% | 1.56 | 42.3% | 46.55 | 0.432% |
| 2001<Q<6000 | 37.1% | FRESH | 100% | 14.5 | 50% | 9.18 | 72% | 1.30 | 8.3% | 46.73 | 1.107% |
| 2001<Q<6000 | 37.1% | FRESH | 100% | 14.5 | 50% | 7.74 | 8% | 0.90 | 40.5% | 47.12 | 0.601% |
| Q>6001 | 10.7% | FRESH | 100% | 14.5 | 50% | 9.32 | 66% | 1.56 | 42.3% | 47.42 | 1.501% |
| Q>6001 | 10.7% | FRESH | 100% | 14.5 | 50% | 9.93 | 19% | 1.93 | 15.4% | 47.51 | 0.157% |
| Q<800 | 9.8% | FRESH | 61.1% | 14.5 | 50% | 8.65 | 4% | 1.30 | 8.3% | 47.56 | 0.010% |
| 801<Q<1500 | 29.8% | FRESH | 80.4% | 14.5 | 50% | 8.65 | 4% | 1.30 | 8.3% | 47.56 | 0.040% |
| 1501<Q<2000 | 12.6% | FRESH | 97.4% | 14.5 | 50% | 8.65 | 4% | 1.30 | 8.3% | 47.56 | 0.020% |
| Q>6001 | 10.7% | FRESH | 100% | 14.5 | 50% | 8.72 | 10% | 1.56 | 42.3% | 48.33 | 0.227% |
| Q>6001 | 10.7% | FRESH | 100% | 14.5 | 50% | 9.32 | 66% | 1.93 | 15.4% | 48.37 | 0.547% |
| 2001<Q<6000 | 37.1% | FRESH | 100% | 14.5 | 50% | 7.74 | 8% | 1.30 | 8.3% | 49.12 | 0.123% |
| Q>6001 | 10.7% | FRESH | 100% | 14.5 | 50% | 8.72 | 10% | 1.93 | 15.4% | 49.26 | 0.083% |

# Attachment I

# Performance of Tee Diffusers in Shallow Water with Crossflow

This page intentionally left blank.

# PERFORMANCE OF TEE DIFFUSERS IN SHALLOW WATER WITH CROSSFLOW

By Il Won Seo,[1] Hong Sik Kim,[2] Daeyoung Yu,[3] and Dong Soo Kim[4]

**ABSTRACT:** The dilution and plume trajectory of the tee diffuser has been investigated via the collection of experimental data for a wide range of ambient current conditions. A new dilution equation in which the stagnation effect between ambient current and diffuser discharge is assumed to be a function of the ratio of the ambient momentum to the discharge momentum, $m_r$, is proposed modifying the conventional theory of Adams that significantly underpredicts mixing for large $m_r$. A simple equation for the plume trajectory including the dependency of the momentum ratio is also derived by dimensional analysis. Experimental results on the near field dilution show that when $m_r < 1$ the dilution decreases with $m_r$, whereas when $m_r > 1$ it increases with increasing $m_r$, and approaches the stagnant water dilution for very large values of $m_r$. The equation is applied to aid the preliminary design of a diffuser discharging heated water from a power station in Korea.



## INTRODUCTION

Submerged multiport diffusers are generally thought to be the most effective means for handling the rapid initial dilution of thermal discharges. A multiport diffuser is a linear diffusion structure that consists of a manifold containing many closely spaced ports through which heated water is discharged, at high velocity, in the form of a turbulent jet into the receiving water. By discharging the heated water through a large number of ports at a high velocity, the total area available for jet entrainment is increased, thus, rapidly diluting the discharged water. Submerged thermal diffusers are characterized by the low buoyancy of the discharge under shallow water conditions.

A number of basic diffuser types for a thermal discharge have been proposed (Jirka 1982; Miller and Brighouse 1984; Akar and Jirka 1991). As shown in Fig. 1, these diffusers are distinguished by an angle $\gamma$ between the ambient current and the diffuser axis. A tee diffuser is a diffuser in which the diffuser alignment is parallel to the ambient cross flow ($\gamma = 0°$). Tee diffusers have the advantage of directing the thermal effluent away from the shoreline, and they perform equally well when the flow is in either direction. Because of certain advantages, tee diffusers have been used as the diffusion structure for heated water which is discharged from large steam electric generating stations in coastal environments (Miller and Brighouse 1984). The dilution characteristics and the plume trajectory of the tee diffusers have been studied by several investigators (Adams 1972, 1982; Lee et al. 1977; Lee and Jirka 1980; Jirka 1982; Lee 1984; Lee and Greenberg 1984) in order to provide basic information for the siting and design of the diffuser. Most of the prediction models for initial dilution of the tee diffusers in shallow water, except the semianalytic vortex model developed by Lee and Greenberg (1984), have been derived using energy and momentum equations in two dimensions. However, these models have not been rigorously tested against a wide range of field and experimental data. Most previous analyses of the dilution characteristics of tee diffusers have focused on conditions in which the ratio of the momentum of ambient current to the discharge momentum is small, usually less than 1. However, in some coastal areas where nuclear power plants are located, including Korean nuclear power plants, it is possible for combinations of strong tidal currents and relatively deep water depths to generate very large momentum ratios. For example, the current velocity in the coastal regions where some of the Korean nuclear power plants are located ranges from 40–80 cm/s, and the average water depth is from 10 to 20 m. Assuming that a typical tee diffuser with a length of 200 m, which has a discharge of 60 $m^3/s$ with the discharging velocity of 3 m/s, has 100 ports with a diameter of 0.5 m, then the momentum of the ambient current in this coastal region becomes ten times as large as the momentum of the thermal discharge. This momentum ratio value is very large compared with typical values of the momentum ratio under which most of the previous studies on tee diffusers have been performed. It has been reported that the dilution equation for tee diffusers leads to inaccurate predictions, especially in strong ambient momentum conditions (Miller and Brighouse 1984; Seo and Kim 1998).

The objective of this study is to investigate the characteristics of the near field dilution and plume trajectory for tee diffusers over a wide range of momentum ratios. In this study, extensive experimental works have been carried out in order to collect mixing and dilution data for the tee diffuser. The measured data were used to test the existing dilution equations as well as to derive the new equation for the near field dilution and the plume trajectory over the complete range of momentum ratios.

## EVALUATION OF PREVIOUS STUDIES

### Dilution in Near Field

It has been reported that the near field dilution of the tee diffuser tends to decrease with increasing ambient current (Lee et al. 1977; Adams 1982; Li and Lee 1991). Adams (1982) presented two explanations for the reduction in dilution of tee diffusers when a cross flow exists. One is that the cross flow deflects the jets, causing interference between individual jets, thus reducing the effective jet cross-sectional area. A second explanation is that the ambient current and the effluent discharge from the diffuser collectively create a region of high pressure, which is represented by an increase in water surface elevation on the downstream side of the diffuser plume. This increased pressure is associated with partial stagnation of the ambient current, thus restricting the ambient water to entrain into the effluent plume boundary.

Adams (1972, 1982) first derived a dilution equation for a tee diffuser by applying Bernoulli equations for the approach

[1]Assoc. Prof., Dept. of Civ. Engrg., Seoul Nat. Univ., Kwanak-Gu, Seoul 151-742, Korea. E-mail: seoilwon@plaza.snu.ac.kr
[2]Grad. Student, Dept. of Civ. Engrg., Seoul Nat. Univ., Kwanak-Gu, Seoul 151-742, Korea.
[3]Grad. Student, Dept. of Civ. Engrg., Seoul Nat. Univ., Kwanak-Gu, Seoul 151-742, Korea.
[4]Grad. Student, Dept. of Civ. Engrg., Seoul Nat. Univ., Kwanak-Gu, Seoul 151-742, Korea.

Note. Discussion open until June 1, 2001. To extend the closing date one month, a written request must be filed with the ASCE Manager of Journals. The manuscript for this paper was submitted for review and possible publication on April 24, 2000. This paper is part of the ***Journal of Hydraulic Engineering***, Vol. 127, No. 1, January, 2001. ©ASCE, ISSN 0733-9429/01/0001-0053–0061/$8.00 + $.50 per page. Paper No. 22308.

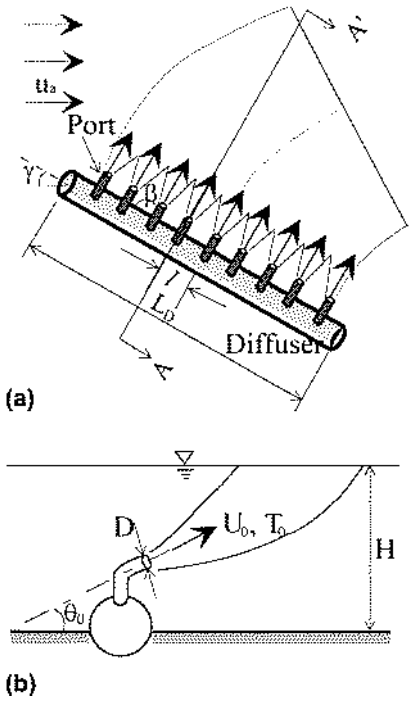


**FIG. 1. Definition Sketch of Multiport Diffuser: (a) Alignment of Diffuser; (b) Diagram of A-A′ Section**

and accelerating flows and a momentum equation for the pressure discontinuity across the diffuser axis. For the tee diffuser, he considered momentum loss caused by stagnation of the ambient current in a momentum equation for sections between the back and the front of the diffuser. The assumptions introduced are that the turbulent side entrainment in the near field region can be neglected, and the induced flow from behind the diffuser is separated from the ambient fluid at the ends of the diffuser. Combining energy and momentum equations, he derived the dilution equation for tee diffusers in the near field as

$$\frac{S_t}{S_0} = 1 - c_d m_r \tag{1}$$

where $c_d$ = coefficient associated with the stagnation effect of the ambient current. $m_r$ is the momentum ratio of the ambient current to the effluent discharge, which is expressed as

$$m_r = \frac{u_a^2 H}{U_0^2 B} \tag{2}$$

where $u_a$ = ambient current; $H$ = depth of the ambient water; and $U_0$ = velocity of the effluent discharge. $B$ is the width of an equivalent slot diffuser, which is defined as

$$B = \frac{A_0}{l} \tag{3}$$

where $A_0$ = cross-sectional area of an individual port; and $l$ = port spacing. $S_0$ is dilution in the case of stagnant ambient, which is given (Adams 1982) as

$$S_0 = \sqrt{\frac{H \cos \theta_0}{2B}} \tag{4}$$

where $\theta_0$ = angle between the port and sea bed, which is usually taken to be $\theta_0 < 45°$.

In (1), the stagnation effect is incorporated into the coefficient $c_d$, which is treated as a constant by Adams (1972, 1982). Thus, if $c_d$ is treated as a constant, predictions given by (1) show a monotonous decrease with increasing ambient momentum. Adams and Stolzenbach (1977), in order to obtain a better fit to the experimental data, proposed the following empirical equation

$$\frac{S_t}{S_0} = (1 + 5m_r)^{-1/2} \tag{5}$$

Lee et al. (1977) suggested a different empirical relation for the near field dilution for the tee diffuser, depending upon the $m_r$. In cases where $m_r < 0.1$, the authors postulated that the near field dilution is not affected by the ambient current, whereas in cases where $m_r > 0.1$, the near field dilution can be considerably lower than that of the stagnant water, and they suggested a linear relation between dilution and the momentum ratio.

Eqs. (1) and (5), and the relations suggested by Lee et al. (1977), are plotted against the available data in Fig. 2. Most of the data was collected from experiments involving a tee diffuser in which $\theta_0 = 0°$, except for the data reported by Seo and Kim (1998), in which the dilution data was collected from experiments involving tee diffusers with $\theta_0 = 22.5°$. For regions of weak to moderately strong currents, $m_r < 1$, (1) for various constant values of $c_d$ gives a poor fit whereas (5) provides a better fit. This is natural, since (5) is empirically derived by fitting it to some of the data in the region of $m_r < 1$ shown in Fig. 2. The relation suggested by Lee et al. (1977) also provides a poor fit. This is because their relation was obtained by limited data sets, i.e., data by Acres (1974) and Lee et al. (1977). For regions involving significantly strong currents, $m_r > 1$, predictions by all of the existing equations are far off the actual measured data. The measured dilution for the tee diffuser shows that, when $m_r < 1$, the dilution decreases with $m_r$, whereas when $m_r > 1$, it increases back as $m_r$ increases further. However, all existing equations provide predictions of monotonous decreasing dilution with increasing $m_r$. Moreover, Adams' theoretical equation with constant values of $c_d$ gives a negative dilution when $m_r$ is large, which is physically impossible.

It is generally thought that the discrepancies between predictions and measurements arise from the fact that the mixing process in the tee diffuser has not been correctly modeled, especially in the range where strong ambient momentum exists. The stagnation effect of the tee diffuser which results from

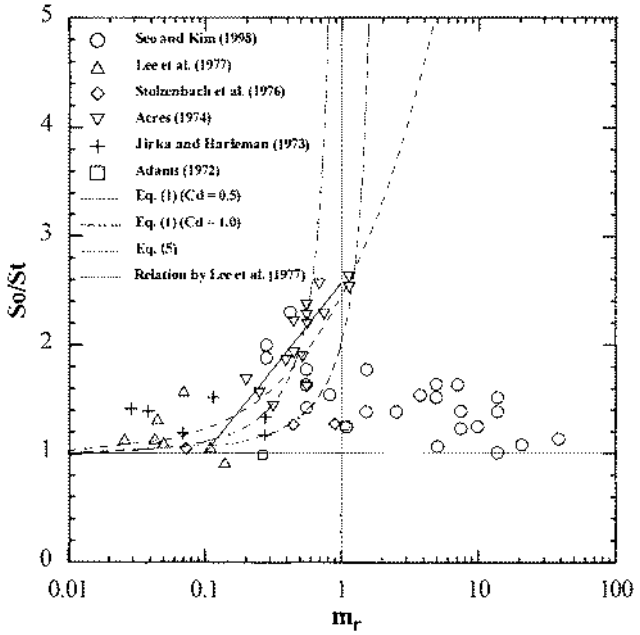


**FIG. 2. Comparison of Existing Dilution Equations with Observed Dilution**

a 90° mismatch between the ambient current and diffuser effluent discharge is known to be dependent upon momentum ratio, $m_r$. However, existing equations, including Adams' theoretical equation, do not incorporate this changing nature of the stagnation effect into their model. Li and Lee (1991), based on the results of their numerical study using a two-dimensional model of the tee diffuser, maintained that when the cross current is strong, the momentum source representation in which they approximated the jets as a line source of momentum in a two-dimensional flow cannot account for the highly complicated three-dimensional nonlinear interaction between the jet group and the crossflow. For very strong crossflow, individual jets from each port are deflected and overlap significantly, so the control volume approach breaks down entirely.

### Plume Trajectory

The prediction of the plume trajectory of the tee diffuser under various ambient current conditions is necessary in estimating the distance of the thermal plume from the shoreline. Lee et al. (1977) developed a theory calculating the plume trajectory of the tee diffuser in a crossflow based on a vertically fully mixed assumption. They integrated the continuity and momentum equations in both the axial and normal directions of the plume in which the bottom friction and the bending force due to ambient momentum are incorporated. They verified the predicted plume trajectory using the experimental data collected by Acres (1974) and Lee et al. (1977). Based on both theoretical prediction and experimental results, they postulated that the larger the value of $m_r$, the more the plume is deflected. They also found that a larger assumed value of blocking coefficient, which is associated with the bending force in the normal momentum equation, leads to a more pronounced plume deflection. Even though a satisfactory agreement between the computed plume trajectory and the observed data is obtained, their study was performed for conditions under weak to moderately strong momentum ratios, i.e., $m_r < 1$. Therefore, a comprehensive study for a wide range of momentum ratios is needed to properly predict the plume trajectory of the tee diffuser.

## PROPOSED THEORY

In this paper, to correctly explain the dilution behavior of the tee diffuser for a complete range of momentum ratios, an improved model modified from Adams' (1972, 1982) theory is proposed. In the proposed model, unlike Adams' theory, the stagnation effect between ambient current and diffuser effluent discharge is assumed to be a decreasing function of the momentum ratio, $m_r$. Physically, these assumptions indicate that, when the momentum ratio is small, the blocking effect produced by the effluent discharge is dominant, and the reduction in dilution gradually increases. So, for this region, as modeled by Adams (1972, 1982), back entrainment behind the diffuser plays a major role in the mixing of the effluent discharge. However, when the cross flow momentum becomes stronger than the discharge momentum, i.e., $m_r > 1$, the cross flow begins to overcome the blocking effect of the effluent plume, tending to be entrained into the effluent plume, and as a result, direct entrainment from the cross flow now plays an important role in the dilution process. Therefore, when $m_r > 1$, as the ambient momentum increases, dilution begins to increase.

As a relation between $c_d$ and the ratio of jet velocity to the ambient velocity, Subramanya and Porey (1984) suggested an exponential function based on the experimental data of the three-dimensional jet in crossflow. In this study, even though the mechanics of the two-dimensional plume in shallow water are quite different from the three-dimensional jet dealt with in Subramanya and Porey (1984), it is assumed that $c_d$ is expressed as the following functional form:

$$c_d = a \exp(-bm_r^c) \tag{6}$$

Substituting (6) into (1) yields

$$\frac{S_0}{S_t} = \frac{1}{1 - [a \exp(-bm_r^c)]m_r} \tag{7}$$

In this study, constants in (7) are determined from the experimental data.

## LABORATORY EXPERIMENTS

The laboratory model was constructed in a 20-m-long, 4.9-m-wide, and 0.6-m-deep flume in the Hydraulics Laboratory at Seoul National University, Seoul, Korea. A schematic diagram of the laboratory flume and the experimental setup is shown in Fig. 3. The model of the diffuser, analyzing the geometry of diffusers and the conditions of heated water discharged from power plants operating presently, is manufactured to indicate the representative characteristics (Jirka 1982). The principles of hydraulic similitude were used as guidelines in determining the appropriate scale of the model. Among the many similitude principles that are relevant to the modeling of thermal discharge, the similitude of the densimetric Froude number is used in this study, because Reynolds similarity is usually relaxed if the flow in the model is turbulent and the phenomenon of surface heat discharge is usually not of importance near the discharge, so that if the model covers mainly the nearfield area, it may be ignored (Fischer et al. 1979). Here, the densimetric Froude number is defined as $F_j = (U_0/\sqrt{g_0' D})$, where $g_0' = (\Delta\rho/\rho)g$; $\Delta\rho$ = density difference between discharging fluid and ambient fluid; and $g$ = gravitational acceleration. The total length of the model diffuser, $L_D$, is 120 cm. The inner diameter of the port is 0.43 cm with a variable spacing of 4.0−12.0 cm. The angle between the port and the channel bottom is selected to be 22.5°.

Flow rates were measured using an electromagnetic flow meter. Water temperature was measured using CC-type thermocouple sensors, installed on the instrument carriage. The thermocouple sensors were connected to a 40-channel data logger in which measured temperatures are stored in digital form. The thermal effluent was supplied from a specially manufactured hot water bath, which consisted of a preheating bath and a constant head tank, which provided hot water of constant temperature and flow rate. The discharge from the constant head tank to the diffuser pipe was measured using an electromagnetic flow meter.

Three sets of data were collected in connection with the experimental program. The ranges of experimental parameters

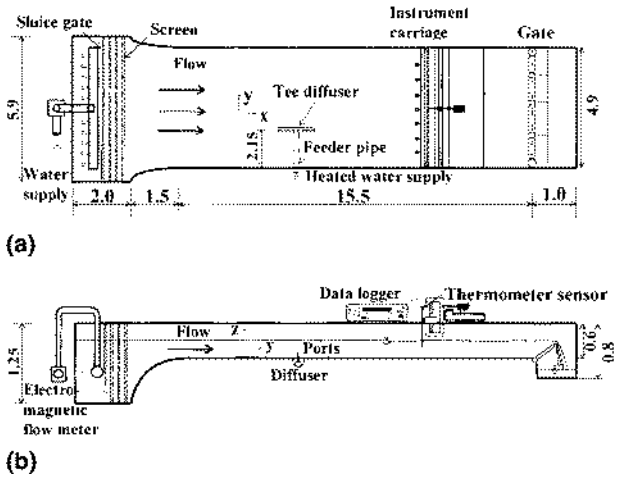


**FIG. 3. Schematic Diagram of Laboratory Flume and Experimental Setup (Unit: m): (a) Plan View; (b) Side View**



J. Hydraul. Eng., 2001, 127(1): 53-61

for series TS, TD, and TT are listed in Tables 1–3. These sets were arranged to study the effects of port spacing on the mixing of the tee diffuser. In this study, the experimental approach is focused on the conditions of strong ambient momentum, which is relevant to the oceanographic conditions of the Korean shoreline, where the existing nuclear power plants are located. Furthermore, whole experiments were conducted without distorting the physical mixing processes in real situations.

The assumption that the flow is vertically well mixed, and as a result, that buoyancy may be neglected, is considered using a criterion proposed by Jirka (1982), in which a densimetric Froude number based on water depth, mixed flow velocity, ambient velocity, and density difference at the diffuser is greater than unity. This criterion for a small slot width in an ambient current is given as follows:

$$\phi = \frac{m_0}{j_0^{2/3} H} + \frac{m_a + m_0 \cos \theta_0}{j_0^{2/3} H} \geq \phi_c \tag{8}$$

in which $m_a$, $m_0$ = momentum fluxes per unit length of ambient and discharge fluid, respectively; and $j_0$ = buoyancy fluxes per unit length of discharge fluid. Jirka suggested that the value of $\phi_c$ is approximately 0.54.

**TABLE 1. Experimental Parameters for TS Series ($B$ = 0.0375)**

| Case (1) | $H$ (cm) (2) | $u_a$ (cm/s) (3) | $U_0$ (cm/s) (4) | $m_r$ (5) | $\phi$ (6) | $S_t$ (7) |
|---|---|---|---|---|---|---|
| TS301 | 10.0 | 18.8 | 56.8 | 30.2 | 86.3 | 9.5 |
| TS302 | 10.0 | 15.3 | 57.3 | 19.6 | 59.9 | 9.5 |
| TS303 | 11.0 | 11.8 | 63.6 | 10.5 | 37.9 | 8.7 |
| TS304 | 19.0 | 1.6 | 95.9 | 0.14 | 9.78 | 11.1 |
| TS305 | 15.0 | 3.9 | 80.2 | 0.99 | 10.2 | 10.5 |
| TS306 | 12.0 | 8.6 | 71.8 | 4.77 | 19.7 | 9.1 |
| TS307 | 13.0 | 7.8 | 74.4 | 3.93 | 17.7 | 10.0 |
| TS308 | 13.0 | 6.8 | 74.7 | 2.94 | 15.3 | 10.5 |
| TS309 | 14.0 | 5.5 | 77.7 | 1.93 | 12.3 | 11.8 |
| TS310 | 14.0 | 5.0 | 76.2 | 1.69 | 11.6 | 9.5 |
| TS311 | 15.0 | 4.5 | 84.4 | 1.16 | 11.1 | 9.5 |
| TS312 | 15.0 | 3.9 | 82.0 | 0.96 | 12.6 | 10.0 |
| TS313 | 16.0 | 3.5 | 82.9 | 0.80 | 11.6 | 10.0 |
| TS314 | 16.0 | 3.1 | 81.7 | 0.65 | 13.1 | 10.0 |
| TS315 | 17.0 | 2.5 | 88.3 | 0.36 | 12.7 | 9.5 |
| TS316 | 18.0 | 2.2 | 92.0 | 0.28 | 8.21 | 10.5 |
| TS317 | 20.0 | 1.3 | 97.0 | 0.10 | 9.57 | 10.5 |
| TS601 | 15.8 | 6.3 | 34.7 | 14.3 | 15.3 | 12.5 |
| TS602 | 17.2 | 6.4 | 35.4 | 15.5 | 15.3 | 13.3 |
| TS603 | 17.0 | 6.9 | 35.4 | 18.0 | 17.6 | 14.3 |
| TS604 | 17.4 | 7.3 | 35.4 | 20.2 | 19.0 | 13.3 |
| TS605 | 17.5 | 7.7 | 35.7 | 22.7 | 21.1 | 13.3 |
| TS606 | 17.0 | 7.9 | 51.5 | 11.0 | 19.4 | 11.1 |
| TS607 | 13.9 | 9.2 | 53.7 | 11.1 | 25.2 | 10.5 |
| TS608 | 14.2 | 9.4 | 51.1 | 13.4 | 26.5 | 10.0 |
| TS609 | 14.2 | 9.8 | 50.6 | 14.5 | 27.9 | 9.1 |
| TS610 | 14.2 | 10.2 | 47.5 | 18.0 | 30.5 | 12.5 |
| TS611 | 14.3 | 10.4 | 55.4 | 14.0 | 30.8 | 11.8 |
| TS612 | 11.3 | 15.0 | 46.0 | 33.2 | 63.7 | 10.0 |
| TS613 | 11.2 | 15.7 | 46.2 | 35.7 | 68.6 | 9.5 |
| TS614 | 11.3 | 16.0 | 46.5 | 37.0 | 70.7 | 10.5 |
| TS615 | 11.0 | 17.0 | 44.7 | 43.5 | 81.4 | 9.5 |
| TS616 | 10.5 | 15.1 | 46.1 | 31.2 | 65.2 | 9.1 |
| TS617 | 9.0 | 16.0 | 35.7 | 49.8 | 83.4 | 8.7 |
| TS618 | 9.0 | 16.4 | 35.9 | 52.0 | 87.0 | 8.7 |
| TS619 | 9.0 | 17.2 | 35.0 | 60.0 | 96.2 | 8.7 |
| TS620 | 9.3 | 19.4 | 32.1 | 92.9 | 126.1 | 9.5 |
| TS621 | 9.2 | 20.5 | 35.8 | 83.3 | 132.0 | 9.5 |
| TS622 | 15.1 | 0.8 | 104.1 | 0.03 | 13.5 | 10.5 |
| TS623 | 15.8 | 0.9 | 51.5 | 0.12 | 5.11 | 10.5 |
| TS624 | 16.1 | 1.0 | 51.3 | 0.16 | 5.05 | 9.5 |
| TS625 | 16.3 | 1.2 | 50.4 | 0.23 | 4.94 | 8.7 |
| TS626 | 16.3 | 1.3 | 49.8 | 0.31 | 4.96 | 10.5 |
| TS627 | 16.0 | 1.7 | 54.5 | 0.41 | 5.91 | 11.1 |
| TS628 | 16.0 | 1.0 | 55.2 | 0.14 | 5.44 | 8.0 |
| TS629 | 16.0 | 0.9 | 54.7 | 0.13 | 5.41 | 9.5 |
| TS630 | 16.0 | 0.8 | 54.6 | 0.09 | 5.30 | 9.1 |
| TS631 | 15.8 | 0.7 | 55.5 | 0.07 | 5.45 | 8.7 |
| TS632 | 9.0 | 21.4 | 33.2 | 103.1 | 150.6 | 8.7 |

**TABLE 2. Experimental Parameters for TD Series ($B$ = 0.0194)**

| Case (1) | $H$ (cm) (2) | $u_a$ (cm/s) (3) | $U_0$ (cm/s) (4) | $m_r$ (5) | $\phi$ (6) | $S_t$ (7) |
|---|---|---|---|---|---|---|
| TD401 | 15.0 | 11.3 | 59.0 | 30.0 | 49.5 | 16.7 |
| TD402 | 14.8 | 0.5 | 58.8 | 0.05 | 5.19 | 14.3 |
| TD403 | 15.8 | 0.7 | 62.4 | 0.10 | 5.31 | 14.3 |
| TD404 | 17.0 | 1.8 | 65.7 | 0.69 | 8.46 | 12.5 |
| TD405 | 18.0 | 2.1 | 70.2 | 0.86 | 8.87 | 12.5 |
| TD406 | 18.0 | 2.2 | 69.9 | 0.95 | 8.84 | 14.3 |
| TD407 | 19.0 | 2.4 | 73.2 | 1.17 | 10.2 | 16.7 |
| TD408 | 18.8 | 2.8 | 73.7 | 1.54 | 11.1 | 14.3 |
| TD409 | 19.9 | 3.1 | 74.6 | 1.91 | 11.3 | 20.0 |
| TD410 | 20.1 | 9.8 | 74.3 | 19.2 | 46.5 | 18.2 |
| TD411 | 21.0 | 3.8 | 75.0 | 2.99 | 13.5 | 13.3 |
| TD412 | 21.2 | 4.4 | 78.8 | 3.68 | 15.8 | 13.3 |
| TD413 | 22.1 | 5.1 | 80.6 | 4.89 | 18.1 | 16.7 |
| TD414 | 22.0 | 5.5 | 80.1 | 5.74 | 19.6 | 18.2 |
| TD415 | 23.3 | 6.0 | 84.9 | 6.32 | 21.7 | 22.2 |
| TD416 | 23.3 | 6.3 | 79.9 | 8.10 | 23.4 | 16.7 |
| TD417 | 24.2 | 6.8 | 85.1 | 8.54 | 25.3 | 20.0 |
| TD418 | 25.0 | 7.4 | 86.7 | 9.95 | 27.8 | 16.7 |
| TD419 | 18.2 | 1.6 | 65.1 | 0.64 | 8.25 | 13.3 |
| TD420 | 18.2 | 1.3 | 69.0 | 0.38 | 8.30 | 13.3 |
| TD421 | 18.9 | 1.0 | 70.4 | 0.20 | 7.75 | 12.5 |
| TD422 | 18.8 | 0.6 | 70.2 | 0.07 | 7.36 | 16.7 |

**TABLE 3. Experimental Parameters for TT Series ($B$ = 0.0133)**

| Case (1) | $H$ (cm) (2) | $u_a$ (cm/s) (3) | $U_0$ (cm/s) (4) | $m_r$ (5) | $\phi$ (6) | $S_t$ (7) |
|---|---|---|---|---|---|---|
| TT501 | 15.2 | 10.0 | 63.8 | 30.8 | 70.0 | 20.0 |
| TT502 | 15.5 | 0.4 | 64.7 | 0.05 | 7.06 | 14.3 |
| TT503 | 16.0 | 0.6 | 67.4 | 0.11 | 7.28 | 14.3 |
| TT504 | 16.0 | 1.1 | 69.0 | 0.33 | 7.77 | 15.4 |
| TT505 | 17.0 | 1.4 | 71.4 | 0.51 | 7.96 | 16.7 |
| TT506 | 17.0 | 1.6 | 71.9 | 0.69 | 8.27 | 16.7 |
| TT507 | 18.1 | 1.8 | 76.3 | 0.85 | 9.36 | 18.2 |
| TT508 | 18.0 | 1.7 | 73.0 | 0.85 | 8.71 | 14.3 |
| TT509 | 19.0 | 2.2 | 75.7 | 1.35 | 9.59 | 20.0 |
| TT510 | 18.9 | 2.6 | 76.4 | 1.75 | 10.5 | 15.4 |
| TT511 | 20.0 | 2.8 | 77.9 | 2.10 | 11.2 | 18.2 |
| TT512 | 20.1 | 8.8 | 76.5 | 21.8 | 48.7 | 22.2 |
| TT513 | 20.9 | 3.5 | 81.5 | 3.13 | 13.3 | 22.2 |
| TT514 | 21.2 | 3.8 | 81.7 | 3.88 | 14.5 | 22.2 |
| TT515 | 22.2 | 4.5 | 84.7 | 5.06 | 16.8 | 20.0 |
| TT516 | 21.8 | 4.9 | 81.4 | 6.65 | 19.8 | 20.0 |
| TT517 | 23.0 | 5.4 | 89.6 | 6.84 | 21.5 | 20.0 |
| TT518 | 23.3 | 5.7 | 88.1 | 8.10 | 23.2 | 22.2 |
| TT519 | 24.5 | 6.1 | 90.7 | 9.04 | 24.7 | 22.2 |
| TT520 | 26.0 | 6.3 | 90.8 | 10.4 | 25.6 | 33.3 |

## ANALYSIS OF EXPERIMENT RESULTS

### Near Field Dilution

The observed dilutions for series TS, TD, and TT are listed in Tables 1–3. Among a number of experimental cases, photographs of the plume behavior at the water surface from different typical groups of $m_r$ are shown in Fig. 4. In this figure, the cross current is flowing from left to right. When $m_r$ is smaller than 1, Fig. 4(a) shows that, as explained by Adams (1972, 1982) and Li and Lee (1991), the effluent discharge of the multiple jets restricts the ambient flow to be entrained into the plume boundary. Li and Lee (1991) maintained that the pressure hill is developed at the source line due to the imparted momentum, leading to the formation of the stagnation region near the windward end of the multiple jets. This blocking ef-

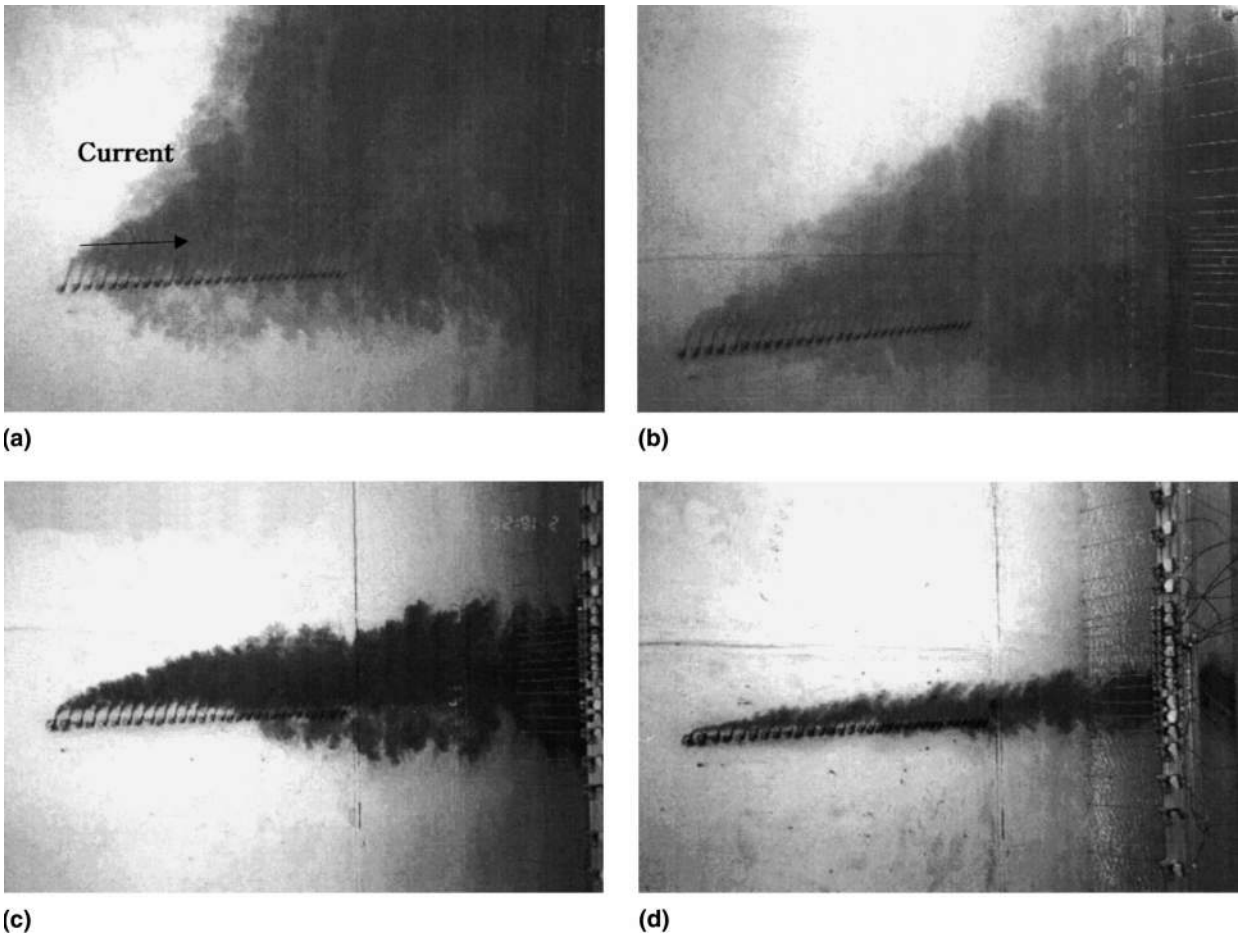


**FIG. 4. Photographs of Plume Behavior at Water Surface: (a) Case TS316 ($m_r$ = 0.28); (b) Case TS312 ($m_r$ = 0.96); (c) Case TS607 ($m_r$ = 11.1); (d) Case TS632 ($m_r$ = 103.1)**

fect remains dominant when $m_r$ is less than 1. However, as shown in Figs. 4(c and d), when the cross flow momentum becomes stronger than the discharge momentum, i.e., $m_r > 1$, the cross flow begins to overcome the blocking effect of the effluent plume, tending to be entrained into the effluent plume. For very large $m_r$, as shown in Figs. 4(c and d), individual jets from each port are deflected and overlap significantly. For these cases, unlike the turbulent jets and plumes, the effluent discharge of the multiple jets loses most of its initial momentum. Thus, the effluent plume from the diffuser is transported by the ambient flow and, at the same time, it is spread by passive dispersion caused by the ambient current. The blocking effect of the effluent plume is now completely overcome, and the discharge momentum has no effect on the mixing of the plume.

The water surface isothermal contours from typical groups of $m_r$ are shown in Fig. 5. In this figure, the isothermal contours are lines of $\Delta T/\Delta T_0$, in which $\Delta T = T - T_b$, and $\Delta T_0 = T_0 - T_b$. Here $T$ = local temperature at the points of measurement; $T_b$ = background temperature of the ambient water; and $T_0$ = initial temperature of the effluent discharge from each port of the diffuser. The plume trajectories are also drawn in this figure. The same arguments on the mechanics of plume for a various range of $m_r$ can be drawn from this figure as Fig. 4.

Results of the experiments reveal that the effects of port spacing on the mechanics of the tee diffuser are not significant, provided the condition of vertically well-mixed flow is achieved. In this study, for most of the experimental cases, the criterion given by (8) was satisfied, as shown in Tables 1–3. Among a number of experimental cases, the vertical distributions of the excess temperature at the near field from different typical groups of $m_r$ are shown in Fig. 6. These temperature data were collected at points of $x/L_D$ = 1.0–1.5; $y/L_D$ = 0.1–1.7. As shown in this figure, at the near field, the temperature distributions of the effluent plume under various cross flow conditions remain approximately uniform in the vertical direction.

The observed dilution, which is normalized by the stagnant water dilution, along with the existing experimental data are plotted in Fig. 7. The observed dilution is defined as the measured discharge temperature rise divided by the highest closed isotherm at the water surface of a scale greater than the port spacing to eliminate the consideration of local hot spots caused by single jets. As described earlier, it is clearly shown in Fig. 7 that when $m_r < 1$, dilution decreases with $m_r$. However, in the range where $m_r > 1$, it increases with increasing $m_r$ and approaches stagnant water dilution, $S_0$, for a very large value of $m_r$. As shown in this figure and Fig. 2, predictions using existing equations by Adams (1982) and Adams and Stolzenbach (1977) are far off the actual measured data, especially for the region where $m_r > 1$.

In this study, constants in (7) were determined by fitting (7) to the available data to yield the following equation:

$$\frac{S_0}{S_t} = \frac{1}{1 - [60 \exp(-5.0 m_r^{0.2})] m_r} \tag{9}$$

This equation has a functional form that is relevant to the distribution characteristics of the measured dilution. Eq. (9) is also plotted in Fig. 7. As shown in this figure, this equation is in excellent agreement with the measured dilution.

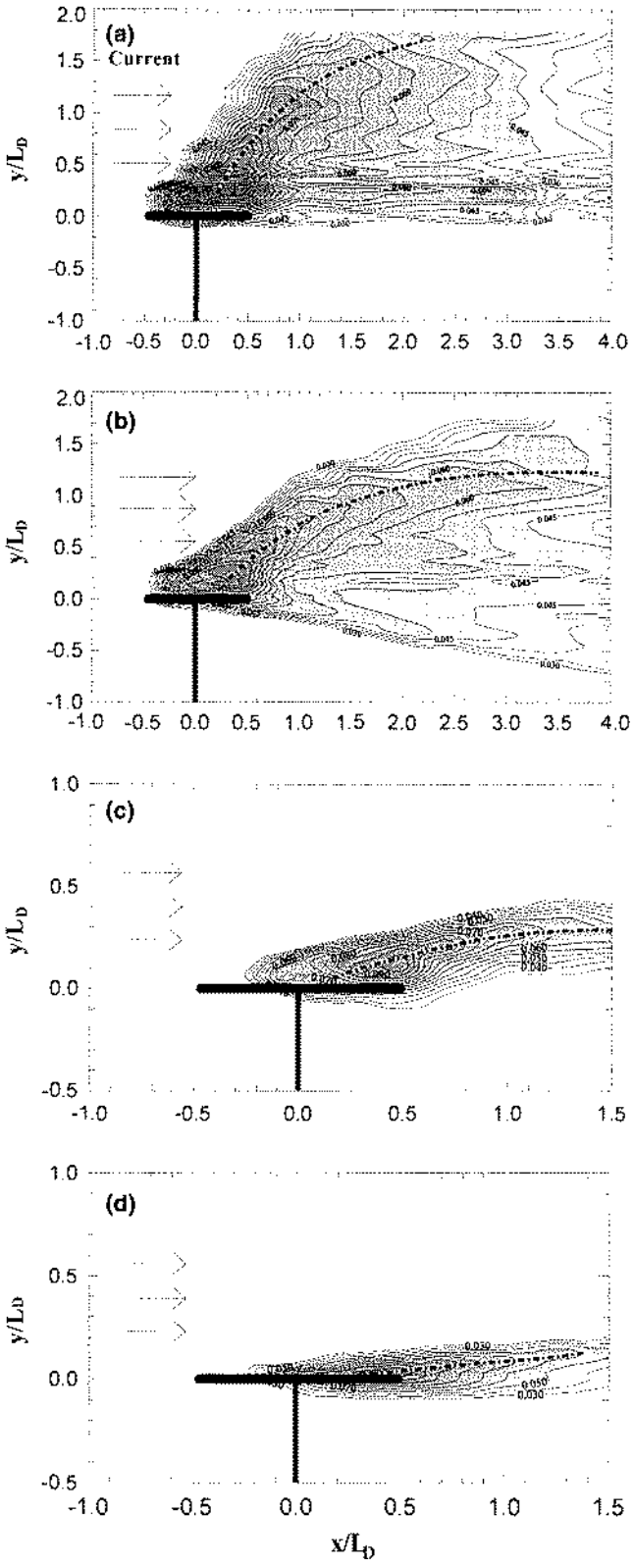


**FIG. 5. Nondimensional Equitemperature Contours at Water Surface: (a) Case TS316 ($m_r$ = 0.28); (b) Case TS312 ($m_r$ = 0.96); (c) Case TS607 ($m_r$ = 11.1); (d) Case TS632 ($m_r$ = 103.1)**

As shown in Figs. 4(c and d), for very large $m_r$, effluent discharge of the multiple jets is advected by the ambient current after it loses most of its initial momentum, which is perpendicular to the ambient flow. Thus, the plume for very large $m_r$ can be treated as those from a continuous line source with no momentum. The width of the plume spreading from a continuous source in two dimensions is proportional to

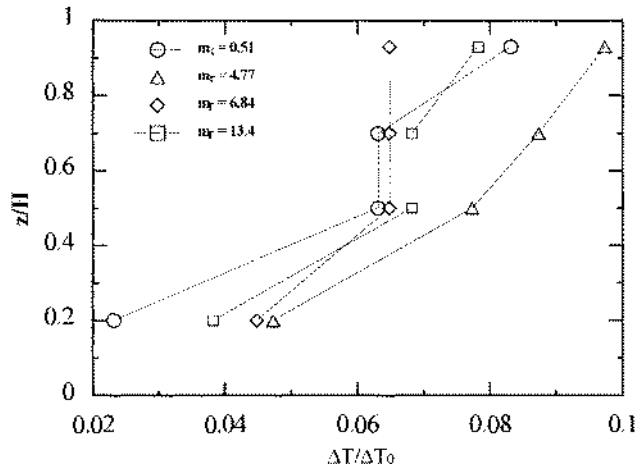


**FIG. 6. Vertical Temperature Distributions at the Near Field**

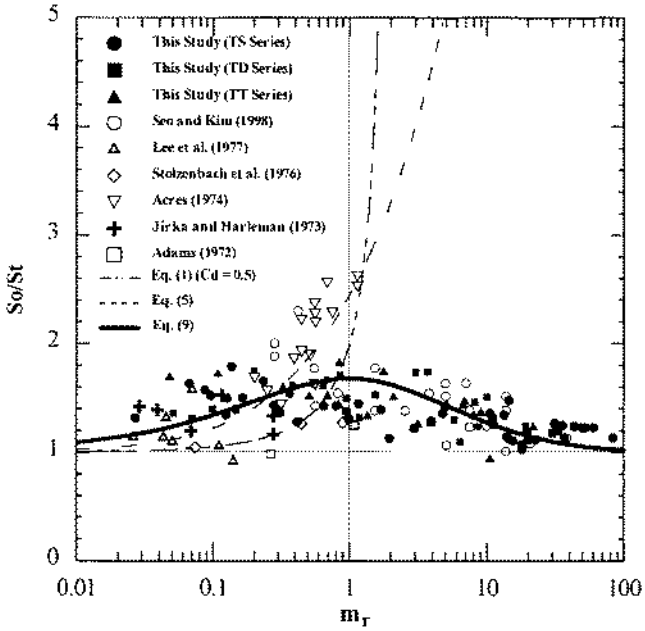


**FIG. 7. Comparison of Observed Dilution with Predictions**

$\sqrt{2\varepsilon_y(x/u_a)}$ (Fischer et al. 1979), where $x$ is the longitudinal distance in the direction of the ambient current. If the ambient diffusion coefficient, $\varepsilon_y$, is expected to be proportional to $u^*H$, where $u^*$ is the shear velocity, then the width of the plume at the end of the diffuser (near field) can be approximated as $k\sqrt{HL_D}$, where $k$ is a coefficient related to the effects of the bottom friction and irregularities. Thus, the bulk flow rate at that section of the plume is given as

$$Q_N = kL_D^{1/2}H^{3/2}u_a \tag{10}$$

The near field dilution can be defined as

$$S_N = \frac{Q_N + Q_0}{Q_0} = \frac{kL_D^{1/2}H^{3/2}u_a}{L_DBU_0} + 1 \approx k\,\frac{u_aH^{3/2}}{U_0L_D^{1/2}B} \tag{11}$$

where $Q_0$ = total flow rate of the diffuser. Eq. (11) can be nondimensionalized by the stagnant dilution $S_0$ as

$$\frac{S_0}{S_N} = \frac{\sqrt{2}}{k}\left(\frac{H}{L_D}\right)^{-1/2} m_r^{-1/2} \tag{12}$$

Eq. (12) with $k$ = 0.5 and $H/L_D$ = 0.075 when $m_r$ = 100 produces the same results as the experiments in which the dilution approaches the stagnant dilution when $m_r$ is very large.

## Excess Isotherm Areas

For environmental impact analysis, excess isotherm areas for different temperature rises should be investigated. In this study, for dimensional analysis, the excess isotherm area normalized by $L_D^2$ is related to various factors as follows:

$$\frac{A}{L_D^2} = f_1\left(\frac{\Delta T}{\Delta T_0}, U_0, B, u_a, H\right) \tag{13}$$

where $A$ = area of the isothermal contour corresponding to $\Delta T/\Delta T_0$. Expressing (13) using nondimensional terms yields

$$\frac{A}{L_D^2} = f_2\left(\frac{\Delta T}{\Delta T_0}, S_t\right) \tag{14}$$

where, as shown earlier, $S_t$ is expressed as

$$S_t = g(U_0, B, u_a, H) \tag{15}$$

Eq. (15) can be rearranged as

$$\frac{\Delta T}{\Delta T_0} S_t = f_3\left(\frac{A}{L_D^2}\right) \tag{16}$$

The relation between the normalized temperature rises and the normalized excess isotherm areas collected in this study, along with some data from previous studies (Acres 1974; Lee et al. 1977) are plotted in Fig. 8. Lee et al. (1977), based on the theoretical approaches in which a set of integral equations containing the bottom friction effect for the plume in the intermediate field was solved, maintained that solutions for the excess isotherm areas depend upon a frictional parameter $\Phi = f_0 L_D/6H$, in which $f_0$ is the Darcy-Weisbach friction factor for the bottom. The frictional parameter for data from Acres (1974) and Lee et al. (1977) ranges 0.01–0.03, whereas values of $\Phi$ for data collected in this study range 0.015–0.03. In Fig. 8, the data by Acres and Lee et al. were collected under stagnant ambient water. As shown in this figure, in general, observed data for different ranges of $m_r$ show a similar trend. However, it indicates that the excess isotherm areas for cases where $m_r > 1$, corresponding to a particular temperature rise, are smaller than those for cases where $m_r < 1$. The regression equations that are best-fitted to the observed data are given as

$$\frac{\Delta T}{\Delta T_0} S_t = 0.67\left(\frac{A}{L_D^2}\right)^{-0.17}, \quad m_r < 1 \tag{17a}$$

$$\frac{\Delta T}{\Delta T_0} S_t = 0.57\left(\frac{A}{L_D^2}\right)^{-0.17}, \quad m_r > 1 \tag{17b}$$

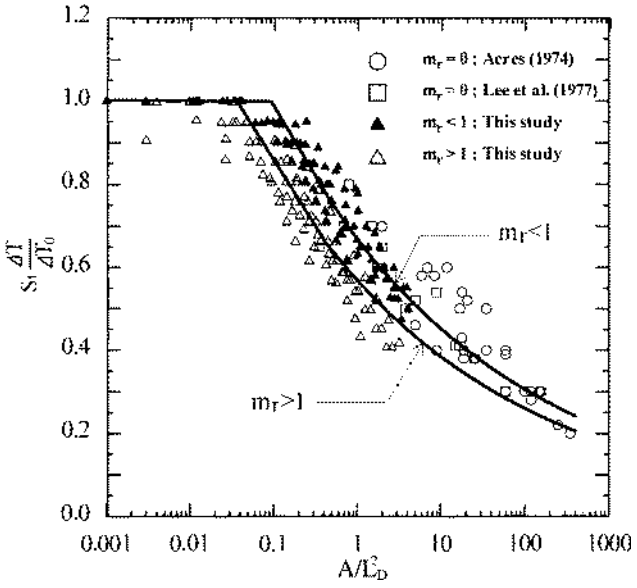


**FIG. 8. Excess Isotherm Areas for Tee Diffuser**

## Plume Trajectory

For dimensional analysis, coordinates of the plume trajectory at the water surface are related to various factors as follows:

$$\phi_1(x, y, U_0, B, u_a, H, L_D) = 0 \tag{18}$$

in which $x$ = coordinate parallel to the direction of the ambient current; and $y$ = coordinate normal to the direction of the ambient current. By applying the Buckingham II theorem, this equation can be rearranged as

$$\frac{y}{L_D} m_r = \phi_2\left(\frac{x}{L_D} m_r\right) \tag{19}$$

In this study, the functional form in (19) is assumed as a power equation as

$$\frac{y}{L_D} m_r = d\left(\frac{x}{L_D} m_r\right)^e \tag{20}$$

The constants in (20) are determined from the experimental data.

The observed data for the plume trajectory collected in this study, along with the regression equation, are plotted in Fig. 9. The plume trajectory data shown in this figure are obtained from the isotherm contours such as those plotted in Fig. 5. In this figure, the data represent series TS from this study. As shown in this figure, the observed data of the plume trajectory plotted in a log-log scale indicate a linear relation. The regression equation can be obtained by best-fitting (20) to the observed data as

$$\frac{y}{L_D} m_r = 0.60\left(\frac{x}{L_D} m_r\right)^{0.55} \tag{21}$$

This equation of the plume trajectory explicitly contains the dependency upon the momentum ratio, $m_r$, as is also suggested by Akar and Jirka (1991). Based on the length scale analysis with momentum conservation, Akar and Jirka (1991) proposed the 2/3 exponent for the trajectory of the tee diffuser in the CORMIX2 model.

## Practical Application

As stated earlier, this study focuses on the conditions of strong ambient momentum, which is relevant to the oceanographic conditions of some coastal areas where nuclear power plants are located, including Korean nuclear power plants. In

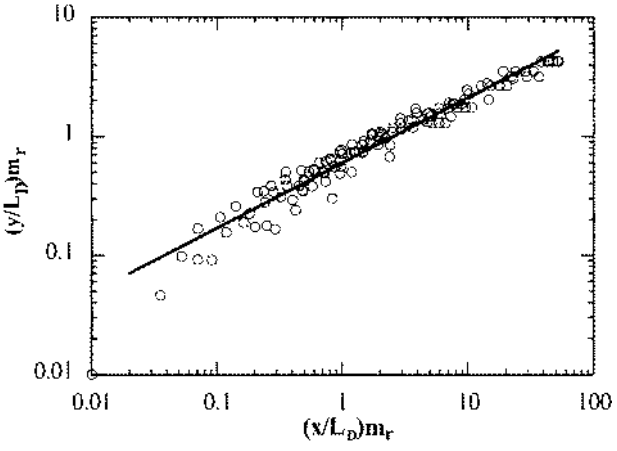


**FIG. 9. Plume Trajectory for Tee Diffuser**



J. Hydraul. Eng., 2001, 127(1): 53-61

this study, a nuclear power plant located on the Korean shoreline was selected as an example of a typical practical application of the performance of the tee diffuser. The power plant is the Kori nuclear power plant, located at the southeastern shoreline of Korean peninsula. At Kori nuclear power plant, in addition to the existing 4 units, 2–4 new units are planned to be constructed. Submerged multiport diffusers are considered to be the most viable option for discharging the heated water from the new units. Thus, in this study, as a preliminary design of the tee diffuser, the dimensions of the diffuser are decided, and dilution characteristics are calculated using the proposed equations.

The location map of the Kori nuclear power plant is given in Fig. 10. The current velocity of the ocean in front of the power plant ranges from 40–80 cm/s, and the water depths are shown in Fig. 10. Dimensions of the tee diffuser, decided in preliminary design considering the overall performance of the diffuser, are listed in Table 4. In this table, $N$ is the number of ports. Dilution characteristics calculated using the equations proposed in this study for typical cases are summarized in Table 5. The centerlines of the plume and the isotherms of surface temperature rise corresponding to $\Delta T = 1$°C are shown in Fig. 10. The isotherms in this figure are drawn following the typical shape of the plume observed in the experiment, such as that shown in Fig. 5(c). The values of the momentum ratio in this practical application example ($m_r$ = 2.72–10.9) are very large compared with values of the momentum ratio under which most of the previous studies on tee diffusers have been performed. Thus, as stated earlier, for these conditions, the proposed equations give more accurate predictions for the dilution characteristics of tee diffusers than existing equations.

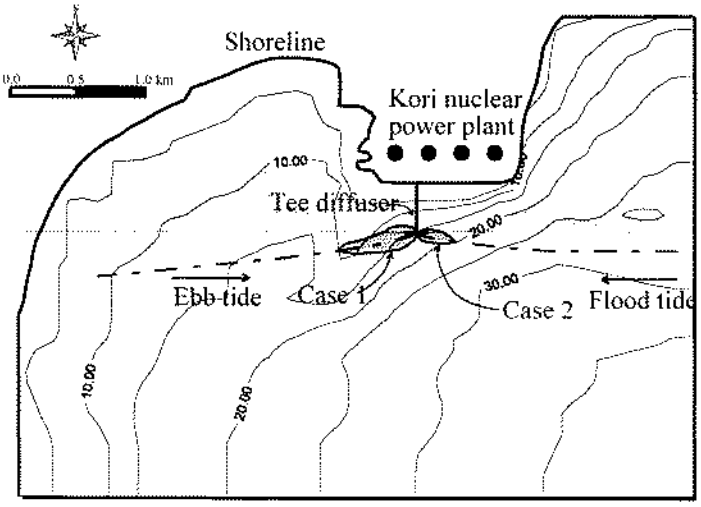


**FIG. 10. Preliminary Design of Tee Diffuser for Kori Nuclear Power Plant**

**TABLE 4. Preliminary Design Example of Tee Diffuser for Kori Nuclear Power Plant**

| $Q$ ($m^3$/s) (1) | $U_0$ (m/s) (2) | $\Delta T_0$ (°C) (3) | $L_D$ (m) (4) | $N$ (5) | $D$ (m) (6) | $\theta_0$ (°) (7) |
|---|---|---|---|---|---|---|
| 58.9 | 3 | 10 | 200 | 100 | 0.5 | 20 |

**TABLE 5. Dilution Characteristics of Tee Diffuser for Kori Nuclear Power Plant**

| Case (1) | $u_a$ (m/s) (2) | $H$ (m) (3) | $m_r$ (4) | $S_0$ (5) | $S_t$ (6) | $A$ [$\Delta T$ = 1°C] ($m^2$) (7) |
|---|---|---|---|---|---|---|
| 1 | 0.4 (flood tide) | 15 | 2.72 | 8.47 | 5.40 | 55,000 |
| 2 | 0.8 (ebb tide) | 15 | 10.9 | 8.47 | 6.72 | 15,000 |

## CONCLUSIONS

A procedure for modifying Adams' theory on the dilution of the tee diffuser has been presented. The distinctive feature of the proposed equation is that the stagnation effect between ambient current and diffuser discharge is correctly incorporated into the momentum equation through the application of the exponential function of the ratio of the discharge momentum to ambient momentum, $m_r$. A simple equation for the plume trajectory including the dependency of the momentum ratio has been derived by applying dimensional analysis. Laboratory experiments involving the tee diffuser were conducted to verify the theoretical equations for a complete range of ambient current conditions.

The experimental results on the near field dilution show that when $m_r < 1$, dilution decreases with $m_r$, whereas when $m_r > 1$, it increases with increasing $m_r$, and that it approaches the stagnant water dilution for very large values of $m_r$. Existing equations provide a reasonable fit to the data in the region where $m_r < 1$; however, predictions by these equations are far off the actual measured data when $m_r$ is larger than 1. A new equation derived in this study has good predictive values, especially when $m_r$ is large.

The observed data for the excess isotherm areas indicate that the relation between the temperature rises and the normalized isotherm areas for different ranges of $m_r$ show similar trends. However, the excess isotherm areas for cases where $m_r > 1$, corresponding to a particular temperature rise, are larger than those for cases where $m_r < 1$. The regression equations which are best-fitted to the observed data from this study can give accurate predictions for complete ranges of the momentum ratio. The observed data for the plume trajectory plotted in a log-log scale indicate a linear relation. The proposed equation for the plume trajectory explicitly contains the factor of the momentum ratio and can accurately predict the plume trajectories for wide ranges of $m_r$.

## ACKNOWLEDGMENTS

This research work was partially supported by the 1997–99 Non Directed Research Fund of Korea Electric Power Corporation and the 1999–2000 Brain Korean 21 Project of the Ministry of Education, Korea. The writers are grateful for the comments provided by Prof. Gerhard H. Jirka, University of Karlsruhe, Germany, and Prof. Joseph H. W. Lee, The University of Hong Kong, China. They have been very helpful in improving the presentation of the material and in clarifying several points.

## APPENDIX I. REFERENCES

Adams, E. E. (1972). "Submerged multiport diffusers in shallow water with current." MS thesis, Massachusetts Institute of Technology, Cambridge, Mass.

Adams, E. E. (1982). "Dilution analysis for unidirectional diffusers." *J. Hydr. Div.*, ASCE, 108(3), 327–342.

Adams, E. E., and Stolzenbach, K. D. (1977). "Comparison of alternative diffuser designs for the discharge of heated water into shallow receiving water." *Proc., Conf. on Waste Heat Mgmt. and Utilization*, Miami Beach, Fla., 1, 171–189.

Akar, P. J., and Jirka, G. H. (1991). *CORMIX2: an expert system for hydrodynamic mixing zone analysis of conventional and toxic multiport diffuser discharges*, Defrees Hydr. Lab., School of Civ. and Envir. Engrg., Cornell University, Ithaca, New York.

Fischer, H. B., List, E. J., Koh, R. C. Y., Imberger, J., and Brooks, N. H. (1999). *Mixing in inland and coastal waters*, Academic, New York.

Jirka, G. H. (1982). "Multiport diffusers for heat disposal: a summary." *J. Hydr. Div.*, ASCE, 108(12), 1423–1468.

Jirka, G. H., and Harleman, D. R. F. (1973). "The mechanics of submerged multiport diffusers for buoyant discharges in shallow water." *Tech. Rep. No. 169*, Ralph M. Parson Laboratory for Water Resources and Hydrodynamics, MIT, Cambridge, Mass.

Lee, J. H. W. (1984). ''Boundary effects on a submerged jet group.'' *J. Hydr. Res.*, Delft, The Netherlands, 22(4), 199–216.
Lee, J. H. W., and Greenberg, M. D. (1984). ''Line momentum source in shallow inviscid fluid.'' *J. Fluid Mech.*, 145, 287–304.
Lee, J. H. W., and Jirka, G. H. (1980). ''Multiport diffuser as line source of momentum in shallow water.'' *Water Resour. Res.*, 16(4), 695–708.
Lee, J. H. W., Jirka, G. H., and Harleman, R. F. (1977). ''Modeling of unidirectional thermal diffusers in shallow water.'' *Rep. No. 228*, Electric Power Program of the MIT Energy Laboratory, MIT, Cambridge, Mass.
Li, C. W., and Lee, J. H. W. (1991). ''Line momentum source in cross-flow.'' *Int. J. Engrg. Sci.*, Great Britain, 29(11), 1409–1418.
Miller, D. S., and Brighouse, B. A. (1984). *Thermal discharges: a guide to power plant cooling water discharges into rivers, lakes and seas*, British Hydromechanics Research Association.
*Perry Nuclear Power Plant, thermal hydraulic model study of cooling water discharge*. (1974). Acres American, Buffalo.
Seo, I. W., and Kim, H. S. (1998). ''Dilution characteristics of unidirectional multiport diffuser.'' *Proc., 3rd Int. Conf. on Hydrodyn.*, Seoul, 517–522.
Stolzenbach, K. D., Almquist, C. W., Adams, E. E., and Freudberg, S. A. (1976). ''Analytical and experimental studies of discharge designs for the Cayuga station at the Somerset alternate site.'' *Rep. No. 211*, Ralph M. Parson Laboratory for Water Resources and Hydrodynamics, MIT, Cambridge, Mass.
Subramanya, K., and Porey, P. D. (1984). ''Trajectory of a turbulent cross jet.'' *J. Hydr. Res.*, Delft, The Netherlands, 22(5), 343–354.

## APPENDIX II. NOTATION

*The following symbols are used in this paper:*

$A$ = cross-sectional area of individual port;
$a, b, c, d, e$ = constants;
$B$ = width of equivalent slot diffuser;
$c_d$ = coefficient associated with stagnation effect of ambient current;
$D$ = port diameter;
$F_j$ = densimetric Froude number;
$g$ = gravitational acceleration;
$g_0$ = effective gravitational acceleration;
$H$ = depth of ambient water;
$j_0$ = buoyancy flux per unit length;
$k$ = coefficient related to effects of bottom friction and irregularities;
$L_D$ = length of diffuser;
$l$ = port spacing;
$m_a$ = momentum flux per unit length of ambient fluid;
$m_r$ = momentum ratio of ambient current to effluent discharge;
$m_0$ = momentum flux per unit length of discharge fluid;
$N$ = number of ports;
$Q_N$ = bulk flow rate at near field;
$Q_0$ = diffuser discharge;
$S_N$ = dilution at near field;
$S_t$ = dilution for tee diffuser in cross flow;
$S_0$ = dilution in stagnant water;
$U_0$ = velocity of effluent discharge;
$u$ = local velocity;
$u_a$ = velocity of ambient current;
$u^*$ = shear velocity;
$\beta$ = horizontal angle between diffuser port and diffuser axis;
$\gamma$ = horizontal angle between diffuser axis and ambient current;
$\Delta\rho$ = density difference between discharging fluid and ambient fluid;
$\varepsilon_y$ = ambient diffusion coefficient;
$\theta_0$ = angle between port and sea bed;
$\phi$ = constant used in criteria for shallow water; and
$\phi_c$ = critical value of $\phi$.

This page intentionally left blank.

# Attachment J

# Maximum and Average 30-Day Total Ammonia Water Quality Objectives

This page intentionally left blank.

**Table 11**
**Maximum Concentration of Total Ammonia Nitrogen for Protection of Aquatic Life (mg/L-N)**

| pH | 0.0 | 1.0 | 2.0 | 3.0 | 4.0 | 5.0 | 6.0 | 7.0 | 8.0 | 9.0 | 10.0 Temp. $^{o}$C |
|---|---|---|---|---|---|---|---|---|---|---|---|
| 6.5 | 27.7 | 28.3 | 27.9 | 27.5 | 27.2 | 26.8 | 26.5 | 26.2 | 26.0 | 25.7 | 25.5 |
| 6.6 | 27.9 | 27.5 | 27.2 | 26.8 | 26.4 | 26.1 | 25.8 | 25.5 | 25.2 | 25.0 | 24.7 |
| 6.7 | 26.9 | 26.5 | 26.2 | 25.9 | 25.5 | 25.2 | 24.9 | 24.6 | 24.4 | 24.1 | 23.9 |
| 6.8 | 25.8 | 25.5 | 25.1 | 24.8 | 24.5 | 24.2 | 23.9 | 23.6 | 23.4 | 23.1 | 22.9 |
| 6.9 | 24.6 | 24.2 | 23.9 | 23.6 | 23.3 | 23.0 | 22.7 | 22.5 | 22.2 | 22.0 | 21.8 |
| 7.0 | 23.2 | 22.8 | 22.5 | 22.2 | 21.9 | 21.6 | 21.4 | 21.1 | 20.9 | 20.7 | 20.5 |
| 7.1 | 21.6 | 21.3 | 20.9 | 20.7 | 20.4 | 20.2 | 19.9 | 19.7 | 19.5 | 19.3 | 19.1 |
| 7.2 | 19.9 | 19.6 | 19.3 | 19.0 | 18.8 | 18.6 | 18.3 | 18.1 | 17.9 | 17.8 | 17.6 |
| 7.3 | 18.1 | 17.8 | 17.5 | 17.3 | 17.1 | 16.9 | 16.7 | 16.5 | 16.3 | 16.2 | 16.0 |
| 7.4 | 16.2 | 16.0 | 15.7 | 15.5 | 15.3 | 15.2 | 15.0 | 14.8 | 14.7 | 14.5 | 14.4 |
| 7.5 | 14.4 | 14.1 | 14.0 | 13.8 | 13.6 | 13.4 | 13.3 | 13.1 | 13.0 | 12.9 | 12.7 |
| 7.6 | 12.6 | 12.4 | 12.2 | 12.0 | 11.9 | 11.7 | 11.6 | 11.5 | 11.4 | 11.3 | 11.2 |
| 7.7 | 10.8 | 10.7 | 10.5 | 10.4 | 10.3 | 10.1 | 10.0 | 9.92 | 9.83 | 9.73 | 9.65 |
| 7.8 | 9.26 | 9.12 | 8.98 | 8.88 | 8.77 | 8.67 | 8.57 | 8.48 | 8.40 | 8.32 | 8.25 |
| 7.9 | 7.82 | 7.71 | 7.60 | 7.51 | 7.42 | 7.33 | 7.25 | 7.17 | 7.10 | 7.04 | 6.98 |
| 8.0 | 6.55 | 6.46 | 6.37 | 6.29 | 6.22 | 6.14 | 6.08 | 6.02 | 5.96 | 5.91 | 5.86 |
| 8.1 | 5.21 | 5.14 | 5.07 | 5.01 | 4.95 | 4.90 | 4.84 | 4.80 | 4.75 | 4.71 | 4.67 |
| 8.2 | 4.15 | 4.09 | 4.04 | 3.99 | 3.95 | 3.90 | 3.86 | 3.83 | 3.80 | 3.76 | 3.74 |
| 8.3 | 3.31 | 3.27 | 3.22 | 3.19 | 3.15 | 3.12 | 3.09 | 3.06 | 3.03 | 3.01 | 2.99 |
| 8.4 | 2.64 | 2.61 | 2.57 | 2.54 | 2.52 | 2.49 | 2.47 | 2.45 | 2.43 | 2.41 | 2.40 |
| 8.5 | 2.11 | 2.08 | 2.06 | 2.03 | 2.01 | 1.99 | 1.98 | 1.96 | 1.95 | 1.94 | 1.93 |
| 8.6 | 1.69 | 1.67 | 1.65 | 1.63 | 1.61 | 1.60 | 1.59 | 1.58 | 1.57 | 1.56 | 1.55 |
| 8.7 | 1.35 | 1.33 | 1.32 | 1.31 | 1.30 | 1.29 | 1.28 | 1.27 | 1.26 | 1.26 | 1.25 |
| 8.8 | 1.08 | 1.07 | 1.06 | 1.05 | 1.04 | 1.04 | 1.03 | 1.03 | 1.02 | 1.02 | 1.02 |
| 8.9 | 0.87 | 0.86 | 0.86 | 0.85 | 0.84 | 0.84 | 0.84 | 0.83 | 0.83 | 0.83 | 0.83 |
| 9.0 | 0.70 | 0.70 | 0.69 | 0.69 | 0.69 | 0.68 | 0.68 | 0.68 | 0.68 | 0.68 | 0.68 |

| | 11.0 | 12.0 | 13.0 | 14.0 | 15.0 | 16.0 | 17.0 | 18.0 | 19.0 | 20.0 |
|---|---|---|---|---|---|---|---|---|---|---|
| 6.5 | 25.2 | 25.0 | 24.8 | 24.6 | 24.5 | 24.3 | 24.2 | 24.0 | 23.9 | 23.8 |
| 6.6 | 24.5 | 24.3 | 24.1 | 23.9 | 23.8 | 24.6 | 23.5 | 23.3 | 23.3 | 23.2 |
| 6.7 | 23.7 | 23.5 | 23.3 | 23.1 | 23.0 | 22.8 | 22.7 | 22.6 | 22.5 | 22.4 |
| 6.8 | 22.7 | 22.5 | 22.3 | 22.2 | 22.0 | 21.9 | 21.8 | 21.7 | 21.6 | 21.5 |
| 6.9 | 21.6 | 21.4 | 21.3 | 21.1 | 21.0 | 20.8 | 20.7 | 20.6 | 20.5 | 20.4 |
| 7.0 | 20.3 | 20.2 | 20.0 | 19.9 | 19.7 | 19.6 | 19.5 | 19.4 | 19.3 | 19.2 |
| 7.1 | 18.9 | 18.8 | 18.7 | 18.5 | 18.4 | 18.3 | 18.2 | 18.1 | 18.0 | 17.9 |
| 7.2 | 17.4 | 17.3 | 17.2 | 17.1 | 16.9 | 16.8 | 16.8 | 16.7 | 16.6 | 16.5 |
| 7.3 | 15.9 | 15.7 | 15.6 | 15.5 | 15.4 | 15.3 | 15.2 | 15.2 | 15.1 | 15.1 |
| 7.4 | 14.2 | 14.1 | 14.0 | 13.9 | 13.9 | 13.8 | 13.7 | 13.6 | 13.6 | 13.5 |
| 7.5 | 12.6 | 12.5 | 12.4 | 12.4 | 12.3 | 12.2 | 12.2 | 12.1 | 12.1 | 12.0 |
| 7.6 | 11.1 | 11.0 | l0.9 | 10.8 | 10.8 | 10.7 | 10.7 | 10.6 | 10.6 | 10.5 |
| 7.7 | 9.57 | 9.50 | 9.43 | 9.37 | 9.31 | 9.26 | 9.22 | 9.81 | 9.15 | 9.12 |
| 7.8 | 8.18 | 8.12 | 8.07 | 8.02 | 7.97 | 7.93 | 7.90 | 7.87 | 7.84 | 7.82 |
| 7.9 | 6.92 | 6.88 | 6.83 | 6.79 | 6.75 | 6.72 | 6.69 | 6.67 | 6.65 | 6.64 |
| 8.0 | 5.81 | 5.78 | 5.74 | 5.71 | 5.68 | 5.66 | 5.64 | 5.62 | 5.61 | 5.60 |
| 8.1 | 4.64 | 4.61 | 4.59 | 4.56 | 4.54 | 4.53 | 4.51 | 4.50 | 4.49 | 4.49 |
| 8.2 | 3.71 | 3.69 | 3.67 | 3.65 | 3.64 | 3.63 | 3.62 | 3.61 | 3.61 | 3.61 |
| 8.3 | 2.97 | 2.96 | 2.94 | 2.93 | 2.92 | 2.92 | 2.91 | 2.91 | 2.91 | 2.91 |
| 8.4 | 2.38 | 2.37 | 2.36 | 2.36 | 2.35 | 2.35 | 2.35 | 2.35 | 2.35 | 2.36 |
| 8.5 | 1.92 | 1.91 | 1.91 | 1.90 | 1.90 | 1.90 | 1.90 | 1.90 | 1.91 | 1.92 |
| 8.6 | 1.55 | 1.54 | 1.54 | 1.54 | 1.54 | 1.54 | 1.55 | 1.55 | 1.56 | 1.57 |
| 8.7 | 1.25 | 1.25 | 1.25 | 1.25 | 1.25 | 1.26 | 1.26 | 1.27 | 1.28 | 1.29 |
| 8.8 | 1.02 | 1.02 | 1.02 | 1.02 | 1.03 | 1.03 | 1.04 | 1.05 | 1.06 | 1.07 |
| 8.9 | 0.83 | 0.83 | 0.84 | 0.84 | 0.85 | 0.85 | 0.86 | 0.87 | 0.88 | 0.89 |
| 9.0 | 0.68 | 0.69 | 0.69 | 0.70 | 0.70 | 0.71 | 0.72 | 0.73 | 0.74 | 0.75 |

**Table 12**
**Average 30-day Nitrogen Concentration of Total Ammonia Nitrogen for Protection of Aquatic Life (mg/L-N)**

| pH | 0.0 | 1.0 | 2.0 | 3.0 | 4.0 | 5.0 | 6.0 | 7.0 | 8.0 | 9.0 | 10.0 Temp.°C |
|---|---|---|---|---|---|---|---|---|---|---|---|
| 6.5-7.1 | 2.08 | 2.05 | 2.02 | 1.99 | 1.97 | 1.94 | 1.92 | 1.90 | 1.88 | 1.86 | 1.84 |
| 7.2 | 2.08 | 2.05 | 2.02 | 1.99 | 1.96 | 1.95 | 1.92 | 1.90 | 1.88 | 1.86 | 1.85 |
| 7.3 | 2.08 | 2.05 | 2.02 | 1.99 | 1.97 | 1.95 | 1.92 | 1.90 | 1.88 | 1.86 | 1.85 |
| 7.4 | 2.08 | 2.05 | 2.02 | 2.00 | 1.97 | 1.95 | 1.92 | 1.90 | 1.88 | 1.87 | 1.85 |
| 7.5 | 2.08 | 2.05 | 2.02 | 2.00 | 1.97 | 1.95 | 1.93 | 1.91 | 1.88 | 1.87 | 1.85 |
| 7.6 | 2.09 | 2.05 | 2.03 | 2.00 | 1.97 | 1.95 | 1.93 | 1.91 | 1.89 | 1.87 | 1.85 |
| 7.7 | 2.09 | 2.05 | 2.03 | 2.00 | 1.98 | 1.95 | 1.93 | 1.91 | 1.89 | 1.87 | 1.86 |
| 7.8 | 1.78 | 1.75 | 1.73 | 1.71 | 1.69 | 1.67 | 1.65 | 1.63 | 1.62 | 1.60 | 1.59 |
| 7.9 | 1.50 | 1.48 | 1.46 | 1.44 | 1.43 | 1.41 | 1.39 | 1.38 | 1.36 | 1.35 | 1.34 |
| 8.0 | 1.26 | 1.24 | 1.23 | 1.21 | 1.20 | 1.18 | 1.17 | 1.16 | 1.15 | 1.14 | 1.13 |
| 8.1 | 1.00 | 0.99 | 0.98 | 0.96 | 0.95 | 0.94 | 0.93 | 0.92 | 0.91 | 0.91 | 0.90 |
| 8.2 | 0.80 | 0.79 | 0.78 | 0.79 | 0.76 | 0.75 | 0.74 | 0.74 | 0.73 | 0.72 | 0.72 |
| 8.3 | 0.64 | 0.63 | 0.50 | 0.49 | 0.48 | 0.48 | 0.48 | 0.47 | 0.47 | 0.46 | 0.46 |
| 8.5 | 0.41 | 0.40 | 0.40 | 0.38 | 0.39 | 0.38 | 0.38 | 0.38 | 0.38 | 0.37 | 0.37 |
| 8.6 | 0.32 | 0.32 | 0.32 | 0.31 | 0.31 | 0.31 | 0.31 | 0.30 | 0.30 | 0.30 | 0.30 |
| 8.7 | 0.26 | 0.26 | 0.25 | 0.25 | 0.25 | 0.25 | 0.25 | 0.24 | 0.24 | 0.24 | 0.24 |
| 8.8 | 0.21 | 0.21 | 0.20 | 0.20 | 0.20 | 0.20 | 0.20 | 0.20 | 0.20 | 0.20 | 0.20 |
| 8.9 | 0.19 | 0.17 | 0.17 | 0.16 | 0.16 | 0.16 | 0.16 | 0.16 | 0.16 | 0.16 | 0.16 |
| 9.0 | 0.14 | 0.13 | 0.13 | 0.13 | 0.13 | 0.13 | 0.13 | 0.13 | 0.13 | 0.13 | 0.13 |

| | 11.0 | 12.0 | 13.0 | 14.0 | 15.0 | 16.0 | 17.0 | 18.0 | 19.0 | 20.0 |
|---|---|---|---|---|---|---|---|---|---|---|
| 6.5 | 1.82 | 1.81 | 1.80 | 1.78 | 1.77 | 1.64 | 1.52 | 1.41 | 1.31 | 1.22 |
| 6.6 | 1.82 | 1.81 | 1.80 | 1.78 | 1.77 | 1.64 | 1.52 | 1.41 | 1.31 | 1.22 |
| 6.7 | 1.83 | 1.81 | 1.80 | 1.78 | 1.77 | 1.64 | 1.52 | 1.41 | 1.31 | 1.22 |
| 6.8 | 1.83 | 1.81 | 1.80 | 1.78 | 1.77 | 1.64 | 1.52 | 1.42 | 1.32 | 1.22 |
| 6.9 | 1.82 | 1.81 | 1.80 | 1.78 | 1.77 | 1.64 | 1.53 | 1.42 | 1.32 | 1.22 |
| 7.0 | 1.83 | 1.81 | 1.80 | 1.79 | 1.77 | 1.64 | 1.53 | 1.42 | 1.32 | 1.22 |
| 7.1 | 1.83 | 1.81 | 1.80 | 1.79 | 1.77 | 1.65 | 1.53 | 1.42 | 1.32 | 1.23 |
| 7.2 | 1.83 | 1.81 | 1.80 | 1.79 | 1.78 | 1.65 | 1.53 | 1.42 | 1.32 | 1.23 |
| 7.3 | 1.83 | 1.82 | 1.80 | 1.79 | 1.78 | 1.65 | 1.53 | 1.42 | 1.32 | 1.23 |
| 7.4 | 1.83 | 1.82 | 1.80 | 1.79 | 1.78 | 1.65 | 1.53 | 1.42 | 1.32 | 1.23 |
| 7.5 | 1.83 | 1.82 | 1.81 | 1.80 | 1.78 | 1.66 | 1.54 | 1.43 | 1.33 | 1.23 |
| 7.6 | 1.84 | 1.82 | 1.81 | 1.80 | 1.79 | 1.66 | 1.54 | 1.43 | 1.33 | 1.24 |
| 7.7 | 1.84 | 1.83 | 1.81 | 1.80 | 1.79 | 1.66 | 1.54 | 1.44 | 1.34 | 1.24 |
| 7.8 | 1.57 | 1.56 | 1.55 | 1.54 | 1.53 | 1.42 | 1.32 | 1.23 | 1.14 | 1.07 |
| 7.9 | 1.33 | 1.32 | 1.31 | 1.31 | 1.30 | 1.21 | 1.12 | 1.04 | 0.97 | 0.90 |
| 8.0 | 1.12 | 1.11 | 1.10 | 1.10 | 1.09 | 1.02 | 0.94 | 0.88 | 0.82 | 0.76 |
| 8.1 | 0.89 | 0.89 | 0.88 | 0.88 | 0.87 | 0.81 | 0.76 | 0.70 | 0.66 | 0.61 |
| 8.2 | 0.71 | 0.71 | 0.71 | 0.70 | 0.70 | 0.65 | 0.61 | 0.57 | 0.53 | 0.49 |
| 8.3 | 0.57 | 0.57 | 0.57 | 0.56 | 0.56 | 0.52 | 0.49 | 0.46 | 0.43 | 0.40 |
| 8.4 | 0.46 | 0.46 | 0.46 | 0.45 | 0.45 | 0.42 | 0.39 | 0.37 | 0.34 | 0.32 |
| 8.5 | 0.37 | 0.37 | 0.37 | 0.37 | 0.37 | 0.34 | 0.32 | 0.30 | 0.28 | 0.26 |
| 8.6 | 0.30 | 0.30 | 0.30 | 0.30 | 0.30 | 0.28 | 0.26 | 0.24 | 0.23 | 0.21 |
| 8.7 | 0.24 | 0.24 | 0.24 | 0.24 | 0.24 | 0.23 | 0.21 | 0.20 | 0.19 | 0.18 |
| 8.8 | 0.20 | 0.20 | 0.20 | 0.20 | 0.20 | 0.19 | 0.17 | 0.16 | 0.15 | 0.15 |
| 8.9 | 0.16 | 0.16 | 0.16 | 0.16 | 0.16 | 0.15 | 0.14 | 0.14 | 0.13 | 0.12 |
| 9.0 | 0.13 | 0.13 | 0.13 | 0.13 | 0.14 | 0.12 | 0.12 | 0.12 | 0.11 | 0.10 |

- the average of the measured values must be less than the average of the corresponding individual values in Table 11.
- each measured value is compared to the corresponding individual values in Table 11.

No more than one in five of the measured values can be greater than one-and-a-half times the corresponding objective values in Table 11.

This page intentionally left blank.

CDM Smith

cdmsmith.com